



**HAL**  
open science

# The development of thermal and spectroscopic methods for the characterization of catalysts for CO<sub>2</sub> storage

José Flavio Benevides Ferreira

## ► To cite this version:

José Flavio Benevides Ferreira. The development of thermal and spectroscopic methods for the characterization of catalysts for CO<sub>2</sub> storage. Other. Université Sciences et Technologies - Bordeaux I, 2013. English. NNT: 2013BOR14812 . tel-00858419

**HAL Id: tel-00858419**

**<https://theses.hal.science/tel-00858419>**

Submitted on 5 Sep 2013

**HAL** is a multi-disciplinary open access archive for the deposit and dissemination of scientific research documents, whether they are published or not. The documents may come from teaching and research institutions in France or abroad, or from public or private research centers.

L'archive ouverte pluridisciplinaire **HAL**, est destinée au dépôt et à la diffusion de documents scientifiques de niveau recherche, publiés ou non, émanant des établissements d'enseignement et de recherche français ou étrangers, des laboratoires publics ou privés.

# THÈSE

PRÉSENTÉE A

**L'UNIVERSITÉ BORDEAUX 1**

ÉCOLE DOCTORALE DES SCIENCES CHIMIQUES

Par **Jose Flavio BENEVIDES FERREIRA**

POUR OBTENIR LE GRADE DE

**DOCTEUR**

SPÉCIALITÉ: PHYSICO-CHIMIE

## **La mise au point de méthodes thermiques et spectrométriques pour la caractérisation des catalyseurs pour le stockage de CO<sub>2</sub>**

Soutenu le : 2 Juillet 2013

Devant la commission d'examen formée de :

Dr ORLANDE, Hécio

Dr DATURI, Marco

Dr FUDYM, Olivie

Dr MIGNANI, Gérard

Dr SERVANT, Laurent

Dr BATSALE, Jean-Christophe

M. PAVAGEAU, Bertrand

Dr MASCETTI, Joëlle

Dr JOLLY, Julien

Dr PRADERE, Christophe

Dr MAGIMEL, Jérôme

Professeur, UFRJ-Brésil

Professeur, Université de Caen

Professeur, Ecole des Mines d'Albi

Fellow Scientist, Solvay-CRTL

Professeur, Université de Bordeaux 1

Professeur, Arts et Métiers ParisTech

Senior Scientist, Solvay-LOF

Directrice de recherche, CNRS, ISM

Ingénieur de recherche, Solvay-LOF

Chargé de Recherche, CNRS, I2M

Chargé de Recherche, CNRS, ICMCB

Président

Rapporteur

Rapporteur

Examineur

Directeur de thèse

Directeur de thèse

Responsable Industriel

Co-encadrant de thèse

Co-encadrant de thèse

Co-encadrant de thèse

Invité



# La mise au point de méthodes thermiques et spectrométriques pour la caractérisation des catalyseurs pour le stockage de CO<sub>2</sub>

**J.F. Benevides Ferreira<sup>a,b,c</sup>, C. Pradere<sup>a</sup>, J. Jolly<sup>c</sup>, G. Le Bourdon<sup>b</sup>, J. Mascetti<sup>b</sup>, B. Pavageau<sup>c</sup>, L. Servant<sup>b</sup>, J-C. Batsale<sup>a</sup>**

*a. 12M, Laboratoire TREFLE, Esplanade des Arts et Métiers, 33405 Talence Cedex, France*

*b. ISM, Université Bordeaux I, 351 cours de la libération, 33405 Talence Cedex, France*

*c. Solvay LOF, 178 avenue du Docteur Schweitzer, 33608 Pessac Cedex, France*

## Résumé:

*La capture de CO<sub>2</sub> par adsorption sur des solides poreux (adsorbants) est une alternative prometteuse en raison de sa sélectivité et de sa faible consommation d'énergie. Nous avons étudié l'adsorption in-situ de CO<sub>2</sub> sur des adsorbants solides en combinant la spectroscopie infrarouge par réflexion diffuse (DRIFT) avec la thermographie infrarouge afin de mieux comprendre les mécanismes d'interaction CO<sub>2</sub>-adsorbant et ainsi optimiser sa captation dans des procédés de capture en post-combustion. La thermographie IR est utilisée pour détecter la source de chaleur transitoire provenant de la surface de l'adsorbant au cours de l'adsorption de CO<sub>2</sub>. Un modèle de transfert de chaleur a été développé afin d'estimer les chaleurs d'adsorption. Un mini réacteur conçu pour la DRIFT nous a permis d'identifier les espèces adsorbées et d'étudier leur évolution sur la surface de l'adsorbant selon la température et l'atmosphère environnante. Enfin, le couplage d'informations provenant des deux approches nous a permis l'investigation haut-débit des paramètres clés pour le choix des adsorbants les plus performants.*

**Mots-clés:** adsorption de CO<sub>2</sub>, thermographie IR, spectroscopie DRIFT, méthodologie haut-débit, modélisation thermique, chaleur d'adsorption, technique inverse.

## The development of thermal and spectroscopic methods for the characterization of catalysts for CO<sub>2</sub> storage

### Abstract:

*CO<sub>2</sub> capture via adsorption process on porous materials (adsorbents) is a promising alternative due to its high selectivity and low energy penalties. We have investigated in-situ CO<sub>2</sub> adsorption on solid adsorbents by combining Diffuse Reflectance Infrared Fourier Transform spectroscopy (DRIFT) with infrared thermography to better understand the mechanisms controlling CO<sub>2</sub>-adsorbent interactions and thus optimize its capture in post-combustion capture processes. Infrared thermography is used to detect the transient heat source coming from the adsorbent surface during CO<sub>2</sub> adsorption. A heat transfer model has been developed in order to estimate the adsorption heats. A model chemical reactor designed for DRIFT allowed us to clearly evidence the adsorbed species and to study the surface species evolution according to the temperature and the surrounding atmosphere. Finally, the coupling of information coming from the two approaches allowed us a high-throughput investigation of key parameters for the selection of the most efficient adsorbents.*

**Keywords:** CO<sub>2</sub> adsorption, IR thermography, DRIFT spectroscopy, high-throughput methodology, thermal modelling, heat of adsorption, inverse technique.



# REMERCIEMENTS

Remerciement...comment remercier tous ceux qui ont contribué directement et indirectement à la concrétisation de cet énorme défis qu'est la thèse? J'avoue que c'est plus difficile que l'attribution de bandes et l'analyse des équations de la chaleur!

J'essaye...Tout d'abord, je tiens à remercier chaleureusement mes directeurs de thèse Pr. Laurent SERVANT et Pr. Jean-Christophe BATSALE pour leur soutien très précieux, pour leur confiance et compétences indispensables pendant ces 3 ans de projet. Comme hommage, je résume leur esprit dans une phrase:

« Flavio, la vie c'est la violence et la brutalité... » ; « Flavio, tu es un ingénieur Arts et Métiers, alors pourquoi faire compliqué si on peut faire simple! »

Je tiens à remercier mon responsable industriel M. Bertrand PAVAGEAU et le directeur du LOF-Solvay M. Patrick MAESTRO pour m'avoir accordé leur confiance sur ce projet de thèse, et pour leur enthousiasme et sympathie constante. Un bon exemple de management!

Je remercie vivement Pr. Marco DATURI et Pr Olivier FUDYM, qui m'ont fait l'honneur de juger ce travail, ainsi que mon compatriote Pr. Hécio ORLANDE pour avoir accepté de présider mon jury de thèse. Je remercie également l'examineur Dr Gérard MIGNANI pour sa vision industrielle et l'invité Dr Jérôme MAGIMEL pour son intérêt porté à ce travail.

Je tiens également à remercier mes co-encadrants de thèse Dr Joëlle MASCETTI pour sa disponibilité, son soutien moral et scientifique, ainsi que son enthousiasme quotidien; Dr Julien JOLLY pour son aide précieuse tout au long de la thèse et pour avoir été un très bon coéquipier; et Dr Christophe PRADERE pour sa bonne humeur et son expertise de thermicien essentielle pour l'avancement du projet.

Je tiens à remercier aussi Dr Gwenaëlle LE BOURDON, Dr Frédéric ADAMIETZ, Dr Cédric SLOSTOWSKI, M. Christian AUPETIT et les stagiaires Adrien FREDON et Sandy POULOU qui m'ont aidé considérablement avec les manipulations et résultats.

Enfin je tiens à remercier ma famille pour le support moral transatlantique, ma copine Mathilde CHAMPEAU pour le soutien professionnel, pour l'encouragement, patience et compréhension.

Comment oublier mes amis et collègues Franck, Sandra, Martha, Thierry T., Aude, Enora, Chris, Stéphanie, Daniela, Elise, Tatiana, Coralie... Un grand merci pour l'ambiance de travail et détente très sympathique et importante durant cette thèse.



## RÉSUMÉ

Ce manuscrit de thèse a comme objet l'étude de la capture de CO<sub>2</sub> par des adsorbants solides, via la mise au point de méthodes de caractérisation thermique et spectroscopique non intrusives devant aider à la sélection haut débit des adsorbant les plus performants.

Ce sujet est motivé par d'importants enjeux environnementaux liés à la capture du CO<sub>2</sub>. En effet, la diminution de la quantité de CO<sub>2</sub> rejetée dans l'atmosphère est devenue un objectif majeur pour de nombreux pays en raison de sa forte contribution au réchauffement climatique. En France, l'objectif est de diviser ces émissions de CO<sub>2</sub> par quatre d'ici 2050. Plusieurs voies peuvent être envisagées: travailler sur le procédé en amont pour réduire les émissions de CO<sub>2</sub> à sa source, diminuer la consommation énergétique des procédés, ou encore capter le CO<sub>2</sub> à la sortie des chambres de combustion (postcombustion). La capture de CO<sub>2</sub> consiste d'abord à l'isoler de ses sources industrielles : pétrochimie, sidérurgie, raffineries. Le CO<sub>2</sub> peut ensuite être comprimé et stocké, ou encore valorisé par transformation chimique pour produire un composé de plus forte valeur ajoutée. Un procédé déjà commercialisé consiste à utiliser un solvant aminé (monoéthanolamine) ayant une forte capacité d'absorption de CO<sub>2</sub>, permettant ainsi de le séparer des autres composés présents dans la fumée de combustion (N<sub>2</sub>, H<sub>2</sub>O majoritairement). Cependant, le coût du processus de séparation reste encore élevé (près de 50 euros par tonne de CO<sub>2</sub>), principalement à cause des étapes de régénération du solvant (augmentation de la température de 60 à 120 °C) pour la thermodésorption de CO<sub>2</sub>. Une autre technologie susceptible d'être économiquement plus viable consiste en l'utilisation d'adsorbants solides qui capteraient de manière réversible des molécules de CO<sub>2</sub> à leur surface avec un faible coût énergétique pour la régénération de l'adsorbant.

La communauté scientifique a rapidement pris conscience de l'intérêt de cette approche et s'est concentrée sur la recherche de matériaux pouvant permettre une capture efficace de CO<sub>2</sub>. Ainsi, cette étude s'est déroulée dans le cadre d'une collaboration scientifique entre le Département TREFLE de l'Institut Mécanique et Ingénierie de Bordeaux (I2M), le Laboratoire du Futur Solvay/CNRS (LOF) et du Groupe de Spectroscopie Moléculaire de l'Institut des Sciences Moléculaires (ISM), qui ont rassemblé leurs expertises afin d'étudier précisément les mécanismes d'adsorption des molécules de CO<sub>2</sub> sur divers adsorbants solides.

De façon générale, les molécules peuvent se lier à des surfaces solides selon deux processus: soit la molécule s'attache à la surface par physisorption, grâce à une interaction de type van der Waals qui s'établit entre elle et le substrat, soit une liaison chimique se forme entre le substrat et la molécule adsorbée: c'est la chimisorption. L'énergie dégagée lors de l'interaction gaz/substrat est dissipée dans le solide (vibrations de réseau) et se traduit par une quantité de chaleur dégagée. La quantité de chaleur dégagée lors d'un processus de physisorption est de l'ordre de 25 kJ.mol<sup>-1</sup> alors qu'elle est considérablement plus élevée (environ 100 kJ.mol<sup>-1</sup>) dans le cas de la chimisorption, qui s'accompagne d'une profonde modification de la répartition des charges électroniques des molécules adsorbées. Les matériaux de capture de CO<sub>2</sub> peuvent donc être classés dans deux grandes catégories: les matériaux de physisorption où se trouvent les zéolithes, les MOF (metal organic framework)

ou encore les charbons actifs et les matériaux de chimisorption où se trouvent les hybrides organique/inorganique et les oxydes métalliques.

La connaissance de ces interactions gaz/solide est donc essentielle en vue d'une capture de CO<sub>2</sub> efficace en matière de performances adsorbant (capacité et cinétique d'adsorption, sélectivité, régénération,...) et de la conception de procédés (bilan énergétique, sécurité procédé, ...).

Dans ce contexte, l'objectif global de ce projet était d'étudier les interactions durant le processus d'adsorption du point de vue énergétique mais aussi chimique. C'est pourquoi nous avons utilisé deux approches complémentaires: la thermographie infrarouge et la spectroscopie infrarouge.

De plus, nous avons développés des outils et des méthodes d'analyse haut-débit afin de répondre aux exigences industrielles qui nécessitent d'accéder rapidement aux paramètres clefs contrôlant l'adsorption de CO<sub>2</sub>. Cette méthodologie nous a alors permis d'évaluer les performances de divers matériaux: des oxydes de terre rare (cérites pures et dopées), des charbons actifs ainsi que des matériaux hybrides (silices imprégnées d'amine).

La stratégie haut-débit a consisté en quatre étapes:

1. **Criblage primaire:** Un dispositif haut débit basé sur la thermographie infrarouge a été utilisé afin d'étudier le comportement thermique d'une couche mince d'adsorbants durant le processus d'adsorption en mesurant la chaleur libérée. Cela a permis une analyse qualitative, en première approche, permettant d'étudier le phénomène et d'identifier les matériaux ayant une bonne affinité avec le CO<sub>2</sub>. Par conséquent, nous avons mis en évidence des paramètres influençant la quantité de chaleur libérée, tel que la concentration en CO<sub>2</sub> dans la phase gazeuse, le débit de gaz injecté, la surface spécifique du matériau, les vitesses d'adsorption et de désorption; et la nature des interactions (physisorption/chimisorption). Nous avons alors émis des hypothèses concernant les comportements adsorptifs de chaque famille de matériaux, par exemple pour la réversibilité de la capture.
2. **Criblage secondaire:** En couplant la thermographie infrarouge et la technique gravimétrique (balance de précision), nous avons pu enregistrer simultanément les évolutions de la température et de la masse adsorbée lors de l'adsorption du CO<sub>2</sub> sur une couche mince d'adsorbant. A partir de ces données, nous avons corrélé les informations concernant les transferts de chaleur et de masse, ce qui a conduit à la confirmation de certaines des hypothèses précédentes. Par exemple, la réversibilité de capture et la chaleur libérée sont fortement influencées par le type d'amine imprégnée sur le support de silice. De plus, la capacité d'adsorption de la plupart des matériaux testés a pu être estimée à partir des profils d'évolution de la masse adsorbée. De manière globale, les matériaux hybrides et les charbons actifs ont démontré des capacités d'adsorption élevées.

Un modèle thermique simplifié a été développé pour mieux comprendre les comportements thermiques, ce qui a permis d'estimer les chaleurs d'adsorption ( $\Delta H_{ads}$ ) et d'étudier les paramètres influençant l'estimation de ces  $\Delta H_{ads}$ , tels que les

pertes thermiques. Par conséquent, en utilisant les données expérimentales, une méthode d'estimation pragmatique et haut débit a été mise en œuvre. Dans l'ensemble, les valeurs les plus élevées de chaleur d'adsorption de CO<sub>2</sub> ( $\Delta H_{ads}$ ) ont été trouvées pour les matériaux hybrides, suivis par les oxydes de terre rare puis les charbons actifs, ce qui est cohérent avec la littérature. Grâce à un modèle simplifié d'évolution de la phase adsorbée, d'autres paramètres clés ont été définis pour comparer les vitesses d'adsorption et de désorption. Les charbons actifs ont montré des vitesses d'adsorption et de désorption les plus élevés parmi les matériaux testés, suivis par les oxydes de terre rare et les matériaux hybrides.

Ainsi, dans ces deux premières parties de l'étude, nous avons identifié et évalué les paramètres clés pour la capture de CO<sub>2</sub> par des adsorbants solides telles que la force d'interaction ( $\Delta H_{ads}$ ), la capacité et la cinétique d'adsorption. Nous avons également pu mettre en évidence la stabilité thermique des matériaux pendant les cycles d'adsorption à température ambiante.

- Première investigation:** Un montage expérimental basé sur la spectroscopie DRIFT (Spectroscopie Infrarouge à Réflexion Diffuse) a été développé pour l'étude haut débit des interactions chimiques entre les molécules de CO<sub>2</sub> et les matériaux. Nous avons donc confirmé la nature des interactions et identifié les espèces formées durant le processus d'adsorption. Ainsi, nous avons confirmé que l'adsorption du CO<sub>2</sub> sur le charbon actif testé était de nature purement physique. De plus, les molécules de CO<sub>2</sub> sont adsorbées sous forme d'espèces carbonatées sur les oxydes de terre rare; et sous forme d'espèces ioniques de carbamates et sous forme d'acide carbamique sur les matériaux hybrides testés. En outre, à partir de l'analyse de l'évolution des espèces adsorbées au cours du protocole expérimental (débit et température de gaz contrôlés), nous avons été en mesure de valider l'ensemble des hypothèses concernant les comportements adsorptifs (cinétique et quantités adsorbées) et d'étudier la stabilité thermique des adsorbants (dégradation des matériaux) et des espèces adsorbées.

Enfin, les informations obtenues au cours des étapes de criblage et de cette première étape d'investigation nous ont permis de faire une comparaison globale des matériaux:

Matériaux	Nature	Espèces adsorbées	$\Delta h_{ads}$ (kJ/mol)	Capacité	Vitesse	Stabilité thermique	Facilité régénération
Oxydes	chimisorption	Carbonates/hydrogénocarbonates	30-40	+	+++	++++	++
Hybrides	chimisorption	Ions carbamates/acide carbamique	40-60	++++	++	++	++++
Charbon	physisorption	CO <sub>2</sub>	20-30	+++	+++++	+++++	+++++

Les oxydes de terres rares ne sont pas des adsorbants appropriés pour la capture du CO<sub>2</sub> dans des flux de postcombustion principalement en raison de leur faible capacité d'adsorption. Toutefois, ces matériaux sont intéressants vis-à-vis de la valorisation du CO<sub>2</sub> (par exemple pour la production de carburant) car il est possible de moduler leurs propriétés de surface (basicité et mobilité de l'oxygène). Parmi les charbons actifs et les matériaux hybrides, deux

matériaux testés ont suscité beaucoup d'intérêt en ce qui concerne la capture réversible de  $\text{CO}_2$  à basse température. En effet, ces deux adsorbants ont des capacités d'adsorption élevées et ils sont régénérables dans des conditions douces (sous flux inerte d'azote, sans chauffer le matériau). Les principales différences entre les matériaux sont leur stabilité thermique et leur vitesse d'adsorption. Etant donné que le charbon actif en question possède la vitesse d'adsorption et la stabilité thermique les plus élevées, il s'avère être l'adsorbant le plus approprié.

4. **Seconde investigation:** Nous avons développé une colonne d'adsorption milli-fluidique dans lequel le champ de température est détecté grâce à la thermographie infrarouge pendant le processus d'adsorption. Ce dispositif milli-fluidique a permis d'explorer les premiers résultats d'une étude haut débit des conditions opératoires influençant le comportement thermique du système milli-fluidique, c'est-à-dire l'évolution de la température et la vitesse de front thermique qui est liée à la saturation du lit. En outre, une analyse multi-échelle, d'une couche mince à une couche épaisse de lit d'adsorbant, a pu être effectuée. Ainsi, nous avons obtenu les premiers résultats reliant les données en couche mince à la vitesse de propagation du front thermique dans le lit d'adsorption milli-fluidique.

Il est important de souligner que ce travail a permis d'accéder rapidement aux principaux paramètres qui régissent les interactions  $\text{CO}_2$ /adsorbant.

La thermographie infrarouge et la spectroscopie infrarouge se sont révélées être une riche combinaison en raison de la complémentarité des informations obtenues.

Enfin, la méthodologie et les outils développés peuvent être appliqués pour l'étude d'autres interactions gaz-solides, comme dans le domaine de la catalyse hétérogène.

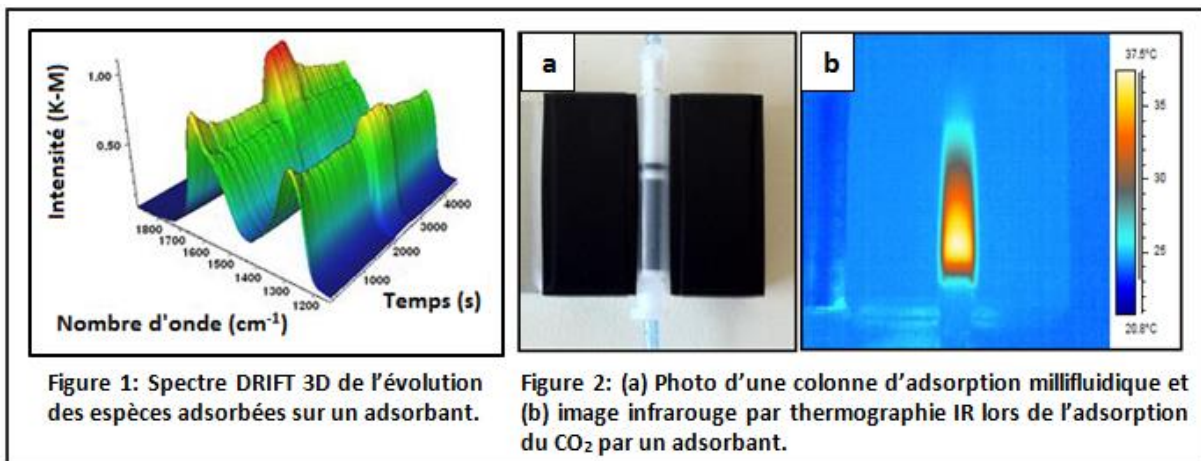


# TABLE OF CONTENTS

GENERAL INTRODUCTION .....	15
CHAPTER I: Adsorption Principles and Materials for Carbon Dioxide Capture .....	23
1 Introduction .....	27
2 Principles of Adsorption.....	27
3 CO <sub>2</sub> molecule description.....	27
4 CO <sub>2</sub> adsorption systems .....	29
5 Solid adsorbents for CO <sub>2</sub> capture .....	30
5.1 Physisorption adsorbents .....	31
5.1.1 Zeolites .....	31
5.1.2 Activated carbons .....	32
5.1.3 Metal Organic Frameworks.....	33
5.2 Chemisorption adsorbents .....	34
5.2.1 Hybrid organic/inorganic adsorbents .....	34
5.2.2 Metal based adsorbents .....	37
6 Studied materials .....	38
6.1 Basic rare Earth oxides .....	38
6.2 Activated carbons .....	41
6.3 Hybrid organic/inorganic materials .....	42
7 Conclusions .....	45
CHAPTER II: Experimental and Modeling Approaches for the Study of Carbon Dioxide Capture .....	47
1 Introduction .....	51
2 Adsorption isotherms .....	51
3 Heat of adsorption evaluation .....	54
3.1 Adsorption heat estimation via adsorption isotherms.....	54
3.2 Adsorption heat measured by calorimetric techniques .....	56
3.3 The <i>pros</i> and <i>cons</i> of classical $\Delta H$ evaluation methods .....	56
4 Modeling adsorption dynamics .....	57
4.1 Mass transfer.....	57
4.1.1 Mass balance for the adsorbed-phase.....	57
4.1.2 Mass balance for the gas-phase .....	58

4.2	Heat transfer .....	59
4.2.1	Heat balance for the adsorbent particle .....	59
4.2.2	Heat balance for the gas-phase .....	59
4.2.3	Heat balance for the wall of adsorption packed column .....	59
5	Critical of classical modeling of adsorption dynamics .....	60
6	Our approach to study CO <sub>2</sub> adsorption .....	60
6.1	IR thermography .....	60
6.1.1	IR thermography cameras .....	61
6.1.2	IR thermography features .....	62
6.1.3	Principles of non-contact temperature measurement .....	63
6.2	IR spectroscopy .....	65
6.2.1	IR Spectrometers .....	66
6.2.2	Sample handling technique .....	66
6.3	Our high-throughput strategy .....	67
7	Conclusions .....	69
CHAPTER III: Primary and Secondary Screening - Qualitative Analysis of Adsorptive Behaviors and Evaluation of Adsorption Capacities.....		71
1	Introduction .....	75
2	Primary Screening: Qualitative Analysis of Adsorptive Behaviors.....	75
2.1	Experimental device .....	75
2.2	Results and discussion .....	77
2.2.1	Rare Earth Oxides (REO).....	77
2.2.2	Hybrid organic/inorganic materials.....	83
2.2.3	Activated Carbon.....	85
2.3	Overall screening results and discussion .....	86
2.4	Summary and conclusions .....	88
3	Secondary Screening: Evaluation of Adsorption Capacities.....	89
3.1	Experimental device .....	89
3.2	Results and discussion .....	90
3.2.1	Activated Carbon.....	90
3.2.2	Hybrid organic/inorganic materials.....	91
3.2.3	Rare Earth oxides .....	93
3.3	Overall screening results and discussion .....	93
3.4	Summary and conclusions .....	94
4	Final Conclusions.....	95

CHAPTER IV: Modeling Adsorption on Thin-Layer and Estimation of Key Parameters.....	97
1 Introduction .....	101
2 Thin-layer Approach .....	101
3 Simplified analysis of experimental data .....	103
4 Adsorption heat estimation.....	105
4.1 General approach to estimate adsorption heats .....	106
4.2 Results and discussion .....	108
4.3 Parameters influencing adsorption heat estimation .....	112
5 Parameters influencing temperature evolution.....	115
6 Key parameters for material selection.....	121
7 Conclusions .....	127
8 Annex .....	128
CHAPTER V: Investigation Level I - Insight into Chemical Interactions via DRIFT Spectroscopy .....	129
1 Introduction .....	133
2 Experimental device .....	133
3 Results and discussion.....	136
3.1 Activated carbon.....	136
3.2 Rare earth oxides (REO).....	137
3.3 Hybrid materials .....	151
3.3.1 33Iminobis impregnated silica HRS1200 .....	151
3.3.2 Monoethanolamine impregnated silica HRS1200.....	160
4 Conclusions .....	163
CHAPTER VI: Investigation Level II - Development of a Millifluic Adsorption Column ..	167
GENERAL CONCLUSIONS and OUTLOOK .....	173
1 Performance of materials: What is the best material for CO <sub>2</sub> capture? .....	175
1.1 Rare Earth oxides.....	175
1.2 Activated carbons .....	176
1.3 Hybrid materials .....	176
1.4 AC1 <i>versus</i> 33Iminobis/HRS1200 .....	177
2 Summary and Outlook .....	178
REFERENCES.....	181



## **GENERAL INTRODUCTION**



## GENERAL INTRODUCTION

According to the Climate Change 2007: Synthesis Report [1] from the Intergovernmental Panel on Climate Change (IPCC), the greenhouse gas (GHG) emissions due to human activities have grown since pre-industrial times, with an increase of 70% between 1970 and 2004. It was also found that carbon dioxide (CO<sub>2</sub>) is the most important anthropogenic GHG, with a rise of annual emissions between 1970 and 2004 by about 80%, with 38 gigatonnes (Gt), representing 77% of total anthropogenic GHG emissions in 2004. The rate of CO<sub>2</sub> emission growth was much higher during the recent 10 year period of 1995-2004 (0.92 GtCO<sub>2</sub> per year) than during the previous period of 1970-1994 (0.43 GtCO<sub>2</sub> per year). The largest growth in GHG emissions between 1970 and 2004 has come from energy supply, transport and industry.

According to released data from US Energy Information Administration in 2009, the map shown in Figure 1 resizes each country conforming to CO<sub>2</sub> emissions.

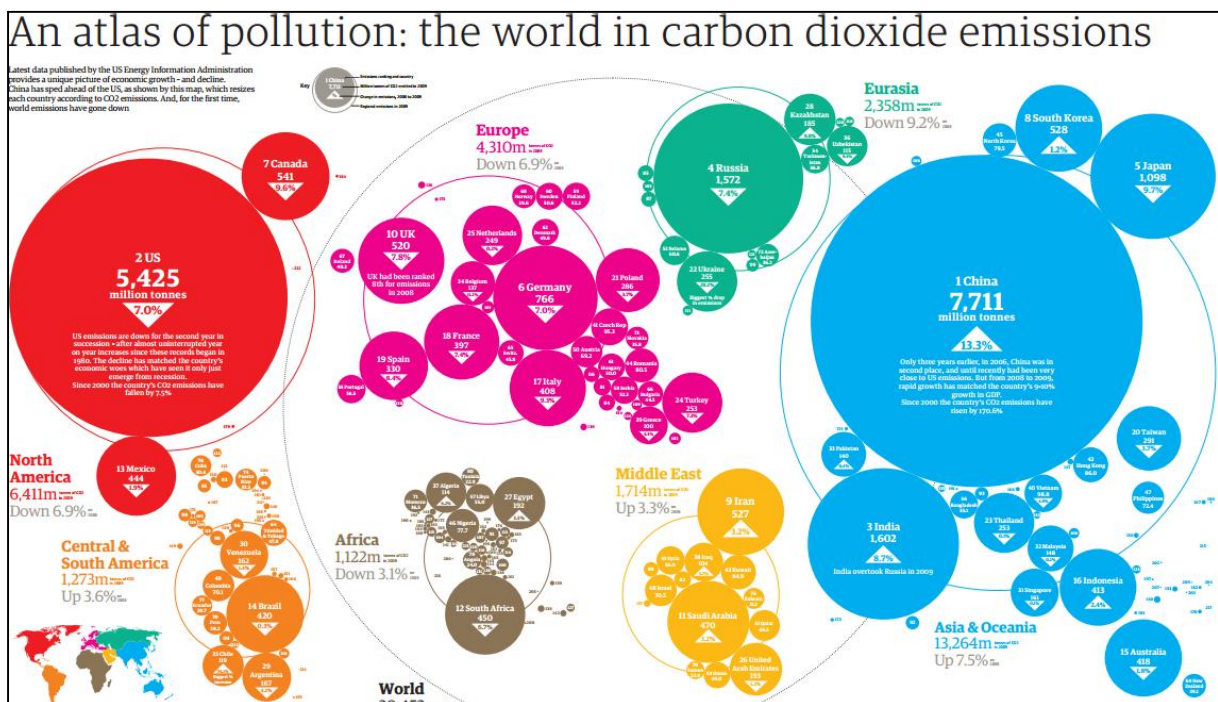


Figure 1: Global CO<sub>2</sub> emission by country in 2009. Source: The guardian. <http://www.guardian.co.uk>.

From the map above, China emits more CO<sub>2</sub> than the US and Canada put together. India is the world's third biggest emitter of CO<sub>2</sub>, just before Russia, fourth place. France was ranked eighteenth in global CO<sub>2</sub> emissions in 2009.

The main sources of CO<sub>2</sub> emissions in the world in 2004 are shown in Figure 2. More than 50% of CO<sub>2</sub> emissions come from localized sources: industry and energy supply.

IPCC 2007 Report states that most of the observed increase in global average temperatures since the mid 20th century is very likely due to the observed increase in anthropogenic GHG concentrations (Figure 3).

Finally, there was affirmed that anthropogenic warming over the last three decades has had a discernible influence at the global scale on observed changes in many physical and biological systems.

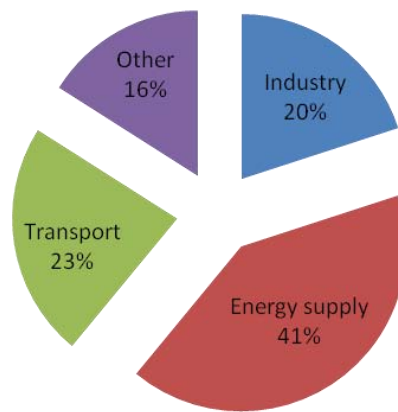


Figure 2: Global CO<sub>2</sub> emissions by source in 2010. Source: [2]

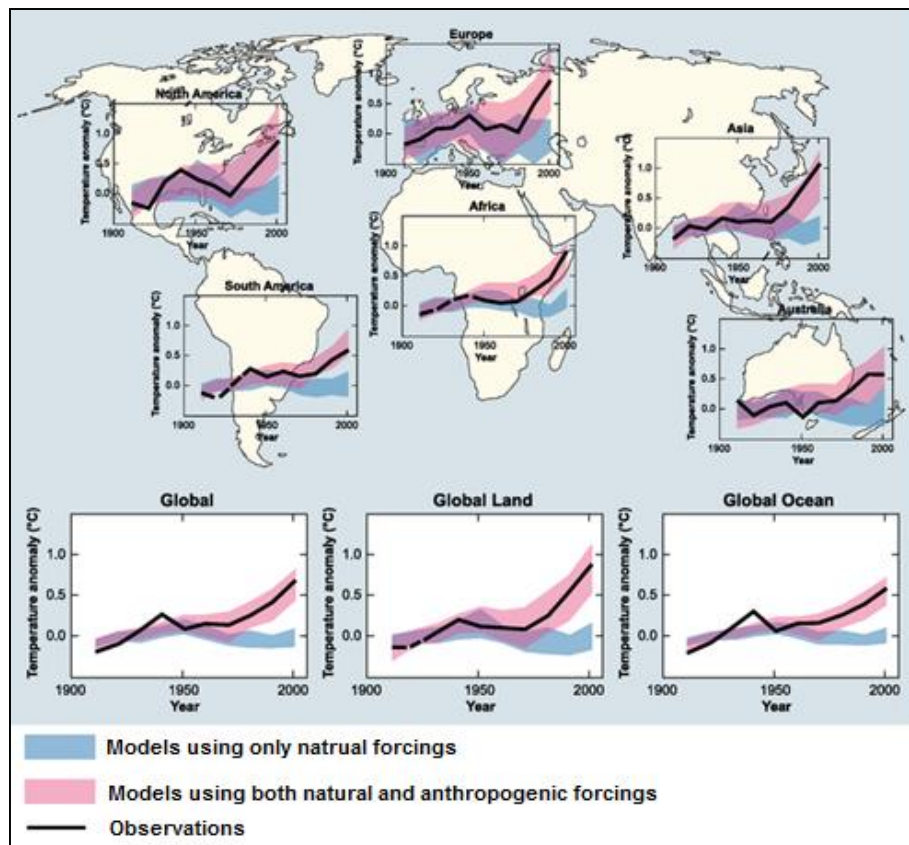


Figure 3: Comparison of observed continental and global scale changes in surface temperature with results simulated by climate models using either natural or both natural and anthropogenic forcings[1].

The scientific message is clear: global warming caused by the accumulation of greenhouse gases generated by human activities is already underway and it will have serious consequences. Therefore, many governments have been developing climate policies to combat global warming. The climate policy in France is based on two pillars: mitigation (reducing emissions of greenhouse gas emissions) and adaptation (policies to anticipate the future damages of climate changes) [3]. As a consequence of these governmental policies,

## GENERAL INTRODUCTION

industrial companies are facing increasingly stringent environmental regulations concerning CO<sub>2</sub> emissions.

There are at least three strategies to reduce CO<sub>2</sub> emissions: the efficient use of energy, the utilization of non-fossil fuels such as hydrogen and renewable energy and the development of technologies for CO<sub>2</sub> capture and storage/utilization [4]. Table 1 summarizes the technologies for controlling the emissions of CO<sub>2</sub> into atmosphere.

Table 1: Technologies for controlling the emissions of CO<sub>2</sub> into atmosphere [5].

Technology	Examples of application	Comments
Efficiency	Production of electric energy	The efficiency of technologies of conversion of chemical-into-electric energy may rise from 32% to over 50%.
Fuel shift	Use of any form of energy	Saving energy through a responsible use.
	Substitution of coal	Emission value expressed as kg CO <sub>2</sub> per kWh electric energy produced: 1 for coal, 0.75 for oil and 0.5 for gas.
Advanced technologies for electric energy production	Integrated gasification combined cycle	Concentration of the production of CO <sub>2</sub> via decarbonization of fossil fuels. CO <sub>2</sub> can either be disposed or used.
Non-carbon-based fuels	Nuclear energy	Use of nuclear fuels for the production of electric energy; used by sectors that require a high intensity.
Perennial energies	Solar, wind, hydro, geothermal	Their exploitation depends on the geographic position of a country.
Renewables	Biomass utilization	Residual and cultivated terrestrial and aquatic biomass can produce liquid or gaseous fuels suitable the transportation sectors.
Carbon dioxide capture and Storage/Utilization (CCSU)	Capture and disposal or utilization of CO <sub>2</sub>	This technology enables the recycle of CO <sub>2</sub> captured from localized sources.

Since the largest source of CO<sub>2</sub> emissions comes from localized sources, Carbon Capture and Storage/Utilization (CCSU) is an important technology solution for controlling CO<sub>2</sub> emissions (Figure 4). CCSU covers the extraction of carbon dioxide of localized sources that strongly emits CO<sub>2</sub> (for example facilities that burn coal, whether they are producing electricity, steam, or supporting industrial processes or production facilities of steel, cement, etc.), its purification and compression, transport (by pipeline or vessel) to storage sites (onshore or

GENERAL INTRODUCTION

offshore) and finally, its injection permanently and safely in suitable geological formations. CO<sub>2</sub> can also be re-utilized [6]. Potential applications of CO<sub>2</sub> are shown in Figure 5.

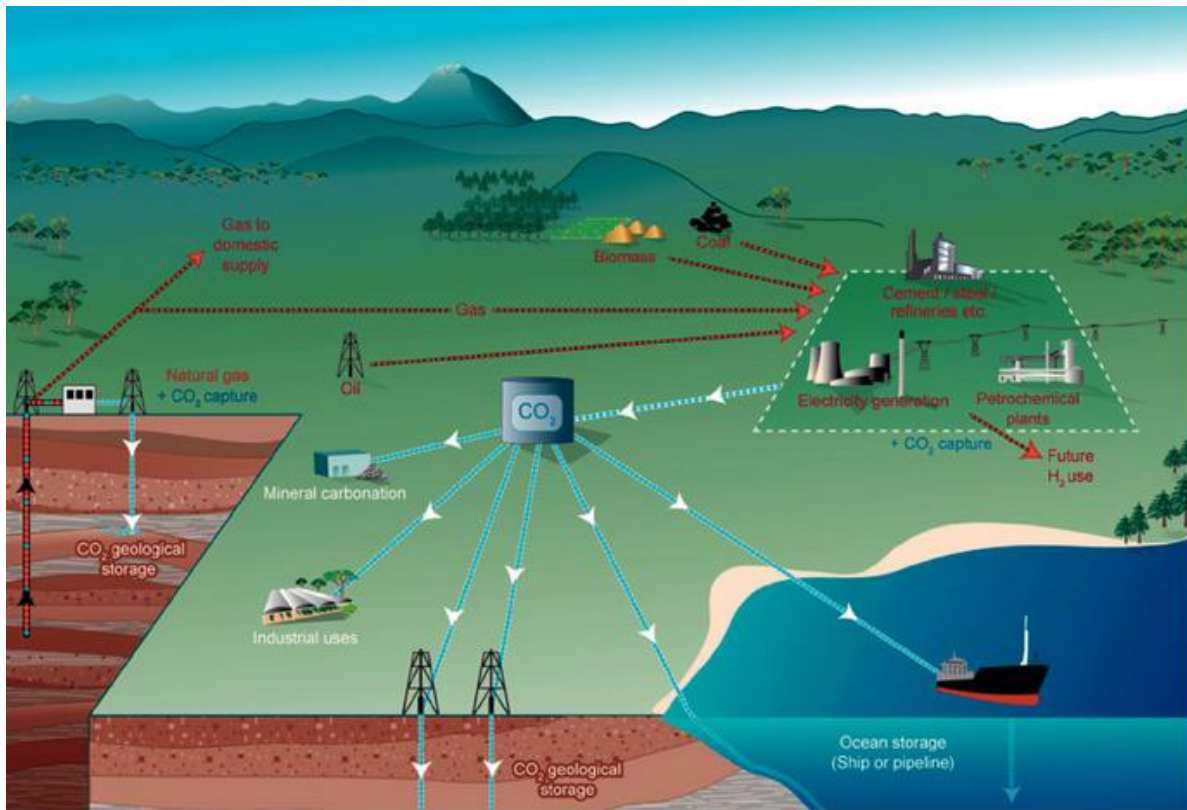


Figure 4: CCS systems showing the carbon sources for which CCS might be relevant, and options for the transport and storage of CO<sub>2</sub>. Source: IPCC, 2005.

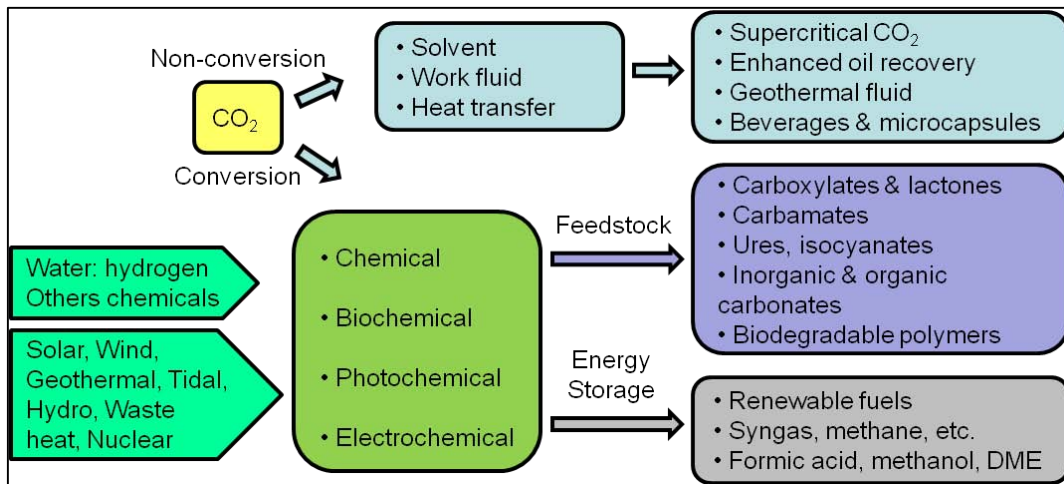


Figure 5: Different pathways for utilizing CO<sub>2</sub>.

CO<sub>2</sub> capture is thus a crucial step in CCSU technology. CO<sub>2</sub> capture can be achieved by various approaches: post-combustion capture, pre-combustion capture, and oxy-combustion [7]. The post-combustion CO<sub>2</sub> capture process is suitable for CO<sub>2</sub> capture from localized sources, which represent the major contribution for global CO<sub>2</sub> emissions (e.g. CO<sub>2</sub> capture from coal-derived power generation) [8-10]. At present, some technologies have been

developed for the post-combustion process: solvent absorption, adsorption using solid sorbent, membrane separation, cryogenic fractionation and ionic liquids [11].

Nowadays, almost all commercial processes for capturing CO<sub>2</sub> from post-combustion streams, use alkaline solutions (e.g. amine gas treating) [12-14]. However, those processes using amines (liquid-phase absorption) are characterized by several disadvantages, such as solvent degradation, corrosion, foaming and high energy consumption. A fraction of amine and its decomposition products are also lost by evaporation, posing several operational problems [15]. CO<sub>2</sub> adsorption on porous materials may be an interesting way to overcome these mentioned disadvantages and it is one of the most promising alternatives to separate and capture CO<sub>2</sub> from major sources, due to its high selectivity and low energy penalties [16]. An American company research using solid sorbents indicates that this process may use as much as 50% less energy than other CO<sub>2</sub> capture technologies [17]. Therefore the scientific community quickly realized the potential benefits of this approach and focused research on finding materials which allow efficient capture of CO<sub>2</sub> [18].

In general, the gas molecules (adsorbate) can bind to material solid surfaces (adsorbent) using two exothermic processes: physisorption interaction (which the molecules attach to the solid surface by van der Waals interactions) or by chemisorption interactions (chemical bonds are formed between the material and the adsorbed molecules).

The energy released when the gas-substrate interaction is dissipated in the solid (lattice vibrations) results in an amount of released heat, defined as “heat of adsorption”. The understanding of those adsorbate-adsorbent interactions is essential when we are looking for efficient CO<sub>2</sub> capture.

In order to study these interactions, Solvay-Laboratory of the Future (LOF), the TREFLE department of the Institute of Mechanical Engineering at Bordeaux (I2M) and the Group of Molecular Spectroscopy (GSM) at the Institute of Molecular Sciences (ISM), have aggregated their expertise to investigate in detail the mechanisms of CO<sub>2</sub> adsorption on various solid adsorbents. Solvay-LOF develops high-throughput tools to quickly test and select potentially interesting families of materials. Depending on the nature of interactions, CO<sub>2</sub> molecules are transformed in different adsorbed species on the surface of the adsorbent. Those species are identified thanks to the spectroscopic techniques available at GSM. Finally, the adsorption heat released during the capture process is studied at TREFLE.

In this collaborative Ph.D. project, the objective was the study of CO<sub>2</sub> adsorption on several types of materials combining and correlating information from *in-situ* infrared thermography and infrared spectroscopy experiments. The first approach allowed us non-contact thermal measurements, in order to study heat transfer and estimate the adsorption heat released during CO<sub>2</sub> adsorption, thanks to a thermal model development. The second approach allowed us the identification of adsorbed species, the study of adsorption kinetics and of the thermal stability of adsorbed species during material regeneration. Finally, by combining thermographic and spectroscopic information, key parameters for CO<sub>2</sub> capture have been investigated.

The studied adsorbents were varied: (1) different types of activated carbons, which were compared in order to investigate their CO<sub>2</sub> adsorption kinetics, selectivity and adsorption heats; (2) basic rare earth oxides where the power of carbonation is assessed through the identification of several species formed on the material surface and (3) hybrid organic/inorganic materials (functionalization of micro porous silica with amine groups), where a screening of several organic molecules has been carried out to understand their reactivity and improve their thermal stability on the inorganic surfaces.

## *GENERAL INTRODUCTION*

Lastly, this Ph.D. work allowed us to better understand the mechanisms controlling the CO<sub>2</sub>-adsorbent interactions. It contributes to a wide project that aims at proposing an effective implementation of an innovative post-combustion CO<sub>2</sub> capture process, and, in the near future, to respond the Solvay objective of 20 percent reduction in its energy consumption and CO<sub>2</sub> emissions by 2020 [19].

This manuscript aims at synthesizing and discussing the results of our investigations. The two first chapters are dedicated to the background and to state-of-the-art of CO<sub>2</sub> capture by solid adsorbents. The first one reviews the principles of adsorption process as well as the most investigated materials for CO<sub>2</sub> capture at low temperature, and presents the materials studied in this work. The second one reviews the classical approaches used to characterize CO<sub>2</sub>-adsorbent interactions. Then, taking into account their main advantages and drawbacks, our methodology is introduced.

As it will be described later on, our strategy is based on four high-throughput steps. Consequently, each following chapter corresponds to one of these steps.

In the third chapter, thanks to infrared thermography and gravimetric technique, a qualitative investigation of the adsorptive behaviors (thermal and kinetics) and an evaluation of the adsorption capacities of our materials are performed.

In the fourth chapter, an in-depth investigation of the thermal behavior during the CO<sub>2</sub> adsorption process is achieved via an analytical thermal model. Then, we present the inverse method used to estimate CO<sub>2</sub> adsorption heats and the key parameters for overall comparison of adsorbent performances.

In the fifth chapter, thanks to Diffuse Reflectance Infrared Fourier Transform (DRIFT) spectroscopy, the CO<sub>2</sub>-adsorbent interactions are analyzed from a chemical point of view.

Finally, the last chapter is dedicated to the first results obtained with a millifluidic adsorption column in which the temperature field is detected by IR thermography during CO<sub>2</sub> capture process.

The final comparison of tested materials is presented in the conclusion, together with the outlook of this work.

## **CHAPTER I**

# **Adsorption Principles and Materials for Carbon Dioxide Capture**



## SUMMARY

1	Introduction .....	27
2	Principles of Adsorption.....	27
3	CO <sub>2</sub> molecule description.....	27
4	CO <sub>2</sub> adsorption systems .....	29
5	Solid adsorbents for CO <sub>2</sub> capture .....	30
5.1	Physisorption adsorbents .....	31
5.1.1	Zeolites .....	31
5.1.2	Activated carbons .....	32
5.1.3	Metal Organic Frameworks.....	33
5.2	Chemisorption adsorbents .....	34
5.2.1	Hybrid organic/inorganic adsorbents .....	34
5.2.2	Metal based adsorbents .....	37
6	Studied materials .....	38
6.1	Basic rare Earth oxides .....	38
6.2	Activated carbons .....	41
6.3	Hybrid organic/inorganic materials .....	42
7	Conclusions .....	45



## 1 Introduction

This chapter presents the principles of adsorption processes and the state of the art of investigated materials for low temperature CO<sub>2</sub> capture, describing as well the studied materials during this work. We start with a brief description of adsorption processes, of CO<sub>2</sub> molecule and of CO<sub>2</sub> capture systems by solid adsorbents. Then, the current status of low temperature adsorbents used for reversible CO<sub>2</sub> capture is presented. Finally, our studied adsorbents are described.

## 2 Principles of Adsorption

We can define adsorption as the adhesion or retention of a thin layer of molecules of a gas or liquid mixture, called adsorbate, brought into contact with a solid surface, called adsorbent, resulting from the force field at the surface (see Figure 1) [20].

There are two types of adsorption process: physisorption and chemisorption. The main difference is the nature and strength of the surface forces. In a physisorption process, the molecules-solid surface interactions are essentially made via Van der Waals and electrostatic forces. This type of adsorption does not significantly modify the molecular structure of the adsorbent and is a reversible process. It means that one may easily desorb the adsorbed molecules from the material surface by reducing the pressure or by rising the temperature [21]. Otherwise, for chemisorption process, there is formation of chemical bonds between adsorbate and adsorbent, resulting in stronger molecules-surface interactions and considerably higher binding energies. For this reason, chemisorption process is hardly reversible. It is then unsuitable for most capture process applications, and most adsorption processes depend on physical adsorption. It is important to note that, generally, all adsorbents involving physisorption process show good cyclability, regarding the material regeneration.

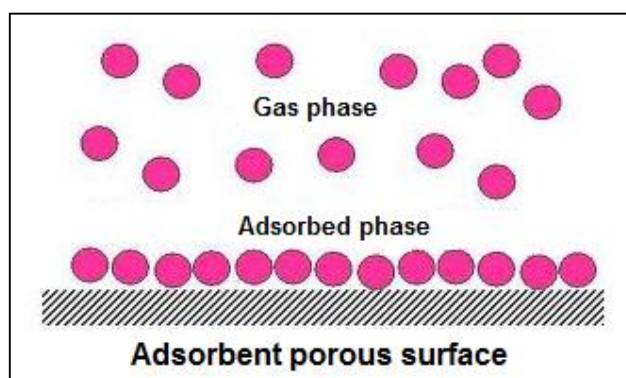


Figure 1: Scheme of adsorption of molecules on a solid surface.

## 3 CO<sub>2</sub> molecule description

Joseph Black, a Scottish chemist and physician, first identified carbon dioxide in the 1750s. At room temperature, carbon dioxide is an odorless, colorless gas, which is faintly acidic and non-flammable. Although carbon dioxide mainly exists in the gaseous form, depending on pressure and temperature, it also has a solid, a liquid and a supercritical phase. (Figure 2a)

Carbon dioxide is an extremely stable oxide composed of two oxygen atoms covalently bonded to a single carbon atom. The two C-O bonds are equivalent and short (Figure 2b), consistent with double bonding [22]. The carbon dioxide molecule is linear and centrosymmetric, then the molecule has no static electrical dipole.

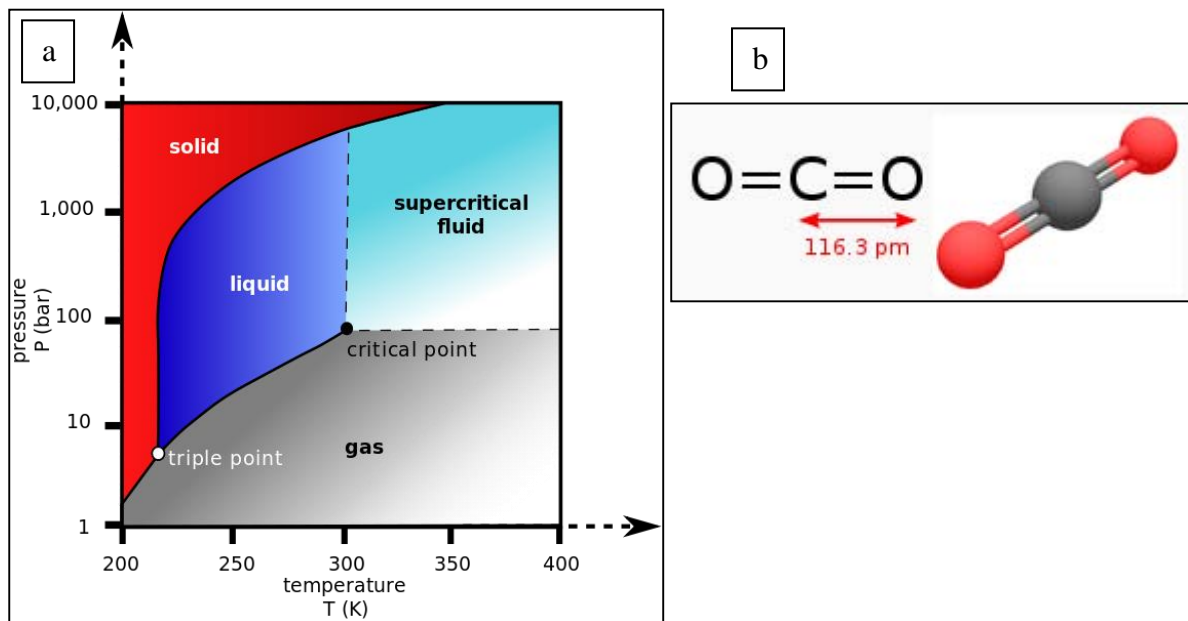


Figure 2: (a) Carbon dioxide pressure-temperature phase diagram. (b) Carbon dioxide molecule.

All matters have the aptitude to interact with surrounding radiation, by absorbing, reflecting or transmitting it. The means by which the radiation energy can be transferred to the molecule when the molecule absorbs radiation energy, involve the dipole moment of the molecule. The selection rule for IR absorption requires that, in order to be IR-active, a molecular vibration must cause a change in dipole moment. Carbon dioxide molecule has four normal vibration modes. Two modes are degenerate in the gaseous state and thus three are distinct (Figure 3). Among these three distinct normal modes, only two are IR-active, because of the selection rule.

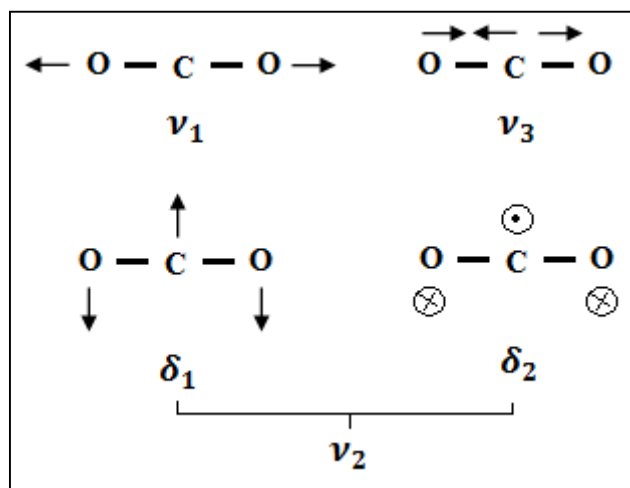


Figure 3: Normal vibration modes of CO<sub>2</sub> molecule.

The bending vibrations  $\delta_1$  and  $\delta_2$  are degenerate:  $\nu_2 = 667 \text{ cm}^{-1}$ . The symmetric stretching mode  $\nu_1$  does not cause a change in dipole moment, thus it is not IR-active. Only  $\nu_2(\delta_1 / \delta_2)$  and  $\nu_3 = 2349 \text{ cm}^{-1}$  are IR-active. Depending on the molecule-surface interaction, the IR spectra exhibit spectral modifications corresponding to the signatures of these interactions.

The adsorption of CO<sub>2</sub> on surfaces is important in a variety of industrial and environmental applications such as methanol synthesis, exhaust cleaning, CO<sub>2</sub> capturing, fuel cell poisoning, fuel synthesis, etc [23].

CO<sub>2</sub> molecule has a weak Lewis acid site over the carbon atom, a weak Lewis base site over the two oxygen atoms and two  $\pi$  bonds which may be involved in adsorption processes on surfaces. Depending on the solid substrate, CO<sub>2</sub> molecules may interact by physisorption or chemisorption. In a physisorption process, CO<sub>2</sub> molecule interacts weakly with the substrate (Van der Waals and electrostatic forces) and remains almost linear (175-180 °).

In the case of a chemisorption, electron transfer from an occupied orbital (type  $1\pi_g$ ) to an empty orbital (type  $2\pi^*_u$ ) of CO<sub>2</sub> causes bending of the molecule, with an angle OCO ranging from 120° for a total electron transfer (carboxylate CO<sub>2</sub><sup>-</sup>) to 175°, depending on the Lewis acid-base interactions (electron transfer) with the substrate. Figure 4 shows a scheme of CO<sub>2</sub>-substrate interactions.

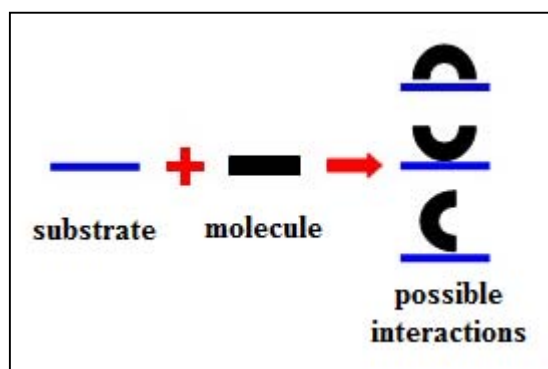


Figure 4: Scheme of CO<sub>2</sub>-material interactions during an adsorption process.

When CO<sub>2</sub> is adsorbed, the interaction with a substrate modifies CO<sub>2</sub> geometry, thus its degrees of freedom of vibration and consequently the frequency of characteristic modes of vibration. These interactions lead to the formation of several adsorbed species such as carboxylates, carbonates, hydrogenocarbonates and carbamates. A review of CO<sub>2</sub>-adsorbent interactions will be presented in detail in the sections *Solid adsorbents for CO<sub>2</sub> capture* and *Studied materials*.

## 4 CO<sub>2</sub> adsorption systems

Adsorption systems operate in a three step cycle (see Figure 5): CO<sub>2</sub> adsorption step, purge (remove impure gases) and evacuate (remove/desorb CO<sub>2</sub>) [3]. The adsorption systems differ in the way that the adsorbent is regenerated. We can list at least 4 systems:

- 1 **TSA:** Thermal Swing Adsorption: the desorption is triggered by an increase in temperature. This is energy intensive and slow since the entire mass of adsorbent must be heated.
- 2 **VSA:** Vacuum Swing Adsorption: the desorption of CO<sub>2</sub> is triggered by creating a near-vacuum. One advantage is that this system will operate at near ambient temperature, so requires less energy. Another advantage is that the energy used is applied only to the CO<sub>2</sub> and so it is thermodynamically more efficient than TSA.
- 3 **PSA:** Pressure Swing Adsorption: the desorption is triggered by a decrease in pressure, usually from an elevated level to near atmospheric pressure.

- 4 **ESA:** Electrical Swing Adsorption: the desorption is triggered by an applied voltage. This method has the advantage of being fast and requiring low energy.

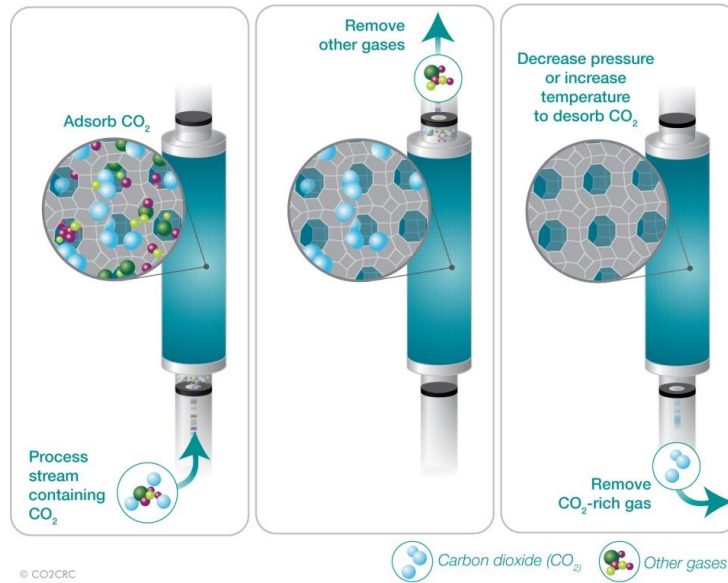


Figure 5: Scheme of an adsorption system for CO<sub>2</sub> capture [3].

Different CO<sub>2</sub> separation process configurations are possible depending on the temperature and pressure of the effluent gas stream (Table 1). Depending on CO<sub>2</sub> capture process, different adsorbents may be better suited for one application or other, given the operational temperatures, pressures, mole fraction of CO<sub>2</sub> in the feed, presence of impurities and other factors.

Table 1: CO<sub>2</sub> capture process regarding operational conditions.

Postcombustion Capture (ambient pressure flue gas)
CO <sub>2</sub> separation from: N <sub>2</sub> , H <sub>2</sub> O (trace O <sub>2</sub> , NO <sub>x</sub> , SO <sub>x</sub> )
<ul style="list-style-type: none"> <li>• Vacuum Swing Adsorption at Ambient Temperature (~30°C)</li> <li>• Vacuum Swing Adsorption at Elevated Temperature (~110°C)</li> <li>• Thermal Swing Adsorption at Ambient Pressure (1atm)</li> </ul>
Precombustion Capture (high pressure synthesis gas)
CO <sub>2</sub> separation from: H <sub>2</sub> , H <sub>2</sub> O, CO, (trace O <sub>2</sub> , S-gases)
<ul style="list-style-type: none"> <li>• Pressure Swing Adsorption at Ambient Temperature (~30°C)</li> <li>• Pressure Swing Adsorption at Elevated Temperature (~110°C)</li> </ul>

## 5 Solid adsorbents for CO<sub>2</sub> capture

Typically the temperatures associated with power plant flue gas (main emission source of anthropogenic CO<sub>2</sub>) range from 50 to 120 °C [24]. For this reason, tremendous efforts have been devoted to develop materials well adapted for reversible CO<sub>2</sub> capture in this range of temperature. The adsorbents are porous materials that have good affinity with CO<sub>2</sub> molecules. The adsorbents have distinct behaviors with regard to several important parameters such as

CO<sub>2</sub> capacity, adsorption/desorption kinetics, operating conditions (e.g. adsorption/desorption temperatures), regenerability, multicycle stability and selectivity [18]. They are classified into two broad categories: materials for physisorption of CO<sub>2</sub> and those for chemisorption.

## 5.1 Physisorption adsorbents

In the category of physisorption materials, we find zeolites, MOFs (Metal Organic Frameworks) and activated carbons [25].

### 5.1.1 Zeolites

Zeolites are porous crystalline inorganic materials with complex structure. They are based on a series of assembled three-dimensional tetrahedra structures of SiO<sub>4</sub> and AlO<sub>4</sub>, joined together in various regular arrangements through shared oxygen atoms. The negative charge created by the substitution of an AlO<sub>4</sub> tetrahedron for a SiO<sub>4</sub> tetrahedron is balanced by exchangeable cations (e.g., Na<sup>+</sup>, K<sup>+</sup>, Ca<sup>2+</sup>, Mg<sup>2+</sup>) located in the channels and cavities throughout the structure.

The CO<sub>2</sub> adsorption mechanism on zeolites has been investigated by various groups and it has been revealed that the physisorption of CO<sub>2</sub> occurs with CO<sub>2</sub> in a linear orientation by an ion-dipole interaction [26]. In addition to physical adsorption, more strongly bound carbonate species are also observed.

The adsorption capacity is relatively high, up to 230 mg of CO<sub>2</sub> per gram of adsorbent (mg<sub>CO<sub>2</sub></sub>/g<sub>ads</sub>). This can be achieved after optimization of the ratio Al/Si and/or the type of cations counterbalancing the negative charges. In the case of faujasite type zeolites (see Figure 6), Harlick *et al.* showed that decreasing the Si/Al ratio, the CO<sub>2</sub> adsorption capacity is increased [27].

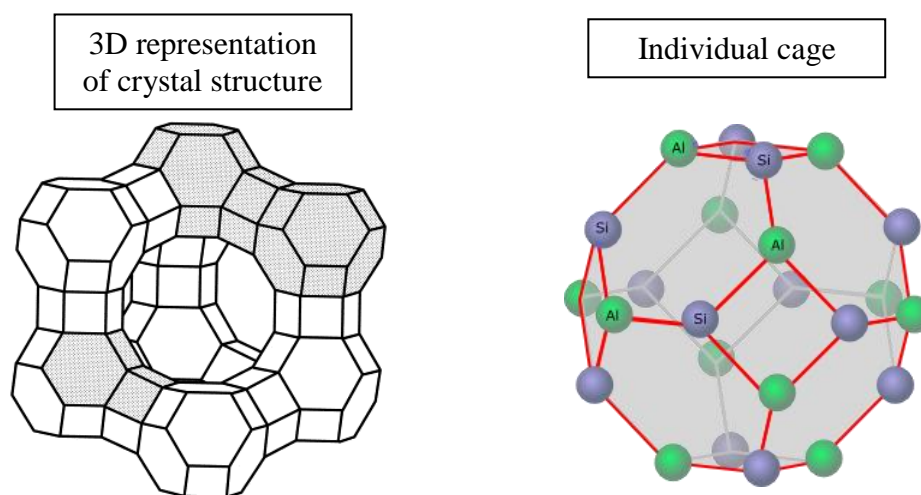


Figure 6: Faujasite structure. The primary building units are corner sharing SiO<sub>4</sub> tetrahedra. Si atoms occupy the vertices while the O atoms are in the middle of the edges. Secondary building units are the sodalite units (truncated cubooctahedra) and the double six-membered rings which connect the sodalite units to a tetrahedral lattice [28].

With regard to Y-type zeolites, Walton *et al.* [29] have clearly demonstrated the importance of the nature and size of cations and then a classification was possible: CsY (114 mg<sub>CO<sub>2</sub></sub>/g<sub>ads</sub>) < RbY < KY < NaY < LiY (228 mg<sub>CO<sub>2</sub></sub>/g<sub>ads</sub>).

The CO<sub>2</sub> adsorption properties of zeolites are also influenced by the porous characteristics of the framework. Siriwardane *et al.* reported that the highest adsorption capacities were

observed in zeolite 13X, the material with the largest pore diameter and volume among those studied [30].

The CO<sub>2</sub> adsorption kinetics is very fast, reaching its equilibrium capacity within a few minutes in most cases. The adsorption is much faster in the initial stage of the process, enabling this material to fill most of the total capacity within several tens of seconds. The CO<sub>2</sub> adsorption rate is affected by diffusion in the micropores of the zeolite crystals and also in the macropores formed during the consolidation of crystals with binders [31].

Although zeolites have shown promising results for separating CO<sub>2</sub> from gas mixtures, their selectivity to CO<sub>2</sub> over other gases (N<sub>2</sub>, CH<sub>4</sub>, H<sub>2</sub>O, etc.) is still low, and their adsorption capacities rapidly decline with increasing temperature [32].

A negative effect on CO<sub>2</sub> capture is observed when water is present in the gas stream, due to the competition between the adsorption of water molecules and CO<sub>2</sub>. One can explain this by the fact that the highly polar water molecule will preferentially adsorb on the cations and thus reduce the electric field in the zeolite structure (neutralization), making the CO<sub>2</sub> adsorption capacity less effective.

### 5.1.2 Activated carbons

Activated carbons are widely used as solid adsorbents, are also an interesting family of materials because of the low cost of raw materials (Figure 7). They are generally obtained after carbonization of carbonaceous materials (bituminous coal, by-products of a process, bio resources, etc ...), followed by chemical activation (KOH, H<sub>3</sub>PO<sub>4</sub>, etc ...) or physical activation (air, water, etc...).

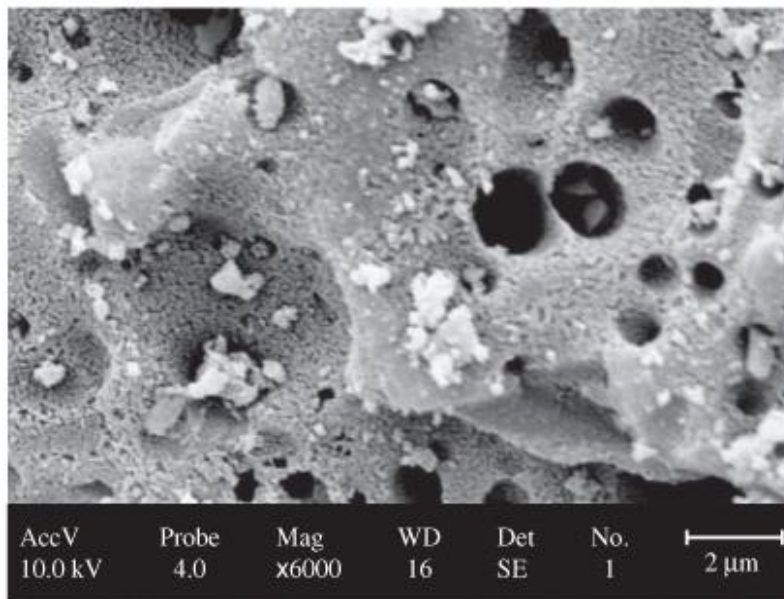


Figure 7: The scanning electron microscope (SEM) micrograph of babassu (brazilian palm) coconut shell activated carbon [33].

Depending on the type of raw material and mode of activation, the porosity, the specific surface and the hydrophilic/hydrophobic characteristics of the obtained active carbon can be highly variable. The specific surface can range from 400 to 2500 (m<sup>2</sup>/g). Micropore structure (d < 2 nm) can be achieved for active carbon synthesized from coconut shells, and macroporous structures (d > 50 nm) for active carbon synthesized from different woods [34]. The CO<sub>2</sub> adsorption capacities on activated carbons are lower than those of zeolites or

molecular sieves under low pressure, ambient conditions. The maximum adsorption capacities of CO<sub>2</sub> on this type of material are generally obtained at high gas pressure equilibrium. For example, Dreisbach *et al.* reported the high-pressure adsorption of CO<sub>2</sub> on Norit R1 of 528 mg<sub>CO2</sub>/g<sub>ads</sub> at a pressure of 56 bars [35].

Activated carbons, despite their general hydrophobic characteristics, are strongly influenced by the presence of water in the gas stream. The dissolved oxygen from adsorbed water attacks the material surface, resulting in gradually surface oxidation. As a consequence, CO<sub>2</sub> adsorption capacities of activated carbons are reduced by the presence of water.

Because of the weak interaction adsorbate-adsorbent, the CO<sub>2</sub> adsorption capacity drops dramatically at increasing temperatures (>30°C) and the selectivity over other gases is relatively poor [24]. The current research efforts are focused on how to enhance the adsorbate-adsorbent interaction and the selectivity for CO<sub>2</sub> by forming different structures such as single-walled carbon nanotubes (CNTs), multi-walled CNTs, ordered mesoporous carbon, microporous carbon. Another efficient approach is to increase the alkalinity by surface modification (e.g. impregnation of basic nitrogen groups).

However, the weak interaction adsorbate-adsorbent leads to less energy requirement regarding material regeneration. Activated carbons have excellent reversibility of adsorption capacities. It has been attributed to the moderate adsorption strength or surface affinity of these materials for CO<sub>2</sub>. Despite lower adsorption capacities compared to zeolites at ambient conditions, activated carbons are often a competitive adsorbent especially for the applications in which the energy requirement for adsorbent regeneration is a critical factor.

The adsorption kinetics of CO<sub>2</sub> on activated carbons are comparable to those on zeolites, which can approach their equilibrium capacity on the time scale of minutes under many conditions. The CO<sub>2</sub> adsorption kinetics of activated carbons have been explained in terms of the diffusional mass transport through these pores between which the adsorbate molecules can be exchanged.

### 5.1.3 Metal Organic Frameworks

Metal-organic frameworks (MOFs) have recently been investigated for use as CO<sub>2</sub> adsorbents. MOFs are constructed from transition metal ions and bridging organic ligands (Figure 8). Defined as tridimensional organic-inorganic hybrid networks, MOFs are a new family of porous materials [36].

One of the most important properties of metal-organic frameworks (MOFs) is their high porosity and high specific surface area, which has led to many applications concerned with gas storage, separations, and catalysis. These properties, more adjustable chemical functionality, ordered and well characterized porous structure, enable high CO<sub>2</sub> capture [37]. Furukawa *et al.* reported Brunauer-Emmett-Teller and Langmuir surface areas of 6240 and 10400 m<sup>2</sup>.g<sup>-1</sup>, respectively, and a total carbon dioxide storage capacity of 2870 mg.g<sup>-1</sup> for MOF-210 [38].

Normally the interaction between adsorbed CO<sub>2</sub> and adsorbents is weak, and the species starts to desorb when the temperature is higher than 30°C. To date, although MOFs have shown exceptionally high CO<sub>2</sub> storage capacity under equilibrium conditions with pure CO<sub>2</sub>, most of them show little uptake in the low pressure regime of 0.1–0.2 bar, which is the pressure range used for CO<sub>2</sub> capture from flue gas streams [39]. Another disadvantage, CO<sub>2</sub> capture selectivity is weak. Many studies have been performed on these materials in order to overcome these problems. These researches are focused on the modification of metal ions, organic linkers, or novel combinations of both [40, 41].

MOFs exhibit potentially superior CO<sub>2</sub> capacities at moderate to high pressures and for this reason should be considered for high pressure gas separation processes and CO<sub>2</sub> storage media.

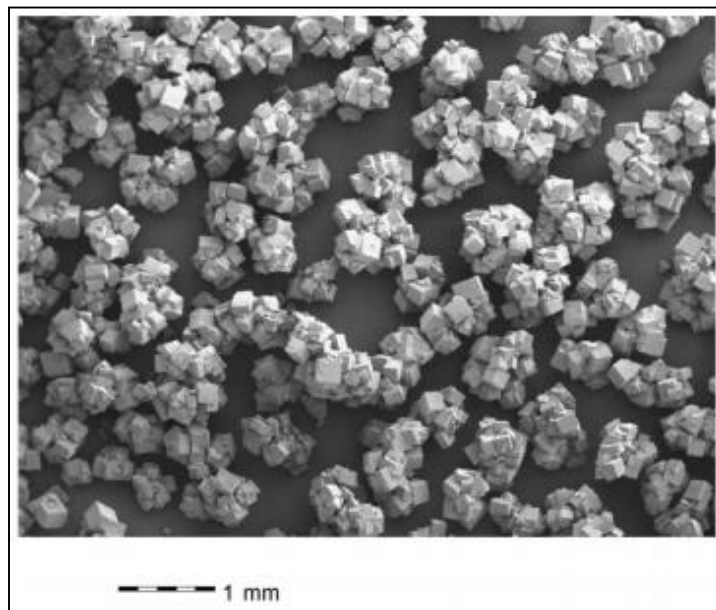


Figure 8: SEM-picture of large MOF crystals (scale bar: 1 mm) [42].

## 5.2 Chemisorption adsorbents

In the category of materials for which CO<sub>2</sub> capture is based on chemisorption process, one finds the hybrid organic-inorganic materials and metal based adsorbents.

### 5.2.1 Hybrid organic/inorganic adsorbents

They are also promising materials for CO<sub>2</sub> capture. They are usually made of basic groups of organic molecules, generally amine groups, supported on inorganic porous materials which develop high specific surface (e.g. porous silica, zeolites, activated carbon, MOFs, etc. ...) and having a high porosity in order to support a maximum loading of these organic molecules [43, 44]. The adsorptive properties of organic and organic/inorganic hybrid adsorbents depend on both the composition and geometry of the chemisorptive moieties and their solid supports.

The interaction of CO<sub>2</sub> with amines can be controlled by different mechanisms [45]. Primary and secondary amines can react directly with CO<sub>2</sub> to produce carbamates through the formation of zwitterionic intermediates, as represented in Figure 9. The first step proceeds with the lone pair on the amine attacking the carbon from CO<sub>2</sub> to form the zwitterion. Free base (another amine, H<sub>2</sub>O, or OH<sup>-</sup>) then deprotonates the zwitterion to form the carbamate. Thus basic amines react with acidic CO<sub>2</sub> under dry conditions (where H<sub>2</sub>O and OH<sup>-</sup> are absent) to form carbamates with a stoichiometric ratio of 1 CO<sub>2</sub> molecule for 2 amine molecules. Under humid conditions, where H<sub>2</sub>O can act as a base, the reaction occurs with a stoichiometric ratio of 1 CO<sub>2</sub> molecule for 1 amine molecule. Therefore, in theory, the presence of water should improve the CO<sub>2</sub> capture.

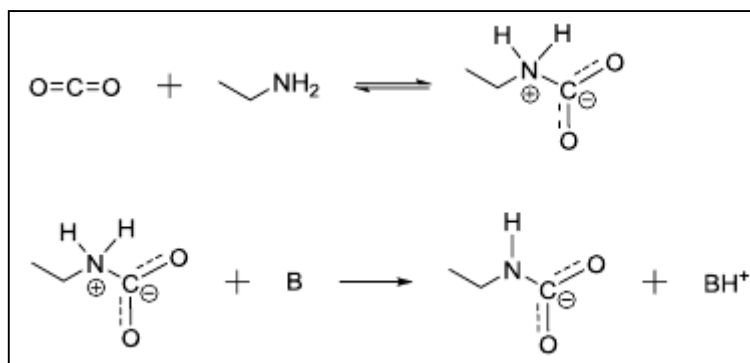


Figure 9: Carbamate formation by reaction of CO<sub>2</sub> with primary or secondary amines.

Tertiary amines react with CO<sub>2</sub> through a different mechanism. Tertiary amines catalyze the formation of hydrogencarbonate at first instead of reacting directly with CO<sub>2</sub> molecules. In the first step, the tertiary amine dissociates H<sub>2</sub>O to form a quaternary cationic species and hydroxide ion. OH<sup>-</sup> then attacks CO<sub>2</sub> to form the hydrogencarbonate anion. The last step is then the ionic association of the protonated amine and hydrogencarbonate. Primary and secondary amines can also react with H<sub>2</sub>O and CO<sub>2</sub> in this manner (see Figure 10).

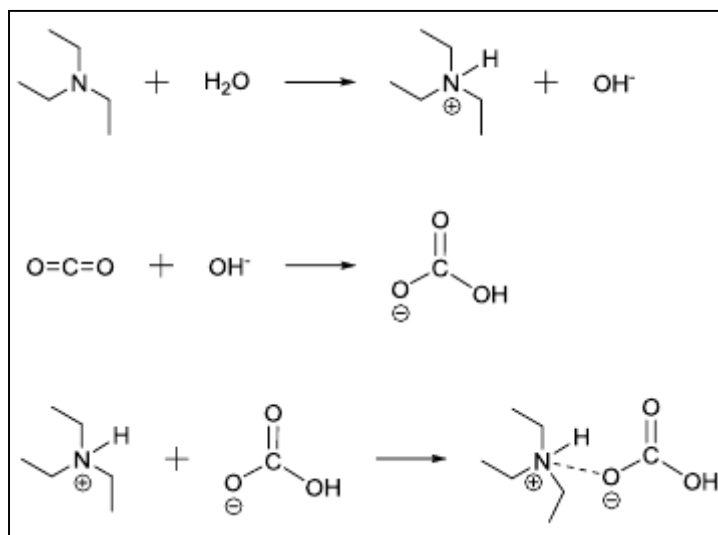


Figure 10: Mechanism for the reaction of CO<sub>2</sub> with tertiary amines.

The immobilization of amines onto a solid support (e.g., porous silica) could have several advantages, such as regeneration costs. In most cases, solid supports have lower heat capacity than H<sub>2</sub>O in the aqueous amine solutions used for CO<sub>2</sub> capture by absorption (0.8 kJ.kg<sup>-1</sup>K<sup>-1</sup> in the case of mesoporous silica SBA-15 vs. 4.2 kJ.kg<sup>-1</sup>K<sup>-1</sup> for H<sub>2</sub>O [46]). The energy costs to heat H<sub>2</sub>O in such systems is thus much higher than that to heat solid supports during regeneration.

Many authors have monitored the CO<sub>2</sub>-amine supported silica interactions by FTIR [47-49]. Under dry conditions, only the formation of carbamate has been considered possible. Under humid conditions, four additional species have been observed: monodentate carbonate, bidentate carbonate, monodentate hydrogencarbonate, and bidentate hydrogencarbonate.

Chuang *et al.* [50] assign the carbamic acid species to bands at 1595, 1441, and 1330 cm<sup>-1</sup>, while Yogo *et al.* [51] assign the bands at 1628, 1563, and 1488 cm<sup>-1</sup>. Chuang *et al.* [46, 50, 52] reported the formation of monodentate carbonate (1337–1363 cm<sup>-1</sup>), bidentate carbonate (1541–1575 cm<sup>-1</sup> and 1390 cm<sup>-1</sup>), monodentate hydrogencarbonate carbonate (1628–1634

$\text{cm}^{-1}$ ). These carbonate species were assigned during humid  $\text{CO}_2$  capture. It has been theorized that humid adsorption first occurs by the formation of carbamate species followed by conversion to carbonates species.

There are at least three groups of supported amine on solid supports. (1) Amine physically adsorbed on oxide supports (2) Amine covalently tethered to oxide supports (3) Amine supported on solid organic materials. Scanning electron microscopy images of supported amine samples are shown in Figure 11 [53].

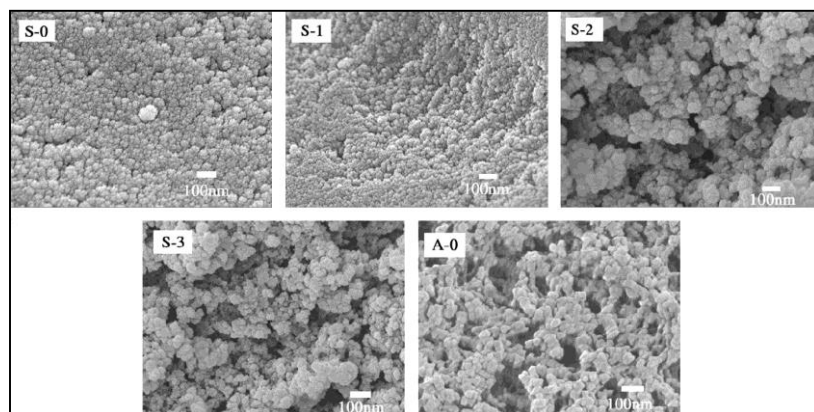


Figure 11: SEM photograph of samples: activated silica gel (S-0), silica gel grafted with (3-Aminopropyl) trimethoxysilane (S-1), silica gel grafted with acrylamide (AAM) polymer (S-2), silica gel impregnated with AAM polymer (S-3), and AAM polymer (A-0).

Physically adsorbed amine groups (described sometimes as wet impregnation method), is the simplest method of supporting amines on oxide or any other supports. This method involves suspending a support such as porous silica in a solution of the amine and a volatile solvent. Amine diffuses into the silica pore space by concentration driving force and in some cases by chemical affinity, after which the solvent is removed by evaporation. The main drawback of these materials is their low thermal stability concerning the supported amines groups. During cycles of adsorption/desorption, the exothermic process resulting from the adsorption of  $\text{CO}_2$  may cause partial desorption of organic molecules and thus reduce the capture efficiency of the adsorbent.

Many amine types have been investigated for impregnation in silica supports. The main selection parameters are the basicity and the weight percentage of nitrogen in the amine group. Strong base amines have high affinity to acid  $\text{CO}_2$  molecules and have strong stability on silica surface. However, regeneration kinetics (i.e. rate and temperature) have shown improved performance with weaker base amines than stronger ones, suggesting a weaker amine may reduce operating costs with lower regeneration temperatures [54]. Selection of amine groups with a high weight percentage of nitrogen leads to high capture capacity per total weight of adsorbent, but may negatively impact other important parameters such as adsorption and desorption kinetics or heats of adsorption.

Considerations during support selection must be done regarding their surface acidity, surface area, thermal stability, thermal conductivity and mechanical durability and cost. An acidic surface is desired to interact with the basic amine group; however, a strong acidic surface may react with the amine, reducing the capture capacity. High surface area is desired to increase the number of adsorption sites; however, high surface area is often achieved by creating small pores which may present a mass transport limitation. If  $\text{CO}_2$  cannot adsorb into the pores with the amine, the active area is reduced and the advantage of the high surface area is not realized. To perform carbon capture quickly and efficiently, the pore size should be large enough to

allow CO<sub>2</sub> to quickly adsorb onto and off the amine [55]. Mass-transfer of the CO<sub>2</sub> into the sorbent material has found to be a function of the surface amine density and pore size. With a pore size smaller than 35 Å, the amine adsorption site inside the pores become inaccessible for CO<sub>2</sub> due to mass-transfer limitations [56].

Silica support has been widely investigated by many authors [57-59]. It is assumed that the amine impregnation on silica surfaces is achieved by amine interactions with hydroxyls on the silica surface (silanols groups). The high surface areas of mesoporous silicas (500 to 1500 m<sup>2</sup>.g<sup>-1</sup>) provide an open, accessible backbone for the stabilization of a large number of active adsorption sites.

Amine-impregnated silicas have relatively high CO<sub>2</sub> capacities, reaching values close to 180 mg of CO<sub>2</sub> per grams of adsorbent. Because of physical interactions with support, their operating conditions are limited to low temperatures regimes. The adsorption capacities of supported amine adsorbents are not negatively affected and in many cases are actually aided by the presence of moisture, unlike inorganic physisorbents. Amine-impregnated silicas are very promising candidates for postcombustion CO<sub>2</sub> capture because of their effectiveness at low CO<sub>2</sub> partial pressures [60].

### 5.2.2 Metal based adsorbents

This group of materials includes alkaline metal oxides (Na<sub>2</sub>O, K<sub>2</sub>O) and alkaline earth metal oxides (CaO, MgO), on which the CO<sub>2</sub> molecules can adsorb forming mono or multidentate species. The acid nature of CO<sub>2</sub> facilitates adsorption on these oxides. For CO<sub>2</sub> capture applications involving high temperatures (from 200 to 700 °C), alkaline earth metal oxides have high adsorption capacities (around 528 mg CO<sub>2</sub> per g ads. for calcium oxide at 650°C, Figure 12 [61]). On the other side, these adsorbents have relatively slow adsorption kinetics and the strong bonds formed with CO<sub>2</sub> during adsorption produce large heats of adsorption and thereby require relatively high temperatures for regeneration. The high operating temperature may result in adsorbent degradation (pore blocking and sintering mechanisms)[18].

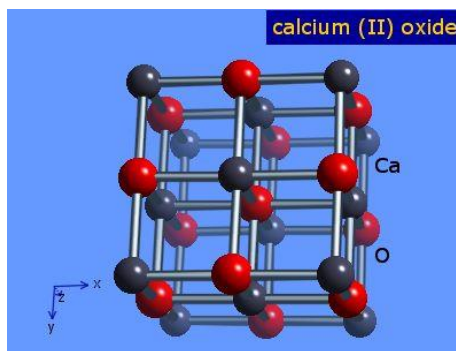
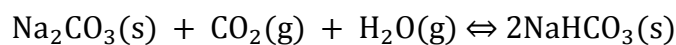


Figure 12: Representation of Calcium oxide structure (oxygen atoms: red, calcium atoms: black).

Researches appoint that alkali metal carbonates are suitable for the treatment of flue gases at temperatures below 200°C [62]. Liang *et al.* [63] studied the mechanism of the capture of CO<sub>2</sub> using Na<sub>2</sub>CO<sub>3</sub> by the following reaction:



This reaction is reversible and highly exothermic and the theoretical CO<sub>2</sub> capture capacity of Na<sub>2</sub>CO<sub>3</sub> is 377 mg<sub>CO2</sub>/g<sub>ads</sub>. K<sub>2</sub>CO<sub>3</sub>-based adsorbents have also been investigated and showed similar results [64]. However, a common problem is that the overall carbonation reaction rate for Na<sub>2</sub>CO<sub>3</sub>/K<sub>2</sub>CO<sub>3</sub> is rather slow.

## 6 Studied materials

In the following topics, a description of the materials studied during this work is presented. As commented in the *general introduction*, the studied materials for CO<sub>2</sub> capture are basic rare earth oxides, activated carbons, and hybrid organic/inorganic materials.

### 6.1 Basic rare Earth oxides

Owing to their low adsorption capacities, basic rare earth oxides have found applications mainly as heterogeneous catalysts to improve reactivity, selectivity and thermal stability of catalysts, rather than as adsorbents [65, 66]. The catalytic activity of basic rare earth oxides has been understood in terms of Lewis acid/base framework, in which the oxygen atoms on the rare earth surface act as the electron-donating species, that provides an overall basic nature to the material [67]. Since acid/base properties of solid catalysts have been evaluated typically by their chemisorptive interactions with probe molecules, most of the understanding of CO<sub>2</sub> adsorption properties of basic rare earth oxides have been reported in studies of its surface basicity, where CO<sub>2</sub> was used as an acidic probe molecule [68-70]. Investigations of the basic properties of these rare earths have been conducted by the use of various techniques, including Fourier Transform Infrared spectroscopy (FTIR), Temperature-Programmed Desorption (TPD) and molecular modeling [71, 72]. The basic properties of rare earth oxides are attributed to lanthanide contraction: the strength of the basic sites decreases with decreasing radius of the rare earth cation [72]. Rare earth oxides with a low charge/radius ratio are thus more ionic in nature and present stronger basic sites.

The most used of rare earth oxides is cerium oxide (CeO<sub>2</sub>), also known as ceria. It has a fluorite structure (Figure 13), which consists in a simple cubic oxygen sub-lattice with the cerium ions occupying alternate cube centres. In perfect ceria, the oxygen atoms have a formal charge of -2; they are tetrahedrally coordinated to the cerium and octahedrally coordinated to the surrounding oxygen atoms. The oxygen-oxygen distance is 2.705 Å. The cerium atoms have a formal charge of +4 and are coordinated to eight oxygen atoms.

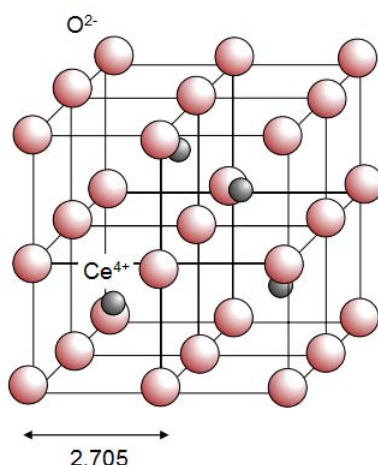


Figure 13: Schema of a unit cell of CeO<sub>2</sub>.

CeO<sub>2</sub> has a range of commercial uses; as a catalyst for the syngas process (the conversion of CO and H<sub>2</sub> to methanol and hydrocarbon) [73], as an active support for various precious metal catalysts, in oxygen sensors [74], and as an electrolyte in Solid Oxide Fuel Cells (SOFC) [75]. The two biggest uses of CeO<sub>2</sub> are as a fast ion conductor in SOFC's and as a promoter in car exhaust catalysts (three way conversion) [76]. These rely on properties of bulk ion migration and surface structure, respectively.

When treated in a reducing atmosphere at elevated temperatures, ceria is known to form a continuum of oxygen-deficient, nonstoichiometric  $\text{CeO}_{2-x}$  oxides (with  $0 < x \leq 0.5$ ) [77]. Even after loss of considerable amounts of oxygen from its lattice and formation of a large number of oxygen vacancies,  $\text{CeO}_{2-x}$  remains in its fluorite crystal structure, and these suboxides are readily re-oxidized to  $\text{CeO}_2$  by exposure to oxidizing environment [78].

Cerium oxide has acid-base character. The description is based on the Lewis acid-base concepts,  $\text{Ce}^{4+}$  being the acidic centre while  $\text{O}^{2-}$  is the basic one [70]. These characteristics allow cerium oxide to adsorb and interact with a wide variety of molecules, such as  $\text{CO}_2$  molecule. Because of ceria properties, oxygen mobility and acid-base character, cerium oxides have aroused interest regarding their reversible and low temperature  $\text{CO}_2$  capture properties. Slostowski [79] studied ceria properties by modulation of composition (doping) or surface characteristics (functionalization). Even though this material has a low adsorption capacity, it is used as model material for the development of characterization techniques [80], and studies reveal interest in this material as a catalyst to  $\text{CO}_2$  valorization, such as methanation of  $\text{CO}_2$  [81-83].

Research conducted by Lavalley *et al.* allowed a better understanding of the mechanisms of  $\text{CO}_2$  adsorption and desorption on ceria surface [70, 84]. Based on FTIR spectroscopic studies, Lavalley *et al.* suggested that  $\text{CO}_2$  molecules interact with cerium oxide by Lewis acid-base reaction.  $\text{CO}_2$  molecule acts as a Lewis acid (an electron-pair acceptor) and ceria anion  $\text{O}^{2-}$  as a Lewis base. They proposed that  $\text{CO}_2$  interact thus with surface  $\text{O}^{2-}$  or with surface basic residual species  $-\text{OH}$  to form carbonate or hydrogencarbonate species, respectively. The formation of carboxylate, via interaction of  $\text{CO}_2$  with surface cerium cations  $\text{Ce}^{4+}$  was also considered. Four adsorption configurations on ceria surface were proposed for carbonate species. In Figure 14, a schematic representation of these interactions is presented.

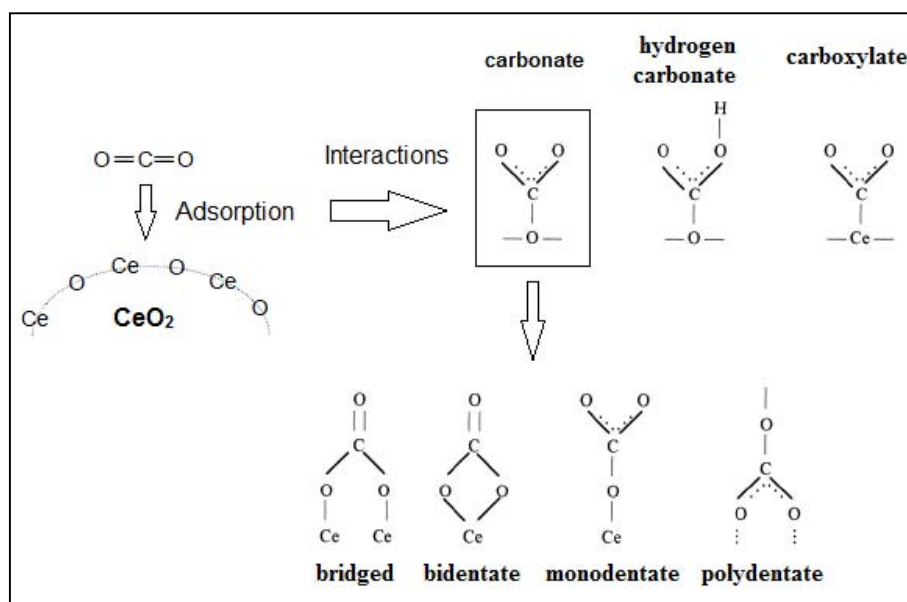


Figure 14: Possible  $\text{CO}_2$ -Ceria interactions [70].

Lavalley *et al.* have also studied the thermal stability of suggested  $\text{CO}_2$ -ceria interactions via FTIR *in situ*. Ceria was subjected to a  $\text{CO}_2$  flow at room temperature, then thermal desorption was conducted. The *in situ* monitoring of ceria surface by FTIR enabled to determine the thermal stability of adsorbed species. The assigned bands of adsorbed species are shown in Table 2. The species related to  $\text{CO}_2$ -ceria interaction were assigned to bands from 800 to 1800

cm<sup>-1</sup>. During thermal desorption, two hydrogencarbonate species have been observed, although their configuration could not be identified. The hydrogencarbonate type I and bridged carbonate have been desorbed under inert gas flow only, without temperature swing (at room temperature), while hydrogencarbonate type II has been desorbed under inert gas flow at 100 °C. Other carbonate species required temperature up to 500 °C to be completely desorbed from ceria surface. The formation of carboxylate species has not been certainly detected.

Table 2: FTIR assigned bands for suggested CO<sub>2</sub>-ceria interactions, from [70].

Species	Desorption temperature	FTIR wave numbers (cm <sup>-1</sup> )			
		$\nu(\text{CO}_3)$	$\pi(\text{CO}_3)$	$\delta(\text{OH})$	$\nu(\text{OH})$
Hydrogencarbonates					
(I)	T <sub>room</sub>	1599,1413, 1025	823	1218	3617
(II)	100°C	1613,1391,1045	836	1218	3617
Carbonates					
Bridged	T <sub>room</sub>	1736, 1135, -	-		
Bidentate	150 °C	1567,1289,1014	856		
Monodentate <sup>a</sup>	200 °C	1504, 1351, -	-		
Polydentate <sup>b</sup>	Above 300 °C	1642,1353 <sup>c</sup> , 1066	854		

<sup>a</sup> Only the high wavenumber band is easily identified in spectra; it was as well assigned to carboxylate species.  
<sup>b</sup> These bands were alternatively assigned to monodentate species.  
<sup>c</sup> When only weak amounts of polydentate carbonates remain on the surface, several bands may be found between 1395 and 1350 cm<sup>-1</sup>.

Solvay manufactures cerium oxide by using conventional closed stirred reactors. The aqueous solution of rare earth salts is first neutralized. After reaction completion, the suspension of solids is filtered. The wet solid pulp may be then dried and/or calcined. The solid dried material may be grinded to adjust particle size. The material is then analyzed for quality and packaged. Solvay-Rhodia ceria is mainly used as such or in formulation for industrial purpose as a high precision polishing agent for glass products, as catalyst or catalyst support for other applications and as raw material in several applications.

The laboratory Solvay-LOF, interested in new applications of Solvay ceria, proposed the study of several types of cerium oxides (concerning the specific surface and doped atoms) as adsorbents for low temperature reversible CO<sub>2</sub> capture. The aim is the use of ceria as adsorbent for CO<sub>2</sub> capture and posterior use as catalyst for CO<sub>2</sub> valorization. In Table 3, we present the different types of Solvay cerium oxides studied in this work.

The studied ceria oxides differ in surface area and concentration/type of doping atoms. The aim is to study these parameters influencing CO<sub>2</sub> capture. It is expected that the atoms with a low charge/radius ratio (La < Ce < Pr) are more ionic in nature and present stronger basic sites, thus having highest affinity towards CO<sub>2</sub> a priori. Doping Zr (transition metal), being less ionic, acts as a counterbalance to modulate the basicity of ceria surface, enabling thus easy material regeneration.

Table 3: Studies Solvay Cerium oxides.

Adsorbent code	Description	B.E.T. specific surface area
Ceria32	undoped cerium oxide	32 m <sup>2</sup> .g <sup>-1</sup>
Ceria50	undoped cerium oxide	50 m <sup>2</sup> .g <sup>-1</sup>
Ceria96	undoped cerium oxide	96 m <sup>2</sup> .g <sup>-1</sup>
Ceria113	undoped cerium oxide	113 m <sup>2</sup> .g <sup>-1</sup>
Ceria149	undoped cerium oxide	149 m <sup>2</sup> .g <sup>-1</sup>
HSA5	undoped cerium oxide	168 m <sup>2</sup> .g <sup>-1</sup>
HSA10	undoped cerium oxide	109 m <sup>2</sup> .g <sup>-1</sup>
CePr	ceria doped with Praseodymium ions	150 m <sup>2</sup> .g <sup>-1</sup>
CeZrPr	ceria doped with Zirconium and Praseodymium ions	137 m <sup>2</sup> .g <sup>-1</sup>
CeLaPr	ceria doped with Praseodymium and Lanthanum ions	147 m <sup>2</sup> .g <sup>-1</sup>

## 6.2 Activated carbons

Several types of commercial activated carbons were investigated as CO<sub>2</sub> adsorbents. The reference names and brief description are shown in Table 4.

Table 4: Studied activated carbons.

Adsorbent code	Description
AC1	Commercial activate carbon derived from polymer precursors which are formed for application requirements (microbeads, pellets, fibers, and monoliths), then pyrolyzed to carbonize polymer precursor.
Norit-R2030	Activated extruded carbon with a diameter of 3 mm. It is used for removal of CO <sub>2</sub> out of cold storage warehouses (B.E.T. specific surface area 800 m <sup>2</sup> .g <sup>-1</sup> )
Norit-GCN	Broken coconut shell based activated carbon designed for use in gold recovery systems.
Chorcarb-130	Activated carbon powder produced by Alfa Aesar (specific surface area 1000 m <sup>2</sup> .g <sup>-1</sup> )

*Note: Norit is the world's largest producer of activated carbon for purification applications.*

The microporous carbon adsorbent AC1 (Figure 15) was used as a model material to study CO<sub>2</sub> adsorption in the context of this thesis. AC1 physical properties are shown in Table 5.

Table 5: AC1 adsorbent physical properties.

Property	Value
Size/Shape	Spherical, ~ 200 $\mu\text{m}$
Isosteric Heat of adsorption ( $\text{CO}_2$ )	25-28 $\text{kJ}\cdot\text{mol}^{-1}$
Bulk Density	~ 0.7 $\text{g}\cdot\text{cm}^{-3}$
$\text{N}_2$ B.E.T. Surface Area	1020 $\text{m}^2\cdot\text{g}^{-1}$
$\text{N}_2$ D-R Micropore Volume	0.4 $\text{cm}^3\cdot\text{g}^{-1}$
Characteristic Pore Dimension	~ 0.6 nm
Heat Capacity	1000-1200 $\text{J}\cdot\text{kg}^{-1}\cdot\text{K}^{-1}$
Thermal Conductivity,	> 1 $\text{W}\cdot\text{m}^{-1}\cdot\text{K}^{-1}$

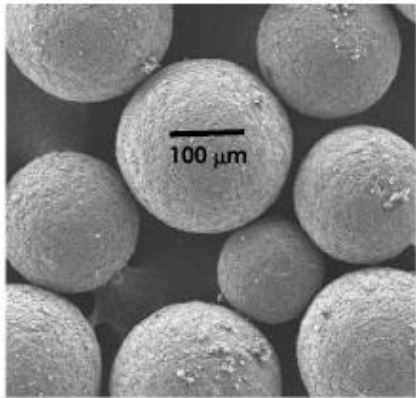


Figure 15: SEM of AC1 microbeads.

### 6.3 Hybrid organic/inorganic materials

Several supported amine on silica supports were synthesized. The supports used in this study consist of two types of Solvay silicas in powder form. The silica supports differ in structural characteristics and production process. These supporting materials were chosen because of their surface acidity, surface area and mechanical resistance. The porous silicas are presented in Table 6. The physical aspect of silica supports is shown in Figure 16.

Table 6: Studied silica supports.

Porous silica code	Physical proprieties		
	Total pore volume	Net pore volume	Specific surface area
HRS1200	1.65 $\text{ml}\cdot\text{g}^{-1}$	1.53 $\text{ml}\cdot\text{g}^{-1}$	199 $\text{m}^2\cdot\text{g}^{-1}$
Z1165	2.00 $\text{ml}\cdot\text{g}^{-1}$	1.86 $\text{ml}\cdot\text{g}^{-1}$	154 $\text{m}^2\cdot\text{g}^{-1}$



Figure 16: Solvay-Rhodia silica.

*Note: HRS1200 and Z1165 micropearls have high absorption capacity for liquids and wear resistance. Net pore volume is obtained after discount the adsorbed water from total pore volume. For more information please see Solvay Silica web page [85].*

Various amine types were used in order to study the affinity with  $\text{CO}_2$  and thermal stability on silica surface. As a matter of confidentiality, we cannot reveal the amine type used in this study. However, the codes used to identify each amine type are shown in Table 7.

Table 7: Amine types used in the synthesis of silica supported amine adsorbents.

Amine type	1	2	3	4	5	6	7
Code	33Iminobis	MEA	PEI	DPTA-T	PTA-YT	DPTA	DPTA-O

Wet impregnation method was used to prepare our samples. The impregnation device (Figure 17) and experimental protocol are then presented.

Amine and ethanol were mixed into a three-necked flask at a 1:8 weight ratio. The support was then added and stirred at 45 RPM and 75 °C until an homogeneous solution was formed. The powder was then dried in the adsorber at 100 °C while flowing argon at 50 ml.min<sup>-1</sup>. The amount of impregnated amine was calculated for maximum saturation of silica pores (net pore volume).

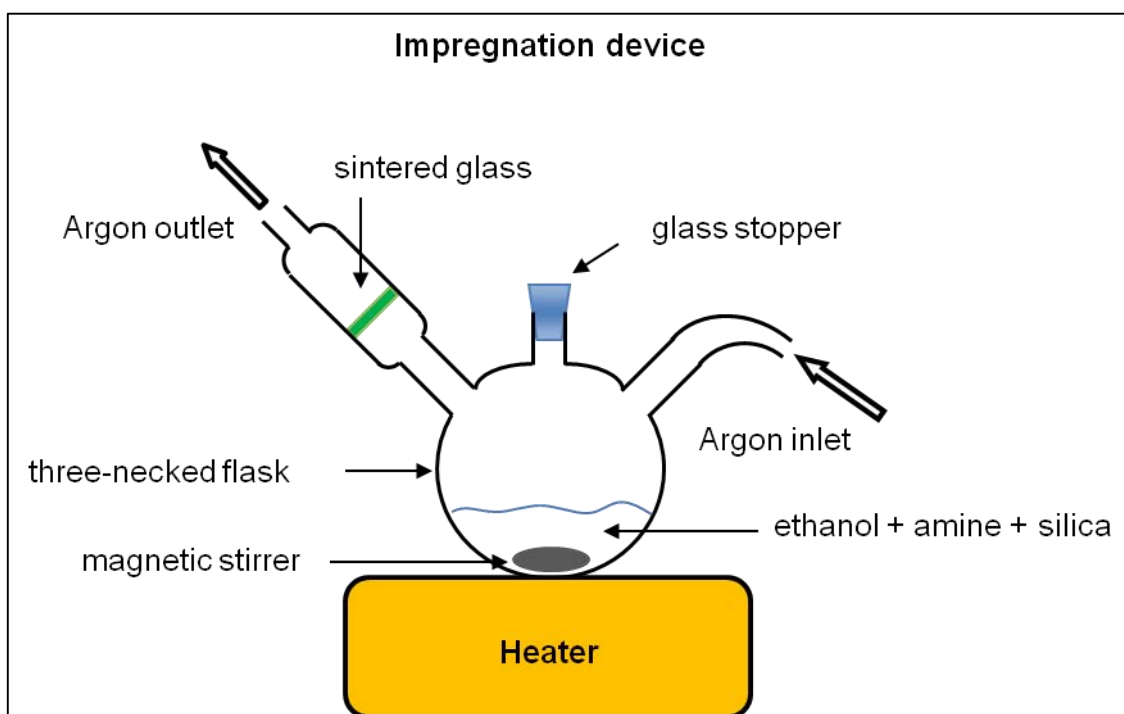


Figure 17: Wet impregnation device.

The aim has been to impregnate the silica support with a maximum load of amine, in order to improve the adsorption capacity. The impregnated silicas are presented in Table 8.

Table 8: amine impregnated silica adsorbents.

Adsorbent code (amine/silica)	Description
PEI/HRS1200	Impregnated PEI on HRS1200
33Iminobis/HRS1200	Impregnated 33Iminobis on HRS1200
33Iminobis/Z1165	Impregnated 33Iminobis on Z1165
MEA/HRS1200	Impregnated MEA on HRS1200
MEA/Z1165	Impregnated MEA on Z1165
DPTA-T/Z1165	Impregnated DPTA-T on Z1165
PTA-YT/Z1165	Impregnated PTA-YT on Z1165
DPTA/Z1165	Impregnated DPTA on Z1165
DPTA-O/Z1165	Impregnated DPTA-O on Z1165

## 7 Conclusions

In this first chapter, base concepts necessary for the understanding of the study of CO<sub>2</sub> capture by solid adsorbents were presented. The adsorption phenomenon was presented as the adhesion of molecules on a solid surface. We have seen that depending on gas-adsorbent interactions, different adsorption processes are possible: physisorption and chemisorption. CO<sub>2</sub> molecules may be captured by physisorption or chemisorption on a substrate. Various adsorbed species may be formed when CO<sub>2</sub> is chemisorbed: carboxylates, carbonates, hydrogencarbonates and carbamates.

A brief presentation of CO<sub>2</sub> adsorption systems was presented. The adsorption systems differ by the way in which the adsorbent is regenerated, and depending on operational conditions, different configurations are possible.

A state-of-the-art of the most investigated materials for reversible CO<sub>2</sub> capture at low temperature was done. Depending on the application and adsorption process, a specific material is suitable. All presented materials have advantages and limitations, concerning the adsorption capacity, adsorption kinetics, thermal stability or selectivity. The different characteristics of reviewed adsorbent are summarized in Table 9.

Table 9: Characteristics of reviewed solid adsorbents for reversible CO<sub>2</sub> capture at low temperature.

Adsorbent type	Process	Ads. kinetics	CO <sub>2</sub> ads. capacity	Selectivity
<b>Zeolites</b>	Physisorption	Fast	+++	low
<b>MOFs</b>	Physisorption	Fast	++++	low
<b>Active carbons</b>	Physisorption	Fast	+++	low
<b>Hybrid (org. /inorg.)</b>	Chemisorption	Moderate	+++	high
<b>Alkali metal carbonates</b>	Chemisorption	Slow	+++++	high

The adsorption capacities of physisorbents are certainly functions of surface area and surface affinity for CO<sub>2</sub>. The adsorptive properties of chemisorbents vary widely according to the nature of their chemical interactions with CO<sub>2</sub>. In the case of organic/inorganic hybrid adsorbents, the adsorptive properties depend on both the composition and geometry of chemisorptive moieties and their solid support.

Finally, the materials used in this study were presented: basic rare earth oxides, activated carbons, and hybrid organic/inorganic materials.



## **CHAPTER II**

# **Experimental and Modeling Approaches for the Study of Carbon Dioxide Capture**

*CHAPTER II: Experimental and Modeling Approaches for the Study of Carbon Dioxide Capture*

## SUMMARY

1	Introduction .....	51
2	Adsorption isotherms .....	51
3	Heat of adsorption evaluation .....	54
3.1	Adsorption heat estimation via adsorption isotherms.....	54
3.2	Adsorption heat measured by calorimetric techniques .....	56
3.3	The <i>pros</i> and <i>cons</i> of classical $\Delta H$ evaluation methods .....	56
4	Modeling adsorption dynamics .....	57
4.1	Mass transfer.....	57
4.1.1	Mass balance for the adsorbed-phase.....	57
4.1.2	Mass balance for the gas-phase.....	58
4.2	Heat transfer .....	59
4.2.1	Heat balance for the adsorbent particle .....	59
4.2.2	Heat balance for the gas-phase.....	59
4.2.3	Heat balance for the wall of adsorption packed column .....	59
5	Critical of classical modeling of adsorption dynamics .....	60
6	Our approach to study CO <sub>2</sub> adsorption .....	60
6.1	IR thermography.....	60
6.1.1	IR thermography cameras .....	61
6.1.2	IR thermography features.....	62
6.1.3	Principles of non-contact temperature measurement .....	63
6.2	IR spectroscopy .....	65
6.2.1	IR Spectrometers .....	66
6.2.2	Sample handling technique .....	66
6.3	Our high-throughput strategy .....	67
7	Conclusions .....	69

*CHAPTER II: Experimental and Modeling Approaches for the Study of Carbon Dioxide Capture*

## 1 Introduction

This chapter reviews a few important methods employed to investigate CO<sub>2</sub>-adsorbent interactions and presents our approach to study CO<sub>2</sub> adsorption. A critical description of each methodology is presented. Concepts and describing phenomena of the adsorption of molecules on adsorbent (specific surface, heat of adsorption, mass and heat transfer between the gas-phase and adsorbed-phase) are discussed.

A classical method, by adsorption isotherms is first presented, then, the usual methods to estimate or measure the heat of adsorption are described. Then, we present the approach by adsorption dynamic modeling. Finally, the methodology used in this work is presented.

## 2 Adsorption isotherms

The adsorption of a gas on the surface of a solid creates an equilibrium state between the gas-phase and the adsorbed phase. To study this equilibrium state, one can represent the relationship between the gas phase pressure (P) and the amount of gas adsorbed per unit mass of solid (q). This equilibrium representation for a constant temperature is named as “adsorption isotherm”. Depending on the nature of the gas-surface interactions, one can observe five types of adsorption isotherms according to BDDT classification (Brunauer, Deming, Deming, Teller) [86]. The evolutions of the amount adsorbed, as a function of the gas phase pressure, are shown for different types of adsorption isotherms in Figure 1.

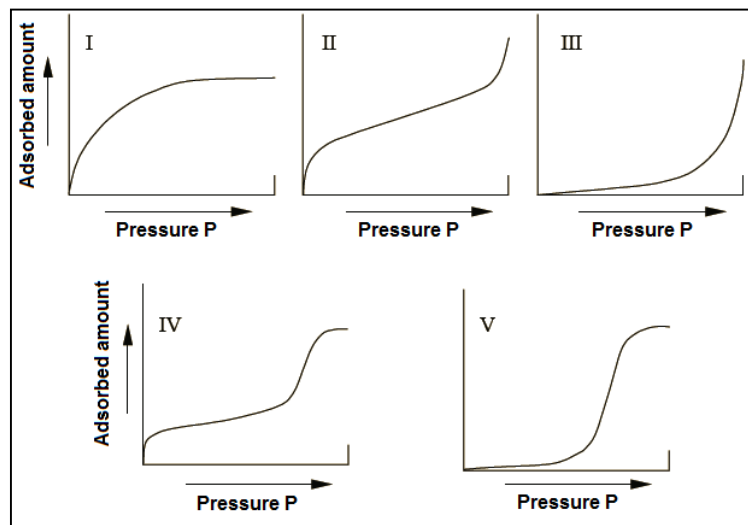


Figure 1: The five types of adsorption isotherms according to BDDT classification.

The equilibrium isotherms for microporous adsorbents are generally of type I (see Figure 2) [20]. It is a Langmuir type isotherm, which corresponds to an adsorption of molecules in a monolayer way on the material surface. The isotherm of type II illustrates the BET (Brunauer, Emmett, Teller) type adsorption or multilayer adsorption. The isotherm of type III corresponds to a so-called unfavorable adsorption, where the adsorbed amounts are weak at low pressures. The increasing of adsorbed amount for high pressures is due to capillary condensation on the mesoporous surface (pores with diameters between 2 and 50 nm). The isotherm of type IV results from the formation of two successive layers of adsorbate on the solid surface. It is the case when interactions between adsorbate molecules and the solid surface are stronger than the interactions between adsorbed molecules themselves. The isotherm of type V reflects the existence of significant intermolecular interactions, when the

interaction between the adsorbate molecules and the solid is weak. Adsorption isotherms of CO<sub>2</sub> on different adsorbents are shown in Figure 2.

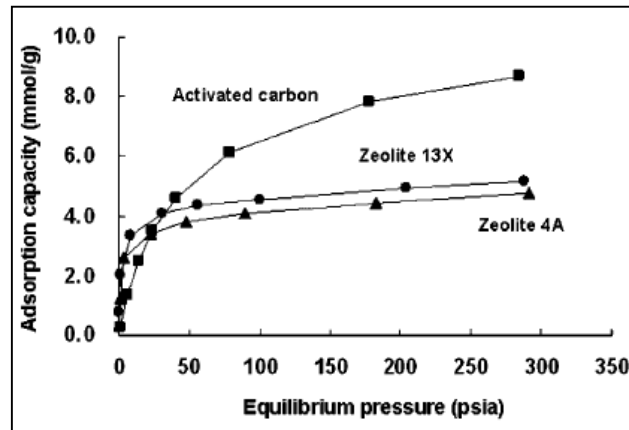


Figure 2: CO<sub>2</sub> adsorption isotherms on activated carbon, zeolite 13X, and zeolite 4A at 298 K [87].

The temperature also has an influence on the adsorbed amount. This quantity decreases with increasing temperature at constant pressure. The plot of equilibrium isotherms at different temperatures represents this dependence (Figure 3). An example of temperature influence on adsorption isotherms for amine-supported solid is shown in Figure 4.

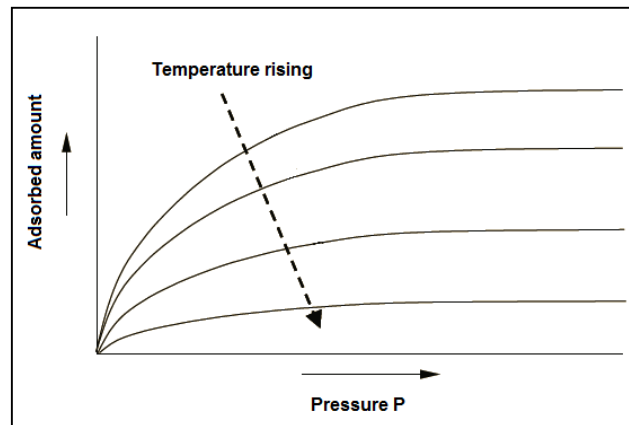


Figure 3: Influence of temperature on the equilibrium isotherms.

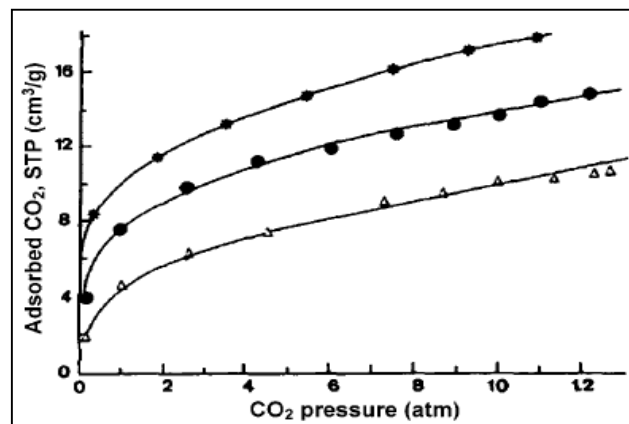
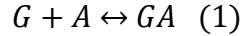


Figure 4: Adsorption isotherms for monosilane-functionalized Davison grade 62 silica gel at three temperatures: small circles: 273 K; big circles: 296 K; triangles: 323 K [88].

*CHAPTER II: Experimental and Modeling Approaches for the Study of Carbon Dioxide Capture*

In order to analytically represent such isotherms, Langmuir proposed a model based on the kinetics of adsorption. It is assumed that when the system is at equilibrium, the rate of adsorption is equal to the rate of desorption:



where  $G$  represents the gas phase,  $A$  the solid surface and  $GA$  the adsorbed phase. The equality of these two rates (adsorption and desorption rates) leads to the equation of the Langmuir isotherm:

$$q_e = q_{sat} \frac{b(T)P}{1 + b(T)P} \quad (2)$$

with

$$b(T) = b_0 \exp\left(\frac{\Delta H_0}{RT}\right) \quad (3)$$

where  $q_e$  is the amount of molecules adsorbed at equilibrium ( $\text{mol.kg}^{-1}$ ),  $q_{sat}$  the maximum amount of molecules adsorbed or saturation capacity ( $\text{mol.kg}^{-1}$ ),  $b$  an equilibrium constant that is directly related to the Henry constant,  $\Delta H_0$  is the limiting heat of adsorption at low coverage,  $R$  the gas constant,  $T$  the absolute temperature, and  $b_0$  the equilibrium constant for standard temperature. Note: the gas phase pressure ( $P$ ) may be expressed by a gas-phase concentration ( $C$ ).

The Langmuir model was originally derived for localized chemisorption on an ideal surface with no interaction between adsorbed molecules. A variety of more sophisticated model isotherms have been developed to take into account such factors as energetic heterogeneity and sorbate-sorbate interactions. But from the perspective of the overall modeling and design of adsorption systems, those sophisticated models offer little advantage over the simple Langmuir model since any increase in accuracy is generally more than offset by the additional complexity of the model and the need for more empirical parameters.

An alternative equation to describe the adsorption isotherms was developed by Brunauer, Emmet and Teller (BET). BET adsorption model is the basis for the widely used analysis technique for the measurement of the specific surface area of a material. Most commercial equipments, used for adsorption isotherm experiments, have been developed using BET method. The BET equation is:

$$\frac{P}{q_e(P_0 - P)} = \frac{1}{q_{sat0}} + \frac{(c - 1)P}{cq_{sat0}P_0} \quad (4)$$

where  $q_e$  is the number of moles of gas adsorbed per gram of adsorbent when the gas pressure is  $P$ ,  $q_{sat0}$  is the monolayer capacity of surface, that is, the number of moles of gas per gram of adsorbent required to form a monomolecular layer,  $P_0$  is the saturation gas pressure at the temperature used, and  $c$  is a coefficient. When  $P/q_e(P_0 - P)$  is plotted as ordinate versus  $P/P_0$  as abscissa, a line is obtained with a slope of  $(c - 1)/cq_e$  and intercepts on ordinate at  $1/cq_{sat0}$ . The coefficient  $c$  is function of the heat of adsorption and depends on the chemical nature of the surface.

From  $q_e$ , calculated from experimental data using the above equation, the surface area is determined from equation:

$$S_{BET} = q_e a_m N_a \cdot 10^{-20} \quad (5)$$

where  $S_{\text{BET}}$  is the specific surface area in square meters per gram, as determined by this method,  $a_m$  the molecular cross-section area of one gas molecule in square angstroms ( $\text{\AA}^2$ ), and  $N_a = 6.10^{23}$  the Avogadro number.

The specific surface area is an important adsorbent parameter, as it is directly related to the adsorption capacity.

### 3 Heat of adsorption evaluation

The adsorption of gas molecules on the material surface results in their immobilization (they are restricted in their movements). It is accompanied by a decrease in entropy. As adsorption also implies a decrease of free energy, thus it can be concluded from the thermodynamic,  $\Delta G = \Delta H - T\Delta S$ , that the adsorption heat will itself be negative and we can say that all adsorption processes are exothermic and happen with heat release, diffusing through the material and the adsorption system. The amount of heat generated in a physisorption process is small, ranging from about 20 to 50  $\text{kJ}\cdot\text{mol}^{-1}$  (kilo joule per mol of adsorbed molecules). Otherwise, in the case of chemisorption, it is considerably higher, within the range of 50-200  $\text{kJ}\cdot\text{mol}^{-1}$ , and accompanied by a profound change in the electronic charge distribution of adsorbed molecules. The temperature rise, occasioned by released heat, contributes for a diminution of the adsorption capacity of the adsorbent and may degrade the performance of the industrial adsorption process. The parameter that characterizes the release of heat is termed ‘‘heat of adsorption’’, which can be measured by calorimetric techniques [89] or estimated by means of adsorption isotherms [90], as we will demonstrate in the following section.

#### 3.1 Adsorption heat estimation via adsorption isotherms

Adsorption processes are processes in equilibrium, which obey an equation like Clausius-Clapeyron:

$$\frac{dP}{dT} = \frac{\Delta H_{diff}}{(V_{gas} - V_{ads})T} \quad (6)$$

where  $V_{gas}$  is the gas phase volume,  $V_{ads}$  the adsorbed phase volume and  $\Delta H_{diff}$  ( $\text{J}\cdot\text{mol}^{-1}$ ) the differential heat of adsorption.

At equilibrium, the volume of the gas phase is much greater than the volume of adsorbed gas, thus the equation reduces to:

$$\frac{dP}{dT} = \frac{\Delta H_{diff}}{V_{gas}T} \quad (7)$$

Considering that the gas phase behaves as a perfect gas, the volume of one mole of gas is given by:

$$V_{gas} = \frac{RT}{P} \quad (8)$$

This relationship is used to modify the equation 7 to:

$$\Delta H_{diff} = RT^2 \left[ \frac{\partial \ln P}{\partial T} \right]_q \quad (9)$$

The subscript  $q$  denotes that the derivative is taken at constant specific adsorbed amount  $q$ .

CHAPTER II: Experimental and Modeling Approaches for the Study of Carbon Dioxide Capture

The integration of this equation leads to:

$$\ln P = \frac{\Delta H_{diff}}{RT} + Cst \quad (10)$$

$\Delta H_{diff}$  therefore can be determined experimentally (thanks to adsorption isotherms) from a straight line representing the variation of  $\ln P$  versus  $1/T$  (Figure 5).

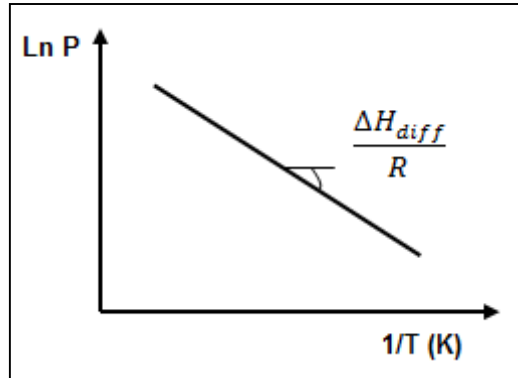


Figure 5: Determination of the differential heat of adsorption.

The differential heat of adsorption represents the amount of heat per mole of adsorbed gas associated with a small change in the solid surface coverage (from  $\theta$  to  $\theta + d\theta$ ). The surface coverage  $\theta$  being defined as follows:

$$\theta = \frac{q}{q_e} \quad (11)$$

where  $q$  is the amount of adsorbed molecules ( $\text{mol.kg}^{-1}$ ) and  $q_e$  is the amount of molecules adsorbed at equilibrium ( $\text{mol.kg}^{-1}$ ).

The differential heat of adsorption depends on the recovery ratio of the solid surface  $\theta$  (Figure 6). In general, the differential heat of adsorption decreases when the amount adsorbed increases.

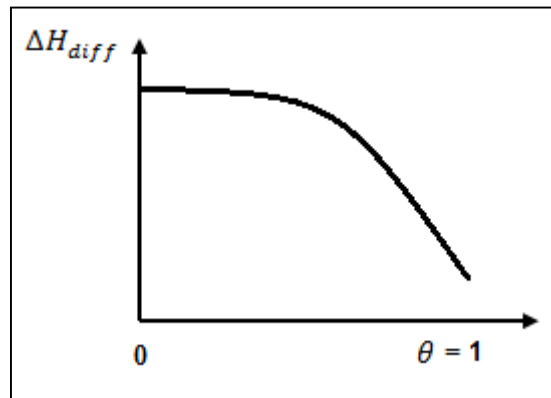


Figure 6: Illustration of the differential heat of adsorption dependence with the solid surface coverage.

*Note: the absolute value of  $\Delta H_{diff}$  is called "isosteric heat".*

If one considers the adsorption heat of a mole of gas on an amount of solid, one can define the integral heat of adsorption  $\Delta H_{int}$  ( $\text{J.mol}^{-1}$ ) as the integration of the differential heat curve:

$$\Delta H_{int} = \frac{1}{q} \int_0^q \Delta H_{diff} dT \quad (12)$$

### 3.2 Adsorption heat measured by calorimetric techniques

The differential heat of adsorption and consequently the integral heat of adsorption can usually be obtained more sensitively and accurately from calorimetric measurements in which increments of gas are admitted successively to a calorimeter which contains the solid substrate. Alternatively, the calorimeter may be operated with continuous admission of gas. Up to date, the differential heat of adsorption can be measured by the combination of manometric/gravimetric techniques and calorimetry [91, 92]. The differential heat of adsorption can then be determined by integrating the heat source curve corresponding to the amount adsorbed as shown in the following example (Figure 7), where a differential scanning calorimetry (DSC) coupled to a thermobalance (ATG) was used for the determination of the differential heat of adsorption and desorption of CO<sub>2</sub> on a catalyst [93].

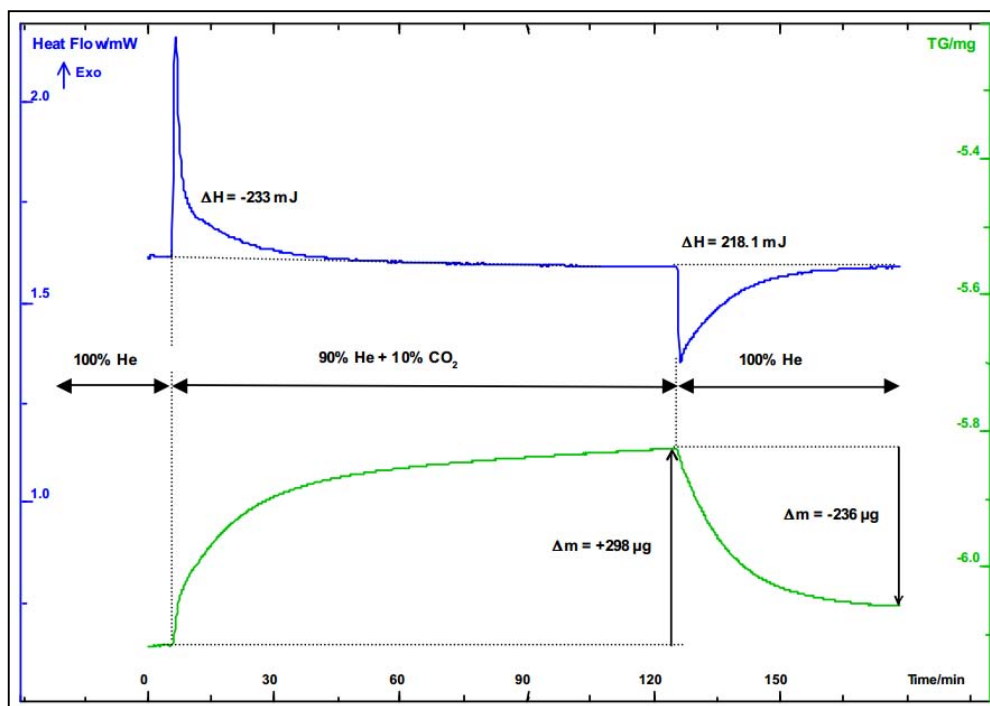


Figure 7: The thermogravimetric signal (green) provides the amount of CO<sub>2</sub> adsorbed or desorbed on the adsorbent and the DSC signal (blue) measures the corresponding adsorption heat: exothermic during adsorption (that means an increase of the temperature during the capture process) or endothermic during the desorption (that means cooling of the coal material). Thermo balance model: Setaram SENSYS evo TG-DSC.

### 3.3 The *pros* and *cons* of classical $\Delta H$ evaluation methods

As described above, the heat of adsorption may be measured by calorimetric techniques or estimated via adsorption isotherms. Both methods are widely used, but they have some limitations. From adsorption isotherms, one may easily estimate the adsorption heat, but its estimation is indirect, based on theoretical evaluation of Van't Hoff type equations. In practice, from several adsorptions isotherms, one determines the values of T and P (at adsorption equilibrium) corresponding to a desired isosteric (specific surface coverage) and then one traces the curve  $\ln P = f(1/T)$  to finally estimate  $\Delta H$ . Therefore, for the achievement of this estimation method, time-consuming experiments are necessary. However, in the case of calorimetric techniques, one evaluates directly the heat of adsorption by measuring the released heat and adsorbed-phase loading during the adsorption phenomenon. The measurements are more sensitive and accurate, but specific and high cost equipments are

necessary (DSC, ATG). Likewise, it is a maladaptive method regarding the high-throughput screening methodologies.

## 4 Modeling adsorption dynamics

In most adsorption processes the adsorbent is contacted with a moving fluid in a packed bed termed adsorption column. The gas stream to be treated flows into the bed under certain conditions of temperature, pressure and speed. The knowledge of adsorption equilibrium (adsorption isotherms) is insufficient to determine the behavior of the column and consequently to control and/or predict the adsorption stage. Many authors [91, 92, 94, 95] have been utilized the simultaneous solution of a set of coupled nonlinear partial differential equations (PDEs) based on heat and mass balances to predict the adsorption column dynamics. In order to present this approach, we describe thus the involved phenomena.

### 4.1 Mass transfer

The mass transfer in the packed bed, from the gas phase to the adsorbed phase, is subjected to different resistances encountered by molecules during their moving through the porous media (Figure 8). The resistances can be described as:

- 1) **External:** resistance to mass transfer (external transfer) through the boundary layer surrounding the grains of adsorbent.
- 2) **Internal:** resistance due to the diffusion of molecules into the pores of the grains (macroporous and microporous internal transfer).
- 3) **Intrinsic:** resistance to adsorption on adsorbent surface. Also called intrinsic adsorption kinetics.

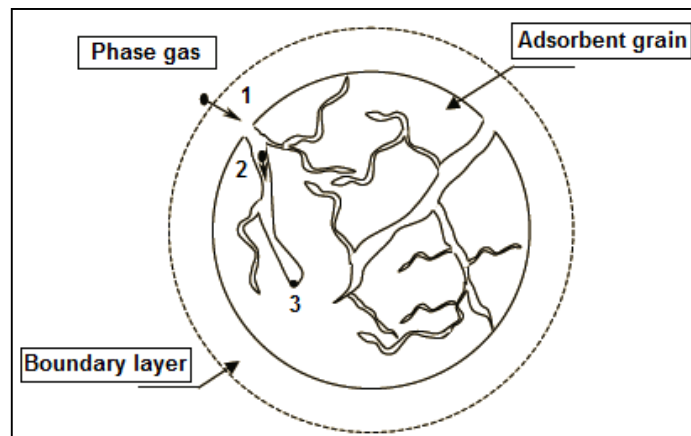


Figure 8: Different resistances to mass transfer [96].

#### 4.1.1 Mass balance for the adsorbed-phase

Depending on the system and the operating conditions, any one of these resistances may be rate controlling, or the rate may be determined by the combined effects of more than one mass transfer resistance. Physical adsorption at a surface is extremely rapid, and the kinetics of physical adsorption are invariably controlled by mass or heat transfer rather than by the intrinsic rate of the surface process. In general, for an adsorption process, resistance due to external mass transfer is negligible compared to that due to internal mass transfer. Therefore, the adsorption kinetics is controlled by internal diffusion which can be approximately

represented by a linearized rate expression according to the Linear Driving Force (LDF) theory:

$$\frac{\partial q}{\partial t} = k_d(q_e - q) \quad (13)$$

The LDF model is the most common model used to describe adsorption rates. It consists in a general expression that lumps together all diffusion mechanisms into one single parameter ( $k_d$ ). The equation above corresponds to mass balance for the adsorbed phase, where variable  $q$  is the amount of molecules adsorbed ( $\text{mol.kg}^{-1}$ ) and parameter  $q_e$  is the amount of molecules adsorbed at equilibrium ( $\text{mol.kg}^{-1}$ ), obtained via an adsorption isotherm. The effective rate constant  $k_d$  is related to the diffusional time constant  $D_M$  ( $\text{m}^2/\text{s}$ ) by:

$$k_d \approx \frac{15D_M}{r^2} (\text{s}^{-1}) \quad (14)$$

where  $r$  is the particle radius (m).

*Note: the effective rate constant is often used as an adjustable parameter.*

### 4.1.2 Mass balance for the gas-phase

In order to realize a balance for the gas phase, one considers a portion of the packed column (Figure 9) of length  $dz$ , crosssectional area  $A(\text{m}^2)$ , and constant bed porosity  $\varepsilon$ .

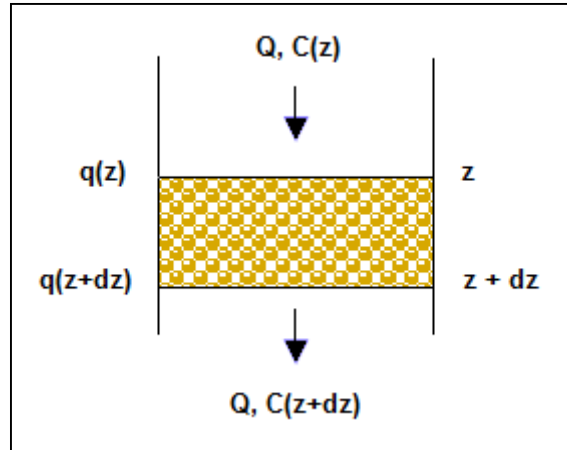


Figure 9: A differential slice of a packed adsorption column.

Assuming that radial effects are negligible, an unsteady-state material balance on the solute may be performed.

$$\underbrace{QC|_z - QC|_{z+dz}}_{\text{Fluid flow}} + \underbrace{\varepsilon A \left[ -D_m \frac{dC}{dz} \right]_z - \varepsilon A \left[ -D_m \frac{dC}{dz} \right]_{z+dz}}_{\text{Axial Dispersion}} = \underbrace{\varepsilon \frac{dC}{dt} Adz}_{\text{Accumulation in fluid phase}} + \underbrace{(1 - \varepsilon) \frac{dq}{dt} Adz}_{\text{Accumulation in solid phase}} \quad (15)$$

Dividing by  $Adz$  and taking limits:

$$-u_0 \frac{\partial C}{\partial z} + \varepsilon D_m \frac{\partial^2 C}{\partial z^2} = \varepsilon \frac{\partial C}{\partial t} + (1 - \varepsilon) \frac{\partial q}{\partial t} \quad (16)$$

with  $u_0 = Q/A$  (17)

where  $u_0$  is the average pore velocity ( $\text{m.s}^{-1}$ ),  $Q$  the gas flow rate ( $\text{m}^3.\text{s}^{-1}$ ),  $C$  the gas-phase concentration of adsorbate ( $\text{mol.m}^{-3}$ ) and  $D_m$  coefficient of axial dispersion of mass ( $\text{m}^2.\text{s}^{-1}$ ).

## 4.2 Heat transfer

The study of heat transfer in adsorption columns requires the heat balance for heat transfer between the gas, solid particles and walls. In a similar way, one may write a differential heat balance for a column element. One considers that thermal properties are constant and the heat transfers by radiation are neglected in comparison with other modes of heat transfer.

### 4.2.1 Heat balance for the adsorbent particle

There are many heat transfer models for packed beds of spherical particles appearing in the literature. The most accurate of all models takes into account heat conduction and dispersion in the solid energy equation:

$$\underbrace{\frac{\partial T_s}{\partial t}}_{\text{temperature derivative}} = \underbrace{\frac{\lambda_s}{\rho_s C p_s} \frac{1}{r^2} \frac{\partial}{\partial r} \left( r^2 \frac{\partial T_s}{\partial r} \right)}_{\text{heat transfer inside a particle}} + \underbrace{\frac{1}{C p_s} \Delta H_{diff} \frac{\partial q}{\partial t}}_{\text{heat generated by adsorption}} \quad (18)$$

with the boundary conditions:

$$-\lambda_s \frac{\partial T_s}{\partial r} = h_{sg} (T_{sg} - T_{gas}) \quad \text{on} \quad A_{gs} \quad (19)$$

$$\text{Note: } T_{sg} = T_s \quad \text{on} \quad A_{gs}$$

where  $T_{sg}$  is the temperature in the interface gas-solid (K),  $A_{gs}$  the interfacial surface area ( $\text{m}^2$ ),  $h_{sg}$  the interfacial heat transfer coefficient between solid particle of adsorbent and the gas-phase ( $\text{W.m}^{-2}.\text{K}^{-1}$ ),  $T_s$  the temperature of adsorbent particle (K),  $T_{gas}$  the temperature of gas-phase (K),  $\lambda_s$  is the conductivity of adsorbent particle ( $\text{W.m}^{-1}.\text{K}^{-1}$ ),  $\rho_s$  the density of adsorbent particle ( $\text{kg.m}^{-3}$ ),  $C p_s$  the heat capacity of adsorbent particle ( $\text{J.mol}^{-1}.\text{K}^{-1}$ ) and  $\Delta H_{diff}$  the differential heat of adsorption ( $\text{J.mol}^{-1}$ ).

### 4.2.2 Heat balance for the gas-phase

Likewise, a thermal balance is applied to gas-phase in the adsorption column. It includes the terms of heat transport, heat diffusion, heat dispersion and heat transfer between the solid adsorbent and the wall of adsorption column:

$$\frac{\partial T_g}{\partial t} + \underbrace{u_0 \frac{\partial T_g}{\partial z}}_{\text{heat transport}} = \underbrace{\frac{1}{\varepsilon} \left( \frac{\lambda_e}{\rho_g C p_g} + D_h \right) \frac{\partial^2 T_g}{\partial z^2}}_{\text{heat diffusion and dispersion}} - \underbrace{\frac{h_{sg} A_0}{\varepsilon \rho_g C p_g} (T_g - T_{sg})}_{\text{heat transfer gas-solid}} - \underbrace{\frac{h_{wall} A_{0\_wall}}{\varepsilon \rho_g C p_g} (T_g - T_{wall})}_{\text{heat losses}} \quad (20)$$

Where  $\lambda_e$  is the effective conductivity of packed bed ( $\text{W.m}^{-1}.\text{K}^{-1}$ ),  $\rho_g$  the gas density ( $\text{kg.m}^{-3}$ ),  $C p_g$  the gas heat capacity ( $\text{J.mol}^{-1}.\text{K}^{-1}$ ),  $D_h$  the coefficient of axial dispersion of heat ( $\text{W.m}^{-1}.\text{K}^{-1}$ ),  $A_0 = A_{gs}/V$  the specific surface area ( $\text{m}^{-1}$ ),  $A_{0\_wall} = A_{wall}/V$  the specific surface area of adsorption column wall ( $\text{m}^{-1}$ ),  $h_{wall}$  the heat transfer coefficient between gas-phase and the wall of adsorption column ( $\text{W.m}^{-2}.\text{K}^{-1}$ ) and  $T_{wall}$  is the temperature of adsorption column wall (K).

### 4.2.3 Heat balance for the wall of adsorption packed column

Thermal balance for the wall of packed column results in:

$$\frac{\partial T_{wall}}{\partial t} = \frac{h_{wall} A_{0\_wall} (T_g - T_{wall})}{\rho_{wall} C p_{wall}} - \frac{h_{ex} A_{0\_wall} (T_{wall} - T_{ex})}{\rho_{wall} C p_{wall}} \quad (21)$$

where  $\rho_{wall}$  is the wall density ( $\text{kg}\cdot\text{m}^{-3}$ ),  $Cp_{wall}$  the wall heat capacity ( $\text{J}\cdot\text{mol}^{-1}\cdot\text{K}^{-1}$ ),  $h_{ex}$  the heat transfer coefficient between wall and ambient ( $\text{W}\cdot\text{m}^{-2}\cdot\text{K}^{-1}$ ) and  $T_{ex}$  the room temperature (K).

The simultaneous solution of the presented coupled equations (mass and heat transfer) enables an accurate prediction of the thermal and dynamic behaviors (temperature evolution, maximum temperature, adsorption rates, saturation time, etc.) during adsorption process inside an adsorber.

## 5 Critical of classical modeling of adsorption dynamics

The presented modeling of mass transfer is widely used in the dynamic study of adsorption columns. The present Ph.D. thesis did not focus on the study of the mass transfer, although we have based the adsorption rates of our adsorbents on LDF model.

The described modeling for heat transfer in porous media is the most accurate among the models in the literature, because heat transport, diffusion and dispersion are taken into account during adsorption of molecules on adsorbent surface. However, the involved phenomena are complex and their modeling is not always easy.

Many parameters have to be evaluated experimentally ( $h$ ,  $Cp$ ,  $\Delta H$ ,  $\lambda$ ,  $D$ ,  $q$ ...) and are hardly measured or estimated. Moreover, different techniques have to be used for the estimation of these parameters (BET, ATG, DSC...), hindering the use of high-throughput methodologies.

A direct methodology is used by these authors, which consists in fitting experimental results (adsorbent temperature and gas-phase concentration) with the mentioned PDEs. The disadvantage of this method is the use of adjustable parameters.

The experimental data are usually recorded by thermocouples and gas-phase analyzers along the model adsorber. The intrusiveness and the influence of thermocouple thermal inertia may be a limitation for transient measurements such as adsorption processes [97].

## 6 Our approach to study CO<sub>2</sub> adsorption

In the general introduction, we have presented the project goal, which is to study CO<sub>2</sub> adsorption on several types of materials, combining and correlating information from *in-situ* infrared thermography and *in-situ* infrared spectroscopy measurements. As will be shown further, IR spectroscopy and IR thermography are suitable techniques for the study of CO<sub>2</sub> adsorption on solid adsorbents and well adapted regarding a high-throughput strategy. In the following topics, we explain the principles and characteristics of each technique. Finally, a description of our high-throughput strategy based on IR thermography and IR spectroscopy is presented.

### 6.1 IR thermography

All matters continuously emit electromagnetic radiation as a result of molecular and atomic agitation associated with the internal energy of the material. The internal energy is in direct proportion to the temperature of the substance at equilibrium state (Figure 10). The detected radiation as heat (thermal radiation) is situated in an intermediate wavelength range (0.1 to 100  $\mu\text{m}$ ) [98].

Etymologically, the word thermography from the Latin *thermos* and *graphia*, means “write the heat”. It refers to any technique representing in space and/or time the thermal state (i.e. temperature) of a scene. If that representation comes from the thermal radiation emitted by the

scene, more precisely, if it is detected as heat radiation, one may use the term infrared thermography [99].

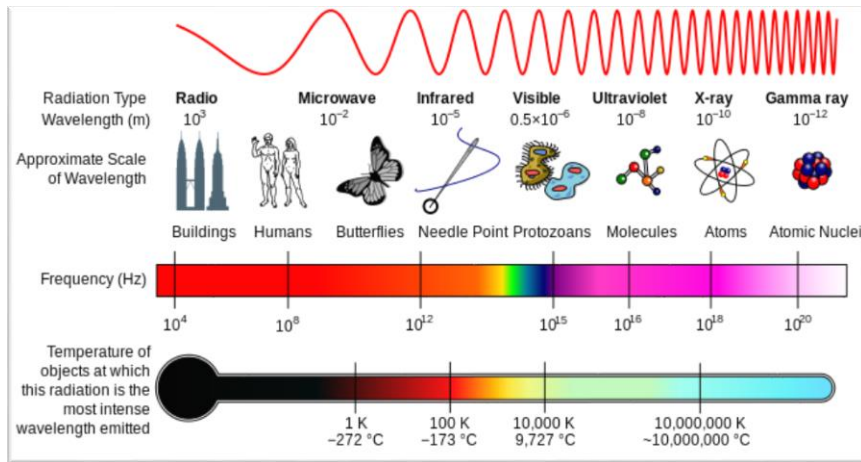


Figure 10: Diagram of the electromagnetic spectrum [100].

### 6.1.1 IR thermography cameras

Although heat radiation or infrared radiation (IR) is not detectable by the human eye, an IR camera can convert it to a visual image that describes thermal variations across an object or scene. IR covers a portion of the electromagnetic spectrum from approximately 0.9 to 14  $\mu\text{m}$  and is emitted by all objects at temperatures above absolute zero, and the amount of radiation emitted increases with temperature [101].

IR Thermography is a type of imaging that is accomplished with an IR camera designed and calibrated for a specific range of the IR spectrum (Figure 11) to display temperature values across an object or scene.

The main components of an IR camera are a lens that focuses IR onto a detector, plus electronics and software for processing and displaying the signals and images. IR detectors technologies are broken down into two categories: thermal detectors (microbolometers) and quantum detectors (Table 1). Microbolometers react to incident radiant energy and are much slower and less sensitive than quantum detectors. The operation of quantum detectors is based on the change of state of electrons in a crystal structure reacting to incident photons. These detectors are generally faster and more sensitive than thermal detectors. However, they require cooling, sometimes down to cryogenic temperatures using liquid nitrogen or a small Stirling cycle refrigerator unit.

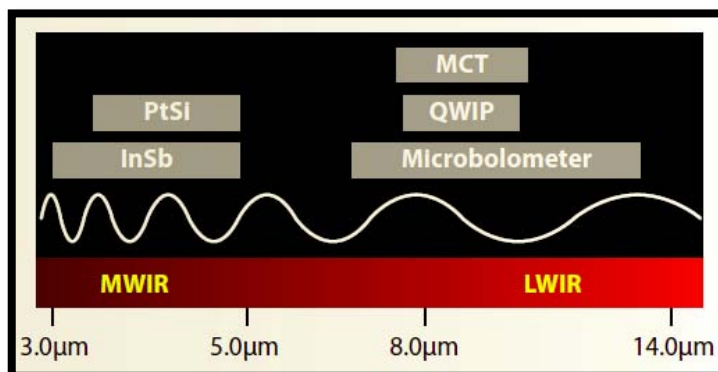


Figure 11: Spectral response regions, IR midwaves (MWIR) and IR longwaves (LWIR), for various detector materials.

Table 1: IR detector's material and associated detector technology.

IR detector's material	Detector technology
Silicon (Si)	Thermal detector (microbolometer)
Germanium (Ge)	Thermal detector (microbolometer)
Indium Arsenic Gallium (InAsGa)	Quantum detector
Platinum Silicon (PtSi)	Quantum detector
Indium Antimony (InSb)	Quantum detector
Mercury Cadmium Tellurium (MCT = HgCdTe)	Quantum detector
Aluminum Arsenic Gallium (Layered GaAs/AlGaAs)	QWIP (Quantum Well Infrared Photon)

### 6.1.2 IR thermography features

In many cases, IR thermography improves the temperature measurements because of its singular characteristics: *instantaneous*, *global*, *discriminative* and *non-intrusive*.

- **Instantaneous:** the measurements may be made at high speed (up to 230 Hz). It is essential for applications in which the evolution of object or scene temperature is relatively fast, for example, transient heat transfer experiments. It is the case of heat released by an adsorption phenomenon (tens of seconds). On the contrary, classical measurement instruments such as thermocouples may have some limitations for transient measurements [97] because of the influence of thermocouple thermal inertia [102].
- **Global:** the IR camera provides a thermal image of the whole scene. It is an important aspect for fault diagnostic applications [103-105] and process monitoring [106]. For our problematic, we can observe the temperature evolution of an entire experimental device, for example, a millifluidics adsorption column (presented in Chapter VI).
- **Discriminative:** the IR camera detector is a focal plane array (FPA) of micrometer size pixels (about 230  $\mu\text{m}$ ) made of various materials sensitive to IR wavelengths (see Table 1), which resolution can range from about  $160 \times 120$  up to  $1024 \times 1024$  pixels, allowing the differentiation of temperatures from a scene. Therefore, we can observe a localized zone of the interaction  $\text{CO}_2$ -adsorbent.
- **Non-intrusive:** IR thermography is a non-intrusive measurement technique, because it allows non-contact measurements of an object/scene temperature and it passively receives the heat radiation. It is a well suited technology to prevent any alteration of the observed phenomenon behavior (i.e. heat flux through porous media).

Those characteristic are explored by many applications, such as non-destructive testing and characterization [107-110], thermophysical properties measuring [111-113], thermal analysis of chemical reactions [114], medical applications [115], etc.

### 6.1.3 Principles of non-contact temperature measurement

The intensity of the emitted energy from an object varies with temperature and radiation wavelength. In addition to the emitted radiation, the object interacts with the surrounding radiation by absorbing and reflecting a portion of it, or allowing some of it to pass through (Figure 12).

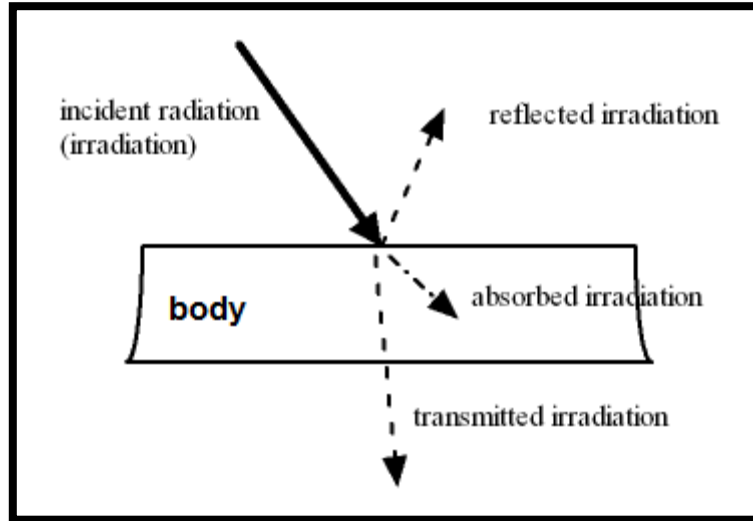


Figure 12: Scheme of the matter/radiation interaction.

The total radiation law can be expressed by the following equation:

$$W = \alpha W + \rho W + \tau W \quad (22)$$

It can be simplified to:

$$1 = \alpha + \rho + \tau \quad (23)$$

The coefficients  $\alpha$ ,  $\rho$  and  $\tau$  describe the object's incident energy absorption ( $\alpha$ ), reflection ( $\rho$ ), and transmission ( $\tau$ ). They represent the object ability to absorb, reflect, or transmits incident radiation and those assume values from zero to one. If an object absorbs 100% of incident radiation ( $\alpha = 1, \rho = 0, \tau = 0$ ), this object is called a perfect blackbody.

A formal definition (stated mathematical as Kirchhoff's Law) is a body that absorbs and emits, at any temperature, the max amount of possible radiation [99]. This concept is important in IR thermography because it relates IR radiation and body temperature. Nonetheless, in the real world, there are no objects that are perfect absorbers, reflectors, or transmitters, although some may come very close to one of these properties.

To take into account the radiative properties of a real body, one use the emissivity ( $\varepsilon$ ) coefficient, which values vary with the radiation wavelength. Since Kirchhoff's law states that for any surface the absorbed radiation is equal to emitted radiation, we obtain  $\alpha(\lambda) = \varepsilon(\lambda)$ .

The radiative properties of a perfect blackbody can also be described mathematically by Planck's Law, easily represented as a series of curves (see Figure 13). These curves show the radiation per wavelength unit and area unit, called the *spectral radiant emittance* of the blackbody.

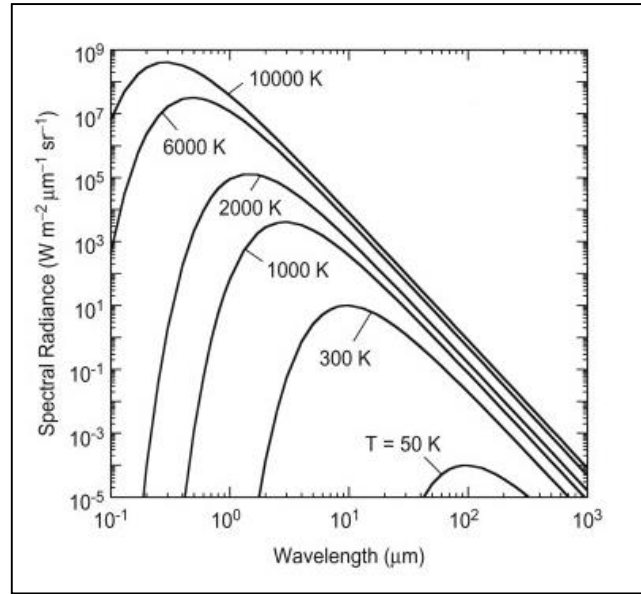


Figure 13: Relationship between emitted radiation and the wavelength (Planck's law) for distinct temperatures.

From Planck's law, the total radiated energy (the area under a curve) from a blackbody can be calculated. This is expressed by a formula known as the Stefan-Boltzmann law, expressed by the following equation:

$$W_T = \sigma T^4 \text{ (W/m}^2\text{)} \quad (24)$$

where  $\sigma$  is the Stefan-Boltzmann's constant equal to  $5.67 \times 10^{-8} \text{ (W/m}^2\text{K}^4\text{)}$ .

This equation provides a relationship between emitted radiation and temperature of a perfect blackbody.

For a normal object, the emitted energy is related to the blackbody emitted energy by the emissivity coefficient ( $\epsilon$ ):

$$W_{obj} = \epsilon \times W_{bb} \quad (25)$$

In fact the emissivity varies with wavelength. As IR thermography operates only inside limited spectral ranges because of the atmospheric attenuation (IR absorption by gases and scattering by particles, see Figure 14), in practice, it is often possible to treat objects as greybodies which are objects that have the same emissivity for all wavelengths. Consequently, for a greybody, Stefan-Boltzmann's law takes the form:

$$W_{Tobj} = \epsilon \times \sigma T^4 \text{ (W/m}^2\text{)} \quad (26)$$

This represents the total emissive power of a greybody.

To summarize, an IR camera receives radiation from the target object, plus radiation from its surroundings that has been reflected onto the object's surface. Both of these radiation components become attenuated when they pass through the atmosphere, since the atmosphere absorbs part of the radiation. If one takes into account these influences and if the object emissivity ( $\epsilon$ ) is known, from the previous equation (total emissive power of a greybody), it is possible to calculate the object's temperature from a calibrated IR camera's output (calibration relative to blackbody temperature).

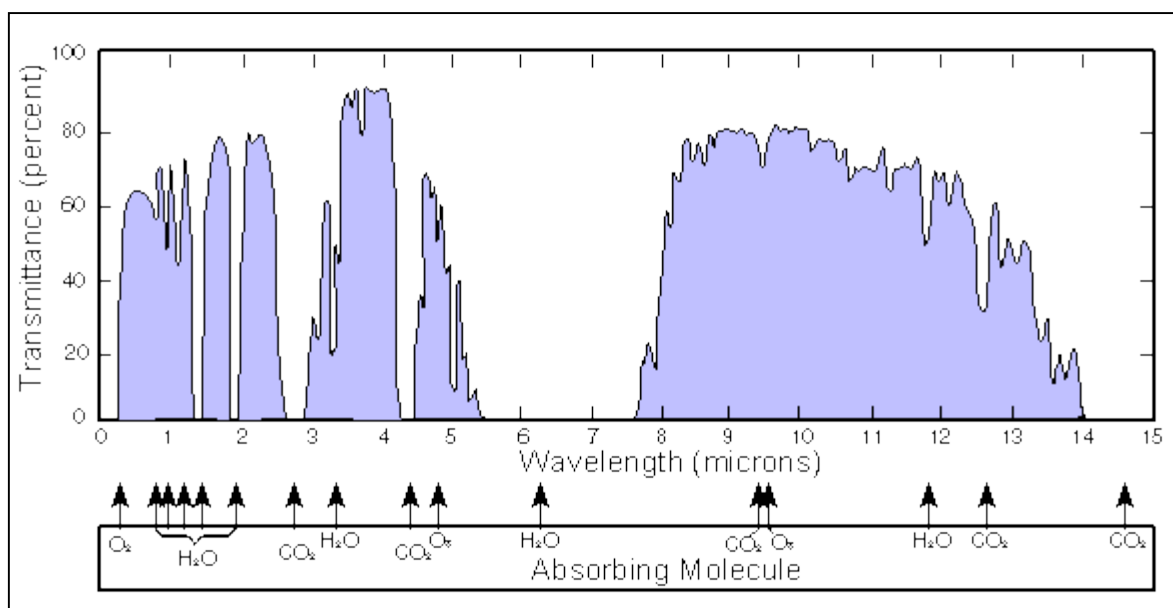


Figure 14: Atmospheric attenuation (white areas) with a chart of the gases and water vapor causing most of it. The areas under the curve represent the highest IR transmission.

## 6.2 IR spectroscopy

With the purpose of elucidating how CO<sub>2</sub> molecules interact with adsorbent surfaces, infrared spectroscopy was chosen as a suitable technique.

It is indeed a high selective technique that allows the investigation of specific chemical groups "active" by interaction with the infrared radiation (one say IR-active). It is also a non-intrusive technique, working in the intermediate wavenumber range from 400 to 4000 cm<sup>-1</sup> (2.5-25 μm), which corresponds to the vibrations related to CO<sub>2</sub>-surface interaction.

In a spectrometer, a source of IR radiation sends all IR wavelengths of interest through a sample. The IR radiation causes some of the molecules to vibrate with increased amplitude, which increases the vibrational energy. The increase in vibrational energy is at the expense of radiation energy, resulting in the absorption of IR radiation at certain frequencies. The absorption frequency of a fundamental absorption band in the IR is the same as the frequency of the molecular vibration that caused the absorption [116]. IR spectra represent types of "fingerprints" unique to every molecule, which are identified from the position, profile and intensity of absorption bands.

Infrared spectroscopy is the most widely used, and usually most effective, spectroscopic method for characterization of the surface chemistry. Infrared spectroscopy played an important role in characterization of heterogeneous catalysts, as it permits direct monitoring of the interaction between adsorbed molecules and catalysts [117]. So, this technique can provide valuable information about the nature of interactions between CO<sub>2</sub> molecules and substrate.

The interactions CO<sub>2</sub>-surface are widely investigated by IR spectroscopy, by the fact that CO<sub>2</sub> is used as a probe molecule to surface characterization [118-120]. IR spectroscopy is therefore frequently employed to study the CO<sub>2</sub>-adsorbent interactions concerning CO<sub>2</sub> capture by solid adsorbents [121-123].

## 6.2.1 IR Spectrometers

Infrared spectrometers come in a variety of types but have many common features. All have a source that emits all the IR radiation of interest. As for IR cameras, they have a thermal or quantum detector. In between the source and detector, the spectrometer has a device employed to analyze the radiation, where intensity can be deduced for each wavelength resolution element. Monochromators were used in dispersive instruments, but they are no longer used and have been replaced by interferometers.

The Fourier transform infrared spectroscopy (FTIR) was developed to obtain faster measurements than a dispersive spectrometer, because of its ability to measure intensities of all of the wavelength elements simultaneously, thanks to a Michelson interferometer. The IR beam is aimed to a sample where it is absorbed and scattered. After the interaction with the sample, the resulting radiation is focused to the detector to be converted into an electrical signal. The interferogram cannot be interpreted directly, it is necessary to correlate the intensity as a function of frequency. It is obtained by means of Fourier transform treatment.

## 6.2.2 Sample handling technique

Depending on the nature of sample (solids, liquids or gases), a specific sample handling technique is suitable. Diffuse reflectance was chosen as sample handling technique for the study of our adsorbents. It is an excellent sampling tool for powdered materials, thus it is well adapted for the studied porous adsorbents. It eliminates the time-consuming process of pressing pellets for transmission measurements and enables the direct analysis of powdered adsorbents.

Diffuse reflectance is well adapted to *in-situ* studies of temperature effects and gas-solid interactions, thanks to a reaction chamber. A powdered sample is placed in a small container, where the source radiation strikes it and is diffusely reflected in various directions (Figure 15). This radiation is collected by a mirror and measured by the detector of a FTIR spectrometer.

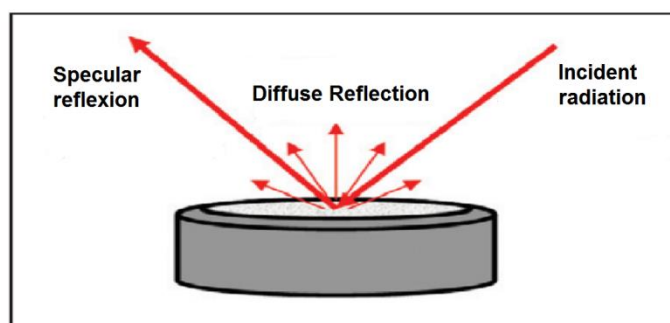


Figure 15: Scheme of source radiation/sample interaction (the spectrometer beam is reflected, scattered and transmitted through the sample material).

Usually the sample must be grounded and mixed with a non-absorbing matrix such as KBr. The spectrum is ratioed against a reference spectrum of this pure powdered non-absorbing matrix. The ratioed spectrum is processed by a computer using a function  $f(R_\infty)$  derived by Kubelka and Munk, which changes the reflectance spectrum into one resembling a linear absorbance spectrum:

$$f(R_\infty) = \frac{(1 - R_\infty)^2}{2R_\infty} = \frac{K}{s} \quad (27)$$

Where  $R_{\infty}$  is the reflectance of a thick scattering layer,  $K$  the molar extinction coefficient, and  $s$  a scattering coefficient, which is a function of particle size.

The Kubelka-Munk equation creates a linear relationship for spectral intensity relative to sample concentration. It assumes infinite sample dilution in a non-absorbing matrix, a constant scattering coefficient and an “infinitely thick” sample layer. These conditions can be achieved for highly diluted, small particle samples and a thick sample layer.

Diluting ensures a deeper penetration of the incident beam into the sample which increases the contribution of the scattered component in the spectrum and minimizes the specular reflection component. The specular reflectance component in diffuse reflectance spectra causes change in band shapes, their relative intensity, and, in some cases, it is responsible for complete band inversions. Dilution of the sample with a non-absorbing matrix minimizes these effects (particle size and sample loading mechanics also play an important role). Other factors related to high spectral quality for diffuse reflectance sampling are listed below:

- **Particle Size:** reducing the size of the sample particles reduces the contribution of reflection from the surface. Smaller particles improve the quality of spectra (narrow bandwidths and better relative intensity). The recommended size of the sample/matrix particles is 50 micrometers or less.
- **Refractive Index:** effects result in specular reflectance contributions (spectra of highly reflecting samples will be more distorted by the specular reflectance component). This effect can be significantly reduced by sample dilution.
- **Homogeneity:** samples prepared for diffuse reflectance measurements should be uniformly and well mixed. Non-homogenous samples will lack reproducibility will be difficult to quantify.
- **Packing:** the required sample depth is governed by the amount of sample scattering. The minimum necessary depth is about 1.5 mm. The sample should be loosely but evenly packed in the cup to maximize IR beam penetration and minimize spectral distortions.

### 6.3 Our high-throughput strategy

One of the major objectives of this work was to propose a methodology to study CO<sub>2</sub>-adsorbent interactions in line with Solvay LOF’s industrial point of view, which aims at a significant impact on its productivity, through an increase of its capability to access basic data for processes as well as physico-chemical properties of complex systems. Therefore, this work has followed a high-throughput strategy.

High-throughput method allows a researcher to quickly conduct investigation tests. This method reduces the time required in the discovery of new materials and is used in many areas as pharmaceuticals and catalysis [124-126].

As the aim of rapid study of materials for CO<sub>2</sub> capture, our high-throughput methodology consists in two levels of selection and two levels of investigation. The first level, called primary screening, quickly selects materials with high productivity, but the information access is limited. After this step, the best candidates are then analyzed on a second level of selection, called secondary screening, which provides higher information access, but with lower productivity. The two further investigation levels lead to a better understanding of CO<sub>2</sub> capture mechanisms by the studied materials and bring knowledge about the utilization of these materials as adsorbents in final applications.

*CHAPTER II: Experimental and Modeling Approaches for the Study of Carbon Dioxide Capture*

In the primary screening, an innovative characterization device based on infrared thermography was developed [126], allowing the thermal analysis of several samples, up to 12, in the same experiment. Temperature variations (observed during cycles of adsorption/desorption of CO<sub>2</sub>) provide information about the material. Characteristics, such as the nature of the adsorption process (physisorption or chemisorption), process reversibility and kinetics of adsorption/desorption, can be studied during this first approach.

In the secondary screening, infrared thermography technique is coupled with a precision weighing balance to estimate the amount of CO<sub>2</sub> adsorbed on the material (mg<sub>CO2</sub>/g<sub>ads</sub>) while observing the temperature variations on the material surface. The experimental data acquired from secondary screening are used as input for a heat transfer model, which was developed in order to identify influencing parameters and also estimate the heat source to finally deduction of CO<sub>2</sub> adsorption heats. A high-throughput methodology was employed as strategy to the development of this model. The heat transfer model is simplified (analytical model with reduced number of parameters to be analyzed or estimated) in order to obtain a deeper insight in the physical behavior of the system.

In the first investigation level, Diffuse Reflectance Infrared Fourier Transform Spectroscopy (DRIFT) is employed for the identification of adsorbed species on the material surface and to study the surface species evolution according to the temperature and the surrounding atmosphere (CO<sub>2</sub> or N<sub>2</sub>).

In the second investigation level (final level), a milli-fluidic adsorption column was designed in order to simulate the CO<sub>2</sub> capture process in industrial adsorption columns. IR thermography was employed as approach technique to study the adsorber thermal behavior during CO<sub>2</sub> capture. In Figure 16, our high-throughput methodology is illustrated by a scheme.

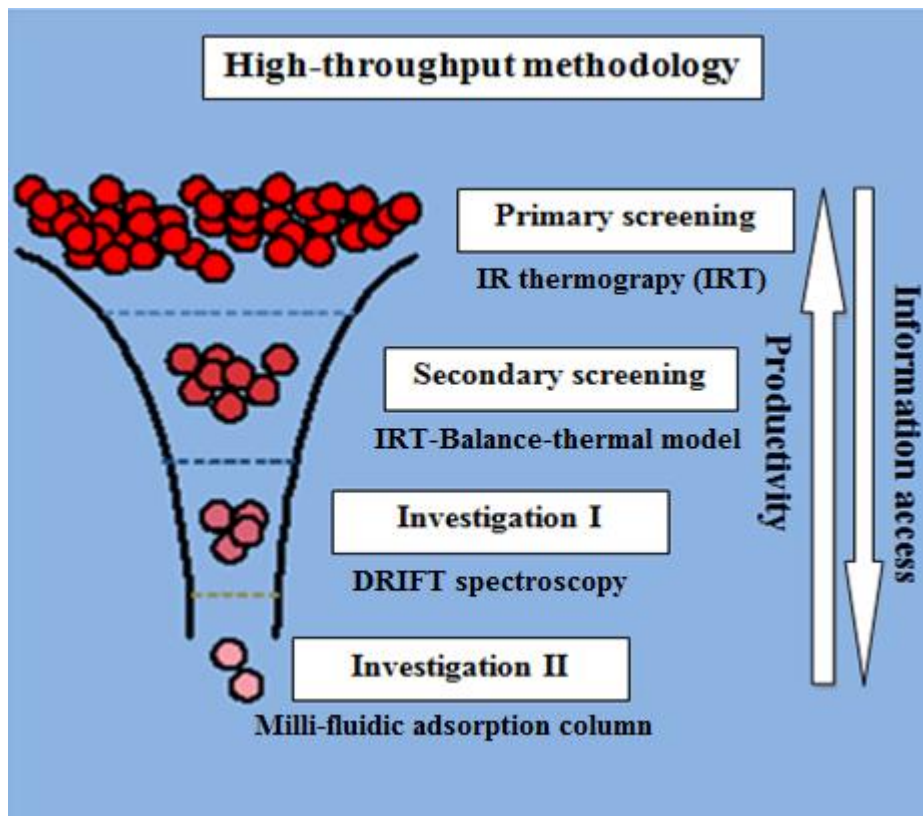


Figure 16: Scheme of our high-throughput methodology.

## 7 Conclusions

In this second chapter, a state-of-the art was done concerning some approaches employed to study a solid adsorbent and its interactions with a gas. The chapter allowed us to acquire knowledge on different concepts necessary for understanding CO<sub>2</sub> capture by solid adsorbents.

Adsorption isotherms were described as the relationship between the gas phase pressure and the amount of gas adsorbed per unit mass of solid at equilibrium, then, influence parameters were represented by a Langmuir isotherm model. BET isotherm model was also presented. Most commercial equipments have been developed using BET method for the estimation of specific surface area of a material. The specific surface area is directly related to adsorption capacities.

Heat of adsorption was defined as the energy released during the adsorption. The heat of adsorption for chemisorption processes is higher than for physisorption processes. We have seen also that the differential heat of adsorption is influenced by the solid surface coverage and temperature. The heat of adsorption can be measured by calorimetric techniques or estimate thanks to adsorption isotherms. Both methods are widely used but have limitations: for example, time-consumption and the necessity of high cost equipments to achieve experiments. Therefore, they are maladaptive methods regarding high-throughput screening methodologies.

In most adsorption processes, the adsorbent is in contact with the fluid in a packed bed. The analysis and rational design of such processes therefore require an understanding of the dynamic behavior of such systems. Until recently, many authors have utilized the simultaneous solution of a set of coupled nonlinear partial differential equations (PDEs) based on heat and mass balances to predict the adsorption column (adsorber) dynamics. The balance equations take into account complex phenomena (e.g. diffusion, dispersion...) and many parameters have to be used as inputs in the models. Moreover, these parameters are hardly measured or estimated. A direct methodology is used, which consists in fitting experimental results (adsorbent temperature and gas-phase concentration) with the mentioned PDEs. The disadvantage of this method is the use of adjustable parameters. The experimental data are usually recorded by thermocouples and gas-phase analyzer along the model adsorber. The intrusiveness and the influence of thermocouple thermal inertia may be a limitation for transient measurements such as adsorption processes

In order to fulfill the Ph.D. thesis goals, a new methodology for the study of adsorbent was then proposed. It consists in the study of CO<sub>2</sub> adsorption on several types of materials combining and correlating information from *in-situ* infrared thermography and *in-situ* infrared spectroscopy experiments, where a high-throughput strategy is employed. The approach techniques were presented and main concepts were discussed. These techniques are distinct but at the same time complementary. The principal features and limitations of these approaches are summarized in Table 2.

Finally, a description of the high-throughput methodology was presented. This methodology includes two levels of selection (thanks to a high-throughput device based on IR thermography) and two levels of investigation (thanks to DRIFT spectroscopy and a millifluidics adsorption column). In the next chapters, for each high-throughput level, the experimental devices and main results are presented and discussed.

Table 2: Features and limitation of IR thermography and IR spectroscopy

<b>IR Thermography</b>	<b>IR Spectroscopy</b>
<p style="text-align: center;"><b>Employed to</b></p> <p style="text-align: center;">Measuring temperature fields</p>	<p style="text-align: center;"><b>Employed to</b></p> <p style="text-align: center;">Identify chemical groups</p>
<p style="text-align: center;"><b>Characteristics</b></p> <p>High speed measurements, visualization of whole scene, discriminative (differentiation of temperatures from a scene) and non-intrusive measurement</p>	<p style="text-align: center;"><b>Characteristics</b></p> <p style="text-align: center;">Highly selective and no-intrusive</p>
<p style="text-align: center;"><b>Limitations</b></p> <p>For accurate temperature measurements, the scene emissivity has to be known or a previous calibration in terms of absolute temperature has to be done (e.g. Joule effect calibration).</p>	<p style="text-align: center;"><b>Limitations</b></p> <ul style="list-style-type: none"> <li>- Sample handling precautions have to be done (highly diluted, small particle samples and a thin sample layer)</li> <li>- Slow spectra acquisition (the spectra acquisition frequency is lower in comparison with the temperature acquisition frequency in the case of IR thermography)</li> </ul>

## **CHAPTER III**

### **Primary and Secondary Screening**

-

### **Qualitative Analysis of Adsorptive Behaviors and Evaluation of Adsorption Capacities**



## SUMMARY

1	Introduction .....	75
2	Primary Screening: Qualitative Analysis of Adsorptive Behaviors .....	75
2.1	Experimental device .....	75
2.2	Results and discussion .....	77
2.2.1	Rare Earth Oxides (REO).....	77
2.2.2	Hybrid organic/inorganic materials.....	83
2.2.3	Activated Carbon.....	85
2.3	Overall screening results and discussion .....	86
2.4	Summary and conclusions .....	88
3	Secondary Screening: Evaluation of Adsorption Capacities.....	89
3.1	Experimental device .....	89
3.2	Results and discussion .....	90
3.2.1	Activated Carbon.....	90
3.2.2	Hybrid organic/inorganic materials.....	91
3.2.3	Rare Earth oxides .....	93
3.3	Overall screening results and discussion .....	93
3.4	Summary and conclusions .....	94
4	Final Conclusions.....	95



## 1 Introduction

As we have seen in Chapter II, our studies of CO<sub>2</sub> capture by solid adsorbents start with a first step based on IR thermography, which was termed “primary screening”. This part of studies consists in selecting materials with good affinity with CO<sub>2</sub> molecules. First assumption about adsorption behaviors are done thanks to qualitative analysis of thermal profiles obtained during CO<sub>2</sub> adsorption on thin-layer of adsorbent. Then, we pass to the next study step, the “secondary screening”, where IR thermography technique is coupled with a precision balance for simultaneous recording of temperature and mass variation during adsorption. We can thus estimate the amount of adsorbed CO<sub>2</sub> on material. The assumption made after primary screening can be thus validated thanks to coupled analysis of thermal and mass variation profiles during CO<sub>2</sub> adsorption.

## 2 Primary Screening: Qualitative Analysis of Adsorptive Behaviors

### 2.1 Experimental device

An experimental device based on IR thermography, for high-throughput characterization of materials, was developed by Julien Jolly (research engineer Solvay-Rhodia) during his Ph.D. thesis [126]. It was based on the thermal effect due to the adsorption (exothermic reaction) or desorption (endothermic reaction) of specific gas phase molecules on solid porous material. For this purpose, a dedicated cell was built (9-well cell) to record by means of an infrared camera, the surface temperature of the porous material when it comes in contact with a specific molecule (Figure 1).

As a primary screening, the developed device was employed in this work to identify adsorbents having high interaction with CO<sub>2</sub> molecules.

The experiment consists in measuring the average temperature variations of the material surface by means of an IR camera, during cyclic injections of gas (CO<sub>2</sub> or N<sub>2</sub>) into filtering cartridges (diameter:  $d = 8\text{ mm}$ ), which are filled with a thin layer of adsorbent (thickness within the range of 1-3 mm). A differential temperature measurement is recorded by using a reference material for each sample in order to take into account the material emissivity and the temperature variations during experimentation.

A bolometric FLIR System A20M camera allows the detection of the thermal radiation (from 7.5 to 13  $\mu\text{m}$ ) coming from the adsorbent surface with a specific sampling frequency. The temperature values can be directly measured through calibration parameters. The high sensibility limit of IR camera (0.1K) and good signal/noise ratio ensure reliable and reproducible thermal measurements.

An injection system (multi-position valve, flow meters and 3-way valves) allows the switch on either N<sub>2</sub> gas (inert gas used to study CO<sub>2</sub> desorption) or CO<sub>2</sub> gas with a controlled injection time, thanks to a home-made Lab view interface. The 3-way valves are used to prevent excessive pressure between gas switching, thus the flow rate can be controlled without variation during adsorption/desorption cycles.

The screening device allows us to evaluate the strength of gas-solid interaction. We may study, as a first approach, the adsorption/desorption kinetics and the reversibility of CO<sub>2</sub> capture at room temperature. Therefore, a large number of different candidates for CO<sub>2</sub> capture can be tested via a first qualitative analysis of adsorbent thermal behaviors.

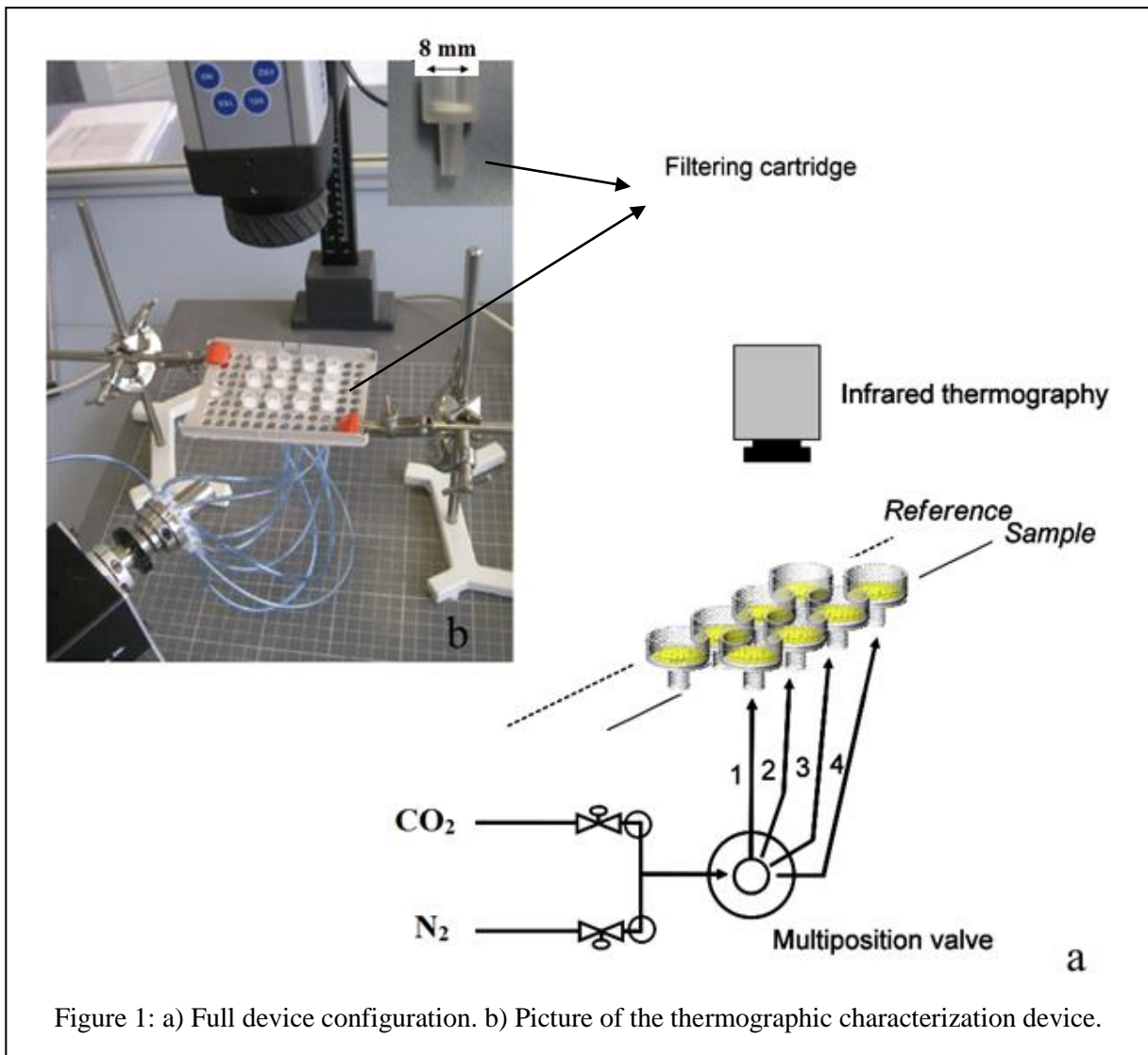


Figure 1: a) Full device configuration. b) Picture of the thermographic characterization device.

In Figure 2, we can see an example of thermal images taken during CO<sub>2</sub> adsorption and desorption processes on a thin-layer of carbon material AC1.

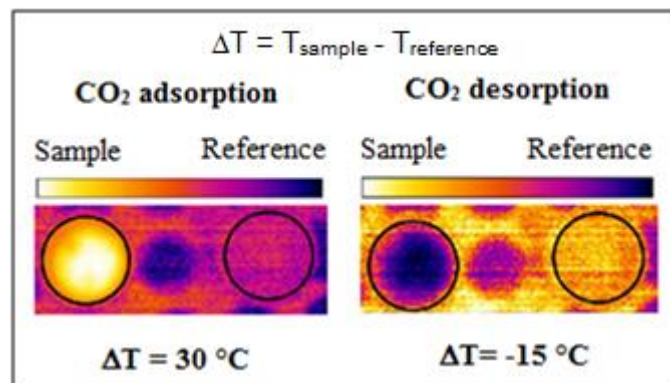


Figure 2: Thermal images during adsorption and desorption of CO<sub>2</sub> on AC1 carbon adsorbent.

## 2.2 Results and discussion

If the studied material has some affinity with CO<sub>2</sub> molecules, CO<sub>2</sub> adsorption on material surface is expected during CO<sub>2</sub> injection through the thin layer of adsorbent. The adsorption is characterized by a release of heat which will cause an elevation of adsorbent temperature. In Figure 3, we show the thermal behavior of some studied adsorbents during CO<sub>2</sub> adsorption.

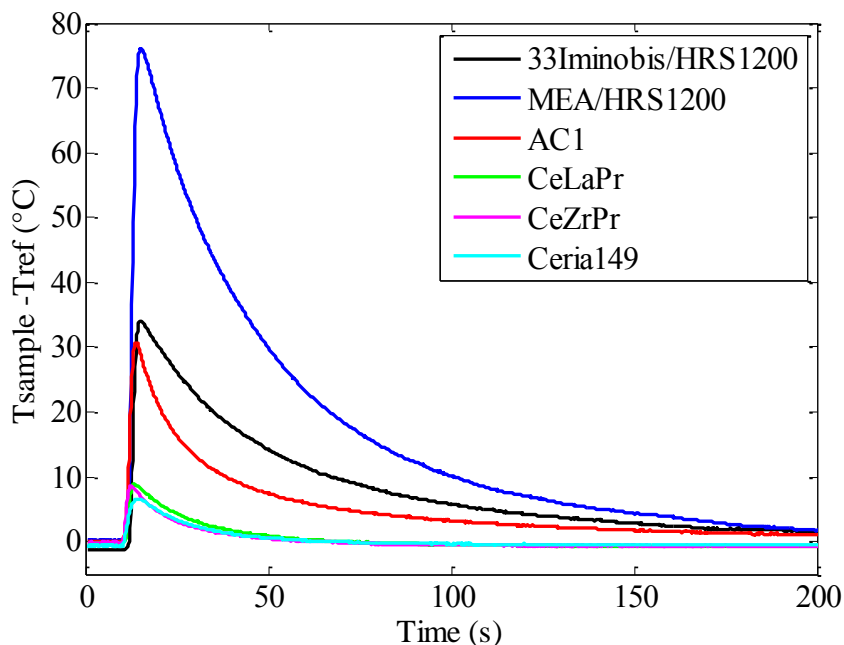


Figure 3: Adsorption peaks observed during CO<sub>2</sub> adsorption on different adsorbents. Continuous CO<sub>2</sub> flow rate (50 ml/min) was injected through an adsorbent thin layer (70 mg).

We can notice that a specific thermal behavior occurs for each adsorbent. Depending on CO<sub>2</sub>-adsorbent interactions, a specific temperature evolution during CO<sub>2</sub> adsorption is observed.

In general, during CO<sub>2</sub> injection, an intense temperature rise is observed in the first seconds of adsorption, then, the adsorbent temperature gradually decreases to reach the initial temperature (room temperature).

In order to study the thermal behaviors of studied materials during CO<sub>2</sub> adsorption, a qualitative study based on analysis of thermal profiles obtained during successive injections of CO<sub>2</sub> and N<sub>2</sub> is presented for the three families of studied materials.

### 2.2.1 Rare Earth Oxides (REO)

Our REO adsorbents were tested using the screening device (see Chapter I.6 “studied materials” for information about the samples). The filtering cartridges were filled with a thin layer (100 mg) of each adsorbent. They were submitted to successive gas injection cycles of N<sub>2</sub> and CO<sub>2</sub>. The flow meter was setup to inject a continuous flow rate of gas (50 ml/min). The protocol was configured to start with N<sub>2</sub> injection during 2000 s, in order to desorb possible contaminants (adsorbed water and other species) from material surface (pretreatment), then, five injection cycles, 400 s of CO<sub>2</sub> + 400 s of N<sub>2</sub> were operated. After the injection cycles, the gas flow was stopped but IR camera continued to record the average surface temperature of the thin layer during 2000 seconds.

For example, a thermal profile is shown in Figure 4, consisting in the average surface temperature of a thin layer of a non-doped ceria (HSA5) recorded during CO<sub>2</sub> adsorption and desorption processes.

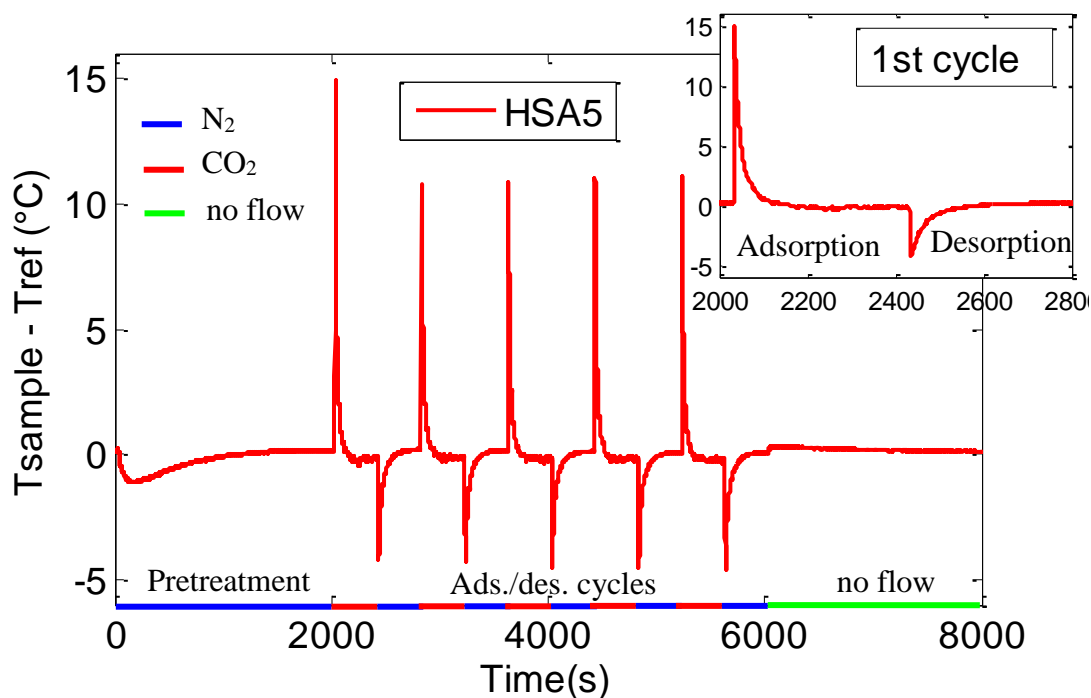


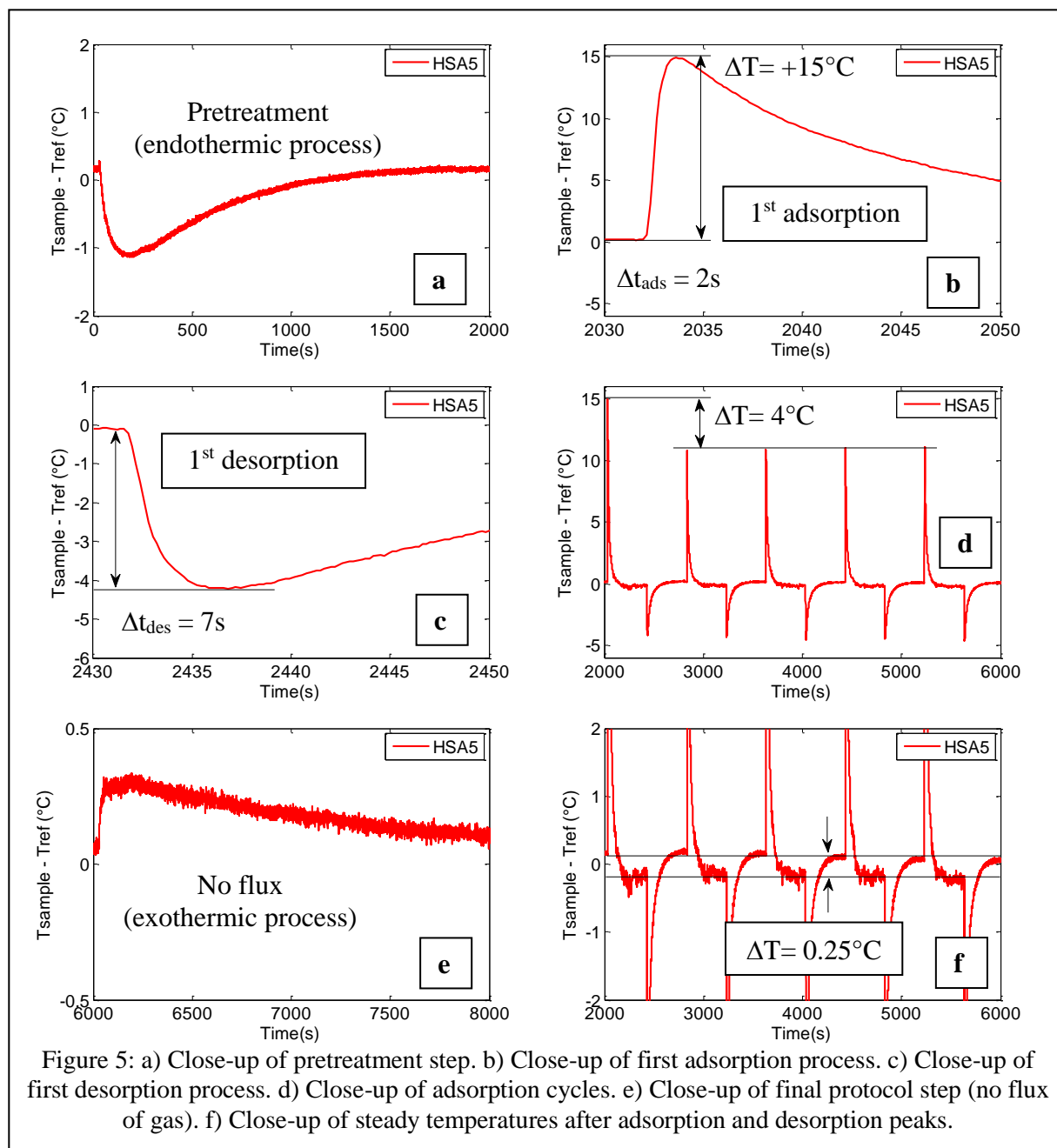
Figure 4: Thermal profile after N<sub>2</sub>/CO<sub>2</sub> injections on HSA5 at room temperature. Inset is a close-up of first adsorption and desorption of CO<sub>2</sub>.

The first N<sub>2</sub> injection (pretreatment) leads to sample temperature decrease ( $\Delta T = -1.2^\circ\text{C}$ ), characterizing thus an endothermic preprocess (see Figure 5a). This suggests desorption of contaminants from sample surface. As a first assumption, we suggest desorption of adsorbed water. After pretreatment, when the gas flow is switched to CO<sub>2</sub>, an intense ( $\Delta T = +15^\circ\text{C}$ ) and fast (2s) temperature increase is observed (see Figure 5b). This exothermic peak suggests a rapid CO<sub>2</sub> adsorption, characterized by fast heat release. Then, still under CO<sub>2</sub> flux, the sample temperature gradually decreases, suggesting a negligible heat release (saturation of adsorption capacity) or/and the influence of heat losses. After that, when N<sub>2</sub> is injected again, an endothermic temperature response is suddenly observed ( $\Delta T = -4^\circ\text{C}$ ), indicating thus CO<sub>2</sub> desorption from the sample surface (see Figure 5c). The switch from CO<sub>2</sub> flow to N<sub>2</sub> flow causes a fast decrease in CO<sub>2</sub> concentrations in the gas phase, which shifts the equilibrium towards desorption of CO<sub>2</sub>. For other adsorption/desorption cycles, the same pattern of thermal responses is observed.

The intensity of desorption peaks is weaker than that of adsorption peaks. As one can see in Figure 5b and 5c, this can be explained by distinct kinetic of adsorption ( $\Delta t_{\text{ads}} = 2\text{s}$ ) and desorption ( $\Delta t_{\text{des}} = 7\text{s}$ ). The differences between adsorption peaks (AP) and desorption peaks (DP) may be an indicator of the strength of the interaction between the adsorbed species, and thus, signaling a chemisorption process.

A difference in maximum temperature rise between the two first adsorption peaks was observed ( $\Delta T = 4^\circ\text{C}$ ), suggesting an irreversible chemisorption of CO<sub>2</sub> molecules on HSA5.

No variation of adsorption peaks was observed after the second adsorption, suggesting that the adsorption process becomes reversible (see Figure 5d).



Finally, when the gas flow was cut off, an exothermic process occurred attributed to re-adsorption of contaminants (water) from atmospheric moisture (see Figure 5e). There was observed a slight difference between the steady temperature after adsorption peaks and the steady temperature after desorption peaks ( $\Delta T = 0.25^\circ\text{C}$ ), which is represented in Figure 5f. We suggest that changes in sample emissivity may occur during  $\text{CO}_2$  adsorption. The adsorbed species may completely change the surface characteristics. The apparent temperature is thus modified. Slight changes on sample emissivity do not disturb the temperature measurements.

The thermal profiles obtained for HSA5, CePr, CeZrPr and CeLaPr thin-layers, using the same experimental protocol described before, are shown in Figure 6 a, b, c and d respectively.

The results suggest almost the same adsorption/desorption behavior for  $\text{CO}_2$ -REO interactions. Differences have been found concerning the intensity of exothermic/endothermic peaks and adsorption/desorption kinetics.

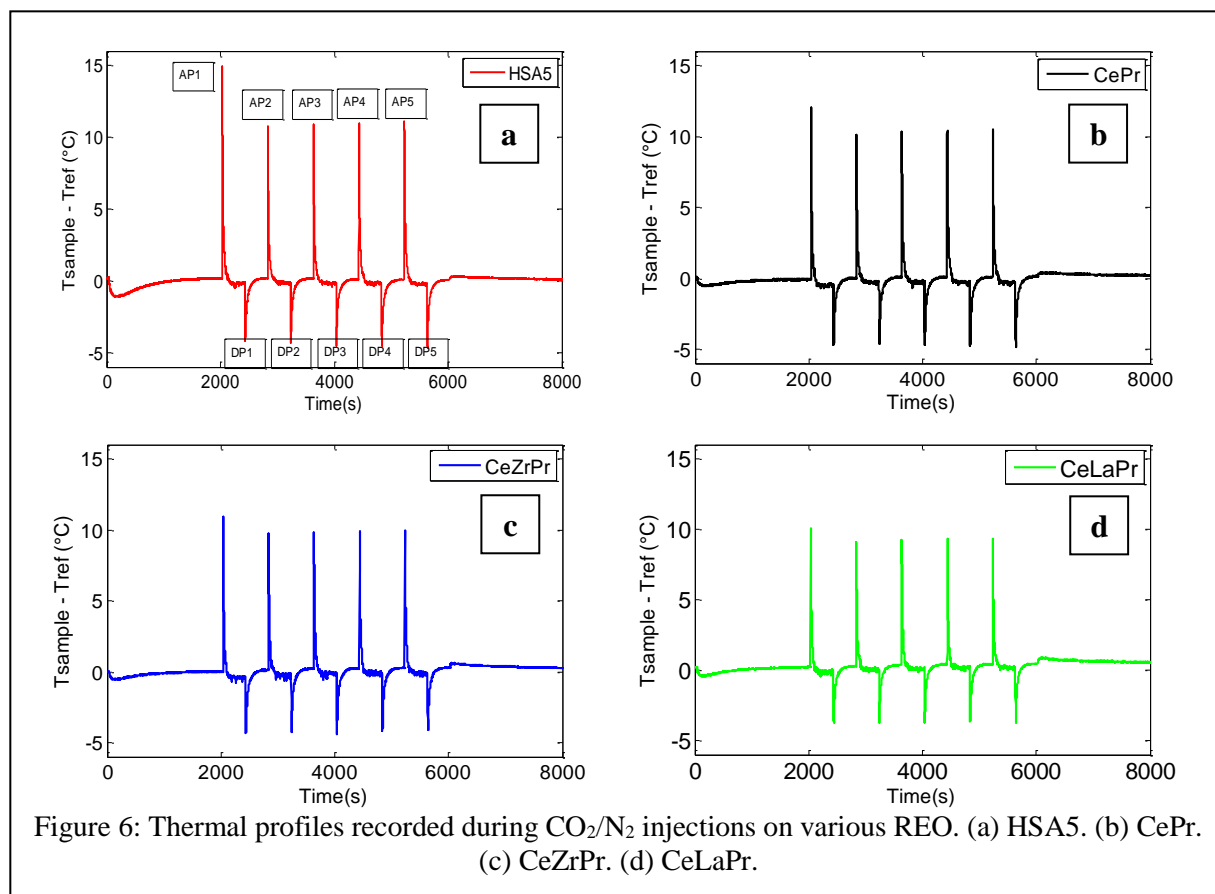


Figure 6: Thermal profiles recorded during  $\text{CO}_2/\text{N}_2$  injections on various REO. (a) HSA5. (b) CePr. (c) CeZrPr. (d) CeLaPr.

For better visualization of these results, the temperature values of the first three adsorption (AP1, AP2 and AP3) and desorption peaks (DP1, DP2 and DP3) of REO thin-layers are shown in Figures 7a and 7b. Adsorption time and desorption times values are shown in Figures 7c and 7d, for the same adsorption/desorption peaks.

In this qualitative study of REO adsorbents, we suppose as a first approach that the main  $\text{CO}_2$  adsorption/desorption process occurs during the temperature increase (adsorption) or decrease (desorption). Therefore, the adsorption/desorption process times are estimated to be equal to time intervals during which temperature increase or decrease.

Globally, the temperature values of adsorption peaks are higher than those of desorption peaks, and adsorption times are lower than desorption times. These results suggest that the adsorption process is faster than the desorption one. As will be shown later, since adsorption or desorption rates are directly related to the heat released or absorbed during adsorption or desorption process, these results suggest higher adsorption rates than desorption rates. The distinct adsorption/desorption rates have thus a significant impact on temperature intensities of adsorption/desorption processes.

As we have stated before, the first adsorption peak of REO is higher than other adsorption peaks, suggesting an irreversible chemisorption of  $\text{CO}_2$  molecules on REO. The desorption condition ( $\text{N}_2$  flux at room temperature) are not enough effective to desorb all adsorbed species formed during the first  $\text{CO}_2$  adsorption on REO. In the next adsorption, a smaller number of adsorption sites are available for  $\text{CO}_2$  adsorption. The temperature rise being proportional to the  $\text{CO}_2$  adsorbed quantity and, consequently, to heat released, adsorption peaks are thus less intense. The reproducibility of thermal responses after second injection cycle is related to possible formation of physisorbed or second-layer chemisorbed  $\text{CO}_2$ -phase,

which is less stable regarding the strength of CO<sub>2</sub>-adsorbent interactions and thus, the adsorption process becomes reversible.

The first adsorption peak for HSA5 is the most intense in comparison with others REO. This results may be explained by the specific surface area of the sample, which is the greatest of the studied samples (HSA5 = 168 m<sup>2</sup>.g<sup>-1</sup>, CePr = 150 m<sup>2</sup>.g<sup>-1</sup>, CeZrPr = 137 m<sup>2</sup>.g<sup>-1</sup> and CeLaPr = 147 m<sup>2</sup>.g<sup>-1</sup>).

Overall, doped samples (CePr, CeZrPr and CeLaPr) show higher desorption time values than undoped ceria, suggesting thus slower CO<sub>2</sub> desorption process, which can be explained by the higher basic character of these adsorbents.

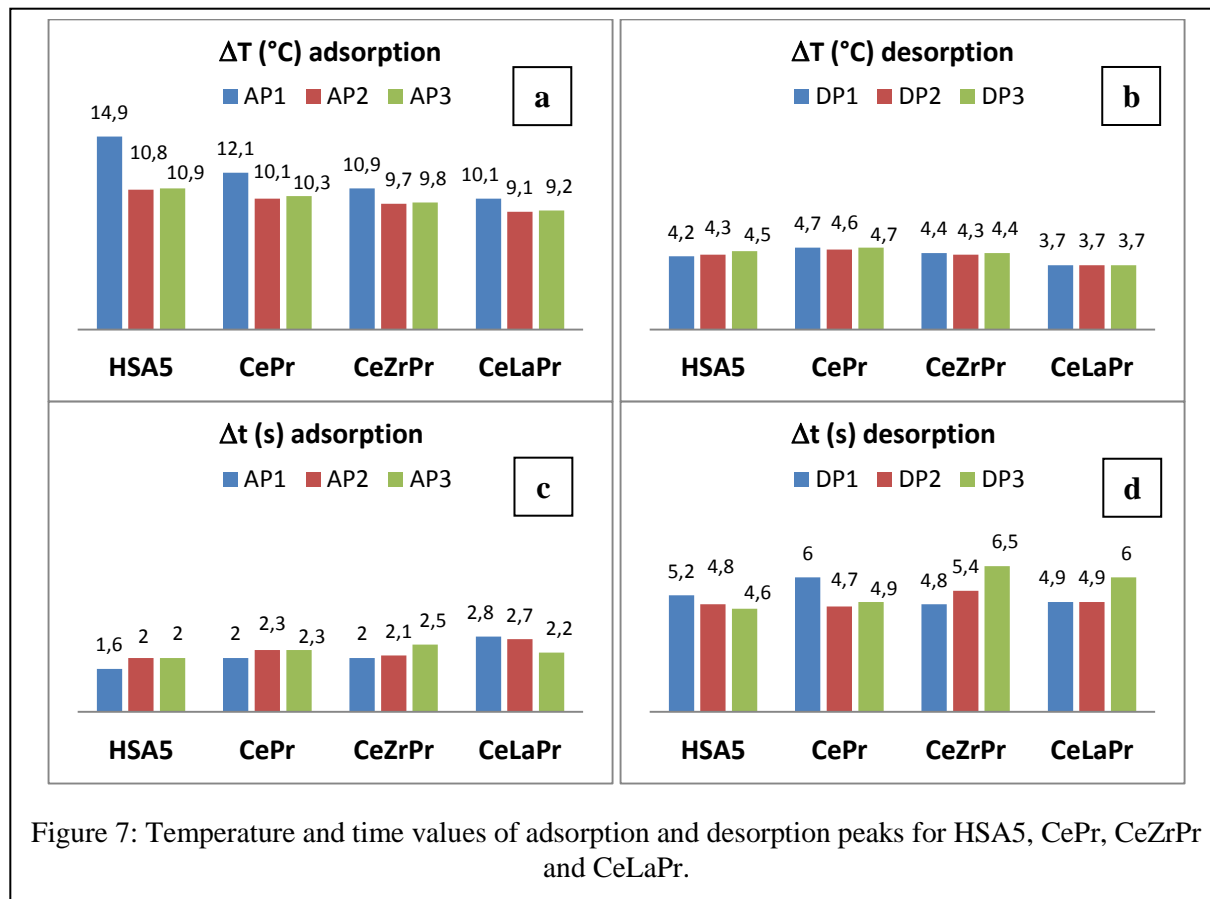


Figure 7: Temperature and time values of adsorption and desorption peaks for HSA5, CePr, CeZrPr and CeLaPr.

A study of the influence of specific surface area on thermal profiles was done. In this study, ceria samples with different specific surfaces were subjected to injection cycles of CO<sub>2</sub>/N<sub>2</sub>. The same operational conditions and experimental protocol were applied. The thermal profiles obtained for Ceria149 (149 m<sup>2</sup>.g<sup>-1</sup>), Ceria113 (113 m<sup>2</sup>.g<sup>-1</sup>), Ceria96 (96 m<sup>2</sup>.g<sup>-1</sup>), Ceria 50 (50 m<sup>2</sup>.g<sup>-1</sup>) and Ceria32 (32 m<sup>2</sup>.g<sup>-1</sup>) are shown in Figure 8. One notices that the intensities of adsorption peaks are directly proportional to the specific surface areas of ceria samples (Figures 9a and 9b). These results suggest a linear correlation between thermal responses and specific surface area of ceria samples. Moreover, this linearity suggests that the adsorption process follows a Langmuir mechanism: a monomolecular layer covers the material surface and the adsorbed CO<sub>2</sub> is proportional to the specific surface area (see chapter II: Adsorption isotherms).

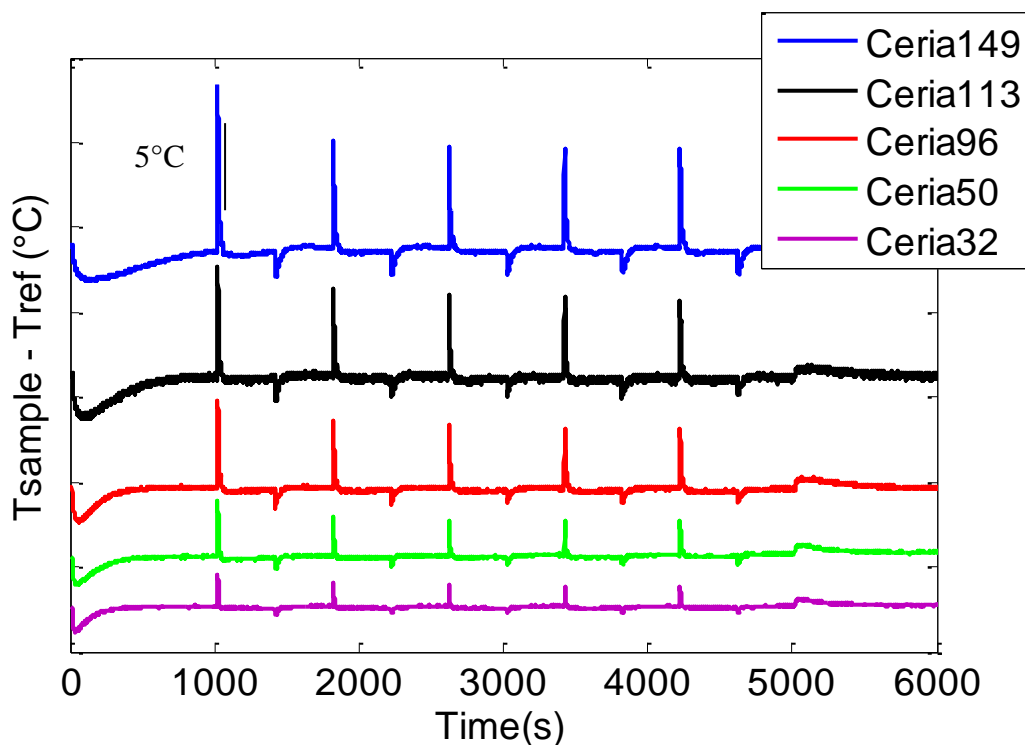


Figure 8: Temperature profiles obtained during subsequent CO<sub>2</sub> injections on ceria samples with different specific surface areas.

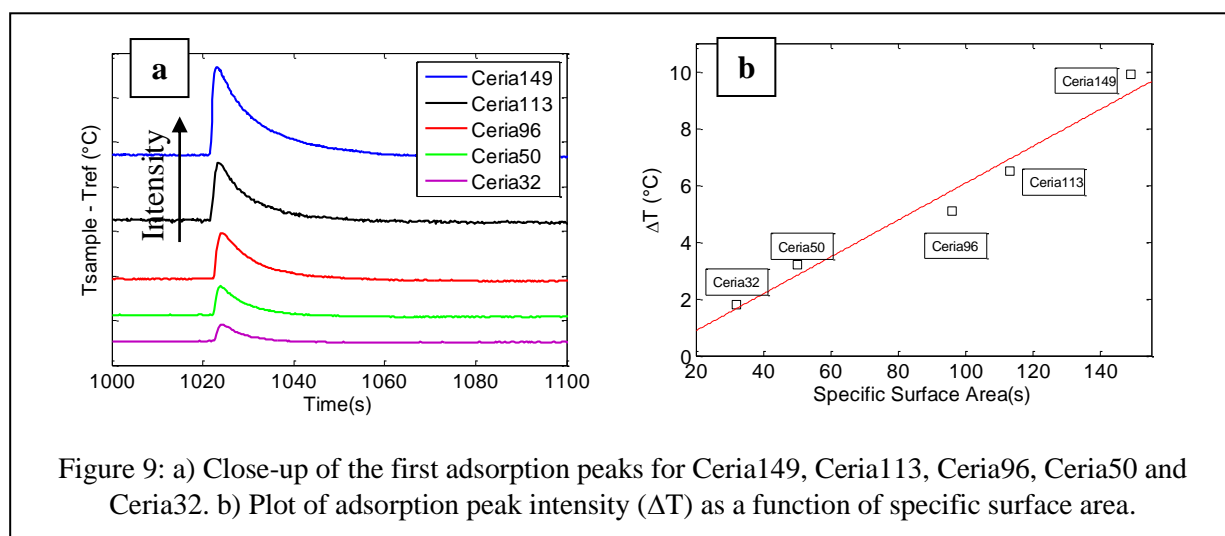


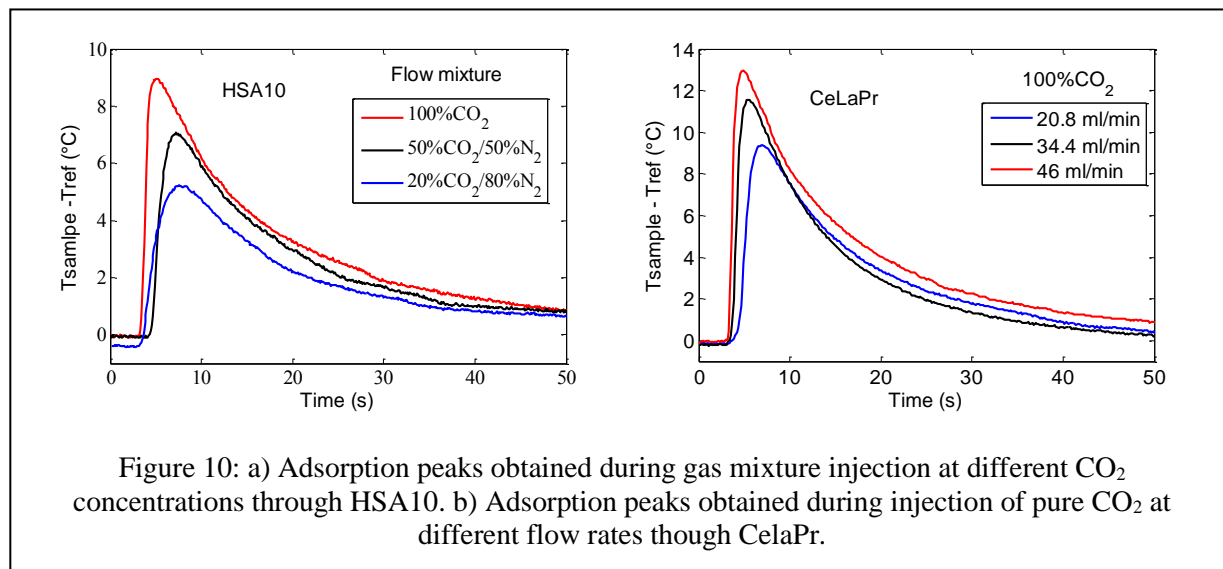
Figure 9: a) Close-up of the first adsorption peaks for Ceria149, Ceria113, Ceria96, Ceria50 and Ceria32. b) Plot of adsorption peak intensity ( $\Delta T$ ) as a function of specific surface area.

The influence of operational conditions on adsorption peaks has been also reported. In Figure 10a, we show the first adsorption peaks obtained during injection of gas mixtures (diluted CO<sub>2</sub> in N<sub>2</sub>) at different CO<sub>2</sub> concentrations, through HSA10 thin layer ( $m = 114$  mg, surface area =  $109 \text{ m}^2 \cdot \text{g}^{-1}$ ), and in Figure 10b, we show the first adsorption peaks obtained during injection of pure CO<sub>2</sub> for different flow rates, through CeLaPr thin layer ( $m = 60$  mg, surface area =  $147 \text{ m}^2 \cdot \text{g}^{-1}$ ).

The intensity of adsorption peaks increases with the increase of CO<sub>2</sub> concentration in the injected gas mixture. We observe the same behavior for adsorption isotherms, for which the adsorbed amount increases with the increase of CO<sub>2</sub> partial pressures. This analogy reinforces the assumption about the correlation between adsorption peaks and adsorbed amount of CO<sub>2</sub>.

Influences on kinetics of adsorption must also be noticed. The adsorption times decrease with the increase of CO<sub>2</sub> concentration ( $\Delta t_{ads}=5s$  for 20% CO<sub>2</sub> and  $\Delta t_{ads}=2s$  for 100% CO<sub>2</sub>).

The injected CO<sub>2</sub> flow rate also impacts the adsorption peaks, especially low flow rates. The CO<sub>2</sub> gas mixes with the purge gas (N<sub>2</sub>) already filling the injection system by axial dispersion, and this dilutes the CO<sub>2</sub> concentration at the flow front. Consequently, the intensity of adsorption peaks is weaker and adsorption times are longer. These results suggest that CO<sub>2</sub> adsorption on ceria adsorbents is mass transfer limited.



## 2.2.2 Hybrid organic/inorganic materials

The thermal profiles of amine supported silicas have also been examined. The study was conducted by analysis of thermal profiles before and after amine impregnation on silica supports. Figure 11 shows the thermal profile obtained during CO<sub>2</sub>/N<sub>2</sub> injection cycles on silica support Z1165. The silica thin layer (40 mg) was submitted to N<sub>2</sub> flow during 2000 s, than to five CO<sub>2</sub>/N<sub>2</sub> injection cycles (400 s of CO<sub>2</sub> + 400 s of N<sub>2</sub>). The flow meter was setup to inject a continuous flow rate of gas (40 ml.min<sup>-1</sup>).

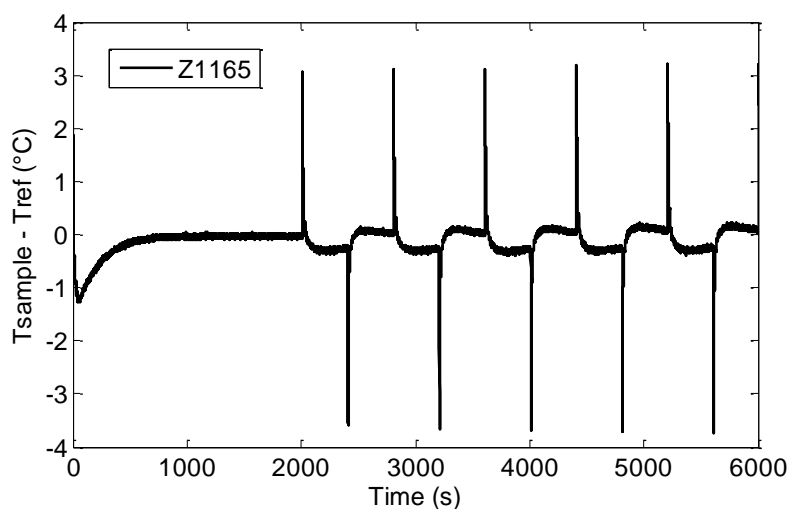


Figure 11: Thermal profile of CO<sub>2</sub> adsorption-desorption on silica support Z1165.

Weak adsorption peaks ( $\Delta T=+3^{\circ}\text{C}$ ) were obtained during  $\text{CO}_2$  adsorption/desorption on Z1165. This result confirms that  $\text{CO}_2$ -Z1165 interactions are weak. The acidic character of the silica surface does not facilitate the adsorption of acidic molecules such as  $\text{CO}_2$ .

Furthermore, desorption peaks have the same intensity that adsorption ones. This suggests identical rates of adsorption and desorption. This behavior is possible for weak  $\text{CO}_2$ -material interactions, like physisorption process.

As for REO, we have noticed a gap between steady temperatures after adsorption and desorption peaks ( $\Delta T=0.4^{\circ}\text{C}$ ). The white color of silica supports may intensify changes in sample emissivity during  $\text{CO}_2/\text{N}_2$  injections. The thermal behavior for HRS1200 silica support was also examined and similar results were found.

The acidic character of silica support is ideal for the interaction with basic molecules such as amines. In Figure 12, we show the thermal profiles obtained during  $\text{CO}_2/\text{N}_2$  injection through amine impregnated silica: 33Iminobis/Z1165 and MEA/Z1165.

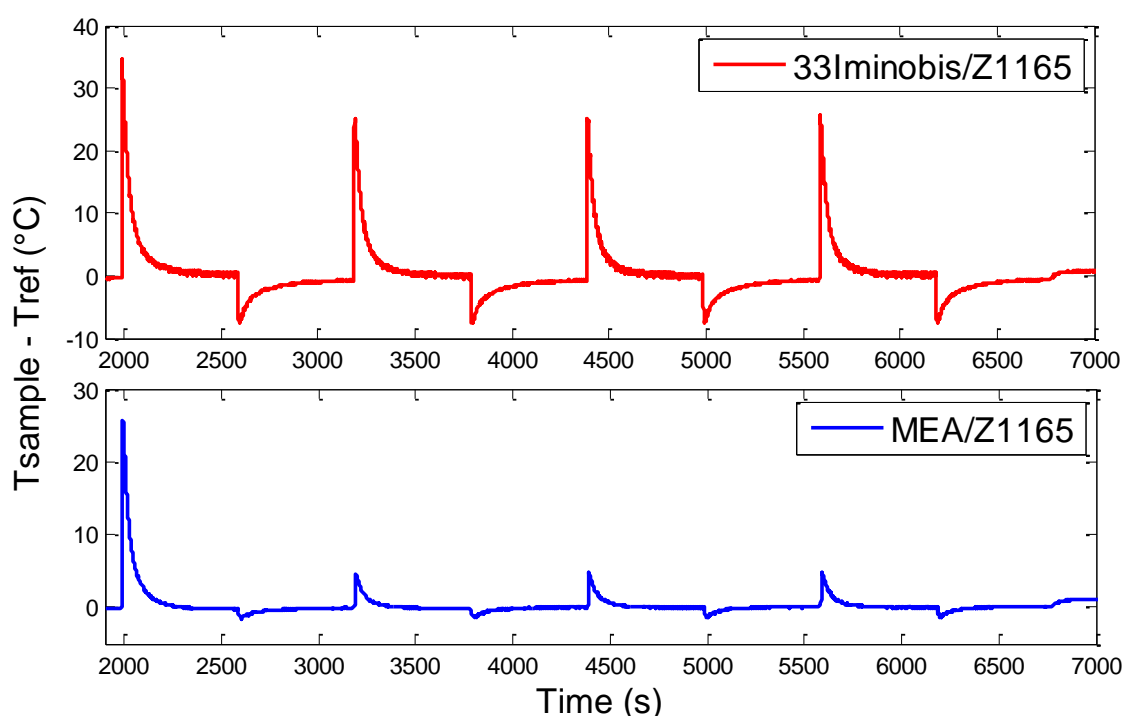


Figure 12: Thermal profiles obtained during  $\text{CO}_2/\text{N}_2$  injection cycles (400 s of  $\text{CO}_2$  + 400 s of  $\text{N}_2$ , flow rate =  $40 \text{ ml}\cdot\text{min}^{-1}$ ) through impregnated silica thin layer ( $m = 70 \text{ mg}$ ).

The thermal profiles obtained during  $\text{CO}_2$  adsorption/desorption are much more intense than those obtained on silica supports. This attests efficient impregnation of 33Iminobis and MEA on silica supports. The adsorption peaks are stronger compared to adsorption peaks obtained for rare earth oxides. These results suggest high  $\text{CO}_2$ -adsorbent interactions which are characterized by a large amount of heat released during  $\text{CO}_2$  adsorption and consequently intense adsorption peaks. As already observed for REO, a difference between the first adsorption peak and others adsorption peaks occurs, indicating thus partial irreversible adsorption. In the case of MEA/Z1165, this peak difference is much more marked ( $\Delta T = 21^{\circ}\text{C}$ ). This suggests thus higher irreversibility of  $\text{CO}_2$  adsorption. As will be shown after (DRIFT investigation), the MEA has a low thermal stability on silica support. During cycles of adsorption/desorption, the high exothermic process causes desorption of MEA molecules over Z1165 and thus the reduction of the capture efficiency of the adsorbent. After the first adsorption cycle, the adsorption peaks are therefore much less intense.

For 33Iminobis/Z1165, the intensity of desorption peaks is much less intense than that of adsorption peaks. This is a signal of distinct kinetic of adsorption and desorption ( $\Delta t_{\text{ads}} = 3.2$  s and  $\Delta t_{\text{des}} = 9.4$  s). The differences between adsorption and desorption peaks suggest slow desorption rates of CO<sub>2</sub> (by N<sub>2</sub> gas purge at room temperature) compared to adsorption rates. This also indicates a high stability of the adsorbed species on the surface, like a chemisorption process.

As already observed for REO and silica supports, a slight difference between the steady temperature after adsorption and after desorption occurs for impregnated silica. As explained before, this suggests changes in sample emissivity during CO<sub>2</sub> adsorption.

The thermal profiles of other impregnated silicas (PEI/HRS1200, 33Iminobis/HRS1200, MEA/HRS1200, DPTA-T/Z1165, PTA-YT/Z1165, DPTA/Z1165 and DPTA-O/Z1165) were also examined. Only 33Iminobis/HRS1200, DPTA/Z1165 and DPTA-O/Z1165 have shown CO<sub>2</sub> capture reversibility (case of 33Iminobis/Z1165), others hybrid materials have shown similar thermal behavior to that of MEA/Z1665, indicating thus a high irreversibility of CO<sub>2</sub> adsorption.

### 2.2.3 Activated Carbon

In order to present the most significant thermal behaviors of the studied activated carbons, we show in Figure 13 the thermal profile obtained during CO<sub>2</sub>/N<sub>2</sub> injections on AC1.

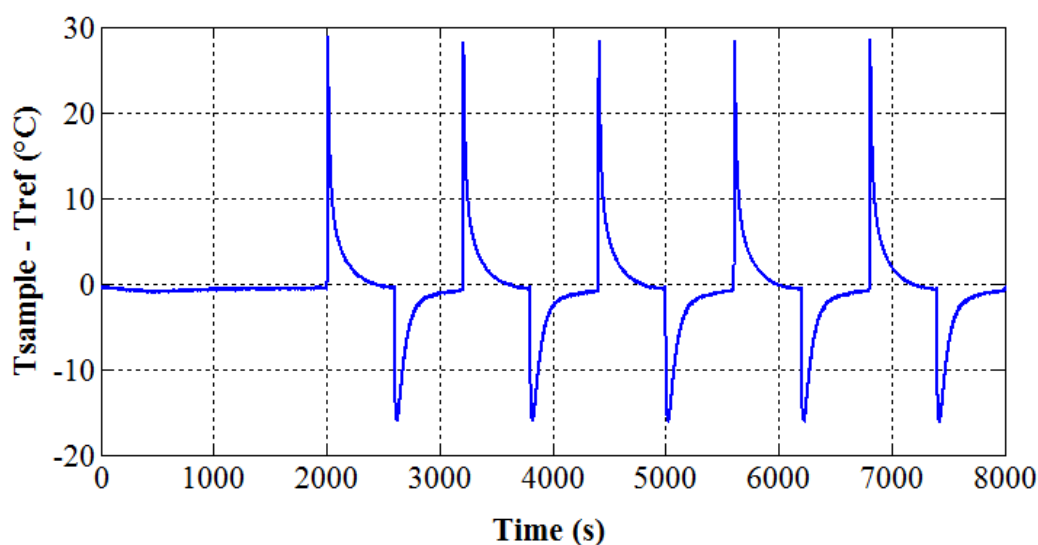


Figure 13: Thermal profile after N<sub>2</sub>/CO<sub>2</sub> injection cycles on AC1 at room temperature.

A thin layer of adsorbent (144 mg) was submitted to gas injection cycles (N<sub>2</sub> + CO<sub>2</sub>). The flow meter was setup to inject a continuous flow rate of gas (40 ml/min). The protocol was configured to starts with N<sub>2</sub> injection during 2000 s, than five injection cycles, 600 s of CO<sub>2</sub> + 600 s of N<sub>2</sub> are operated.

Strong adsorption peaks were observed ( $\Delta T = 30^\circ\text{C}$ ). This suggests large amount of heat released during CO<sub>2</sub> adsorption. As we have seen in the first chapter, activated carbons adsorb CO<sub>2</sub> via physisorption process. Since physisorption process leads to weak adsorbate-adsorbent interactions, it is thus expected lower values for heats of adsorption. For this reason, the strong adsorption peaks observed for AC1 are directly related to high adsorption rate or/and high adsorption capacity. No difference has been observed between the first adsorption peak and others adsorption peaks. Moreover, strong desorption peaks have been observed. This

suggests high desorption rates, consequently a reversible CO<sub>2</sub> adsorption and an easy CO<sub>2</sub> desorption by inert gas purge at room temperature.

Because of its black color, AC1 behaves as an ideal blackbody. No difference between the steady temperature after adsorption peaks and after desorption have been noticed for this activated carbon. This result suggests no changes in material emissivity and no chemical modification of the surface. Consequently no significant changes of surface characteristics during CO<sub>2</sub> adsorption are expected.

No significant endothermic response has been observed during pretreatment. If we consider that endothermic responses during pretreatment are related to desorption of contaminates such as adsorbed water, this results suggests a hydrophobic character of AC1.

## 2.3 Overall screening results and discussion

The maximum temperature values of adsorption peaks were used in order to identify materials having good interaction with CO<sub>2</sub> molecules. The maximum temperatures of adsorption  $\Delta T_{\max}$  are related directly to the heat released during CO<sub>2</sub> adsorption process, and are thus used as the first selection approach.

An easy way to understand the correlation between maximum adsorption temperature and released heat is to consider the heat transfer phenomena during CO<sub>2</sub> adsorption on adsorbent particle:

$$\underbrace{m_p \cdot C_{p_s} \cdot \frac{dT(t)}{dt}}_{\text{accumulation of heat}} = \underbrace{\phi(t)}_{\text{heat generated by the adsorption}} - \underbrace{h_o \cdot A_{\text{eff}} \cdot (T(t) - T_0)}_{\text{heat losses}} \quad (1)$$

where  $m_p$  is the particle mass (kg),  $C_{p_s}$  the particle heat capacity (J.kg<sup>-1</sup>.K<sup>-1</sup>),  $T(t)$  the temperature of particle (K),  $t$  the time (s),  $\phi(t)$  the adsorption heat source (W) generated by the adsorption process,  $h_o$  the overall heat transfer coefficient (W.m<sup>-2</sup>.K<sup>-1</sup>),  $A_{\text{eff}}$  the particle surface area (m<sup>2</sup>) and  $T_0$  the gas-phase temperature (K).

This simplified thermal model represents the heat balance for adsorbent particle. The adsorbent particle is assumed to be isothermal because the characteristic time for heat diffusion in the micrometer particle is very low (around 10<sup>-3</sup> s).

Assuming that the main release of heat is during rising temperature period, the integration of equation 1 from the start of adsorption process ( $t_0$ ) to the time at maximum temperature ( $t_{\max}$ ) gives the following expression:

$$m_p \cdot C_{p_s} \cdot \int_{t_0}^{t_{\max}} dT(t) = \int_{t_0}^{t_{\max}} \phi(t) dt - \int_{t_0}^{t_{\max}} h_o \cdot A_{\text{eff}} \cdot (T(t) - T_0) dt \quad (2)$$

Resulting in:

$$m_p \cdot C_{p_s} \cdot \Delta T_{\max} = Q - \int H dt \quad (3)$$

where  $Q$  is the accumulated adsorption energy (J), which represents the total amount of heat generated during adsorption process and  $\int H dt$  is the accumulated heat losses (J).

From equation 3, we state a correlation between the total amount of released heat  $Q$  and the maximum temperature of adsorption peak  $\Delta T_{\max}$ . Even though the presented heat equation does not take into account other important parameters, it allows easy visualization of the relationship between  $\Delta T_{\max}$  and the release of heat during CO<sub>2</sub> adsorption. A more detailed and accurate study of the heat transfer in the thin-layer of adsorbent will be presented in the next chapter.

Therefore, using the same operational conditions (thin-layer mass and injected gas flow rate), we can compare the temperature adsorption peak obtained during CO<sub>2</sub> adsorption for each studied material. This procedure allows the selection of adsorbents developing affinity towards CO<sub>2</sub> molecules. The  $\Delta T_{\max}$  values for two adsorption cycles are shown in Figure 14.

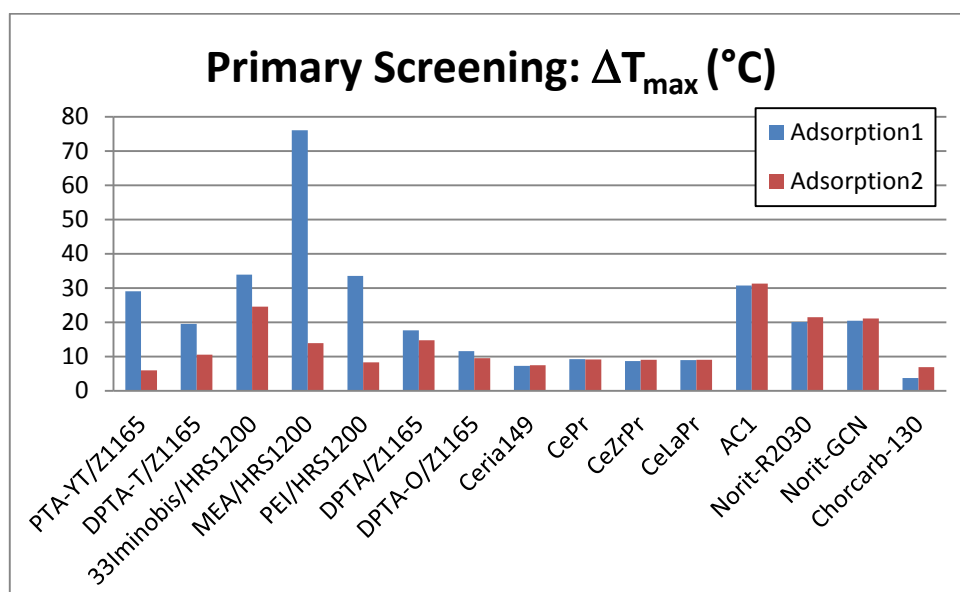


Figure 14: Overall screening of studies material. The first two adsorption peaks are shown for each material. Adsorption peaks were obtained during CO<sub>2</sub> injection (40ml.min<sup>-1</sup>) through adsorbent thin-layer (70 mg).

The comparison between first and second adsorption peak allows us to make assumptions about CO<sub>2</sub> adsorption reversibility.

Overall, we state that CO<sub>2</sub> adsorption on hybrid materials (amine supported silica) have led to the highest  $\Delta T_{\max}$  values for the first adsorption cycle. Particularly for MEA/HRS1200 which have developed the first most intense adsorption peak. However, the second adsorption has led to much weaker  $\Delta T_{\max}$ . This result suggests high adsorption irreversibility on this material. CO<sub>2</sub> adsorptions on PTA-YT/Z1165 and PEI/HRS1200 have led also to large difference between  $\Delta T_{\max}$  values, suggesting thus capture irreversibly.

Among hybrid materials, only 33Iminobis/HRS1200 has developed intense  $\Delta T_{\max}$  values in the first and second adsorption cycle. These results indicate thus high affinity towards CO<sub>2</sub> molecules and good capture reversibility.

Activated carbons have developed the second most intense adsorption peaks, with CO<sub>2</sub> capture reversibility.

The weakest  $\Delta T_{\max}$  values have been observed for rare earth oxides. This result suggests low adsorption capacity for REO.

## 2.4 Summary and conclusions

In this first part of our study, assumptions about adsorption behaviors have been done thanks to qualitative analysis of thermal profiles on thin-layers of adsorbents. Thanks to maximum temperature of adsorption, we have identified the materials having good affinity with CO<sub>2</sub> molecules.

Adsorption and desorption peaks are directly correlated to the heat released or absorbed, consequently to adsorption or desorption behaviors. Various parameters influence the quantity of heat released:

- CO<sub>2</sub> concentration in gas-phase;
- Gas flow rate;
- Specific surface area;
- Adsorption and desorption rates;
- Nature of interaction (physisorption/chemisorption);

Each family of studied materials has shown specific adsorption behaviors. The main assumptions are described below.

CO<sub>2</sub> adsorption on REO is a chemisorption process. The rates of adsorption are higher than those of desorption. The release of heat during CO<sub>2</sub> adsorption is the lowest among studied materials. REO show a partial CO<sub>2</sub> capture reversibility.

CO<sub>2</sub> adsorption on amine impregnated silicas is also a chemisorption process. The rates of adsorption are also higher than those of desorption. The release of heat during CO<sub>2</sub> adsorption is the highest among the studied materials. Impregnated silica show a partial CO<sub>2</sub> capture reversibility. The capture reversibility and release of heat are strongly influenced by the type of impregnated-amine on silica supports.

CO<sub>2</sub> adsorption on activated carbons is a physisorption process. The rates of adsorption are not much higher than those of desorption. High release of heat during CO<sub>2</sub> adsorption is also observed, which is related to fast adsorption kinetics. Activated carbons show full CO<sub>2</sub> capture reversibility.

In order to validate a part of the assumptions described above, and obtain data on mass transfer, we proceed to the second step of our study, the “secondary screening”.

### 3 Secondary Screening: Evaluation of Adsorption Capacities

#### 3.1 Experimental device

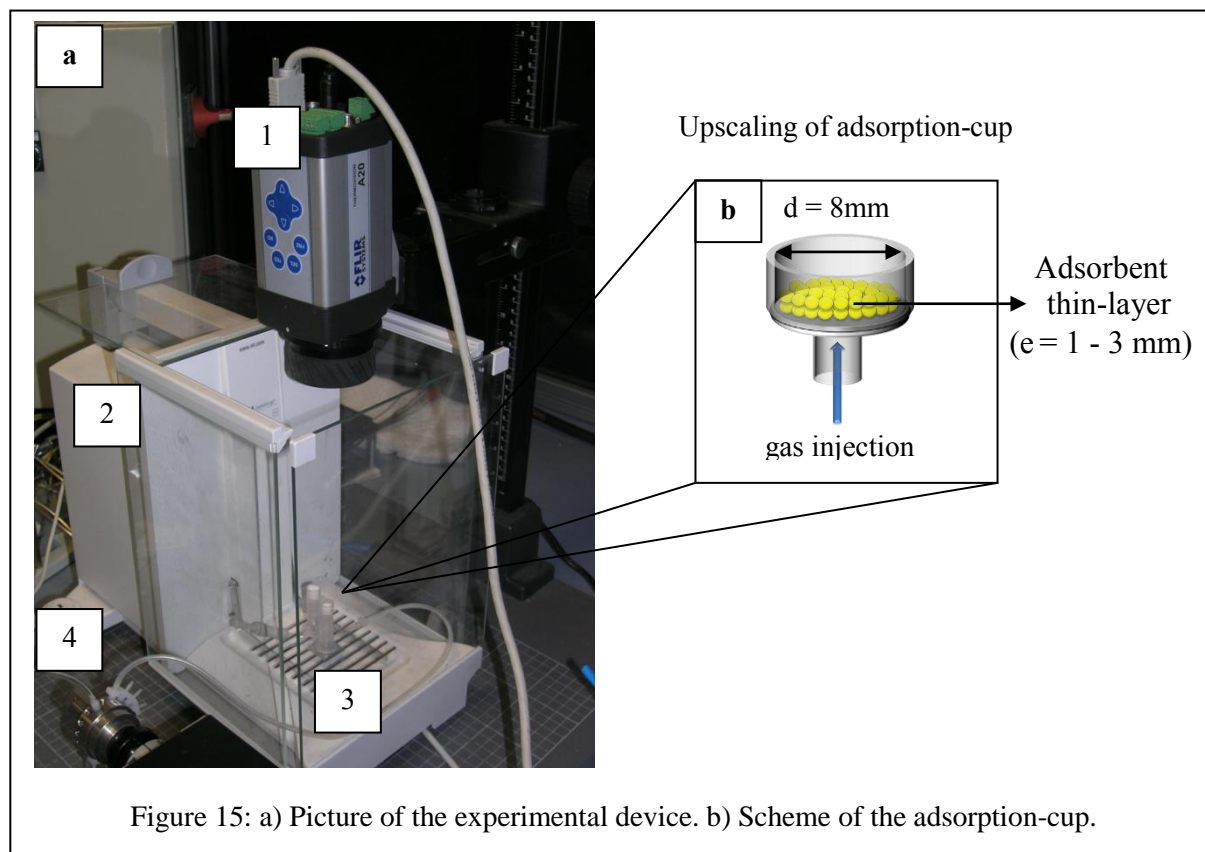


Figure 15: a) Picture of the experimental device. b) Scheme of the adsorption-cup.

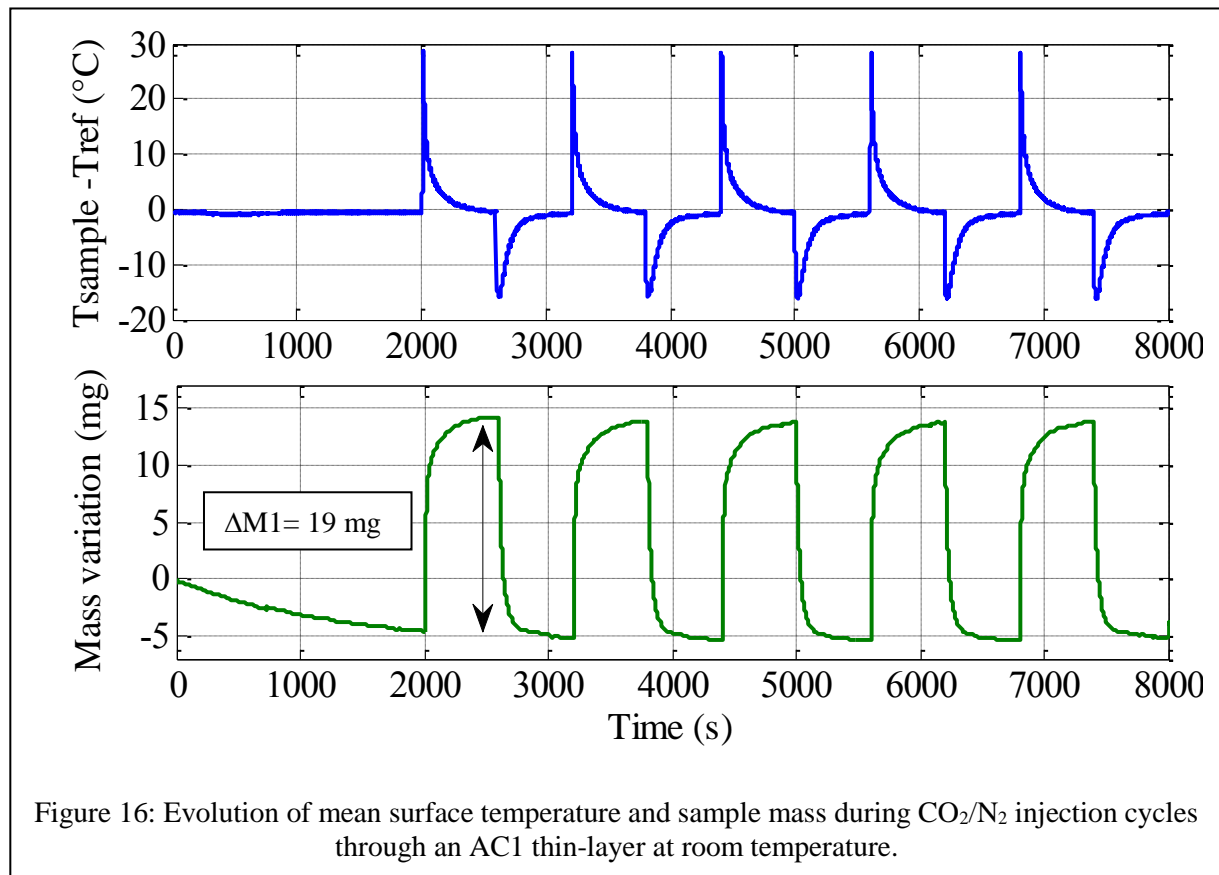
In the secondary screening step, the same infrared camera was used (FLIR A20M, Figure 15: number 1) and coupled with a precision weighing balance (METTLER TOLEDO XS204 DeltaRange, Figure. 15: number 2) to record simultaneously the average temperature and the mass variation of a thin layer of adsorbent during  $\text{CO}_2$  adsorptions and desorptions at room temperature. The principle of differential temperature measurement is maintained for this device (sampling rate = 12 Hz). The sample mass variation is associated with adsorbed-phase evolution during  $\text{CO}_2$  adsorption/desorption. The precision balance measures the sample mass, and, thanks to home-made Labview interface, the sample mass evolution is recorded (sampling-rate = 1 Hz). Two filtering cartridges filled with a thin layer of adsorbent (thickness= 1 - 3 mm) are placed on the balance scale pan (Figure. 15: number 3) and one of them is connected with the gas injection system (Figure. 15: number 4). The same injection system as the one used in primary screening (multi-position valve, flow meters and 3-way valves) allows the switch on either  $\text{CO}_2$  gas or  $\text{N}_2$  gas with a controlled injection time (home-made Labview interface).

This device allows thus *in-situ* measurements of the amount of adsorbed  $\text{CO}_2$  and of the material surface temperature as a function of a specific protocol (cycles of  $\text{CO}_2$  adsorption/desorption).

## 3.2 Results and discussion

### 3.2.1 Activated Carbon

Figure 16 shows average temperature and mass variation recorded during CO<sub>2</sub> adsorption and desorptions on an AC1 thin-layer. The same experimental protocol, as used in primary screening, was employed: pretreatment under inert gas (2000 seconds under N<sub>2</sub> flow), than five adsorption cycles (600 s of CO<sub>2</sub> + 600 s of N<sub>2</sub>, flow rate = 40 ml.min<sup>-1</sup>, thin-layer mass = 144 mg).



As already seen in primary screening, CO<sub>2</sub> injections through an adsorbent thin-layer have led to exothermic peaks (adsorption peaks). We state from recorded data that adsorption peaks have been followed by intense mass uptake during the first seconds of adsorption. This time interval corresponds in general to the defined adsorption time in primary screening (time of temperature rise). The mass uptake corresponds to adsorbed-phase evolution on adsorbent surface (CO<sub>2</sub> loading). The results confirm that the heat released during CO<sub>2</sub> adsorption is related to adsorption rates. High mass variation means high adsorption rate, consequently intense heat release. After this short-time, a progressive mass uptake has been observed, which led to low or negligible heat release. The influence of heat losses on thermal behavior is higher than that of heat source (heat released) and then, a gradual temperature relaxation has thus been observed.

During N<sub>2</sub> injections, endothermic peaks (desorption peaks) and mass losses have been observed. These results confirm CO<sub>2</sub> desorption from the adsorbent surface.

Identical mass variations during subsequent adsorption cycles have been observed (Table 1). The mass uptake profiles confirm thus reversible CO<sub>2</sub> capture by AC1 under inert gas flow only, without temperature swing.

Table 1: Mass variation values for CO<sub>2</sub> adsorption cycles on AC1.

Adsorption Cycle	$\Delta M$ (mg)
1	18,8
2	19
3	19,1
4	19,1
5	19,2

As will be shown in the next chapter, thanks to quantitative analysis of temperature and mass profiles, we will show that the adsorption rates are higher than desorption ones. This result will confirm the dissymmetry observed between adsorption and desorption peaks.

Mass losses have been observed during pretreatment. However, no significant endothermic responses have been observed in the presented thermal profile. This suggests low interactions between contaminates (adsorbed water) and AC1. No thermal responses have been thus observed.

Note: the assumption about hydrophobic character of AC1 will be confirmed by DRIFT analysis and will be presented later on (*Chapter V: investigation level I*).

From the presented mass variation profile, using the equation below, we have estimated an average adsorption capacity ( $C_{ads}$ ) equals to 132 mg<sub>CO<sub>2</sub></sub>/g<sub>ads</sub> (milligram of CO<sub>2</sub> per gram of adsorbent) for the tested AC1 sample.

$$C_{ads} = \frac{\Delta M}{m_s} \quad (4)$$

where  $\Delta M$  is the mass variation (mg) (see Figure 16) and  $m_s$  the thin-layer mass (g).

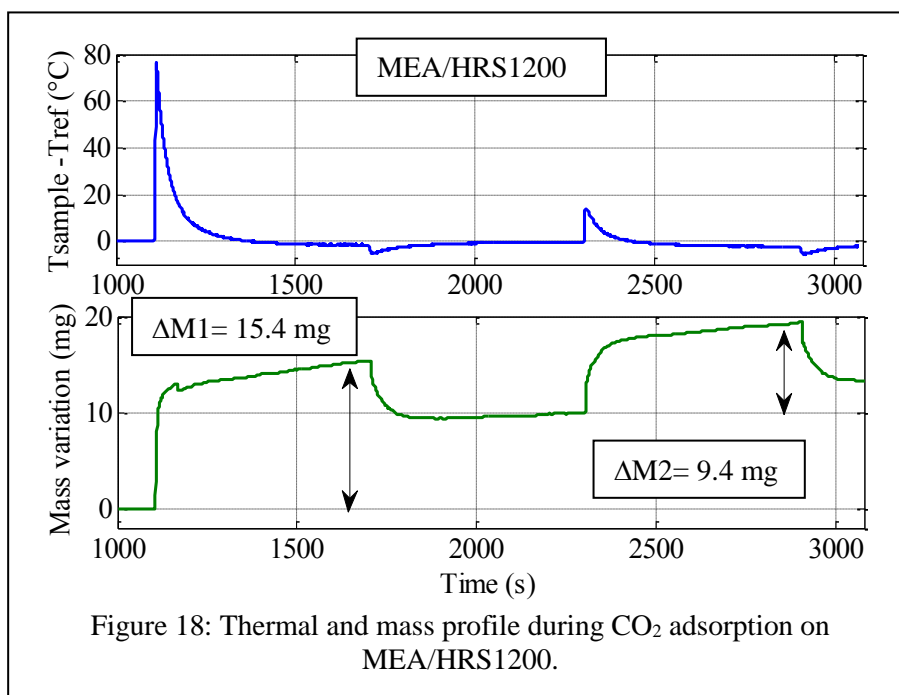
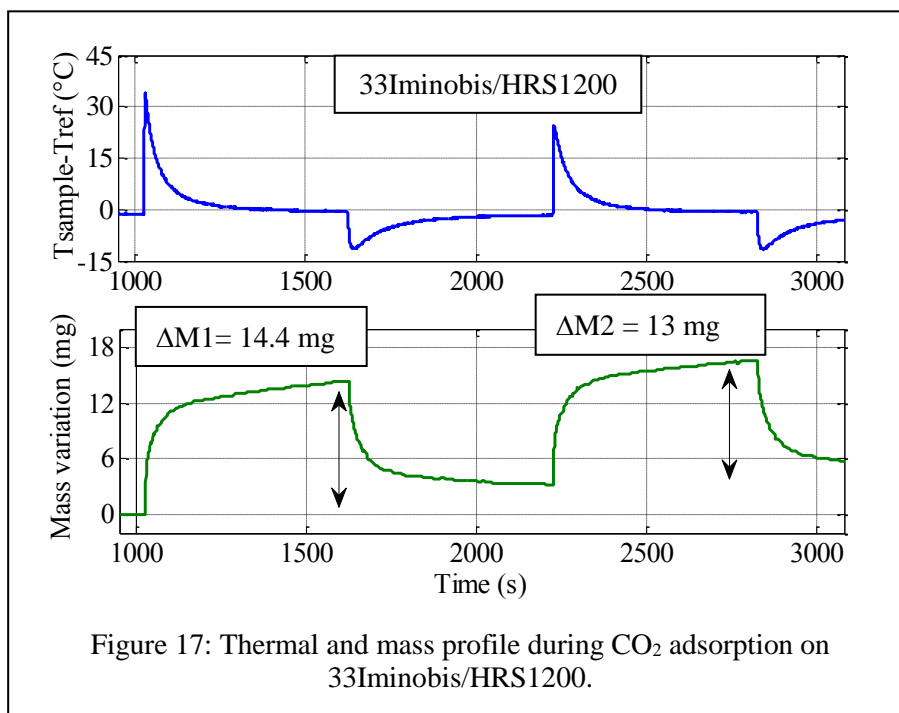
### 3.2.2 Hybrid organic/inorganic materials

The coupled analysis of thermal and mass variation profiles allowed the verification of assumptions about adsorption behavior previously done in primary screening. The obtained results for 33Iminobis/HRS1200 and MEA/HRS1200 silicas are shown in Figures 17 and 18.

The thin-layer of adsorbents were submitted to two adsorption cycles (600 s of CO<sub>2</sub> + 400 s of N<sub>2</sub>, flow rate = 40 ml.min<sup>-1</sup>, thin-layer mass = 70 mg).

As already seen for AC1, CO<sub>2</sub> injections on amine impregnated silicas have led to adsorption peaks followed by simultaneous mass uptake, and N<sub>2</sub> injections have led to desorption peaks followed by mass loss. The first adsorption peaks were higher than second adsorption peaks. From primary screening data, it has been suggested CO<sub>2</sub> capture irreversibility.

As we can observe from mass profiles, the mass variation for second adsorption ( $\Delta M_2$ ) is lower than first adsorption ( $\Delta M_1$ ). The adsorption capacities were thus reduced between first and second adsorption. This proves the correlation between the adsorption peaks and the adsorbed amount of CO<sub>2</sub>.



In the case of 33Iminobis/HRS1200, a small difference in intensity has been found between adsorption peaks. This result is in accordance with the low difference between first and second mass variation ( $\Delta M1 - \Delta M2 = 1.4$  mg).

In the case of MEA/HRS1200, as already observed in primary screening, a significant difference between adsorption peaks has been observed. This result is also in accordance with the large difference between first and second mass variation ( $\Delta M1 - \Delta M2 = 6$  mg). These results allow thus to confirm the low thermal stability of impregnated MEA on silica support.

### 3.2.3 Rare Earth oxides

The same experimental protocol has been used to study rare earth oxides. The thermal and mass profile of CeLaPr and CeZrPr are shown in Figure 19. As we can see, the thermal and mass evolution behaviors are similar to those observed for AC1 and amine-impregnated silicas. However, the mass variations during CO<sub>2</sub> adsorption are weaker than those measured for previous materials (over 5 mg). These results are in agreement with lower adsorption peaks (over 10 °C).

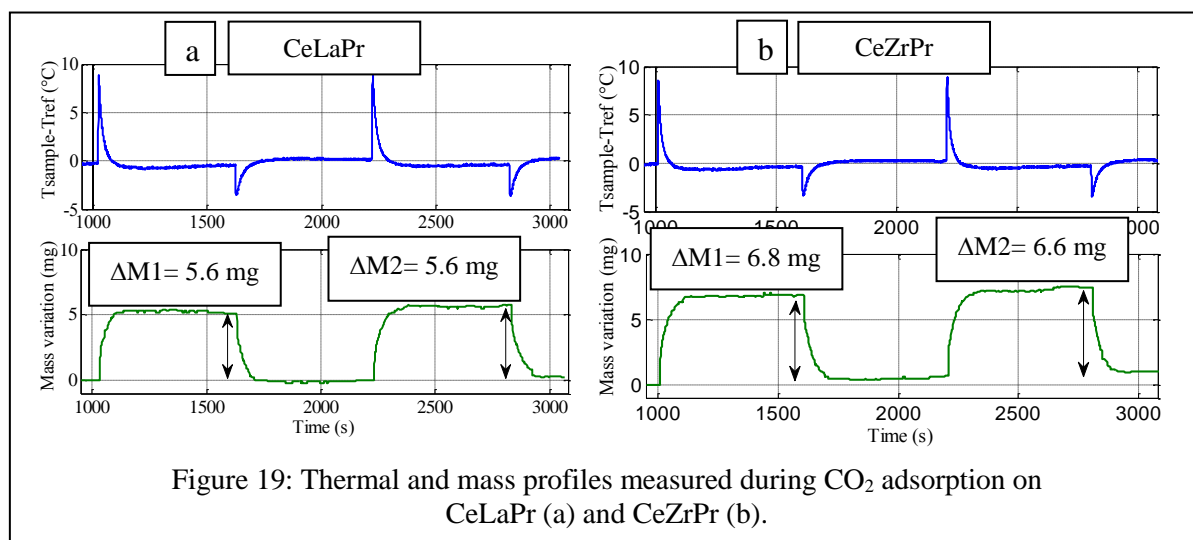


Figure 19: Thermal and mass profiles measured during CO<sub>2</sub> adsorption on CeLaPr (a) and CeZrPr (b).

### 3.3 Overall screening results and discussion

In order to verify the consistency of the mass measurement technique, we have decided to run the experimental device using full experimental protocol without adsorbent filling the adsorption cup (successive gas injections on empty adsorption cup). We have observed a systematic mass variation tendency. We can explain it by an axial thrust observed during gas injection. This force is detected as weight gain by the balance.

This systematic weight gain was thus deducted from mass variation during CO<sub>2</sub> adsorption on adsorbent thin-layer to certainly estimate the adsorption capacity for studied materials. The value of systematic weight gain has been evaluated in few milligrams. If the adsorption capacities of adsorbents are small, which is the case of rare earth oxides, the results may thus be not accurate. Moreover, when the mass of adsorbent is small (thin-layer of adsorbent) the changes in weight can be as small as milligrams or tenths of milligrams, which is close to the sensitivity limits of the balance.

Despite these technical limitations, we have successfully estimated the adsorption capacities of most of studies materials. The adsorption capacities of studied materials for two adsorption cycles are shown in Figure 20.

The results below are in accordance with results obtained from the primary screening. The adsorption capacities of materials are globally related to maximum temperature of adsorptions shown in Figure 14.

Special attention is given to 33Iminobis/HRS1200 and AC1, which have shown the highest adsorption capacities in both adsorption cycles. These results confirm thus the reversibility of the CO<sub>2</sub> capture by these two materials.

Rare earth oxides have shown much lower adsorption capacities. Technique limitations (due to systematic weight errors) may be source of low accuracy of measurements.

Indeed, for some materials (PEI/HRS1200, DPTA-O/ZII65 and Chorc carb-130) the adsorption capacities could not be estimated because the mass variations during CO<sub>2</sub> adsorption were smaller than the systematic weight gain (5 mg).

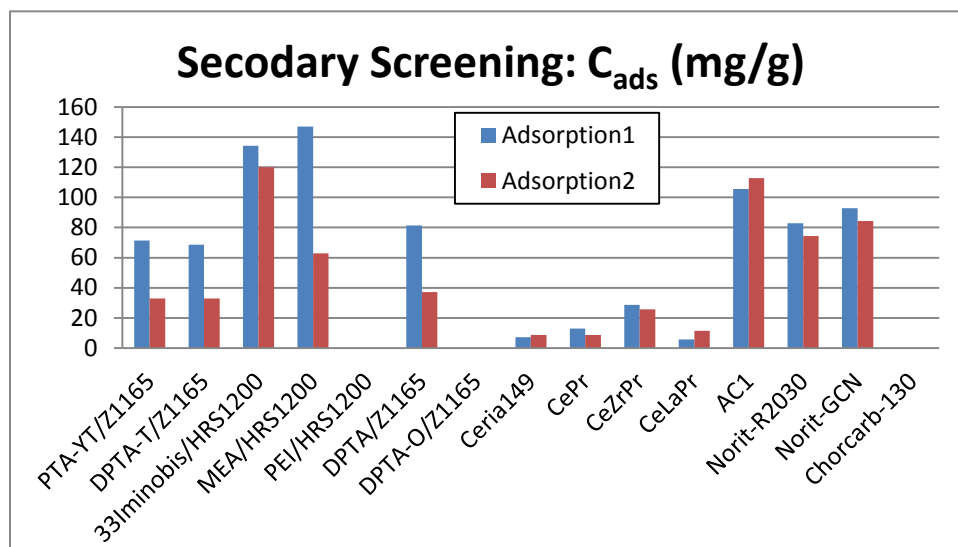


Figure 20: Overall screening of studied materials. The adsorption capacities have been estimated for two adsorption cycles (600 s of CO<sub>2</sub> + 400 s of N<sub>2</sub>, flow rate = 40 ml.min<sup>-1</sup>, thin-layer mass = 70 mg).

### 3.4 Summary and conclusions

In this second part of our study, thanks to IR thermography and gravimetric technique, we have confirmed a part of the assumption previous done after primary screening, and we also have estimated the adsorption capacities of studied materials.

A systematic error of 5 mg has been detected during mass measurements. This is related to axial thrust observed during gas injection, which is detected as weight gain by the balance. Therefore, the adsorption capacities of studied materials have been estimated taking into account this technical limitation.

The analyses of thermal and mass variation profiles led us to the following conclusions:

- The adsorption peaks are related to CO<sub>2</sub> adsorbed loading: CO<sub>2</sub> adsorption leads to exothermic peaks and mass uptake. CO<sub>2</sub> desorption leads to endothermic peaks and mass loss;
- Globally, the mass uptake/loss rates are correlated to temperature evolutions: in short-time adsorption, we observe fast evolution of temperature and sample mass. In long-time adsorption, we observe a slow evolution of temperature and sample mass. These results confirm that adsorption/desorption rates are directly related to heat release;
- The adsorption capacities of materials are globally related to  $\Delta T_{\max}$  values, consequently to the release of heat.
- AC1: identical mass variations measured during adsorption cycles confirm CO<sub>2</sub> capture reversibility on this material;
- Amine impregnated silicas: the adsorption capacities were reduced between first and second adsorption. The results confirm partial CO<sub>2</sub> capture reversibility or thermal instability of impregnated amine;

- Rare earth oxides have shown the lowest adsorption capacities.

Activated carbon and amine impregnated silicas have shown the highest adsorption capacities. The stability of amine on silica supports influences the adsorption capacity and capture reversibility.

Special attention is given to 33Iminobis/HRS1200 and AC1. These materials show both high adsorption capacity and capture reversibility.

## **4 Final Conclusions**

Primary Screening and Secondary Screening allowed us to perform the study of adsorption behaviors of studied materials by means of original experimental approaches.

The analysis of thermal and mass variation profiles during CO<sub>2</sub> adsorptions proved to be a very interesting approach for high-throughput studies of materials.

We have thus identified many influencing parameters controlling CO<sub>2</sub>-adsorbent interactions (CO<sub>2</sub> concentration in gas-phase, gas flow rate, specific surface area, adsorption and desorption rates, interaction nature) and promising adsorbents to reversible CO<sub>2</sub> capture at low temperature (AC1 and 33Iminobis/HRS1200).

This first step of study was based on qualitative analysis. In the next chapter, thanks to thermal modeling and parameter estimation, in-depth analysis of experimental data will be done and a quantitative analysis will be achieved.



## **CHAPTER IV**

-

### **Modeling Adsorption on Thin-Layer and Estimation of Key Parameters**



## SUMMARY

1	Introduction .....	101
2	Thin-layer Approach .....	101
3	Simplified analysis of experimental data .....	103
4	Adsorption heat estimation.....	105
4.1	General approach to estimate adsorption heats .....	106
4.2	Results and discussion .....	108
4.3	Parameters influencing adsorption heat estimation .....	112
5	Parameters influencing temperature evolution.....	115
6	Key parameters for material selection.....	121
7	Conclusions .....	127
8	Annex .....	128



## 1 Introduction

In the previous chapter, temperature and mass evolution of adsorbent thin-layer during CO<sub>2</sub> adsorption were recorded. Thanks to qualitative analysis of thermal and mass variation profiles, the first assumptions about adsorption behaviors were done.

In this chapter the objective is a better understanding of adsorption behaviors by means of in-depth analysis of experimental data. Many parameters influencing adsorption, such as the heat of adsorption, will be quantified. The analysis is based on the heat transfer during CO<sub>2</sub> adsorption on adsorbent thin-layer.

As already presented in chapter II, the heat of adsorption may be measured by calorimetric techniques or estimated via adsorption isotherms. Both methods are widely used, but high cost equipments and time-consuming experiments are necessary, hindering the use of high-throughput methodologies. Many authors have utilized the simultaneous solution of a set of coupled nonlinear partial differential equations (PDEs) based on heat and mass balances to predict the adsorption column dynamics. However the balance equations take into account complex phenomena (e.g. diffusion, dispersion...) and thus many parameters have to be used as an input in the models. Moreover, these parameters are hardly measured or estimated. A direct methodology is used by these authors, which consists in fitting experimental results (adsorbent temperature and gas-phase concentration) with the mentioned PDEs. The disadvantage of this method is the use of adjustable parameters. The experimental data are usually recorded by thermocouples and gas-phase analyzer along the model adsorber. The intrusiveness and the influence of thermocouple thermal inertia may be a limitation for transient measurements such as adsorption processes.

Taking notice of these inconveniences, we have decided to base our approach on high-throughput strategy. Thanks to thin-layer approach, we have developed a simplified thermal model. It means, an analytical model with reduced number of parameters to be analyzed and estimated, in order to obtain a deeper insight into the physical behavior of CO<sub>2</sub> adsorption.

## 2 Thin-layer Approach

In the secondary screening, the infrared camera was coupled with a precision balance to record the average surface temperature and mass variation during CO<sub>2</sub> adsorptions and desorptions at room temperature on a thin-layer of adsorbent (Figure 1).

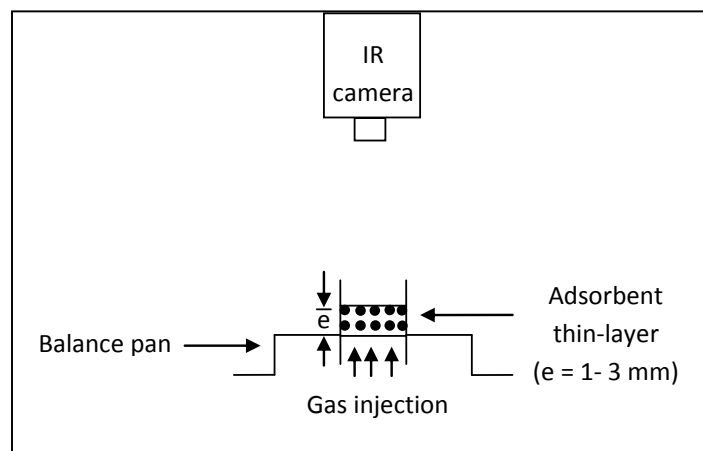


Figure 1: Schema of secondary screening device.

Concerning the heat transfer between the gas-phase and adsorbent grains, the internal resistance (adsorbent grain) is negligible compared with the external resistance (gas-phase) and the grain temperature is thus assumed as isothermal. Moreover, as already presented, the characteristic time for heat diffusion in the micrometer particle is very low (around  $10^{-3}$  s).

As our experimental device leads to CO<sub>2</sub> adsorption on a thin layer of adsorbent, we assumed that there is no temperature gradient in the layer thickness direction. The heat diffusion and dispersion in layer direction can be thus neglected.

An average temperature of the thin layer surface is recorded by the IR camera. The averaging of surface temperatures allows to take into account the heat diffusion in the direction of the plane.

We assume also that the accumulation of heat in the gas-phase is negligible compared with that in the solid adsorbent [127].

Even though heat capacity ( $C_p$ ) varies with temperature, we assume it as a constant physical property, as already done in many other thermal models in the literature. The adsorbed-phase heat capacity ( $C_{p_a}$ ) is set equal to gas-phase heat capacity.

In order to estimate the adsorbed-phase loading ( $q$ ), CO<sub>2</sub> is considered as an ideal gas. The mass variation obtained via the balance (mg) can be thus converted to molar concentration (mol).

Heat loss is negligible in large industrial columns which operate under near adiabatic conditions, contrary to our millimetric scale device. An overall heat transfer coefficient ( $h_0$ ) is thus used to express heat losses.

With these assumptions, the thermal problem can be rewritten as a lumped body model. It means that the thin-layer is substantially isothermal at any instant:

$$\underbrace{\frac{d[(m_s.Cp_s + m_s.Cp_a.q(t)).\bar{T}_s(t)]}{dt}}_{\text{accumulation of heat}} = \underbrace{\phi(t)}_{\text{heat generated by the adsorption}} - \underbrace{h_0(t).A_{eff}.\left(\bar{T}_s(t) - T_\infty\right)}_{\text{heat losses}} \quad (1)$$

where  $m_s$  is the thin-layer mass (kg),  $C_{p_s}$  the adsorbent heat capacity ( $\text{J.kg}^{-1}.\text{K}^{-1}$ ),  $C_{p_a}$  the adsorbed-phase heat capacity ( $\text{J.mol}^{-1}.\text{K}^{-1}$ ),  $q(t)$  the amount of molecules adsorbed ( $\text{mol.kg}^{-1}$ ),  $\bar{T}_s(t)$  the mean temperature of thin-layer (K),  $\phi(t)$  the adsorption heat source term (W),  $h_0(t)$  the overall heat transfer coefficient ( $\text{W.m}^{-2}.\text{K}^{-1}$ ),  $A_{eff}$  the effective surface area ( $\text{m}^2$ ) and  $T_\infty$  the room temperature (K).

with the initial conditions:

$$t = 0, \quad \bar{T}_s(t) = T_\infty \quad (2)$$

As the experimental device leads to a differential temperature measurement, we can write:

$$\bar{T}(t) = \bar{T}_s(t) - T_\infty \quad (3)$$

The first term of equation 1 represents the variation of internal energy in the thin-layer during adsorption, which is influenced by the accumulation of heat in adsorbed-phase (adsorbed CO<sub>2</sub>) and solid phase (adsorbent grains).

The second term represents the heat generated during the adsorption process and the third term represents a behavior model for overall heat losses with surrounding atmosphere.

The heat losses term in equation 1 is written as a product of a transient heat loss coefficient, an effective surface area and transient differential temperature. However, such expression has no physical foundation. It is only a convenient way to express the transient heat losses.

Equation 1 can be rewritten as follows:

$$\frac{d\bar{T}(t)}{dt} = \alpha(t) - H(t)\bar{T}(t) \quad (4)$$

with:

$$\alpha(t) = \frac{\phi(t)}{(m_s.Cp_s + m_s.Cp_a.q(t))} \quad (5)$$

$$H(t) = \frac{h_o(t).A_{eff}}{(m_s.Cp_s + m_s.Cp_a.q(t))} + \frac{m_s.Cp_a}{(m_s.Cp_s + m_s.Cp_a.q(t))} \frac{dq(t)}{dt} \quad (6)$$

where  $\alpha(t)$  is a macro-function describing the heat source; and  $H(t)$  a macro-function describing the heat losses and storage of adsorbed-phase.

### 3 Simplified analysis of experimental data

As already presented in chapter III, we have stated two characteristic times for adsorption process: short-time (ST) and long-time (LT) adsorption. In short-time adsorption, we observe a fast evolution of temperature and sample mass, whereas in long-time adsorption, we observe a slow evolution of temperature and sample mass (Figure 2).

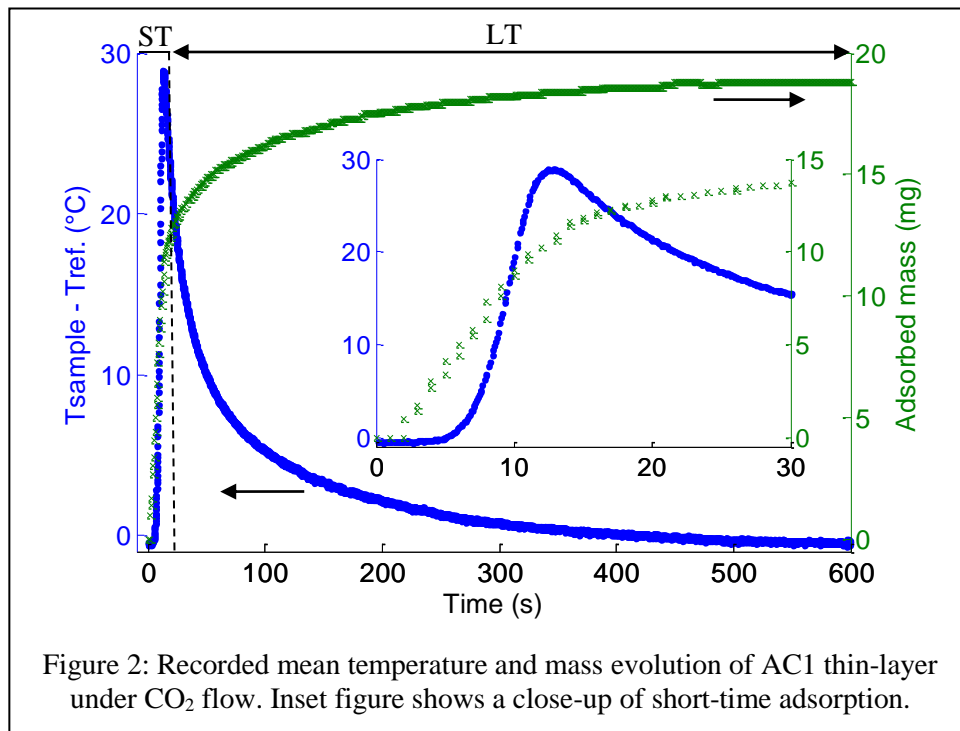
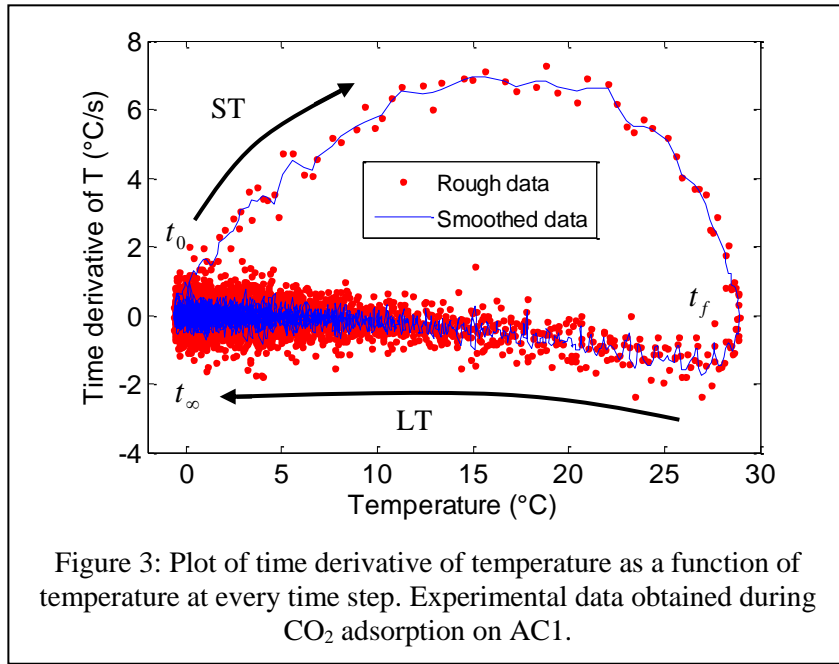


Figure 2: Recorded mean temperature and mass evolution of AC1 thin-layer under CO<sub>2</sub> flow. Inset figure shows a close-up of short-time adsorption.

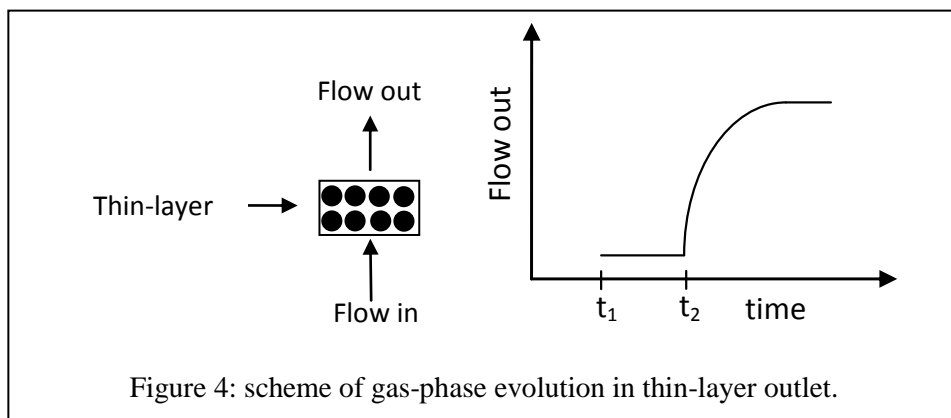
The presented lumped body model allows a simplified analysis of the experimental data, which consists in plotting the time derivative of mean temperature  $d\bar{T}(t)/dt$  versus mean temperature  $\bar{T}(t)$  (Figure 3). The experimental temperature obtained during CO<sub>2</sub> adsorption for AC1 thin-layer was used to present this analysis.



The results show also two adsorption-time behaviors. In short-time adsorption, from  $t_0 = 0$  s to  $t_f = 14$  s, we observe a high non-linear behavior between  $d\bar{T}(t)/dt$  and  $\bar{T}(t)$ . In long-time adsorption, from  $t_f = 14$  s to  $t_\infty = 600$  s, a quasi-linear behavior between  $d\bar{T}(t)/dt$  and  $\bar{T}(t)$  is observed.

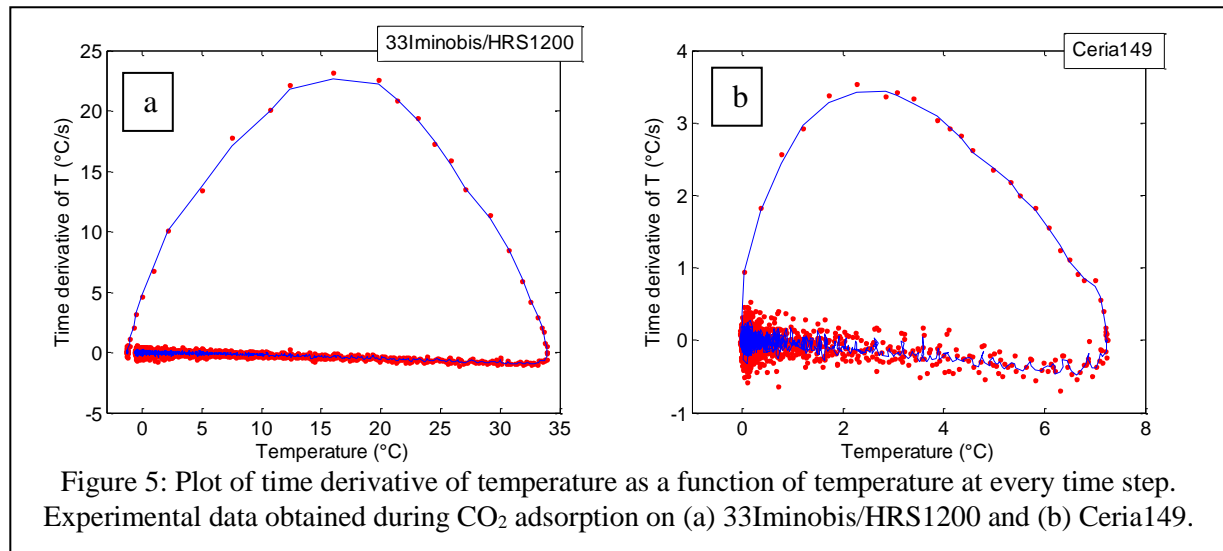
Thanks to the lumped body model (equation 4), we can propose an interpretation of these results. In short-time adsorption, the non-linearity behavior is related to the heat released during the adsorption process. This means that the heat source is “on”. However, in long-time adsorption, the results suggest that the energy released by the adsorption is negligible and that the heat source is “off”:  $\alpha(t_f \rightarrow t_\infty) = 0$ . Therefore, a quasi-linearity behavior is observed. It can be interpreted as an evolution of the macro-function  $H$  during CO<sub>2</sub> adsorption. This evolution is due to adsorbed loading  $q(t)$  on thin-layer and to variation of overall heat transfer coefficient  $h_o(t)$  during CO<sub>2</sub> adsorption (see equation 6).

The adsorbed loading evolution is intrinsic to the CO<sub>2</sub> adsorption on adsorbent. The overall heat transfer coefficient is directly related to the gas-flow going through the adsorbent. In fact, during the adsorption process, we have observed an evolution of the gas-phase flow traversing the adsorbent. Figure 4 shows a scheme of gas-phase evolution in the outlet of thin-layer.



During gas-phase conversion into adsorbed-phase (mainly during short-time adsorption), we have observed a negligible flow rate in thin-layer outlet. After a time interval ( $t_2 - t_1$ ) corresponding to short-time adsorption, the flow rate in outlet start to increase to reach a steady state. Since the overall heat transfer coefficient is related to the flow rates, a heat transfer coefficient evolution during the adsorption process is thus expected.

Similar results have been observed for others adsorbents. Figure 5 shows the plot of time derivative of mean temperature  $d\bar{T}(t)/dt$  versus mean temperature  $\bar{T}(t)$  for 33Iminobis/HRS1200 and Ceria149 thin-layer.



The results suggest that in general, the main release of heat is due to the first interactions between CO<sub>2</sub> molecules and adsorbent surface during the formation of a monolayer of adsorbed-phase (the adsorbates occupy the most energetically favorable positions and adsorbent-adsorbate interactions dominate). The evolution of adsorbed-phase after the short-time adsorption could be explained by the formation of a multilayer of adsorbate on adsorbent surface, which is intensified during the cooling of the adsorbent. In the multilayer, the main interactions are adsorbate-adsorbate, which are less energetic, and the heat source becomes negligible.

## 4 Adsorption heat estimation

One of the aims of this work was the study of adsorption heat during CO<sub>2</sub> adsorption on studied materials. The estimation of adsorption heats is crucial for the understanding of the interactions CO<sub>2</sub>-adsorbent. A high heat of adsorption leads to a high CO<sub>2</sub>-adsorbent interaction. This means that the material has a good affinity with the CO<sub>2</sub> molecules, allowing favorable CO<sub>2</sub> capture. However, too much energetic interactions may impede the material regeneration (desorption of CO<sub>2</sub> from adsorbent).

The release of heat leads to significant temperature rises during adsorption process. As already commented in Chapter II, the adsorption capacities of adsorbents are influenced by the temperature: the adsorbed quantity decreases with increasing temperature. Moreover, intense temperature rises during adsorption process can desorb amines from silica support, which causes reduction of capture efficiency. Therefore, the heat of adsorption is a key parameter for the selection of materials.

The presented analytical heat transfer model was employed to estimate the adsorption heat source, via an inverse technique, and then evaluate the heat of adsorption. The main

originality of our method is to estimate the heat losses directly from the transient heat generated during the adsorption process. This is possible thanks to the calculation of a correlation coefficient between the mean surface temperature of thin layer and its time derivative related to the experimental data zone where no source term (released heat) occurs. Then, the estimated heat loss is taken for an a posteriori calculation of the adsorption heat source. Finally, the heat of adsorption may be deduced.

In the following topics, we present the approach used to estimate adsorption heat by using AC1 as a model material. The experimental data recorded during secondary screening are thus used.

## 4.1 General approach to estimate adsorption heats

From the forward model (lumped body model, equation 4) an inverse thermal model can be written as follows:

$$\alpha(t) = \frac{d\bar{T}(t)}{dt} + H(t)\bar{T}(t) \quad (7)$$

Given  $\alpha(t) = \frac{\phi(t)}{(m_s.Cp_s + m_s.Cp_a.q(t))}$ , equation 7 can be rewritten as:

$$\phi(t) = \left[ \frac{d\bar{T}(t)}{dt} + H(t)\bar{T}(t) \right] (m_s.Cp_s + m_s.Cp_a.q(t)) \quad (8)$$

The integral heat of adsorption can be deduced by the equations below:

$$\Delta H_{ads} = \frac{Q}{N_{mol}} \quad (J.mol^{-1}) \quad (9)$$

with:

$$Q = \int_{t_0}^{t_f} \phi(t).dt \quad (10) \quad \text{and} \quad N_{mol} = m_s \int_{t_i}^{t_f} \frac{dq(t)}{dt} dt \quad (11)$$

where  $Q$  is the integral adsorption energy (J),  $N_{mol}$  the total amount of adsorbed CO<sub>2</sub> (mol),  $dq(t)/dt$  the adsorption rate (mol.s<sup>-1</sup>) and  $t_i, t_f$  the time window where the heat source is active (s).

*Note:  $\Delta H_{ads}$  is the integral heat of adsorption defined in chapter II, representing an overall heat of adsorption.*

Therefore, to estimate the adsorption heat  $\Delta H_{ads}$ , it is necessary at first, to estimate the heat source term  $\phi(t)$ . For this reason, the following inputs have to be used in equation 8:

- $\bar{T}(t)$ , **temperature evolution:** obtained via second screening device. Thanks to IR thermography, the mean temperature of the adsorbent surface is recorded during CO<sub>2</sub> adsorption.
- $d\bar{T}(t)/dt$ , **temporal derivative:** calculated directly from the experimental temperature evolution  $\bar{T}(t)$ .

- $H(t)$ , **heat loss and storage coefficient**: estimated via a calculation of a correlation between the experimental temperature and time derivative of temperature.
- $m_s$ , **sample mass**: it is obtained via balance measurement.
- $q(t)$ , **adsorbed-phase evolution**: obtained via second screening device. Thanks to precision balance, the adsorbed mass evolution is recorded during CO<sub>2</sub> adsorption.
- $Cp_s$ , **heat capacity of adsorbent**: it is obtained via differential scanning calorimetry (DSC) measurements.
- $Cp_a$ , **heat capacity of adsorbed-phase**: it is assumed equal to gas-phase heat capacity and thus obtained from CO<sub>2</sub> gas data sheet ( $Cp_a = 840 \text{ kJ.Kg}^{-1}.\text{K}^{-1}$ ).

The main difficulty is that in such situation, the source term evolution is correlated with heat losses. In order to remove the heat losses information, it is important to detect the adsorption period during which nothing but the heat losses are affecting the thermal behavior.

Our strategy was to look for this adsorption period where the sensitivity to heat losses is at the maximum without heat generation. To detect such zone it is suitable to consider the coefficient of correlation ( $\rho^{F_t}$ ):

$$\rho^{F_t} = \frac{\sum_{F_t} \bar{T}^k \cdot \frac{d\bar{T}}{dt}}{\sqrt{\sum_{F_t} \bar{T}^{k^2}} \cdot \sqrt{\sum_{F_t} \frac{d\bar{T}}{dt}^2}} \quad (12)$$

where  $\bar{T}$  is the thin layer mean temperature,  $d\bar{T}/dt$  the temporal derivative of thin layer mean temperature,  $F_t$  is a temporal window of length  $F_t = [k, k + lt]$ , with  $k$  the time step and  $lt$  the length of temporal window.

The correlation coefficient represents the normalized measurement of the strength of linear relationship between two variables [128], in our case, the mean surface temperature of thin layer and its time derivative. Coefficient values close to 1 suggest that there is a positive linear relationship between the data columns. Coefficient values close to -1 suggest that one column of data has a negative linear relationship to another column of data (anticorrelation). Coefficient values close to or equal to 0 suggest there is no linear relationship between the data columns.

In the case of our thermal model, if such correlation coefficient is close to -1, it is a proof that the thermal model has a linear behavior. It means that the heat source is “off” and that heat losses  $H(t)$  related to the slopes of Figures 3 and 5 can be thus estimated with the formulation:

$$H(t) = \rho^{F_t} \cdot \frac{\sum_{F_t} \bar{T}^k \cdot \frac{d\bar{T}}{dt}}{\sqrt{\sum_{F_t} \bar{T}^{k^2}}} \quad (13)$$

## 4.2 Results and discussion

In order to show how this method has been applied to estimate the CO<sub>2</sub> adsorption heats of the studied materials, we detail the case of AC1 carbon sample.

When applying Equation 12 to experimental data (see Figure 2), we obtain results shown in Figure 6. The experimental mean temperature and coefficient of correlation are plotted as a function of adsorption time (from 0 to 100 s).

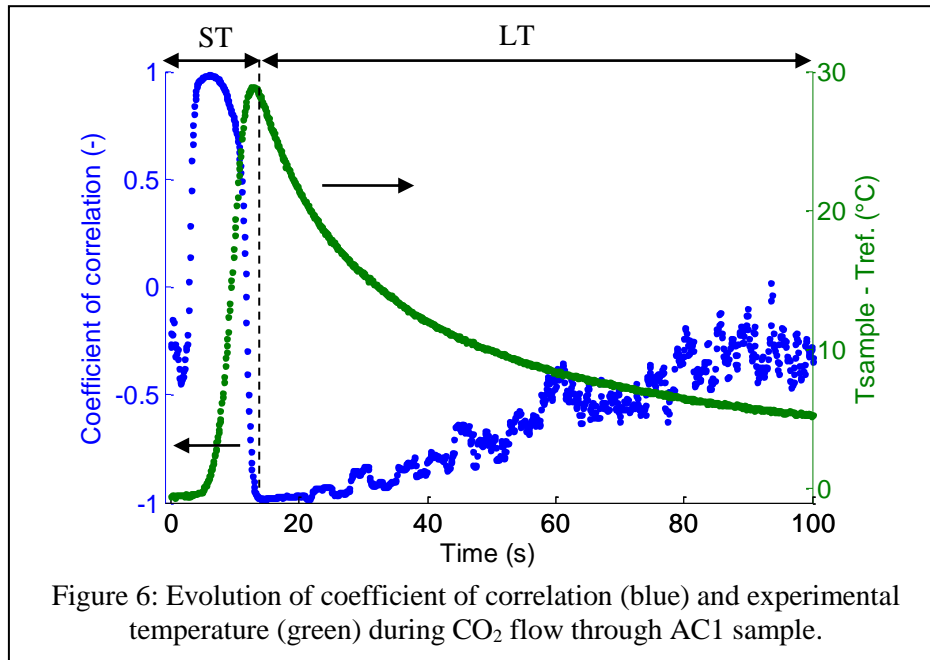


Figure 6: Evolution of coefficient of correlation (blue) and experimental temperature (green) during CO<sub>2</sub> flow through AC1 sample.

Comparing the temperature evolution and the coefficient of correlation, we clearly notice the adsorption behaviors. At the time of the heat source (short-time adsorption) the correlation coefficient evolves to values corresponding to non-linear relationship between temperature and its time derivative. This means that we cannot estimate the heat losses  $H$  at this adsorption time interval. After short-time adsorption, when the heat source is “off”, we obtain a correlation near to -1. This means that the lumped body model has an approximate linear behavior and heat losses can be thus estimated.

For long-time adsorption, the linear relationships are kept during a few seconds (from 14 to 22 s) and then the correlation coefficient evolves to values superiors to -1. This is explained by progressively weaker signal/noise ratio during long-time adsorption. It means that the estimation of heat loss coefficient is less favorable because  $d\bar{T}/dt \approx 0$ .

Therefore, the coefficient of correlation allows the selection of the adsorption period during which a maximum sensitivity of heat losses is observed.

Applying equation 13, the heat losses can be thus estimated: The heat loss coefficient  $H$  is represented in Figure 7.

Even though we have estimated heat losses related to time period during which the lumped body model has a linear behavior, we observe on Figure 7 that heat losses decrease.

As already presented, this can be explained by the adsorbed loading  $q(t)$  on thin-layer and the evolution of flow rate during adsorption, consequently the evolution of overall heat transfer coefficient  $h_o(t)$ .

These results suggest a high influence of adsorbed loading and flow rate on heat loss coefficient. The maximum value of heat loss coefficient equal to  $0.049 \text{ s}^{-1}$  has been used to the estimation of adsorption heat. This value corresponds to the maximum value of correlation coefficient.

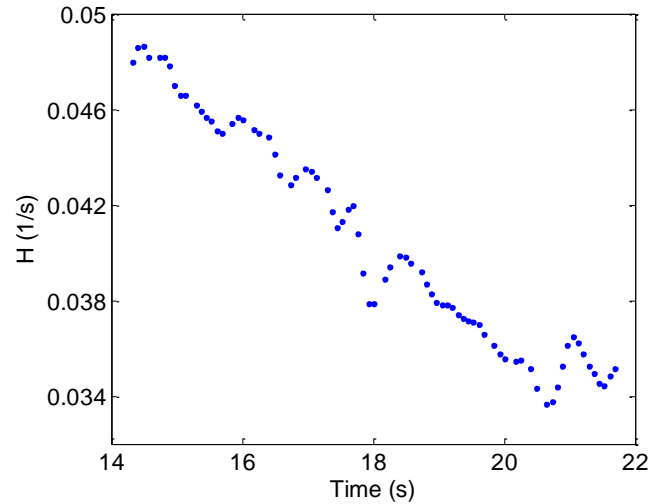


Figure 7: Estimation of heat loss coefficient related to time period from 14 to 22 s, when correlation coefficient is close to -1 ( $-0.99 > \rho^{F_i} > -1$ ).

After heat losses estimation, we can calculate the heat source using equation 8. Figure 8 shows the heat source estimated in short-time period, the experimental temperature, the temperature simulated using the forward model and the residual between experimental temperature and simulated temperature.

The simulated temperature has been obtained by using as input in our thermal model the estimated heat source. To solve the differential equation 4 (lumped body model) a numerical solver was utilized: MATLAB ode45 solver (for more information please see annex at the end of this chapter). An average heat capacity of  $1100 \text{ J.kg}^{-1}.\text{K}^{-1}$  was used to the estimation of heat source term. The residual have been calculated as the differences between experimental temperature and simulated temperature evolutions.

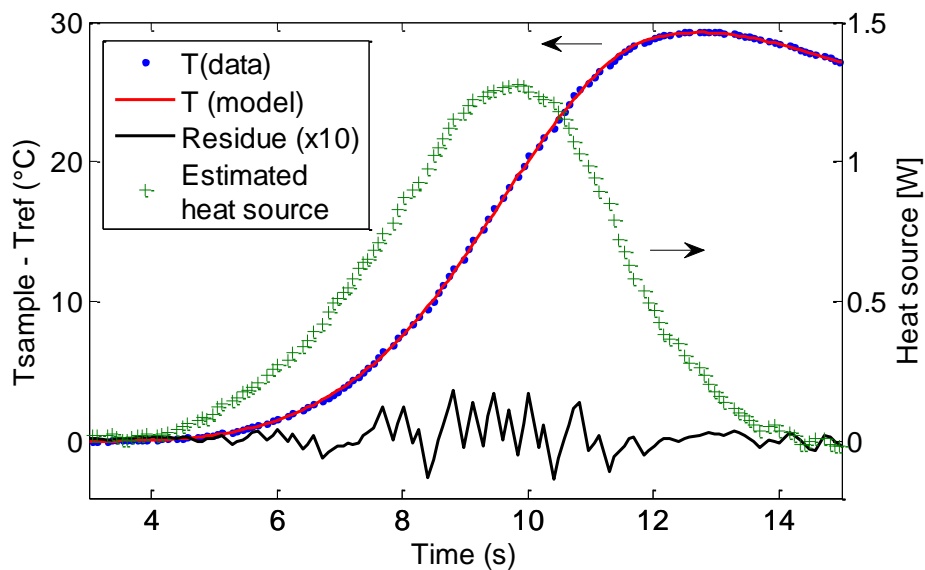


Figure 8: Estimated heat source and temperature evolutions.

A negligible residual was obtained between experimental temperature and simulated temperature. This result thus validates our estimation method.

To estimate the heat of adsorption, the final step consist in integrating the heat source curve from  $t_i = 4$  to  $t_f = 14$  s (for the estimation of the integral adsorption energy  $Q$ ) and calculating, in the same time interval, the total amount of adsorbed  $\text{CO}_2$ :  $N_{mol}$  (from the variation mass data). Finally, applying equation 9, a value of  $\Delta H_{ads} = 28.3 \text{ kJ.mol}^{-1}$  was calculated for the  $\text{CO}_2$ -sample interaction. The result is in very good agreement with the experimental value found in the AC1 data-sheet:  $\Delta H_{ads} = 25 - 30 \text{ kJ.mol}^{-1}$  (see chapter I: studied materials).

Using the described estimation method, we have estimated  $\text{CO}_2$  adsorption heats of most of studied materials (Figure 9). For overall comparison and limitation of systematic errors, we have used the same experimental protocol and operational conditions for all samples (two adsorption cycles: 600 s of  $\text{CO}_2$  + 400 s of  $\text{N}_2$ , flow rate =  $40 \text{ ml.min}^{-1}$ , thin-layer mass = 70 mg).

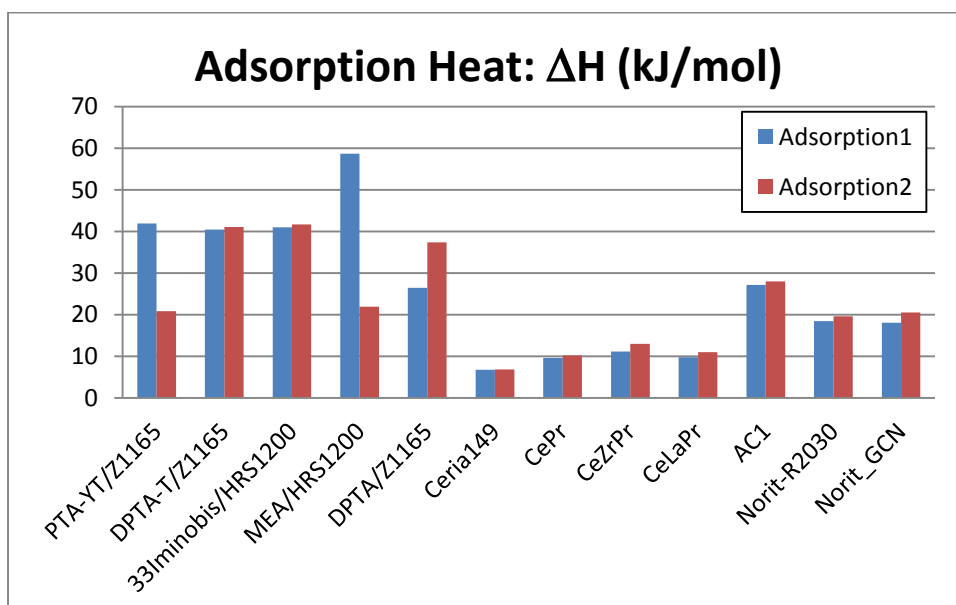


Figure 9: Estimated values of  $\text{CO}_2$  adsorption heats on studied materials.

The heats of adsorption shown in Figure 9 represent the amounts of released heats normalized by the amounts of  $\text{CO}_2$  adsorbed on the adsorbent. Therefore, for the same quantity of adsorbed  $\text{CO}_2$ , hybrid materials have released the highest amount of heat, over  $40 \text{ kJ.mol}^{-1}$  for the first adsorption cycle. Because of these moderate  $\Delta H_{ads}$  values, we suggest that  $\text{CO}_2$  adsorption on these hybrid sorbents is a combination of both physisorption and weak chemisorption process.

The estimated heat of adsorption of  $\text{CO}_2$  on MEA/HRS1200 is the strongest one among hybrid materials ( $59 \text{ kJ.mol}^{-1}$ ). This result indicates high  $\text{CO}_2$ -adsorbent interaction. However, the  $\Delta H_{ads}$  value for the second adsorption cycle is much weaker ( $22 \text{ kJ.mol}^{-1}$ ). As will be presented later on by DRIFT analysis, this result is due to the weak thermal stability of MEA over silica support. The high release of heat during adsorption process leads to an intense temperature increase of material ( $\Delta T = 76^\circ\text{C}$ ), causing desorption of MEA from silica support. The weak  $\Delta H_{ads}$  for the second adsorption cycle is close to values found in literature for  $\text{CO}_2$  adsorption on silica supports [89, 90, 129]. Therefore, the second adsorption on sorbent is

mainly a physisorption process (CO<sub>2</sub> adsorption on silica support). Similar results have been found for PTA-YT/Z1165.

The amine-impregnated sorbent DPTA/Z1165 shows a weaker  $\Delta H_{ads}$  value for the first adsorption cycle, compared to the second one, suggesting possible reorganization of amines on support surface after the first material regeneration. The CO<sub>2</sub>-adsorbent interactions for the second adsorption cycle are thus stronger.

In the case of 33Iminobis/HRS1200,  $\Delta H_{ads}$  values for first and second adsorption cycles are identical. These results reveal good stability of amine group over silica support and capture reversibility. The strength of interactions is strong enough to afford high affinity towards CO<sub>2</sub> molecules, characterized by high adsorption capacity ( $C_{ads} = 134 \text{ mg}_{\text{CO}_2} \cdot \text{g}_{\text{ads}}^{-1}$ ), but is weak enough to allow easy adsorbent regeneration over inert gas only (N<sub>2</sub> flux), without temperature swimming.

The estimated adsorption heats for activated carbons (over 20 kJ.mol<sup>-1</sup>) are just above the enthalpy of condensation of CO<sub>2</sub> (ca. 17 kJ.mol<sup>-1</sup>) [130]. These results confirm CO<sub>2</sub> capture via physisorption process. The weak CO<sub>2</sub>-adsorbent interaction leads to easy material regeneration.

The estimated  $\Delta H_{ads}$  values for AC1, ca. 28 kJ.mol<sup>-1</sup>, indicates stronger CO<sub>2</sub>-adsorbent interactions than other activated carbons, consequently the affinity with CO<sub>2</sub> molecules is higher, reflecting thus high adsorption capacity ( $C_{ads} = 120 \text{ mg}_{\text{CO}_2} / \text{g}_{\text{ads}}$ ).

The estimated adsorption heats of rare earth oxides are the weakest ones among studied materials. However, as already discussed in the previous chapter, these results may not be accurate because of systematic errors due to technique limitations for the measurement of weak variation of mass during CO<sub>2</sub> adsorption (see chapter III: secondary screening).

In order to estimate accurate adsorption heats of REO, we have measured the adsorbed CO<sub>2</sub> amount by ATG measurements in collaboration with Cédric Slostowski at ICMCB (for more information see [79]).

The measured adsorption capacities and estimated heat of adsorption are shown in Figure 10.

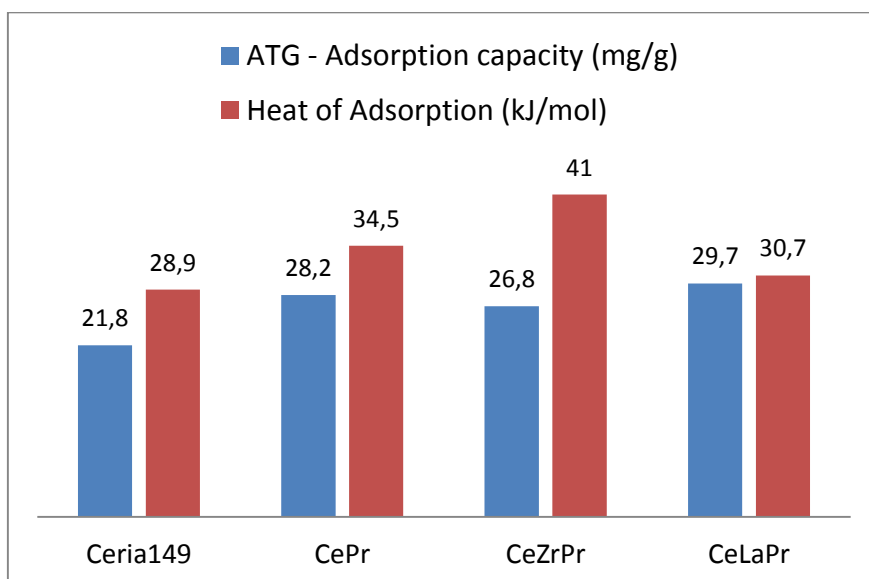


Figure 10: Adsorption capacity measured by ATG (blue) technique and estimated adsorption heats (red) of REO.

The estimated  $\Delta H_{ads}$  values of REO are intermediate between hybrid materials and activated carbons, from 29 to 41 kJ.mol<sup>-1</sup>. These results suggest CO<sub>2</sub> capture by weak chemisorption or/and physisorption process. The measured adsorption capacities are the lowest among studied materials, from 22 to 30 mg<sub>CO2</sub>/g<sub>ads</sub>. CeZrPr shows the strongest CO<sub>2</sub>-adsorbent interactions ( $\Delta H_{ads} = 41$  kJ.mol<sup>-1</sup>) and CeLaPr the highest adsorption capacity ( $C_{ads} = 29.7$  mg<sub>CO2</sub>/g<sub>ads</sub>). The differences in  $\Delta H_{ads}$  and  $C_{ads}$  values between REO are certainly related to doping ratio and cation (La, Pr and Zr) in cerium oxide. The doping creates more strongly basic sites on ceria surface, modifies the reducibility of Ce<sup>4+</sup> and the mobility of O<sup>2-</sup> anions. Therefore, stronger CO<sub>2</sub>-adsorbent interactions and consequently higher adsorption capacities can be obtained.

*Note: As a matter of confidentiality, we cannot reveal the doping ratio of studied cerium oxides.*

### 4.3 Parameters influencing adsorption heat estimation

We have used equation 8 to estimate the transient heat source term and, consequently, the adsorption heats of CO<sub>2</sub>. In order to evaluate the impact of the most influencing parameters of equation 8 on  $\Delta H_{ads}$  estimation, we have imposed some simplifying assumption in the lumped body model, and then, the resulting heat sources and adsorption heats were estimated.

In the literature, the most current assumption to simplify the heat balance equation is to consider that there is no accumulation of heat in the adsorbed-phase. With this assumption, equation 8 can be rewritten as follows:

$$\phi(t) = \left[ \frac{d\bar{T}(t)}{dt} + H(t).\bar{T}(t) \right] . m_s . Cp_s \quad (14)$$

The estimated heat sources and resulting adsorption heats using equation 8 (1) and using equation 14 (2) are shown in Figure 11.

*Note: For each simplifying assumptions, the same experimental data (CO<sub>2</sub> adsorption on AC1) were employed for this study of influences on estimations. The maximum value of heat loss coefficient  $H = 0.048$  s<sup>-1</sup> and the average value of heat capacity  $Cp_s = 1100$  kJ.kg<sup>-1</sup>.K<sup>-1</sup> were used for estimations.*

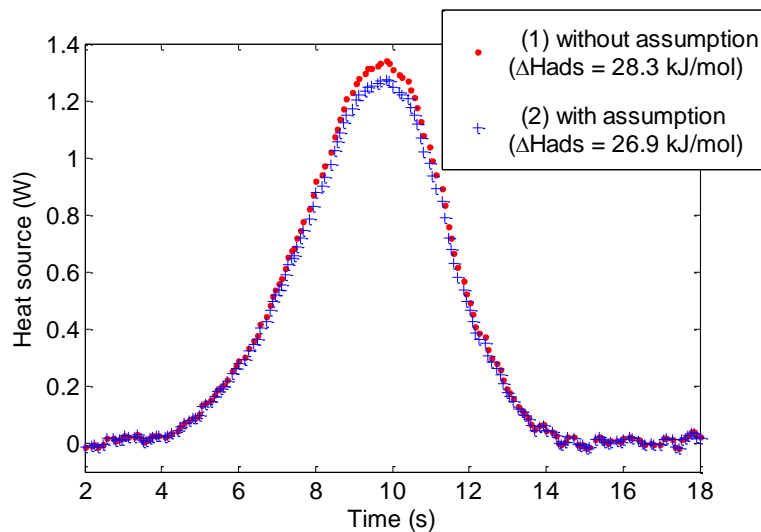


Figure 11: Estimated heat source and adsorption heats using the lumped body model (1) and simplified model without heat accumulation on adsorbed-phase (2).

The results show small differences on  $\Delta H_{ads}$  estimated with or without the assumption of no heat accumulation on adsorbed-phase (difference:  $1.4 \text{ kJ}\cdot\text{mol}^{-1}$ ). This suggests a weak influence of this parameter on  $\Delta H_{ads}$  estimation.

In our  $\Delta H_{ads}$  estimations, we have assumed heat capacity of adsorbents ( $C_{p_s}$ ) as a constant parameter. However it is known that this physical property varies with temperature. The evolution of  $C_{p_s}$  with temperature, obtained via DSC measurements, of AC1 and 33Iminobis/HRS1200 are shown in Figure 12.

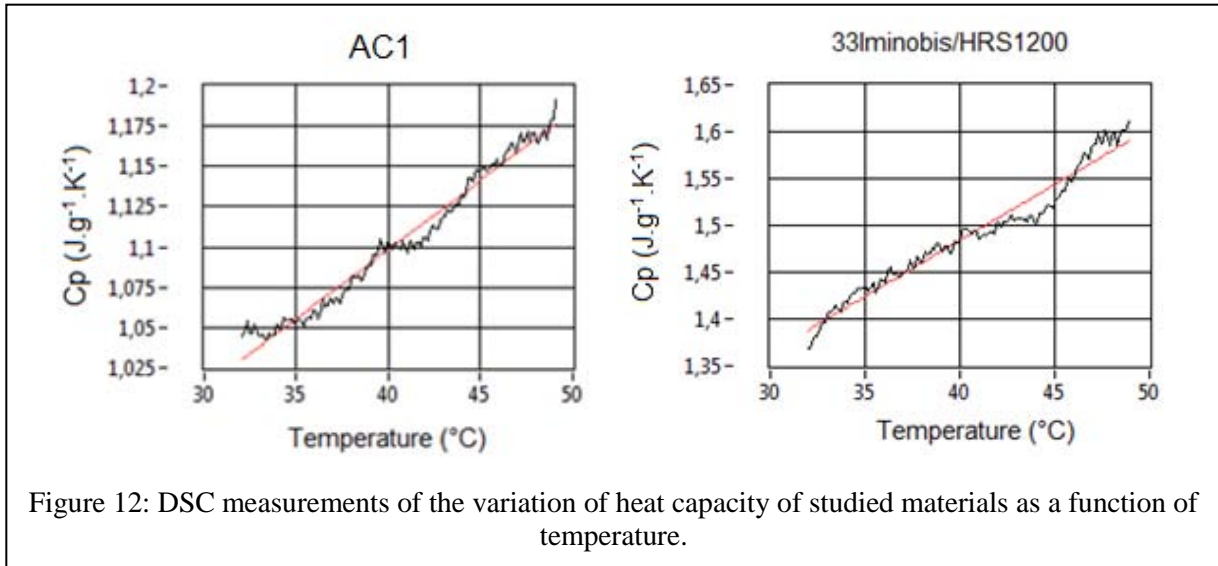


Figure 12: DSC measurements of the variation of heat capacity of studied materials as a function of temperature.

The results show an increase in  $C_{p_s}$  values with increasing temperature. In order to present the influence of this parameter on  $\Delta H_{ads}$  estimation, the heat sources and adsorption heats were estimated using three  $C_{p_s}$  values of AC1. As we can see in Figure 13, major differences on estimated  $\Delta H_{ads}$  have been found using extreme  $C_{p_s}$  values (difference:  $4.9 \text{ kJ}\cdot\text{mol}^{-1}$ ). These results suggest a non negligible influence of  $C_{p_s}$  on  $\Delta H_{ads}$  estimations.

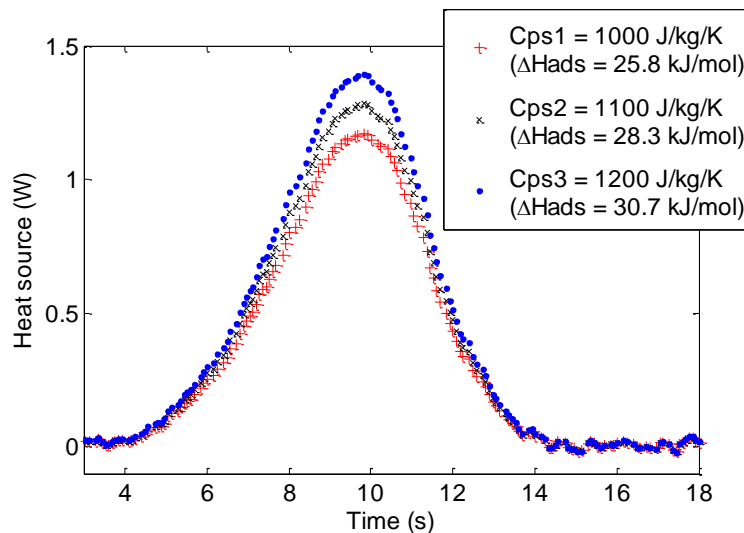
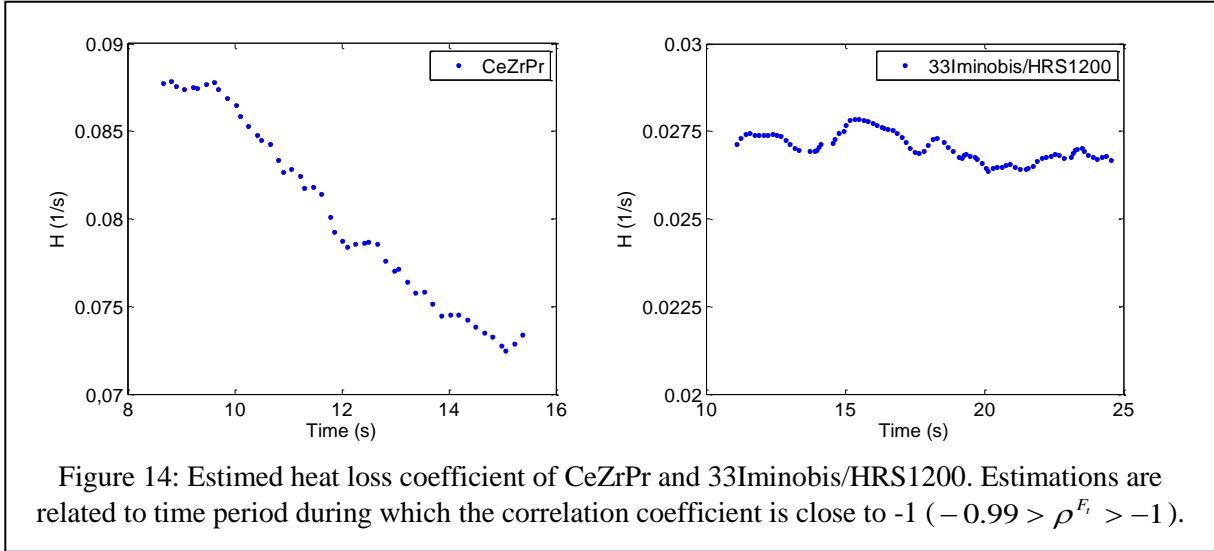


Figure 13: Estimated heat source and adsorption heats using distinct  $C_{p_s}$  values of AC1.

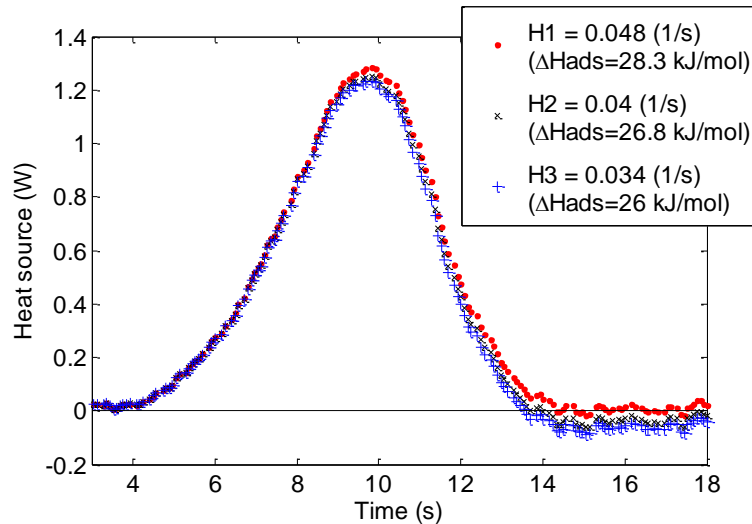
The heat loss coefficient  $H$  is also an influencing parameter. Because of adsorbed-phase loading and variable flow rate traversing the thin-layer, depending on the adsorbent,

significant variations of  $H$  values can be observed during adsorption process. Figure 14 shows the estimated  $H$  values for CeZrPr and 33Iminobis/HRS1200 during CO<sub>2</sub> adsorption.



In the given examples of  $H$  estimations, we observe strong  $H$  variation for CeZrPr and negligible variations for 33Iminobis/HRS1200. Similar tendencies have been reported for other REO and hybrid materials respectively. The  $H$  evolution for activated carbons is similar to that shown for AC1 in Figure 7. These results suggest that the heat losses are strongly dependent of the mass transfer process from gas-phase to adsorbed-phase through each family of adsorbents.

In the case of AC1, this variation ranges from 0.048 to 0.034 s<sup>-1</sup> (see Figure 7). To study the influence of this parameter, we have estimated the heat sources and adsorption heat using  $H$  values in this cited range.



The results (see Figure 15) show that using lower  $H$  values than the maximum estimated value ( $H = 0.048$ ), the heat source evolves to negative values (from 14 to 18 s). As negative values have no physical meaning, the estimations are thus biased. However, using the maximum  $H$  value, we do not detect physical incoherencies. For this reason, we have decided to use the maximum values of estimated  $H$  for the estimation of adsorption heats. As we will

see in the next topic, the variation of heat losses has influence during long-time adsorption only.

## 5 Parameters influencing temperature evolution

High temperature during adsorption process may lead to system degradation and adsorber ignition. The knowledge about temperature evolutions during adsorption process is thus a key point for the design and safety of adsorption systems.

As already presented, we have defined two macro-functions in our lumped body model: heat source  $\alpha(t)$ ; and heat loss and storage coefficient  $H(t)$ . These parameters are directly related to the temperature evolution of the thin-layer during CO<sub>2</sub> adsorption. During adsorption, a competition is established between these parameters. The heat source contributes to temperature increase whereas the heat loss coefficient contributes to temperature decrease.

In order to study the influence of these parameters, we have used the heat source estimated during CO<sub>2</sub> adsorption on AC1 (using equation 8) to simulate the temperature evolution for distinct assumption cases:

- 1) Temperature evolution obtained via lumped body model (Equation 4), using the estimated  $H$  values during adsorption (see Figure 7);
- 2) Temperature evolution obtained via simplified thermal model (Equation 14) in which no accumulation of heat in the adsorbed-phase was considered;
- 3) Temperature evolution obtained via lumped body model (Equation 4), using the maximum estimated value of  $H$ .
- 4) Temperature evolution obtained via lumped body model (Equation 4), considering no heat losses during CO<sub>2</sub> adsorption process ( $H = 0$ ).

The temperature evolutions for each assumption case are shown in Figure 16.

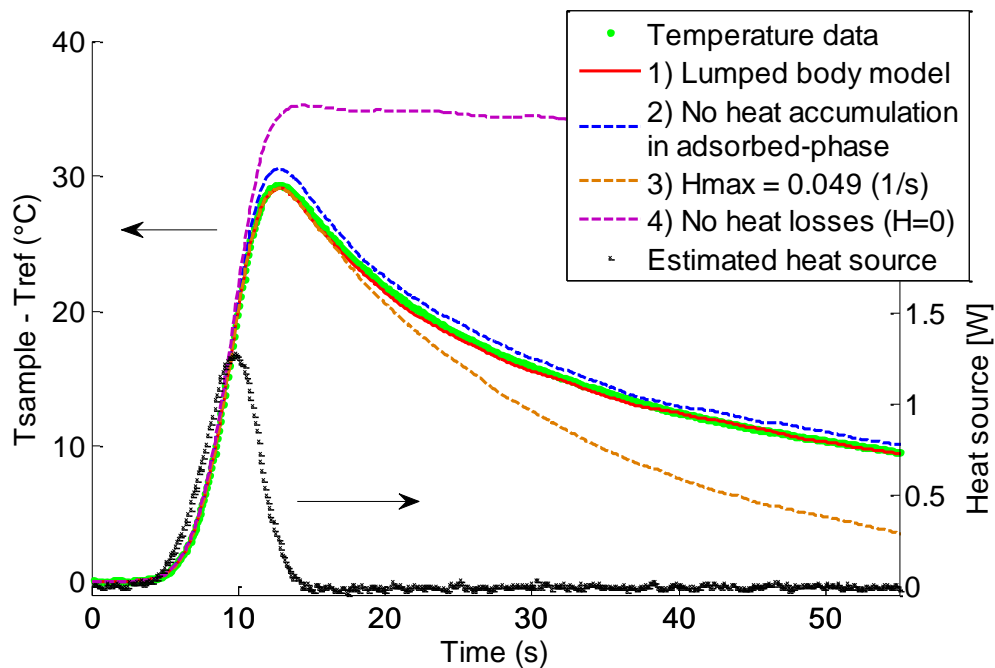


Figure 16: Temperature evolutions for distinct assumption cases. Simulated temperatures were obtained via numerical solver, MATLAB ode45.

As we can see above, in short-time adsorption (from 0 to 15 s), the heat source is the influencing parameter on temperature evolution (see heat source evolution), whereas in long-time adsorption (after 15 s), the heat loss coefficient is the dominating parameter (see the results of assumption case 4). Comparing simulated temperature (case 2) with experimental data (green curve), we verify the low influence of heat accumulation in the adsorbed-phase. This result suggests that the heat accumulation in adsorbed phase is negligible compared with that in the solid adsorbent. Using in lumped body model the constant and maximum value of  $H$  (case 3), the divergences between thermal model and experimental data are only remarkable in long-time adsorption range. The lumped body model (case 1) is in very good agreement with the experimental data (green curve).

The main influencing parameter in  $\alpha(t)$  is the heat source  $\phi(t)$ , which is directly related to the adsorption heat and kinetic (see Equations 9, 10 and 11). From these equations, we state that high adsorption heats and kinetics lead to intense heat release and consequently intense adsorption peaks ( $\Delta T$ ).

To study the heat source influence on temperature evolution and to study the contribution of adsorption heat and kinetic to heat source evolution during  $\text{CO}_2$  adsorption process, we have defined a key parameter directly related to a maximum temperature increase. This parameter describes the total energy released during  $\text{CO}_2$  adsorption normalized by the mass of adsorbent:

$$\Delta H_m = \frac{Q}{m_s} \quad (\text{J} \cdot \text{g}^{-1}) \quad (15)$$

where  $Q$  is the integral adsorption energy (J) (equation 10) and  $m_s$  the mass of the thin-layer of adsorbent (g). So, the same method used to estimate the heat of adsorption  $\Delta H_{ads}$  is employed for the estimation of  $\Delta H_m$ .

An easy way to notice the relationship between  $\Delta H_m$  and the maximum variation of temperature ( $\Delta T_{\max}$ ) is to consider the following expression:

$$\Delta T_{\max} = \frac{\Delta H_m}{Cp_s} \quad (^\circ\text{C}) \quad (16)$$

$\Delta T_{\max}$  is the maximum variation of temperature obtained without heat losses. The heat capacity ( $Cp_s$ ) is expressed in terms of  $\text{J} \cdot \text{g}^{-1} \cdot ^\circ\text{C}^{-1}$ .

Therefore, for a given value of adsorbent heat capacity, the higher the heat released, the greater the elevation of temperature.

Examples of the relationship between maximum temperature increases and  $\Delta H_m$  values are shown in Figure 17.

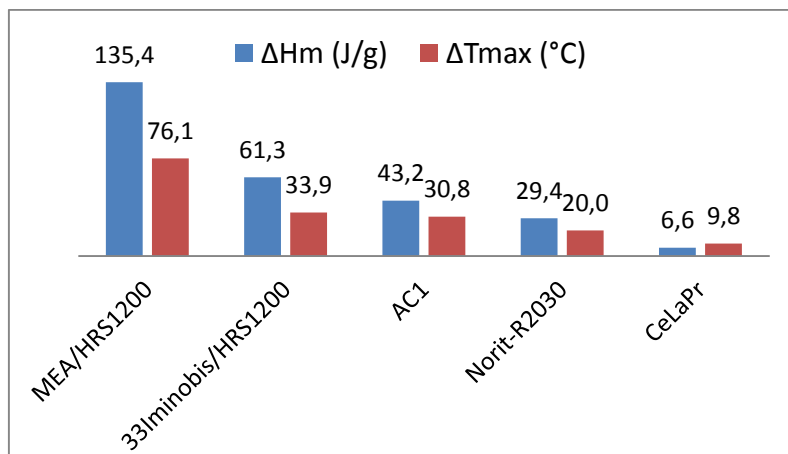


Figure 17: Maximum variation of temperature (red) and released heats (blue) for some materials.

The estimated  $\Delta H_m$  values for CO<sub>2</sub> adsorption on studied materials are shown in Figure 18. As we can see from these results, for the same quantity of adsorbent, MEA/HRS1200 has released the highest amount of heat during the first adsorption process (135.4 J.g<sup>-1</sup>), which has led to a maximum variation of temperature equals to 76°C. As already explained, because of MEA thermal stability over silica support, the second adsorption cycle has led to much weaker heat release (25.7 J.g<sup>-1</sup>). The second most intense  $\Delta H_m$  value has been estimated for 33Iminobis/HRS1200 (61.3 J.g<sup>-1</sup> for AP1). The high  $\Delta H_m$  values estimated for hybrid materials are related to their high adsorption heat values (see Figure 9). Differences between the first and second adsorption cycle are related to adsorption irreversibility.

Even though AC1 has developed low heat of adsorption (ca. 28 kJ.mol<sup>-1</sup>), we have estimated high  $\Delta H_m$  values. This result suggests thus high CO<sub>2</sub> adsorption rates. High adsorption rates may be expected also for other activated carbons.

The weakest  $\Delta H_m$  values have been estimated for rare earth oxides. Since the CO<sub>2</sub> adsorption on REOs has led to moderate heat of adsorption values, we suggest thus moderate adsorption rates during CO<sub>2</sub> capture.

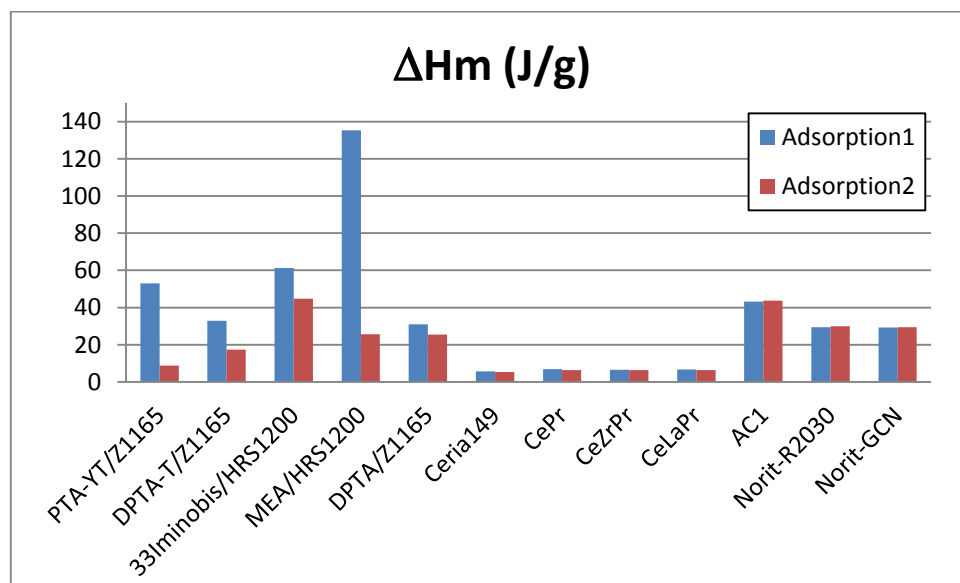


Figure 18: Estimated  $\Delta H_m$  values for two adsorption cycles of CO<sub>2</sub> on studied materials.

Therefore, these results suggest the influence of adsorption rates on heat release. To better understand this influencing parameter, we have carried out two distinct experiments from which we have estimated the heat source during CO<sub>2</sub> adsorption.

In the first one, we have varied the flow rates (22, 39 and 60 ml.min<sup>-1</sup>) injected through AC1 thin-layer (80 mg). In the second one, we have varied the adsorbent thin-layer mass (40, 80 and 120 mg) of AC1 using a flow rate of 50 ml.min<sup>-1</sup>. Figure 19 shows the adsorption and desorption peaks obtained for the first experiments.

As already presented for REO in chapter III, the injected flow rates impact the adsorption and desorption peaks, regarding peaks intensities and kinetics: the higher the flow rate, the greater the intensity of peaks and thermal kinetics.

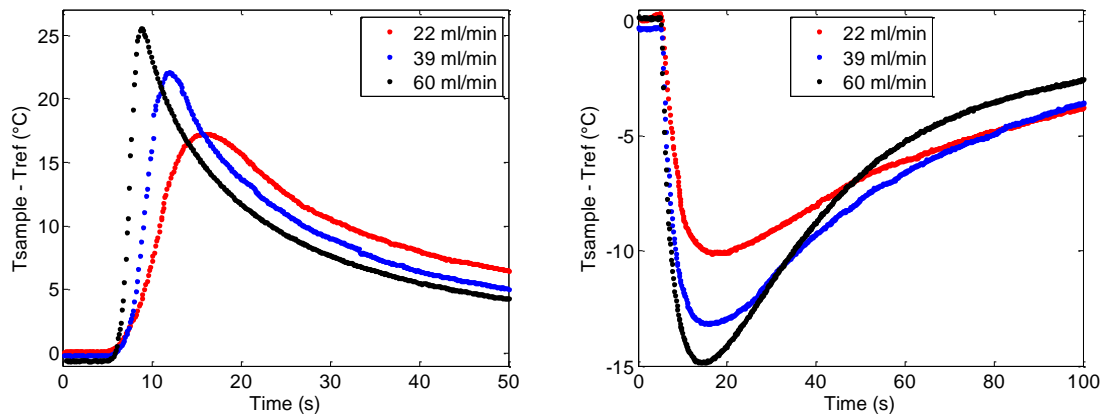


Figure 19: Adsorption and desorption peaks obtained during CO<sub>2</sub> and N<sub>2</sub> injections on AC1 at different flow rates.

The estimated heat sources and  $\Delta H_m$  values for each injected flow rate are shown in Figure 20. The results show evidence of distinct adsorption rates. The increasing flow rates have led to more intense and fast evolution of heat source. As already explained, especially at low flow rates because of CO<sub>2</sub> dilution with N<sub>2</sub> already filling the injection system, the adsorption energy is distributed in a longer time period. As the heat source is the fingerprint of CO<sub>2</sub> adsorption, we can relate it with adsorption rates.

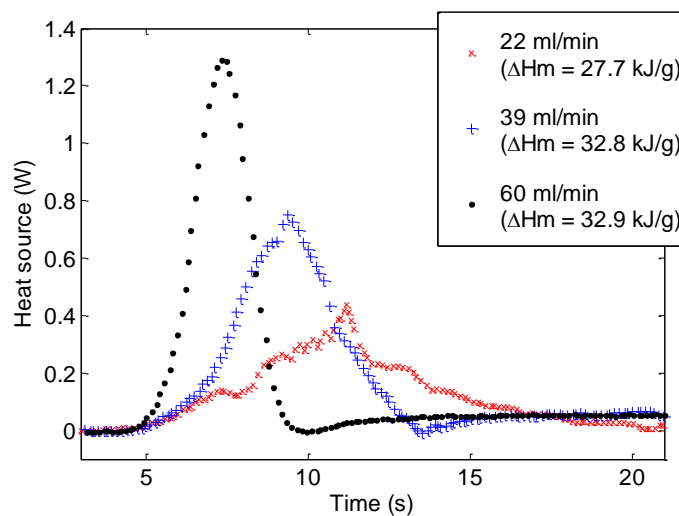


Figure 20: Estimated heat source and  $\Delta H_m$  for distinct CO<sub>2</sub> flow rates injected through AC1.

Since we have used the same amount of thin-layer mass during experiments, the estimated values of  $\Delta H_m$  indicate similar amount of total heat released during adsorption process independently of gas flow rate. The slight difference of  $\Delta H_m$  values obtained for the lowest flow rate ( $22 \text{ ml}\cdot\text{min}^{-1}$ ) can be explained by weak signal/noise ratio, which has led to biased estimations. As shown in Figure 21, the heat losses are also impacted by increasing flow rates.

The results show an increase of  $H$  with increasing flow rates. We can understand this behavior by analyzing equation 6. Higher flow rates lead to higher values of overall heat transfer coefficient ( $h_o$ ) and of adsorption rates ( $dq/dt$ ). Since these parameters are directly proportional to heat loss coefficient, we expect thus higher  $H$  values.

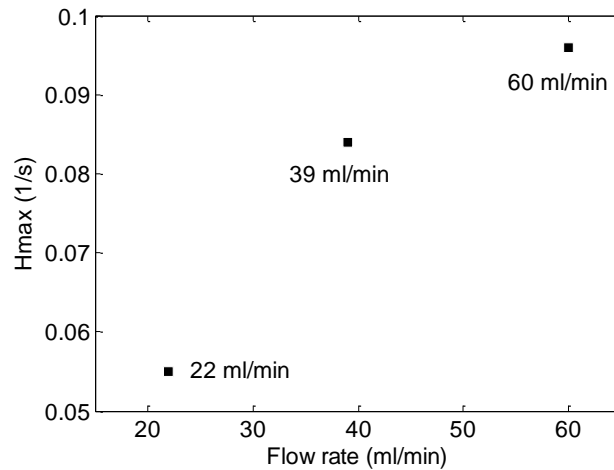


Figure 21: Estimated maximum  $H$  values for each injected flow rate.

Concerning the second experiment in which we have varied the thin-layer mass and consequently the thin-layer thickness, the obtained adsorption and desorption peaks are shown in Figure 22.

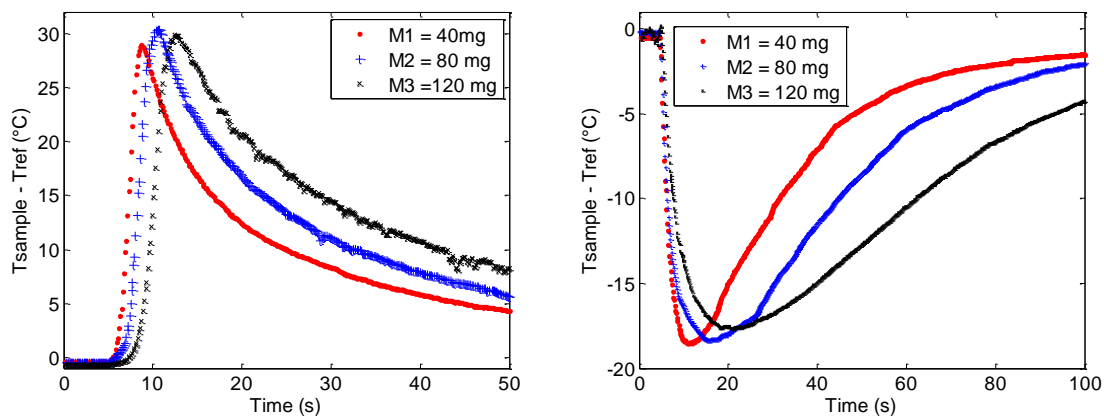


Figure 22: Adsorption and desorption peaks obtained during  $\text{CO}_2$  adsorption/desorption on distinct thin-layer masses of AC1.

According to our results, the peak intensities for  $\text{CO}_2$  adsorption and desorption are both independent on the thin-layer mass. However, we observe a delay in thermal response as the thin-layer mass increases not only during adsorption but also during desorption process.

The estimated heat source and  $\Delta H_m$  values related to adsorptions peaks are shown in Figure 23. From these results, we observe with clarity the delay in thermal responses. Moreover, the

time period during which the heat source is active (short-time adsorption) is longer as the thin-layer mass increases ( $\Delta t = 4.9$  s for 40mg and  $\Delta t = 7.8$  s for 120). As will be presented later on in chapter VI (Investigation level II), the delay in thermal responses and consequently the short-time period ( $\Delta t$ ) of adsorbent thin-layer is related to the propagation speed of the thermal front in a millifluidics adsorption bed.

Even though the total amount of released heat during adsorption process is different for each thin-layer mass, the released heat per mass (or thickness) of thin-layer is constant ( $\Delta H_m \approx 40$  J.g<sup>-1</sup>). This means that each slice of thin-layer release an identical amount of heat, therefore this indicates a homogeneous CO<sub>2</sub> adsorption on this adsorbent.

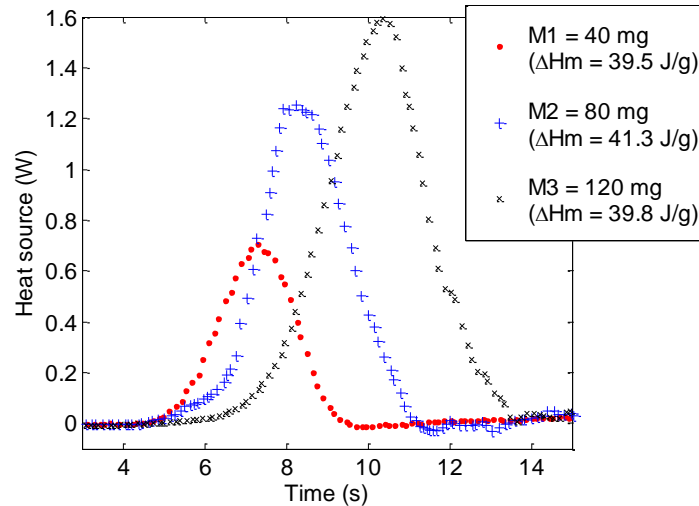


Figure 23: Estimated heat sources and  $\Delta H_m$  values related to different thin-layer masses.

Heat losses also depend on thin-layer mass. The maximum heat loss coefficient  $H$  is plotted as a function of sample mass in Figure 24. From these results, we state that  $H$  values decrease as the thin-layer mass increases. This inverse proportionality can be explained via the analysis of equation 6, that shows that higher the thin-layer mass ( $m_s$ ), the lower the  $H$  values are. Moreover, the increase of thin-layer mass increases the amount of CO<sub>2</sub> adsorbed ( $q$ ), consequently, we must also observe lower  $H$  values.

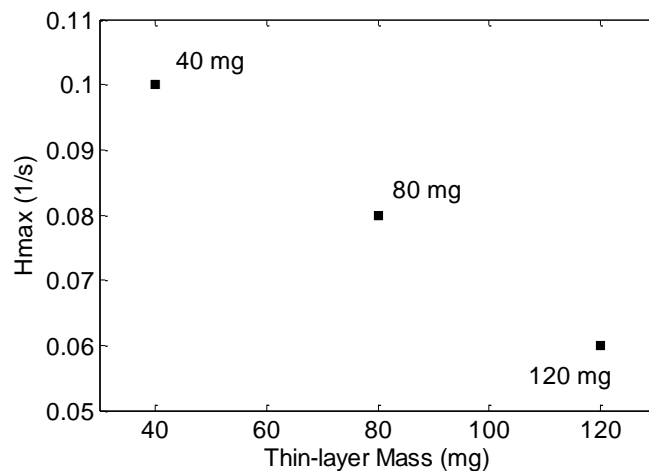


Figure 24: Estimated maximum  $H$  values as a function of thin-layer mass.

## 6 Key parameters for material selection

A major goal of this work was to identify the main influencing parameters of CO<sub>2</sub> capture by solid adsorbents. These influencing parameters will be used as key parameters for the selection and overall comparison of materials.

Most of key parameters have already been defined:

- 1) **Heat of adsorption**,  $\Delta H_{ads}$  (kJ.mol<sup>-1</sup>): indicates the strength of CO<sub>2</sub>-adsorbent interactions.
- 2) **Released heat per mass**,  $\Delta H_m$  (J.g<sup>-1</sup>): indicates how energetic the adsorption process is.
- 3) **Adsorption capacity**,  $C_{ads}$  (mg.g<sup>-1</sup>): indicates the maximum amount of CO<sub>2</sub> adsorbed.
- 4) **Short-time period**,  $\Delta t_{ST}$  (s): defined as the time period of heat release, it indicates the adsorption rate during first CO<sub>2</sub>-adsorbent interactions.

Thanks to secondary screening, we have obtained mass variation profiles associated with adsorbed CO<sub>2</sub> loading during adsorption and desorption process. From mass variation profile we have extracted four others key parameters.

- 5) **Characteristic time of adsorption/desorption**,  $\tau_{ads}$  (s): indicates an overall rate of adsorption or desorption process.
- 6) **Diffusional constant**,  $D_m$  (m<sup>2</sup>/s): indicates the rate of diffusion of molecules inside a particle.
- 7) **Half time**,  $tp50\%$  (s): indicates the rate of saturation of an adsorbent.
- 8) **Short-time uptake**,  $M_{ST}$  (%): indicates the amount of adsorbed mass during strong adsorbate-adsorbent interactions.

For this purpose, we have relied on Linear Driving Force (LDF) theory. As already presented in chapter II, LDF is the most common model used to describe adsorption rates.

Equation 17 represents the analytical expressions for mass uptake during adsorption process obtained under isothermal and constant pressure experiments for the LDF model.

$$m(t) = m_e (1 - e^{-k_d t}) \quad (17)$$

where the adsorbed mass  $m(t)$  is the amount of CO<sub>2</sub> adsorbed (mg),  $m_e$  is the amount of CO<sub>2</sub> adsorbed at equilibrium (mg),  $k_d$  the effective rate constant (s<sup>-1</sup>) and  $t$  the time (s).

To obtain equation 17, assumptions have been imposed, such as that the gas-phase pressure is instantaneously changed from initial pressure  $P^0$  to final condition pressure  $P^\infty$  at  $t=0$ , and then it is held constant at that value during the constant pressure experiment in a gravimetric apparatus.

This analytical solution is frequently used to obtain the diffusional coefficient  $D_M$  of a gas into adsorbent particules, from experimental gravimetric uptake data. It should, however, be emphasized that these solutions are rigorously applicable only for isothermal uptakes and for the case where  $D_M$  is not a function of adsorbate concentration within adsorbent particle [131].

We have tried to fit experimental data with this simplified analytical model, but we did not obtained good agreement. Since the CO<sub>2</sub> adsorption on studied materials has led to intense release of heat, the adsorbent thin-layer operates under non-isothermal conditions. The analytical model is not thus representative of adsorption phenomenon.

Nowadays, the most rigorous approach used to study adsorption dynamics is to couple the solutions of simultaneous mass, heat, and momentum balance equations at the particle, column, and steady state cyclic operation levels. However, because of the complexity of this approach, it is unsuitable for our high-throughput strategy.

According to this strategy, we have looked for a representative model to easy obtain the effective rate constant  $k_d$ , which enables to compare the average rate of adsorption of our materials. We have thus selected a model that best correlates our experimental data. This simplified model is derived from LDF model and takes into account the heterogeneity of adsorbents particles regarding to their shape, size of pores, etc [131].

The modeling adsorbed mass uptake  $m(t)$  has been thus represented by the following expression:

$$m(t) = \frac{m_e \cdot k_d \cdot t}{(1 + k_d \cdot t)} \quad (18)$$

In order to fit the model (equation 18) to experimental results, the least-squares method was applied, based on the maximum coefficient of determination ( $R^2$ ):

$$R^2 = \frac{\sum (\hat{y}_i - \bar{y})^2}{\sum (y_i - \bar{y})^2} \quad (19)$$

where  $R^2$  is the coefficient of correlation,  $\hat{y}_i$  the predicted values,  $\bar{y}$  the average data of measured values and  $y_i$  measured values. The best fit in the least-squares sense minimizes the sum of squared residuals, a residual being the difference between an observed value and the fitted value provided by a model [132].  $R^2$  is a statistic that will give information about how well the model fits the experimental data. An  $R^2$  of 1 indicates that the model perfectly fits the data [132].

For the maximum coefficient of determination, we have estimated the effective rate constant  $k_d$ . As already presented,  $k_d$  is an overall parameter representing the diffusion mechanism of mass transfer. From  $k_d$ , we can define two key parameters related to the characteristic time of diffusion mechanism:

$$\tau_{ads} = \frac{1}{k_d} \quad (20) \quad \text{and} \quad D_M = \frac{r_p^2}{\tau_{ads} \cdot 15} \quad (21)$$

where  $\tau_{ads}$  is the effective characteristic time of adsorption (s),  $D_M$  the diffusional coefficient ( $\text{m}^2 \cdot \text{s}^{-1}$ ) and  $r_p$  the radius of the adsorbent particle (m). The lower the characteristic time  $\tau_{ads}$ , the faster the adsorbent reaches its adsorption capacity.

$D_M$  is an effective intraparticle diffusion coefficient (already presented in chapter II). The higher the diffusional coefficient, the faster molecules diffuse inside a particle.

Example of modeling mass uptake curves and experimental data (first CO<sub>2</sub> adsorption) for some adsorbents are shown in Figure 25. For this example and the following results, the experimental data have been obtained by using the same experimental protocol and operational conditions for all samples (two adsorption cycles: 600 s of CO<sub>2</sub> + 400 s of N<sub>2</sub>, flow rate = 40 ml.min<sup>-1</sup>, thin-layer mass = 70 mg).

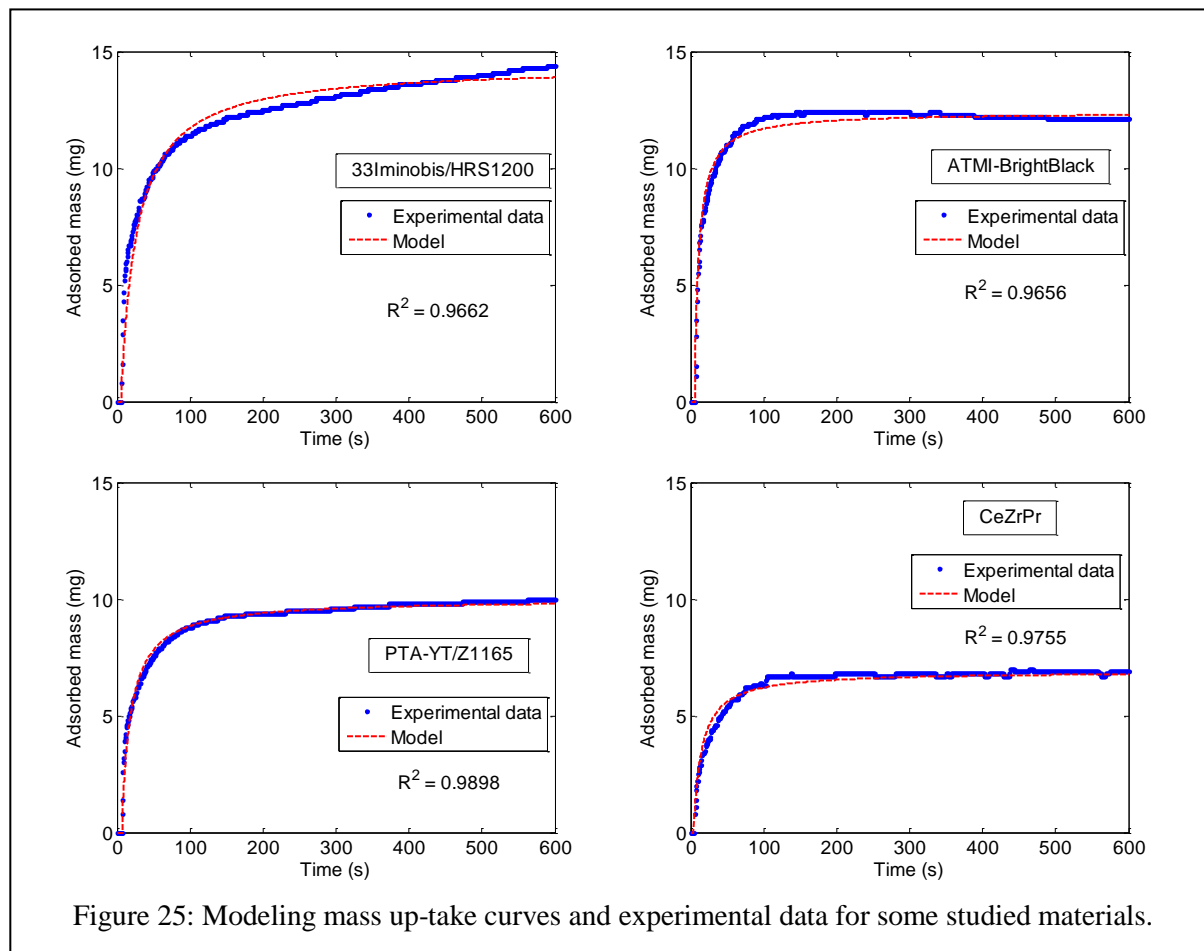


Figure 25: Modeling mass up-take curves and experimental data for some studied materials.

At first sight, in Figure 25, we observe different adsorption behaviors for each studied material, regarding adsorption kinetics and capacities. To better compare overall adsorption kinetic of different adsorbents,  $\tau_{ads}$  and  $D_M$  have been used as quantitative indicators.

The values of characteristic time of adsorption/desorption on studied materials are shown in Figure 26. Overall, the results show the lowest  $\tau_{ads}$  values for activated carbons, the highest values for hybrid materials and moderate values for REO. This suggests thus highest adsorption rates for activated carbons, the lowest for hybrid materials and moderate adsorption rates for REO. The results confirm the relationship between adsorption rate behaviors and the estimated  $\Delta H_m$  values. Among all studied materials, AC1 has reported the highest adsorption rates and 33Iminobis/HRS1200 the lowest adsorption and desorption rates. The strength of CO<sub>2</sub>-adsorbent interactions and the diffusional mass transport seem to be the base of these behaviors. In the literature, CO<sub>2</sub> adsorption on activated carbons have been explained in the terms of the diffusional mass transport through these pores between which the adsorbate molecules can be exchanged [133]. Amine loading, pore diameter of supports, and type of amine have an effect on the rate of CO<sub>2</sub> capture by amine-impregnated silicas

[134]. The common theme for amine-impregnated silicas is a quick adsorption phase followed by a slow approach to equilibrium [60].

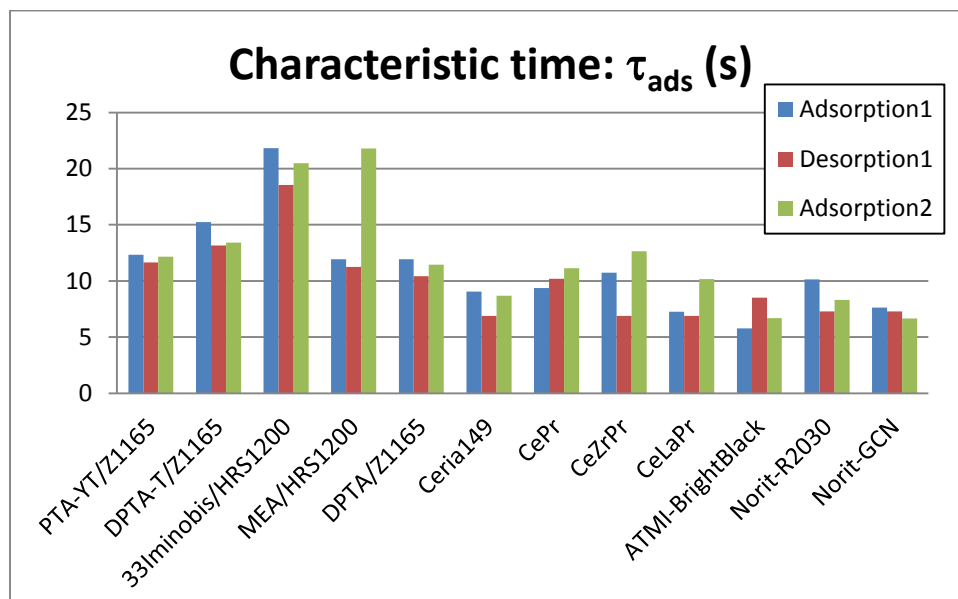


Figure 26: Characteristic times estimated thanks to mass uptake model.

High  $\tau_{ads}$  values have been estimated for MEA/HRS1200 for second adsorption. As already seen, because of low thermal stability of MEA over support, the second CO<sub>2</sub> adsorption leads to low CO<sub>2</sub>-adsorbent interactions. It means that the adsorbent affinity towards CO<sub>2</sub> has been diminished for second adsorption and consequently the adsorption rates are lower.

Differences have been reported between adsorption and desorption process. Overall, desorption rates are lower than adsorption ones. Desorption rates are strongly influenced by the operational conditions of desorption. In our case, the material regeneration has been achieved by N<sub>2</sub> purge without temperature swimming. Inert gas purge only is the less effective one among operational conditions.

The effective diffusion coefficient  $D_M$  can be calculated from the values of characteristic times  $\tau_{ads}$  and average particle diameters (hybrid materials: 330  $\mu\text{m}$ , activated carbons: 200  $\mu\text{m}$  and REO: 20  $\mu\text{m}$ ) by means of equation 21.  $D_M$  values are shown in Table 1. As  $D_M$  is dependent of  $\tau_{ads}$  values, differences on  $D_M$  values have been reported for adsorption and desorptions process.

The results show explicit dependence of  $D_M$  on particle size. The lowest  $D_M$  values (over  $10^{-13} \text{ m}^2 \cdot \text{s}^{-1}$ ) have been estimated for rare earth oxides which have the smallest particle sizes. The diffusion of CO<sub>2</sub> in REO particles is thus slower than in other families of studied materials. Overall, hybrid materials and activated carbons have reported comparable  $D_M$  values (from  $10^{-11}$  to  $10^{-10} \text{ m}^2 \cdot \text{s}^{-1}$ ).

Table 1: Estimated values of effective diffusion coefficient  $D_M$  ( $\text{m}^2.\text{s}^{-1}$ ).

Material	Adsorption1	Desorption1	Adsorption2
PTA-YT/Z1165	1.47E-10	1.56E-10	1.49E-10
DPTA-T/Z1165	1.19E-10	1.38E-10	1.35E-10
33Iminobis/HRS1200	8.31E-11	9.78E-11	8.86E-11
MEA/HRS1200	1.52E-10	1.61E-10	8.33E-11
DPTA/Z1165	1.52E-10	1.74E-10	1.59E-10
Ceria149	7.35E-13	9.69E-13	7.67E-13
CePr	7.12E-13	6.53E-13	5.99E-13
CeZrPr	6.21E-13	9.69E-13	5.27E-13
CeLaPr	9.19E-13	9.69E-13	6.55E-13
AC1	1.15E-10	7.81E-11	9.95E-11
Norit-R2030	6.57E-11	9.15E-11	8.03E-11
Norit-GCN	8.75E-11	9.15E-11	1.00E-10

The last two key parameters have been defined by normalizing the adsorbed mass curve. Using as example the experimental data for PTA-YT/Z1165 (see Figure 25), the normalized curve is shown in Figure 27. The obtained curve is termed fractional uptake curve and is widely used to study adsorption kinetics [133, 135, 136].

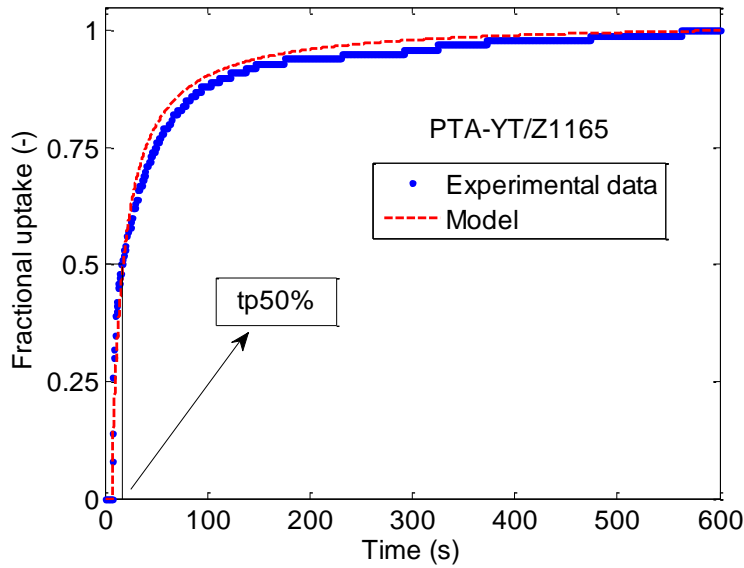


Figure 27: Normalized model and data uptake curves of PTA-YT/Z1165.

The half time  $tp50\%$  is the time required to achieve 50% of adsorption saturation. From the fractional uptake curve above we have estimated a half time of  $tp50\% = 17.1$  s. In the case of desorption process,  $tp50\%$  is the time required to achieve 50% of total desorption.

The half times  $tp50\%$  of studied materials are shown in Figure 28. Overall, the lowest values of  $tp50\%$  have been estimated for activated carbons, and the highest values for hybrid materials. Intermediate  $tp50\%$  values have been estimated for REO. AC1 has reached half of its saturation in just 10.8 s, while 33Iminobis/HRS1200 has reached half saturation in 25.7 s.

These results are in good agreement with other key parameters which indicate the highest adsorption rate for AC1 and the lowest one for 33Iminobis/HRS1200.

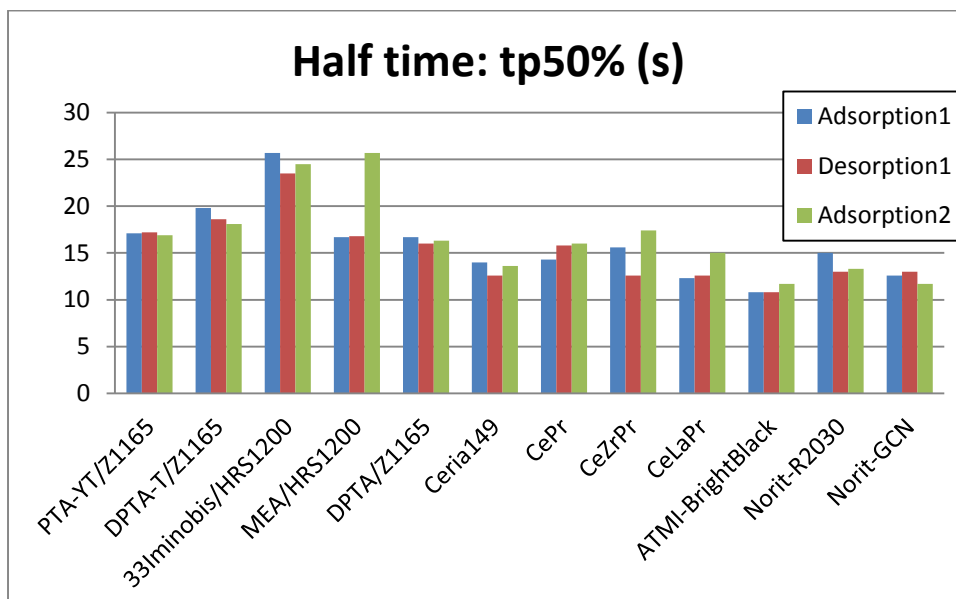


Figure 28: Half time  $tp_{50\%}$  of studied materials.

As already presented, we have stated two adsorption-time behaviors during  $\text{CO}_2$  adsorption on studied materials: short-time and long-time adsorption. In short-time adsorption, because of intense release of heat, we have suggested that  $\text{CO}_2$ -adsorbent interactions are much higher than long-time adsorption.

Taking into account these adsorption-time behaviors, we have thus defined a last key parameter related to short-time period.

The short-time uptake  $M_{st}$  consists in the adsorbed mass percentage during short-time adoption.  $M_{st}$  indicates the amount of adsorbed mass during strong  $\text{CO}_2$ -adsorbent interactions. The short-time uptake  $M_{st}$  of studied materials are shown in Figure 29.

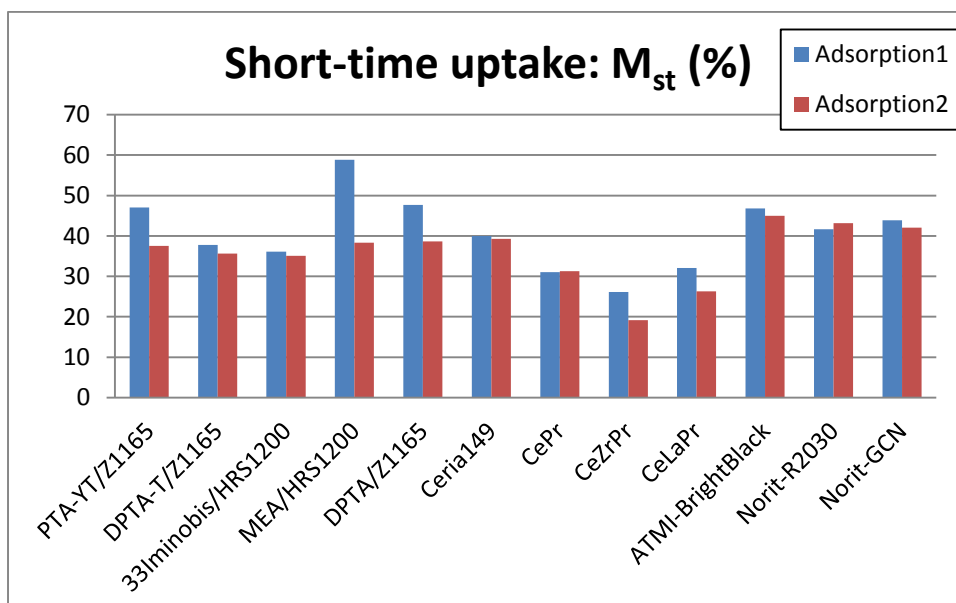


Figure 29: Estimated short-time uptake of studied materials.

Overall, the highest  $M_{ST}$  values have been estimated for activated carbons and MEA/HRS1200, and the lowest values for rare earth oxides. Intermediate  $M_{ST}$  values have been estimated for hybrid materials (except for MEA/HRS1200).

In the first adsorption, MEA/HRS1200 has adsorbed 59 % of its adsorption capacity during short-time adsorption. This result explains the intense release of heat during first adsorption and consequently the highest temperature rise among studied materials.

Among activated carbons, AC1 has adsorbed the highest amount of CO<sub>2</sub> during short-time adsorption (47%). This result is in accordance with fast adsorption rates for this material.

Other hybrid materials show an average  $M_{ST}$  value of 40%. This result appoints that over 60% of CO<sub>2</sub> capture by these materials is achieved in long-time adsorption, by weak CO<sub>2</sub>-adsorbent interactions, such as physisorption or weak chemisorption.

This result confirms the moderate  $\Delta H_{ads}$  values estimated for hybrid materials. As already suggested, CO<sub>2</sub> adsorption on studied hybrid sorbents seems to be a combination of both physisorption and chemisorption process. Identical analogy can be done for REO. The results indicate that CO<sub>2</sub> capture is mainly achieved by weak CO<sub>2</sub>-adsorbent interactions during long-time adsorption. As will be presented in the next chapter, CO<sub>2</sub> capture by REO mainly causes the formation of species weakly bound to the surface of the adsorbent at room temperature.

## 7 Conclusions

In this chapter, we have presented a thin-layer approach which consists in the development of a simplified model (lumped body) to get an insight into the thermal behavior of CO<sub>2</sub> adsorption on studied materials.

The lumped body model has allowed us to develop a simplified analysis of experimental data and to estimate adsorption heats. From an energetic point of view, the heat of adsorption is the most important key parameter to evaluate adsorbate-adsorbent interactions. Therefore, the heats of adsorption  $\Delta H_{ads}$  have been deduced from the transient adsorption heat source estimated via an inverse technique thanks to our heat transfer model.

Two adsorption regimes (short-time and long-time periods) related to the release of heat during CO<sub>2</sub> adsorption process have been characterized. We have thus confirmed that the main release of heat is due to the first interactions between CO<sub>2</sub> molecules and adsorbent surface during short-time period.

The estimated heat of adsorption  $\Delta H_{ads}$  of CO<sub>2</sub> on the studied materials enabled us to evaluate the strength of CO<sub>2</sub>-adsorbent interactions. Overall, the highest values of  $\Delta H_{ads}$  were estimated for hybrid materials, followed by REO and activated carbon.

Thanks to a simplified mass uptake model, we have defined other key parameters related to kinetics of adsorption. Overall, the highest adsorption rates were estimated for activated carbon followed by REO and hybrid materials.

Using these key parameters, an overall comparison of all studied materials will be presented in the “General Conclusions”

In the next chapter, we present the spectroscopic approach used to characterize CO<sub>2</sub>-adsorbent interactions from a chemical point of view.

## 8 Annex

### **MATLAB ode45 solver**

*MATLAB ode45* solve initial value problems for ordinary differential equations. In mathematics, in the field of differential equations, an initial value problem (also called the Cauchy problem by some authors) is an ordinary differential equation together with a specified value, called the initial condition, of the unknown function at a given point in the domain of the solution. In physics or other sciences, modeling a system frequently amounts to solving an initial value problem; in this context, the differential equation is an evolution equation specifying how, given initial conditions, the system will evolve with time.

### **Algorithm**

*Ode45* is based on an explicit Runge-Kutta formula, the Dormand-Prince pair. It is a one-step solver – in computing  $y(t_n)$ , it needs only the solution at the immediately preceding time point,  $y(t_{n-1})$ . In general, *ode45* is the best function to apply as a first try for most problems [137].

### **Solver description**

$[T, Y] = \text{solver}(\text{odefun}, \text{tspan}, y_0)$  with  $\text{tspan} = [t_0 \text{ tf}]$  integrates the system of differential equations  $y' = f(t, y)$  from time  $t_0$  to  $t_f$  with initial conditions  $y_0$ . *odefun* is a MATLAB function handle. Function  $f = \text{odefun}(t, y)$ , for a scalar  $t$  and a column vector  $y$ , must return a column vector  $f$  corresponding to  $f(t, y)$ . Each row in the solution array  $Y$  corresponds to a time returned in column vector  $T$ .

## **CHAPTER V**

### **Investigation Level I**

-

### **Insight into Chemical Interactions via DRIFT Spectroscopy**



## SUMMARY

1	Introduction .....	133
2	Experimental device .....	133
3	Results and discussion.....	136
3.1	Activated carbon.....	136
3.2	Rare earth oxides (REO).....	137
3.3	Hybrid materials .....	151
3.3.1	<sup>33</sup> Iminobis impregnated HRS1200 .....	151
3.3.2	Monoethanolamine impregnated HRS1200 .....	160
4	Conclusions .....	163



## 1 Introduction

In this step of our work, we are interested in the chemical interactions between CO<sub>2</sub> and adsorbents during the adsorption and desorption processes. As already seen in Chapter I, depending on interactions (physisorption or chemisorption), CO<sub>2</sub> molecules may interact with the adsorbent surface by forming adsorbed species. During the adsorption process, one may observe the evolution of adsorbed species amount or/and the evolution of adsorbed species nature. The identification of adsorbed species and the study of adsorbed species evolutions are important for the understanding of the adsorption mechanisms, which is essential to improve the effectiveness of CO<sub>2</sub> capture by an adsorbent.

An experimental device based on Diffuse Reflectance Infrared Fourier Transform (DRIFT) spectroscopy was developed for the *in situ* study of CO<sub>2</sub>-adsorbent interactions. As already presented in chapter II, diffuse reflectance is an excellent sampling tool for powdered materials, thus well adapted for the study of our porous adsorbents.

In the following topic, we present the experimental setup used for the study of CO<sub>2</sub>-adsorbent interactions. Then, we discuss the main results for each family of studied materials.

## 2 Experimental device

In accordance with our high-throughput strategy, an experimental setup based on DRIFT spectroscopy was developed regarding an automatic control of operating conditions (gas flow injection and temperature) and automatic spectra acquisition. DRIFT device allows thus the study of CO<sub>2</sub>-adsorbent interaction according to a defined experimental protocol, in which temperature and surrounding atmosphere (CO<sub>2</sub> or N<sub>2</sub>) are mastered.

The experimental setup consists of (see Figure 1):

- 1) **FTIR spectrometer:** Nicolet 6700 FTIR spectrometer is used for spectral acquisitions during the gas-adsorbent interactions. A resolution of 4 cm<sup>-1</sup> has been used for the achievement of experiments.
- 2) **Diffuse Reflection Accessory:** Praying Mantis™ Diffuse Reflection Accessory is used as a sample handling technique allowing DRIFT measurements.
- 3) **Reaction chamber:** Praying Mantis™ High Temperature Reaction Chamber allows DRIFT measurements under controlled atmosphere and a wide range of temperature (from T<sub>room</sub> up to 900 °C).
- 4) **Temperature controller:** Harrick series 989 temperature controller allows an adjustable temperature of the adsorbent during desorption studies.
- 5) **Injection system:** The injection system composed of two Bronkhorst flow meters (calibrated to CO<sub>2</sub> and N<sub>2</sub> gas) and 3-way valves, allows the switch on gas (N<sub>2</sub> /CO<sub>2</sub>) with a controlled injection time, thanks to a home-made Lab view interface.
- 6) **Minichiller:** HUBER-Minichiller is used to cool the system and so it protects diffuse reflection accessories from excessive heating, avoiding thus the degradation of the experimental device.
- 7) **Spectral acquisition PC:** Personal computer provided with spectral acquisition software.
- 8) **Injection system PC:** Personal computer provided with Lab view interface to control the injection system.

Figure 2 shows a scheme for a better visualization of the experimental setup.

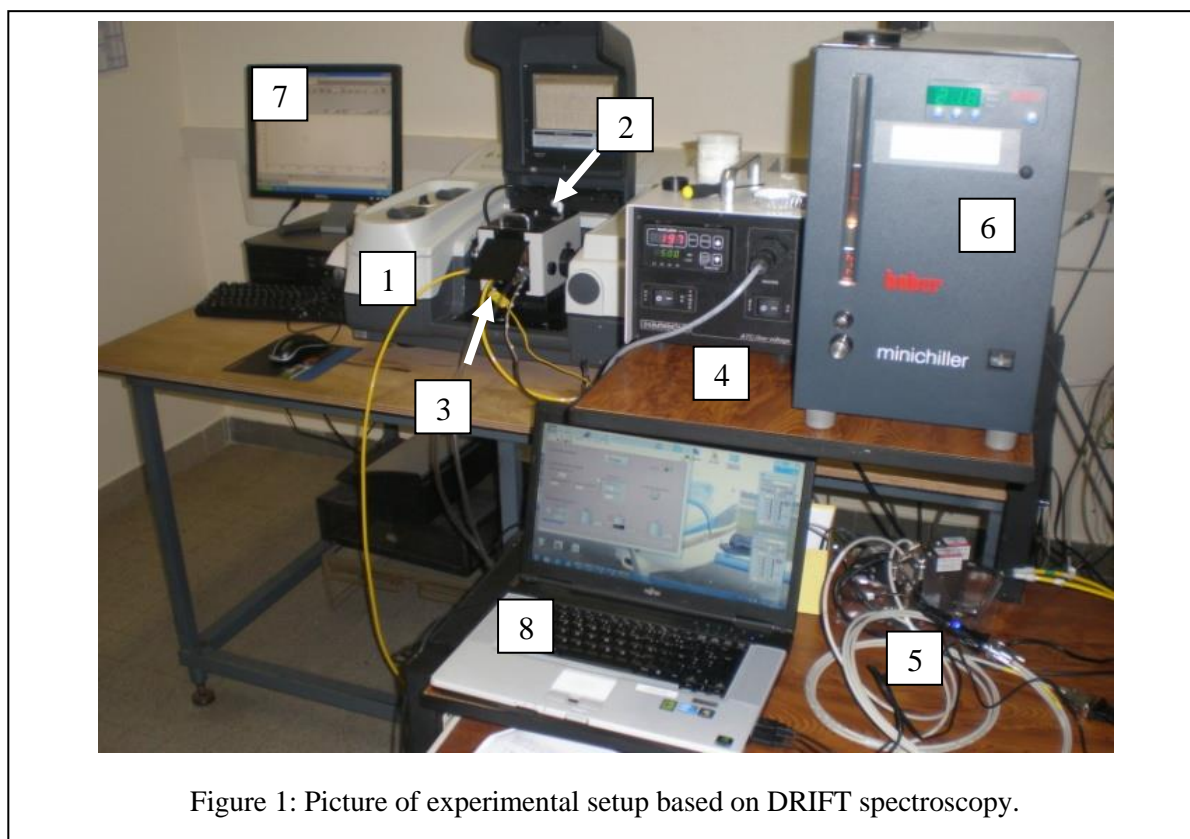


Figure 1: Picture of experimental setup based on DRIFT spectroscopy.

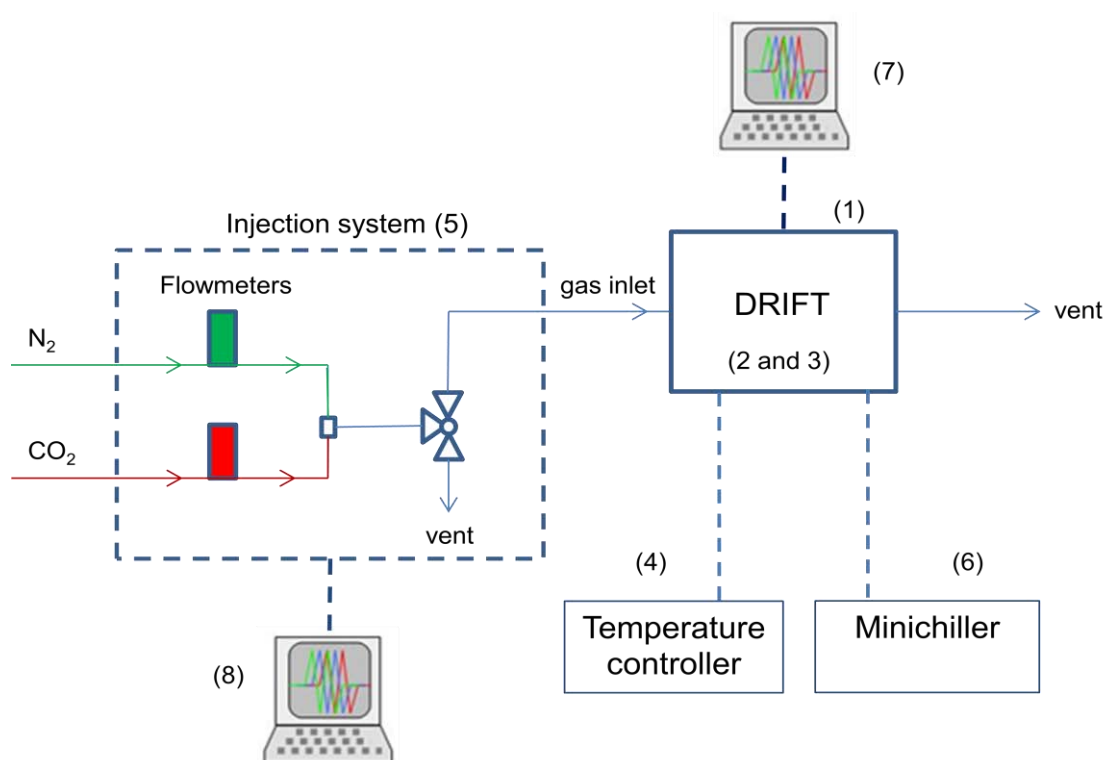


Figure 2: Schema of experimental setup.

Therefore, in order to record the DRIFT spectra of CO<sub>2</sub>-adsorbent interaction, the diluted sample (grounded and mixed with KBr) is placed in the reaction chamber (Figure 3), which is placed in the FTIR spectrometer equipped with a Diffuse Reflection Accessory. The reaction chamber is connected with the injection system, with temperature controller and the minichiller.

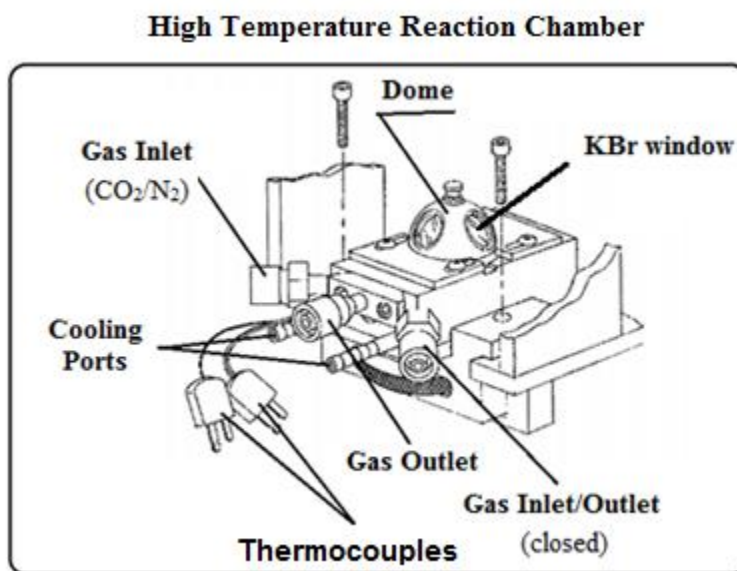


Figure 3: Illustration of the High Temperature Reaction Chamber.

By mean of Diffuse Reflection Accessory, the source radiation strikes the powdered sample and is diffusely reflected in various directions. This diffuse radiation is collected by a mirror and measured by the detector of the FTIR spectrometer (Figure 4).

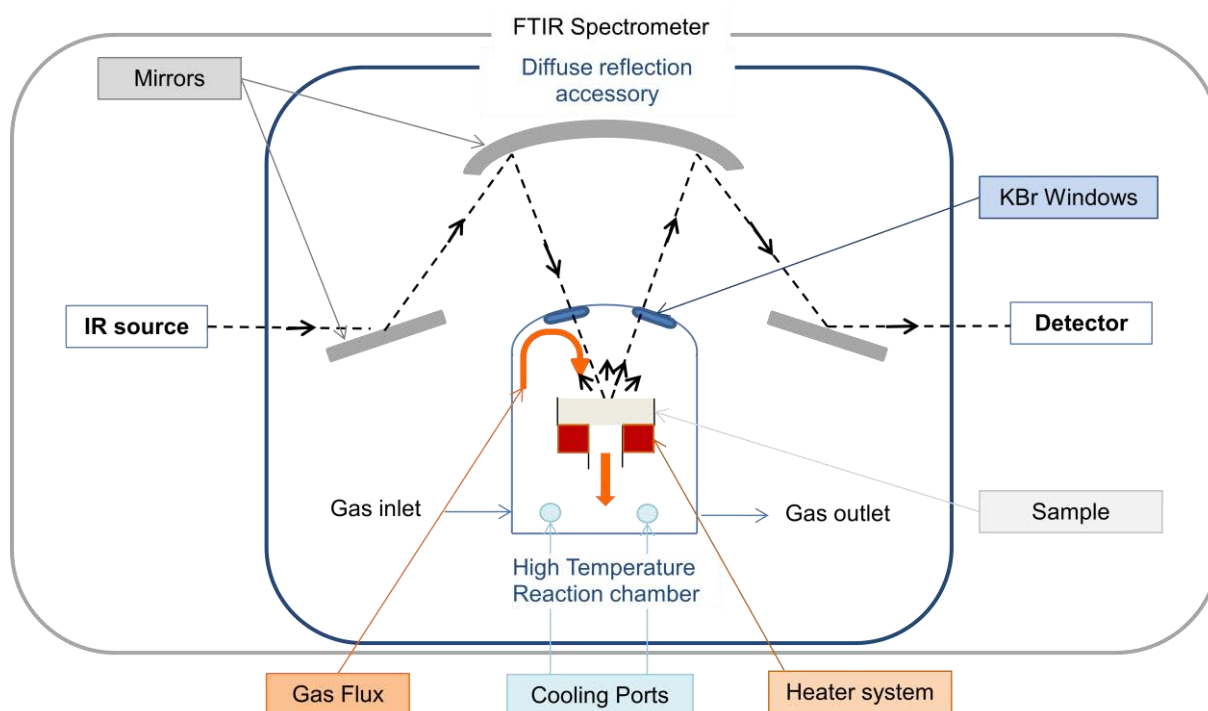
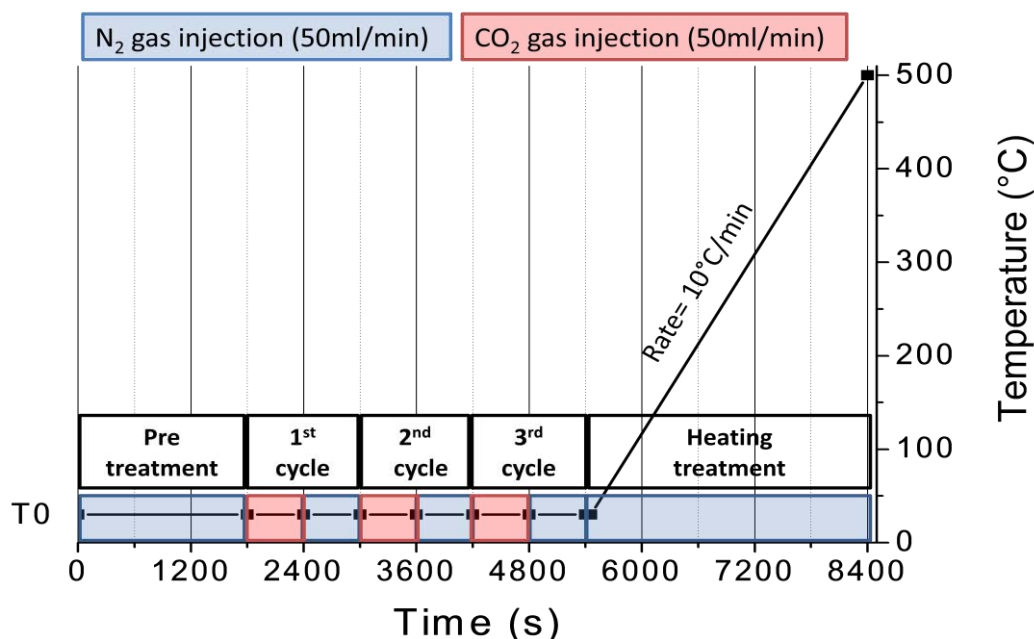


Figure 4: Close-up of FTIR spectrometer equipped with DRIFT device.

Thanks to this experimental, device we record the spectrum evolution during CO<sub>2</sub>/N<sub>2</sub> injections into the reaction chamber.

An experimental protocol has been used to investigate CO<sub>2</sub>-adsorbent interactions (Figure 5). This experimental protocol was designed for high-throughput studies. In other words, from a single experiment, we obtain a maximum amount of information about CO<sub>2</sub>-adsorbent interactions.

Figure 5: Experimental protocol used to study CO<sub>2</sub>-adsorbent interactions via DRIFT device.

The protocol consists of three steps:

- 1) **Pretreatment:** N<sub>2</sub> gas injection during 1800 (s) at room temperature (30°C). The aim is to desorb possible contaminants on sample surface and to prepare sample for CO<sub>2</sub> adsorption cycles.
- 2) **CO<sub>2</sub> adsorption cycles:** 3 cycles of gas injection at room temperature. Each cycle includes CO<sub>2</sub> injection during 600 (s), than N<sub>2</sub> injection during 600 (s). The aim is to study at room temperature, CO<sub>2</sub> adsorptions and desorptions.
- 3) **Temperature swing:** under inert flow (N<sub>2</sub>) during 3000 (s), the sample is heated from T=30 °C to T=500°C. The aim is to study the thermal stability of adsorbed species.

### 3 Results and discussion

#### 3.1 Activated carbon

The obtained results from previous high-throughput steps have indicated AC1 as the most interesting adsorbent among activated carbons regarding a reversible CO<sub>2</sub> capture. These results suggested CO<sub>2</sub> physisorption on this material.

In order to confirm that the physical-sorption occurred and no new species were formed, the DRIFT spectrum of AC1 following CO<sub>2</sub> adsorption was recorded and is shown in Figure 6.

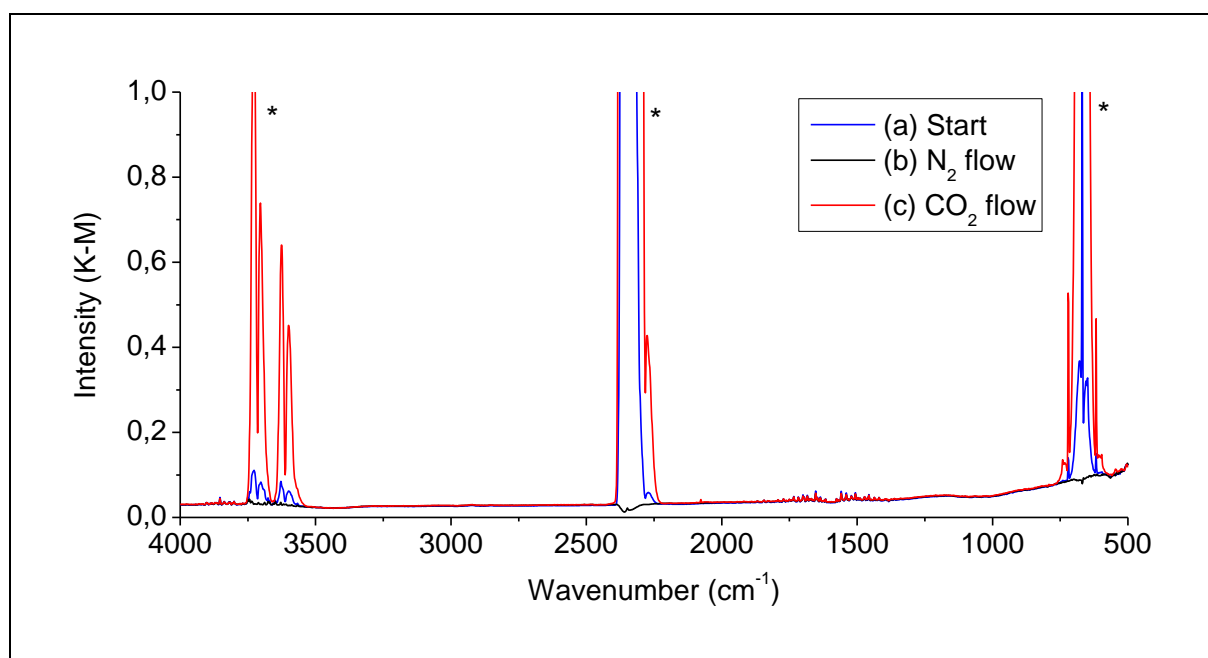


Figure 6: DRIFT spectra of AC1. Start spectrum (a), before adsorption under N<sub>2</sub> flow (b) and after adsorption under CO<sub>2</sub> flow (c).

Compared with the start DRIFT spectrum of the AC1 (a), neither the spectrum obtained under N<sub>2</sub> flow (b) nor under CO<sub>2</sub> flow (c) shows obvious changes, except for the bands at spectral range 3770-3530, 2407-2216 and 770-560 cm<sup>-1</sup> (\*) due to vibration modes of CO<sub>2</sub> in the gas-phase. These results indicate that no new species were formed during CO<sub>2</sub>-adsorbent interactions. The CO<sub>2</sub> capture by AC1 is thus achieved via physisorption process.

No bands in the spectral range corresponding to adsorbed water (3500-3000 cm<sup>-1</sup>) have been observed. This suggests a hydrophobic character of this material and confirms the results obtained in screening steps, in which no significant endothermic response during pretreatment (under N<sub>2</sub> flow) has been observed.

*Note: to achieve this experiment, the sample was ground and mixed with KBr using a 10 tons press because of the high hardness of AC1 particles and because of its black color (and consequentially of its high IR absorption). A study of the optimal dilution ratio of sample in KBr was performed (3, 5 and 10 wt%) to maximize the signal/noise ratio. The best signal/noise ratio was obtained for dilution ratio of 5% by weight.*

### 3.2 Rare earth oxides (REO)

From literature, it is known that CO<sub>2</sub> interacts with rare earth oxides by chemisorption process. Lavalley *et al.* suggested that CO<sub>2</sub> molecules interact with cerium oxide by Lewis acid-base reaction. They proposed that CO<sub>2</sub> interact thus with surface O<sup>2-</sup> or with surface basic residual species -OH to form carbonate or hydrogencarbonate species, respectively.

In order to verify the formation and study the evolution of these species on studied REO, we have recoded the DRIFT spectra during the experimental protocol presented before (Figure 5).

In order to show the main results obtained via DRIFT spectroscopy, we have selected Ceria149 (undoped ceria with a specific surface of 149 m<sup>2</sup>/g) as a model material.

The spectrum of Ceria149 before and after CO<sub>2</sub> adsorption, for the first adsorption cycle, is shown in Figure 7.

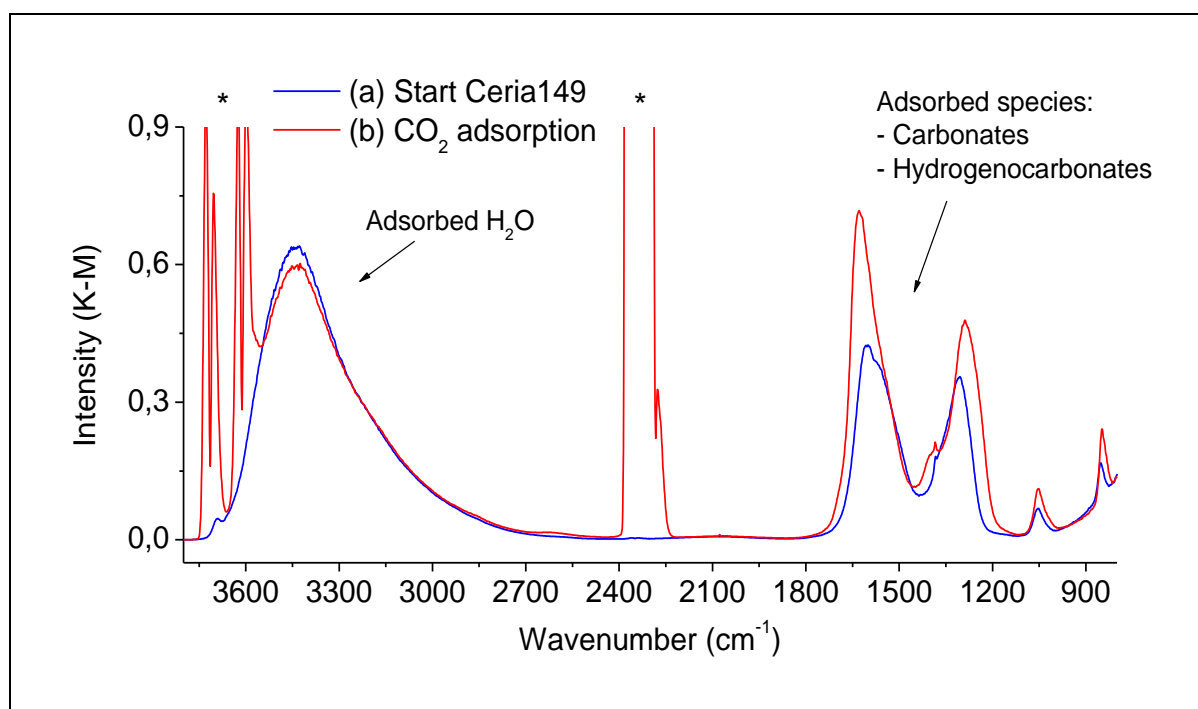


Figure 7: DRIFT spectra of Ceria149. Initial spectrum of Ceria149 under  $N_2$  flow (a) and spectrum of Ceria149 under  $CO_2$  flow (b). (\*) refers to the vibration modes of gas-phase  $CO_2$ .

On the DRIFT spectrum of the starting material Ceria149 under  $N_2$  flow (a), we identify the presence of already existing adsorbed species: a broad band centered at  $3442\text{ cm}^{-1}$  due to adsorbed water and several bands at spectral range of  $1800\text{--}800\text{ cm}^{-1}$  due to carbonates and hydrogencarbonates.

Compared with the starting spectrum (a), the spectrum of sample under  $CO_2$  flow shows considerable changes regarding the intensity and shape of bands. Main changes are observed in the spectral range of carbonates and hydrogencarbonates species. Overall, the intensity of these bands increases during  $CO_2$  adsorption.

The kinetic profile of these species, recorded during the experimental protocol, is shown in Figure 8.

*Note: The kinetic profiles shown in this chapter were obtained by integration of the spectral range related to adsorbed species ( $1800\text{--}1100\text{ cm}^{-1}$ ). The gas flow rate and sampling rate were adjusted to  $50\text{ ml/min}$  and  $1\text{ spectrum each } 11\text{ seconds}$ , respectively. All studied REOs were grounded and mixed (10% in mass) with non-absorbing matrix (KBr).*

The kinetic profile obtained via DRIFT spectroscopy shows similar behaviors to thermal and mass uptake profiles obtained during primary and secondary screening respectively.

In the pretreatment under  $N_2$  flow ( $t_0$  to  $t_1$ ), we observe the decrease of the peak area and intensity related to overall adsorbed species corresponding to carbonates and hydrogencarbonates (a) and adsorbed water (b) respectively. These results confirm a partial desorption of these species from Ceria149 and explain the endothermic response observed during pretreatment under the same conditions in primary screening.

In the second step of protocol, in which  $CO_2$  adsorption cycles are achieved, we observe a sudden increase of the area of bands (a) during  $CO_2$  injections and a decrease of the area of these bands during  $N_2$  injections. These results confirm thus  $CO_2$  adsorption and desorption processes respectively.

The intensity of peak (b) is almost constant in this part of protocol. This indicates that adsorbed water has reached the thermodynamic equilibrium with adsorbent surface at room temperature. Minor differences are observed during CO<sub>2</sub> flow. We suggest that part of adsorbed water interacts with CO<sub>2</sub> molecules to form hydrogencarbonates.

We notice that adsorption rates are not similar to desorption rates. CO<sub>2</sub> adsorption rates are faster than desorption rates, principally at short-time periods. These results are in line with screening results previously obtained.

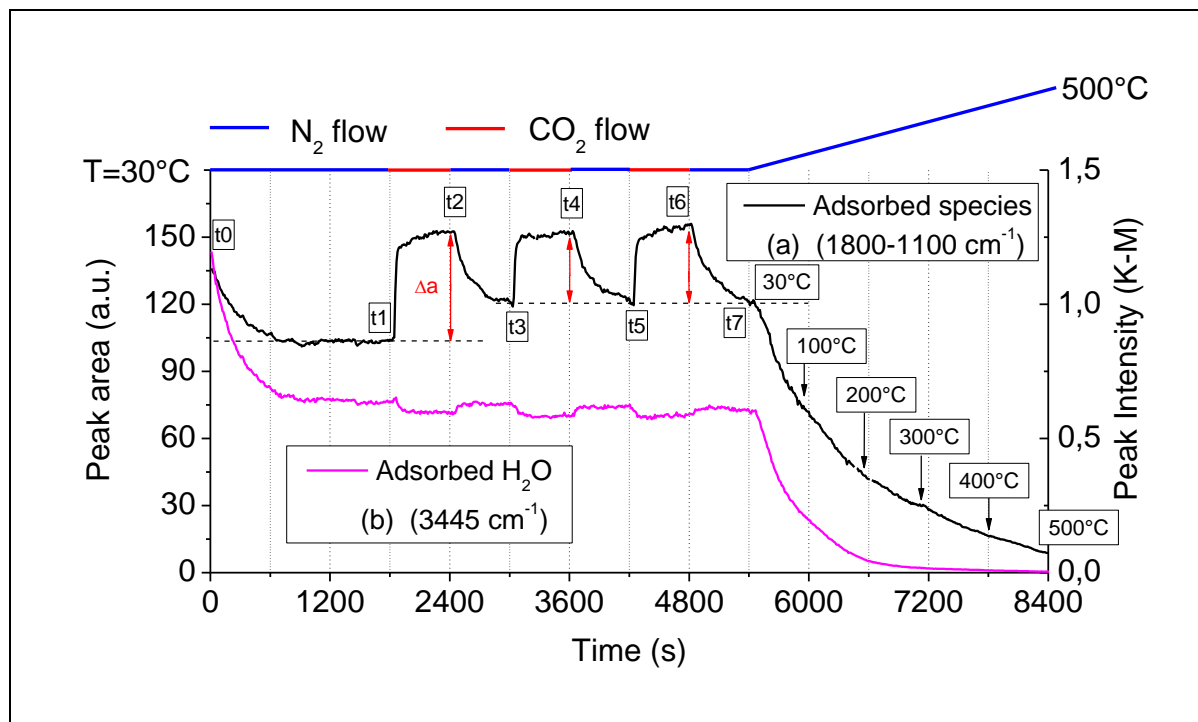


Figure 8: Kinetic profiles obtained via DRIFT spectroscopy. Area of peaks related to adsorbed species (a) and intensity of peak related to adsorbed water (b).

The variation of the area of bands ( $\Delta a$ ) in the first CO<sub>2</sub> adsorption is higher than the following ones. As also observed in thermal profiles, the difference between first and following adsorptions is related to CO<sub>2</sub> capture irreversibility. As already explained for thermal profiles of REO, the desorption conditions (N<sub>2</sub> flow at room temperature) is insufficient to desorb the total of adsorbed species during the first CO<sub>2</sub> adsorption. In following adsorptions, a smaller number of adsorption sites are available for CO<sub>2</sub> capture and consequently the adsorption capacity is reduced. We observe as well that following adsorptions are totally reversible because  $\Delta a$  is almost constant.

In the final step of protocol, in which the sample is heated at a constant rate (10°C/min) from room temperature 30°C to 500°C, we observe a fast decrease of the area of peaks (a) and of the intensity of peak (b) until almost and total disappearance of species (a) and (b) respectively. We state also distinct desorption rates of these species. Water is desorbed much faster than other adsorbed species. These results indicate different thermal stabilities for each adsorbed species on adsorbent surface.

The spectra of Ceria149 obtained during adsorption cycles, at spectral range of 1800-800 cm<sup>-1</sup>, are shown in Figure 9. From t1 to t2, during the first CO<sub>2</sub> adsorption (see Figure 8), the spectrum of Ceria149 evolves to higher intensities. We observe the increase and the shift of bands: from 1600 to 1628 cm<sup>-1</sup> (a), from 1306 to 1286 cm<sup>-1</sup> (b) and from 852 to 848 cm<sup>-1</sup> (c).

We observe as well the increase of band intensity, without shift, at 1400 and 1054  $\text{cm}^{-1}$ . The evolution of these bands is the fingerprint of the formation of species over adsorbent.

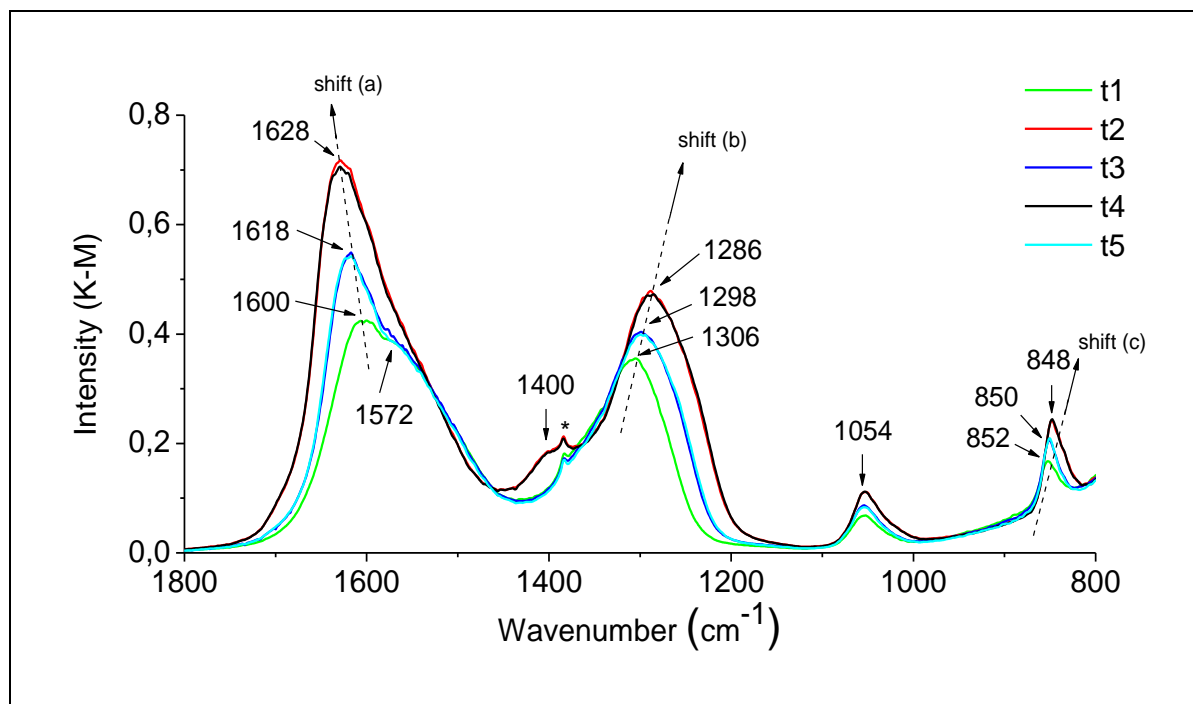


Figure 9: Evolution of DRIFT spectra of Ceria149 during adsorption cycles. (\*) unidentified band.

In the first desorption process, from t2 to t3, the intensity of bands a, b, c and 1054  $\text{cm}^{-1}$  decrease to intermediary levels and the band at 1400  $\text{cm}^{-1}$  totally decreases to initial conditions. These results suggest a partial desorption of species from adsorbent surface.

From t3 to t4 (second  $\text{CO}_2$  adsorption) and from t4 to t5 (second desorption), the sample spectrum evolves to the same position than t2 and t3 respectively. Identical adsorption and desorption behaviors were observed for following adsorption cycles.

Overall, these results confirm that the first adsorption cycle leads to the formation of adsorbed species having stronger strength of interaction with ceria surface than following adsorption cycles, and that after the first adsorption,  $\text{CO}_2$  adsorption process becomes reversible.

In order to strictly identify the adsorbed species during the first and following adsorptions, subtraction spectra were obtained (Figure 10) by subtracting spectrum t2 from t1 (a), t4 from t3 (b), and t3 from t1 (c). All subtraction spectra are shown in Figure 10 d.

The subtraction spectra is a valid technique only if we consider that  $\text{CO}_2$  adsorption process at room temperature has not significantly modified the already existing adsorbed species on adsorbent surface.

Subtraction1 and subtraction2 exalt the spectra of the species adsorbed during the first and second adsorption processes respectively. Comparing these results, we suggest that first adsorption leads to different nature and amount of adsorbed species because of distinct intensities and shapes of resulting bands. As second and following adsorptions are totally reversible under soft conditions (desorption under  $\text{N}_2$  flow at room temperature), subtraction2 represents the most instable adsorbed species on Ceria149.

From studies by Lavalley *et al.* (see Table 2 in chapter I), bands at 1647, 1600, 1452, 1403, 1235, 1052, 844 and 834  $\text{cm}^{-1}$  are assigned to hydrogencarbonates [70] formed during the second and the following adsorption cycles.

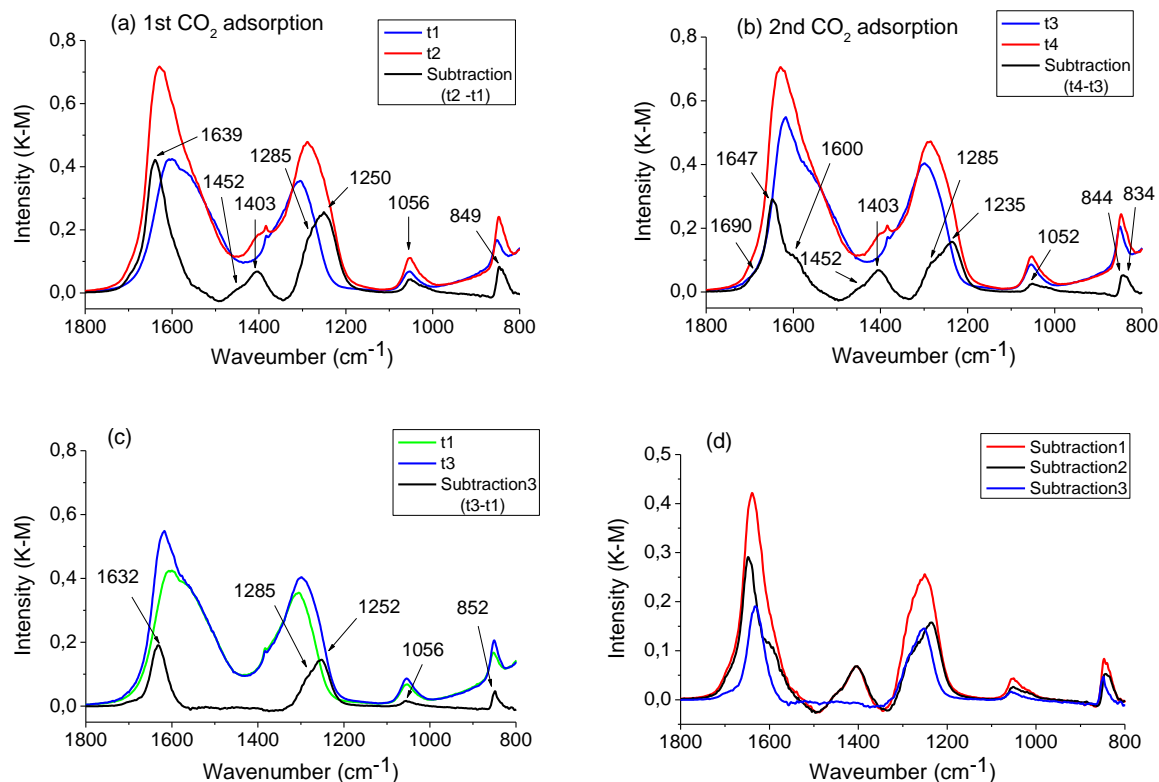


Figure 10: Subtraction spectra of Ceria149.

Substarction3 exalts the spectrum of adsorbed species during the first adsorption process, but which were not desorbed from sample under soft conditions. The strength of interaction between these species and adsorbent are therefore higher than adsorbed species during following adsorptions. We suggest that the bands at 1632, 1285, 1252, 1056 and 852  $\text{cm}^{-1}$  are due to more stable hydrogencarbonates and to bidentate carbonates formed during the first adsorption cycle of  $\text{CO}_2$ .

As reported by Lavalley, these results indicate the formation of two types of hydrogencarbonates, type II being more stable than type I. They suggest that the two different compounds may result from  $\text{CO}_2$  interaction with OH groups either mono- or bicoordinated with cerium surface cations (Figure 11 a), and that the type I OH groups are mainly involved in the formation of hydrogencarbonate species. The following mechanism of type I hydrogencarbonate has been proposed by Tsyganenko [138] (Figure 11 b):

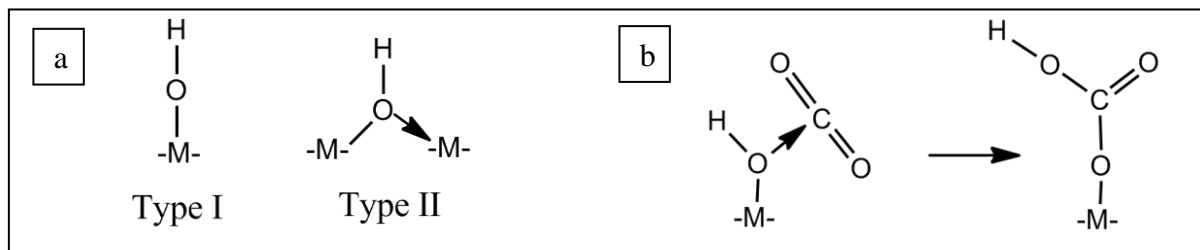


Figure 11: a) OH groups of type I and II. b) Mechanism of formation of hydrogencarbonates type I.

The temperature swing during the final step of experimental protocol (see Figure 8) confirmed the presence of the two types of OH groups, and also allowed the identification of already existing adsorbed species on adsorbent surface. Figure 12 shows the DRIFT spectra of Ceria149 during temperature swing at spectral range of 3800-2650  $\text{cm}^{-1}$ .

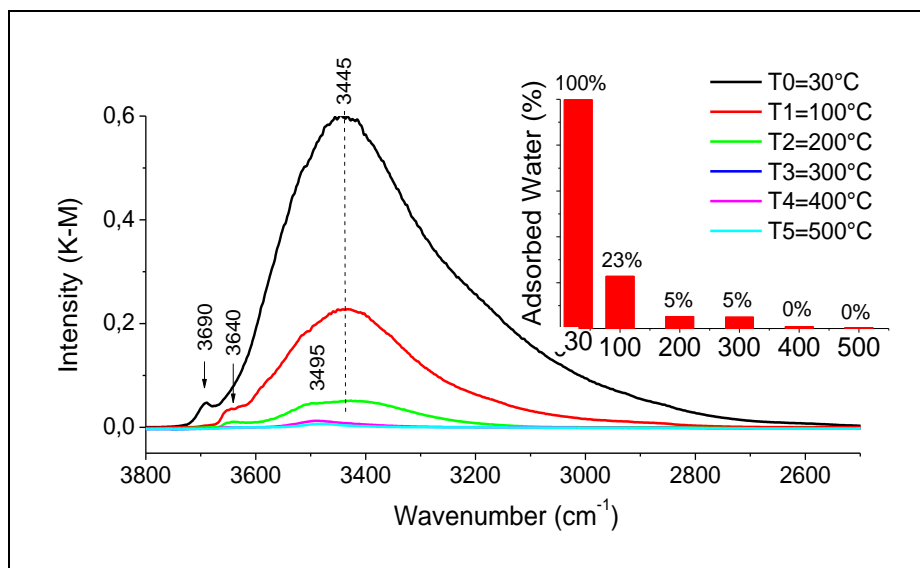


Figure 12: Evolution of adsorbed water during temperature swing. Inset figure show the percentage of remaining adsorbed water

The results show that the intensity of the band at  $3445\text{ cm}^{-1}$  due to adsorbed water strongly decreases during temperature swing, mainly from 30 to  $100^\circ\text{C}$ . At room temperature, we observe a band at  $3690\text{ cm}^{-1}$  assigned to type I hydroxyls and at  $100^\circ\text{C}$  we observe a band at  $3640\text{ cm}^{-1}$  assigned to type II hydroxyls. These results shows that type I hydrogencarbonates completely vanishes during temperature swing from 30 to  $100^\circ$  and just a few amount of type II hydrogencarbonates remains on adsorbent surface.

The DRIFT spectra of Ceria149 recorded during the final step of experiment in the spectral range of  $1800\text{-}800\text{ cm}^{-1}$  is shown in Figure 13.

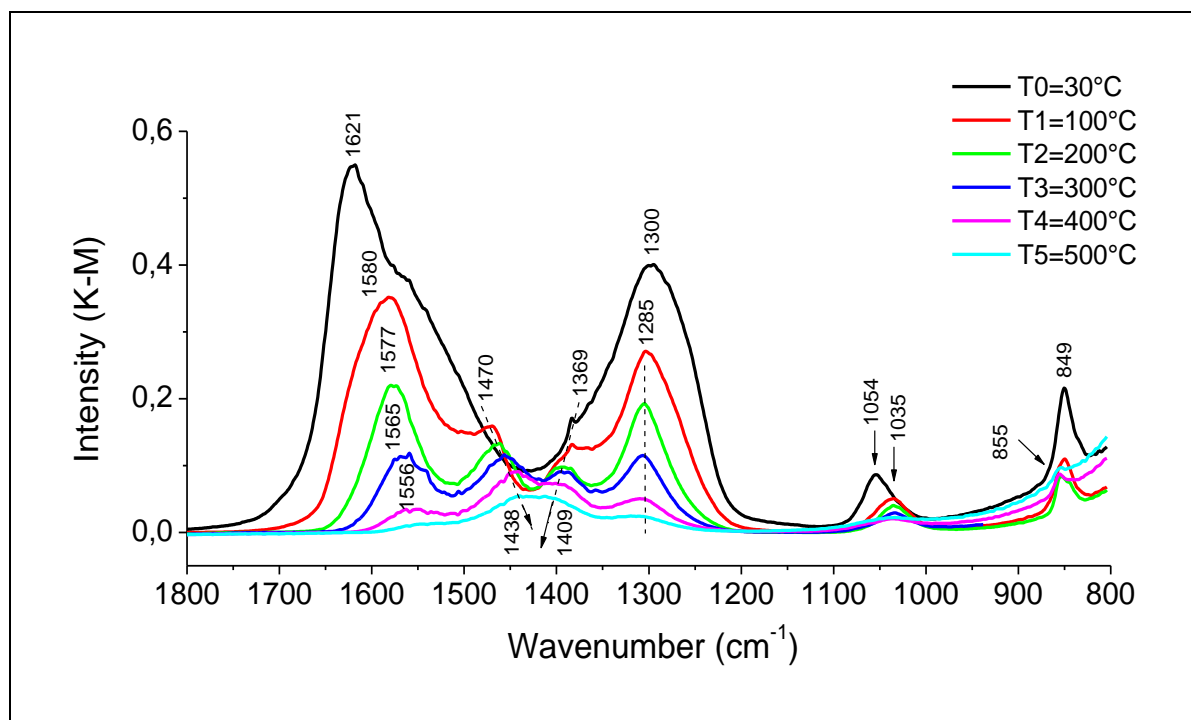


Figure 13: DRIFT spectra of Ceria 149 obtained during temperature swing step.

Overall, we observe the decrease of the intensity of bands during temperature swing. The shapes of these bands are also influenced by rising temperature. These results suggest that

desorption process leads to surface reorganization of already existing adsorbed species on Ceria149 during temperature swing. For this reason, we could not apply subtraction spectra technique for identification of these species.

Using peak resolve software, in which a model fits a number of individual synthetic peaks to a set of overlapping peaks in a spectrum (deconvolution technique), we have identified several bands related to different adsorbed species (Figure 14).

The deconvolution technique enables to identify hidden bands and to evidence the ratio between bands for each temperature of desorption.

As we can see from results, at room temperature, a large number of peaks have been identified, suggesting thus various types of adsorbed species. As the sample is heated, we observe a decrease of the intensity and the number of bands, indicating thus successive desorptions of species.

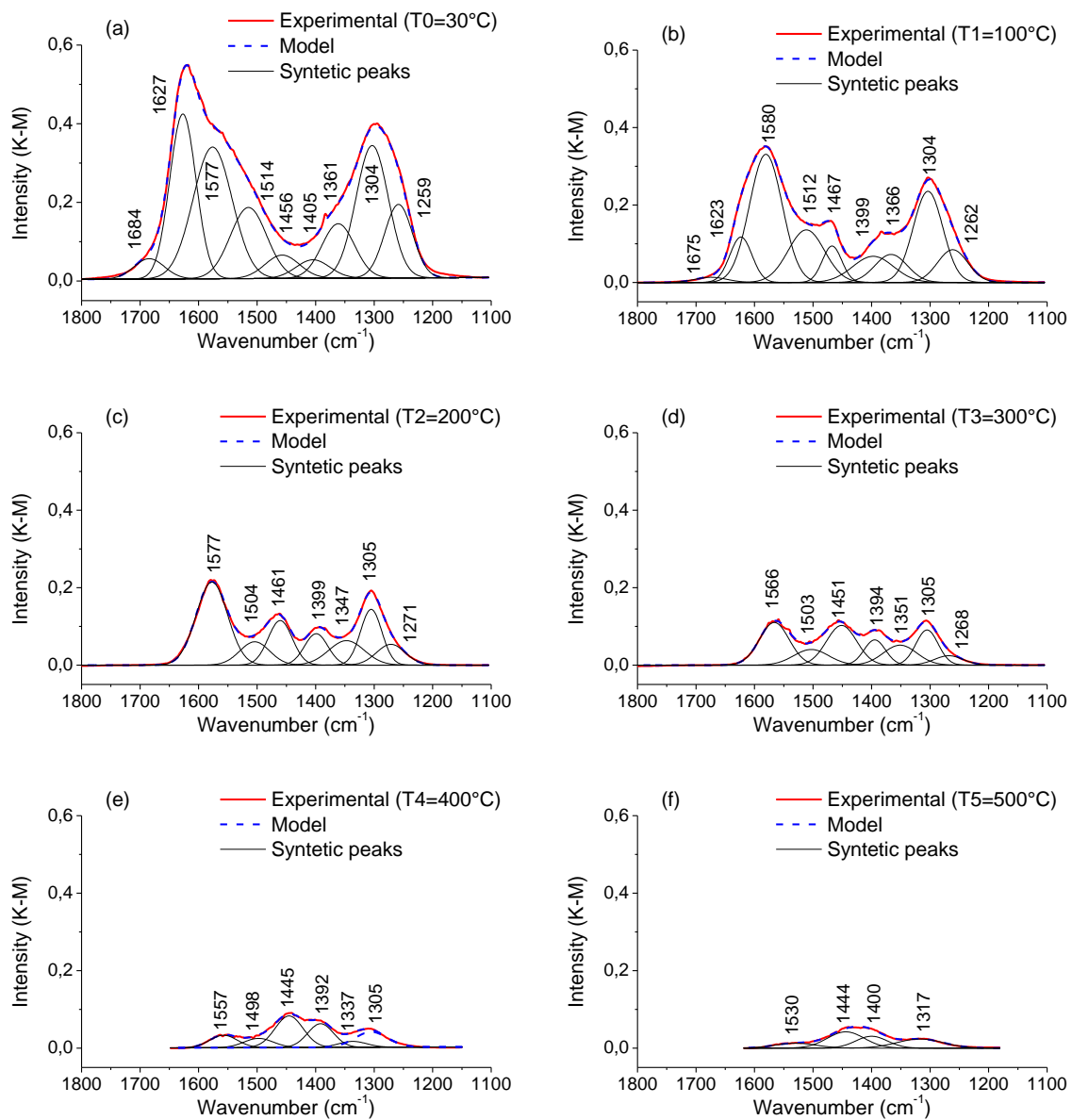


Figure 14: Identification of bands via deconvolution technique.

As already seen in chapter I, different kinds of carbonate species can be formed depending how CO<sub>2</sub> is bonded to material surface in a monodentate, bidentate or polydentate way.

Designed as bulk carbonates, polydentate species correspond to an incorporation of carbonate ions into the oxide. Therefore these species are the most stable of adsorbed species.

The free carbonate ion presents three IR active bands: one asymmetric  $\nu(\text{CO})$  vibration at  $1415 \text{ cm}^{-1}$ , one out-of-plane  $\pi(\text{CO}_3)$  deformation at  $879 \text{ cm}^{-1}$  and in plane  $\delta(\text{CO}_3)$  deformation at  $680 \text{ cm}^{-1}$ . In adsorbed state, two  $\nu(\text{CO})$  bands either side of a wavenumber of  $1415 \text{ cm}^{-1}$  are generally observed. These two bands result from the splitting of the degenerate  $\nu(\text{CO})$  vibration of free carbonate ion.

The splitting between the two highest frequency modes of the carbonates  $\Delta\nu(\text{CO})$  is related to the symmetry of the  $\text{CO}_3$  moiety. The most symmetric carbonates manifest the smallest splitting and are in general more stable than other carbonates.

The splitting between bands  $\Delta\nu(\text{CO})$  has been used to characterize the structure of the species formed: it is about 100, 300 and  $400 \text{ cm}^{-1}$  for monodentate, bidentate and bridged species, respectively [139]. We have used this criterion and literature review to propose band assignment.

Table 1 summarizes the bands found for each temperature of desorption, in which similar bands are organized in the same row.

Table 1: Summary of bands found via deconvolution technique.

Temperature (°C)	Wavenumber ( $\text{cm}^{-1}$ )									
30	1627	1577	1514	1456	1405	1361	1304	1259	1054	849
100	1623	1580	1512	1467	1399	1366	1304	1262	1035	849
200		1577	1504	1461	1399	1347	1305	1271	1035	850
300		1566	1503	1451	1394	1351	1305	1268	1035	850
400		1557	1498	1445	1392	1337	1305		1033	855
500		1530		1444	1400	1317			1033	855
	A1	B1	C1	D1	D2	C2	B2	A2		

Therefore, we suggest that bands at A1, A2, 1054 and  $849 \text{ cm}^{-1}$  are due to hydrogencarbonates, bands at B1, B2, 1035 and  $850 \text{ cm}^{-1}$  are due to bidentate carbonates, bands at C1, C2, D1, D2 are due to monodentate and polydentate carbonates respectively together with bands at 1033 and  $855 \text{ cm}^{-1}$ .

We have also identified at low temperatures (30-100 °C) a very weak band at 1684-1675. This band may indicate traces of bridged carbonates, defined as carbonates with two oxygen atoms coordinated to two different cerium cations.

At 500°C the bands at B1, C1 and C2, B2 converge to single bands at 1530 and  $1317 \text{ cm}^{-1}$  respectively. These results reinforce the assumption about a reorganization of adsorbed species on material surface during thermal desorption.

The difference between splitting bands  $\Delta\nu(\text{CO})$  of species is shown in Table 2. Overall, the results are in accordance with literature: polydentate < monodentate < bidentate.

There is a lot of controversy about bands assignment of surface carbonate species. Because of low symmetry, monodentate species should be normally less stable on a surface than the corresponding bidentate structure. However, as for our results and most of reported results in the literature, thermal desorption studies have revealed smaller splitting  $\Delta\nu(\text{CO})$  for monodentate species, suggesting thus higher stability.

Table 2: Splitting between the two highest frequency modes of the carbonates.

Temperature (°C)	Bidentate $\Delta\nu(\text{CO})$	Monodentate $\Delta\nu(\text{CO})$	Polydentate $\Delta\nu(\text{CO})$
<b>30</b>	273	153	51
<b>100</b>	276	146	68
<b>200</b>	272	157	62
<b>300</b>	261	152	57
<b>400</b>	252	161	53
<b>500</b>	213		44

Vayssilov *et al.* recently reported good correlation about the splitting between the two highest frequency modes of the carbonates and the symmetry of adsorbed species on ceria nanoparticles [71]. Using a combination of computational modeling and FTIR spectroscopy, they proposed partly new assignment of the vibrational bands. Comparing our results to these new assignments, the bands previously assigned to monodentate and bidentate carbonates are actually due to different types of tridentate carbonates (carbonates bound by three oxygen atoms to the ceria surface) regarding their stability on ceria surface. However, in order to compare our results with classical results in the literature, we have decided to keep the usually band assignments. The characteristic bands are thus reported in Table 3.

Table 3: Adsorbed species from CO<sub>2</sub> adsorption on Ceria149 at r.t.: wavenumbers of their characteristic bands.

Species	Desorption temperature	DRIFT wavenumbers (cm <sup>-1</sup> )			
		$\nu(\text{CO}_3)$	$\pi(\text{CO}_3)$	$\delta(\text{OH})$	$\nu(\text{OH})$
Hydrogencarbonates					
(I)*	r.t. (30°C)	1647, 1403, 1052	844	1235	3690
(II)	30-100°C	1627, 1452, 1056	852	1252	3640
Carbonates					
Bidentate*	30-300°C	1580, 1305, 1035	850		
Monodentate*	300-400°C	1503, 1351, 1033	855		
Polydentate*	400-500°C	1444, 1400, 1033	855		
*The wavenumbers assigned to Hydrogencarbonate of type I were obtained from subtraction spectra technique.					

Figure 15 shows the kinetic of desorption for each species during temperature swing. The results bring out the thermal stability of adsorbed species.

We notice distinct desorption rate of adsorbed species, with highest desorption rates for hydrogencarbonates and slowest rates for polydentate carbonates.

Hydrogencarbonates are thus the most unstable species and polydentate the most stable ones. These results are in good agreement with literature, in which the thermal stability of species is established as: hydrogencarbonates < bidentate carbonates < monodentate carbonates <

polydentate carbonates [140, 141]. We can also observe the rearrangement of surface species as the ratio of polydentate species slightly rises between 100 and 200°C.

The percentage of remaining adsorbed species on adsorbent during temperature swing is shown in Figure 16. Temperature swing from room temperature 30 up to 500 °C almost desorbs the total amount of species. We observe the highest desorption rates at relatively low temperature swing, from 30 to 200°C.

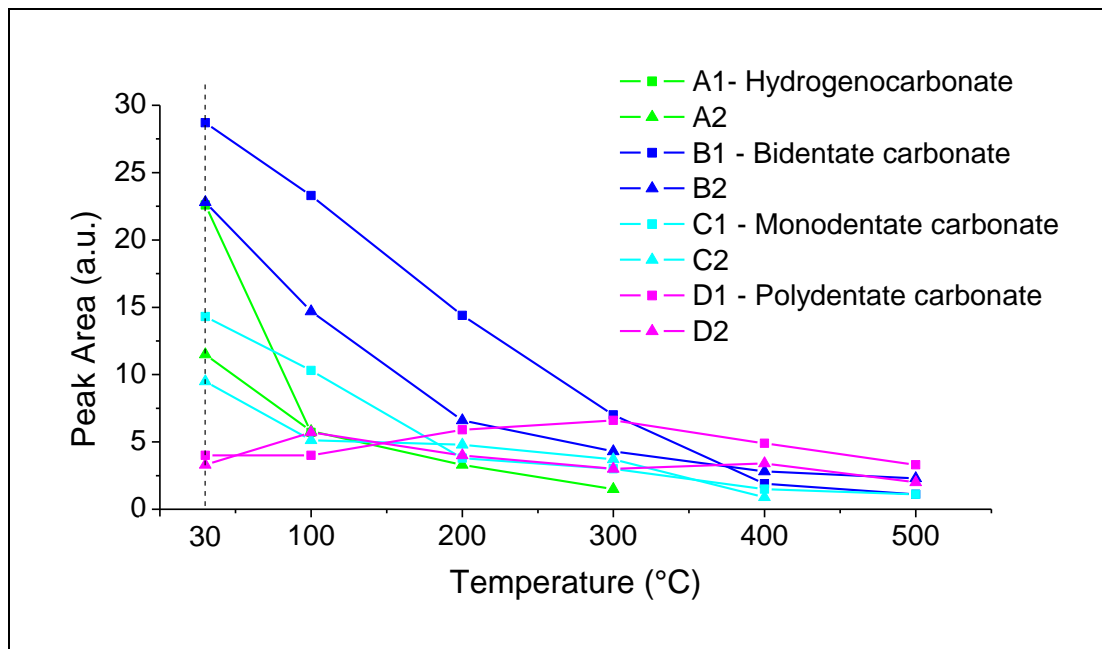


Figure 15: Kinetic of desorption of species from Ceria149.

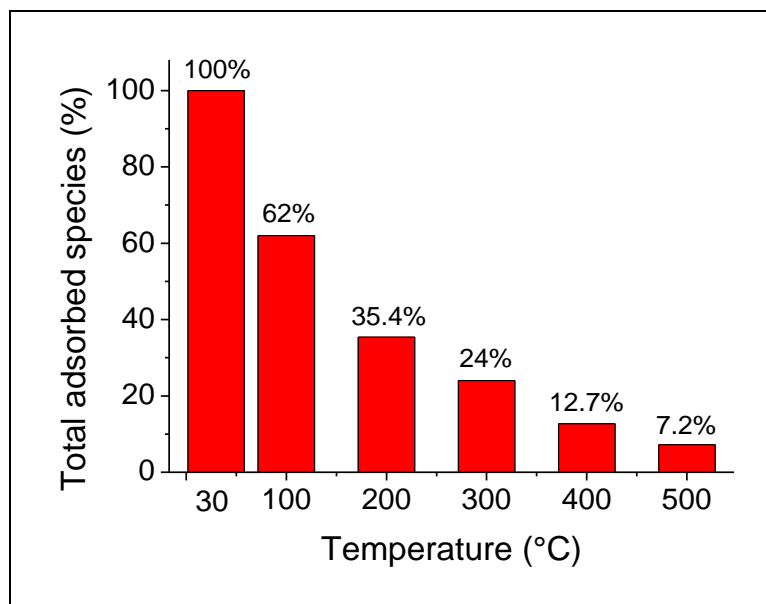


Figure 16: Percentage of remaining adsorbed species during thermal desorption.

As deconvolution technique allowed differentiating various bands related to different adsorbed species, we could calculate the ratio between species for each desorption temperature (Figure 17). The results indicate that bidentate species are the main adsorbed species on ceria surface, mainly at low temperatures. Hydrogenocarbonate species are mostly desorbed from ceria at low temperature swing (30 to 100°C), and then we observe the

progressive desorption of bidentate carbonates. At higher temperatures (400 to 500 °C), monodentate and polydentate species are the only remaining adsorbed species on the sample surface.

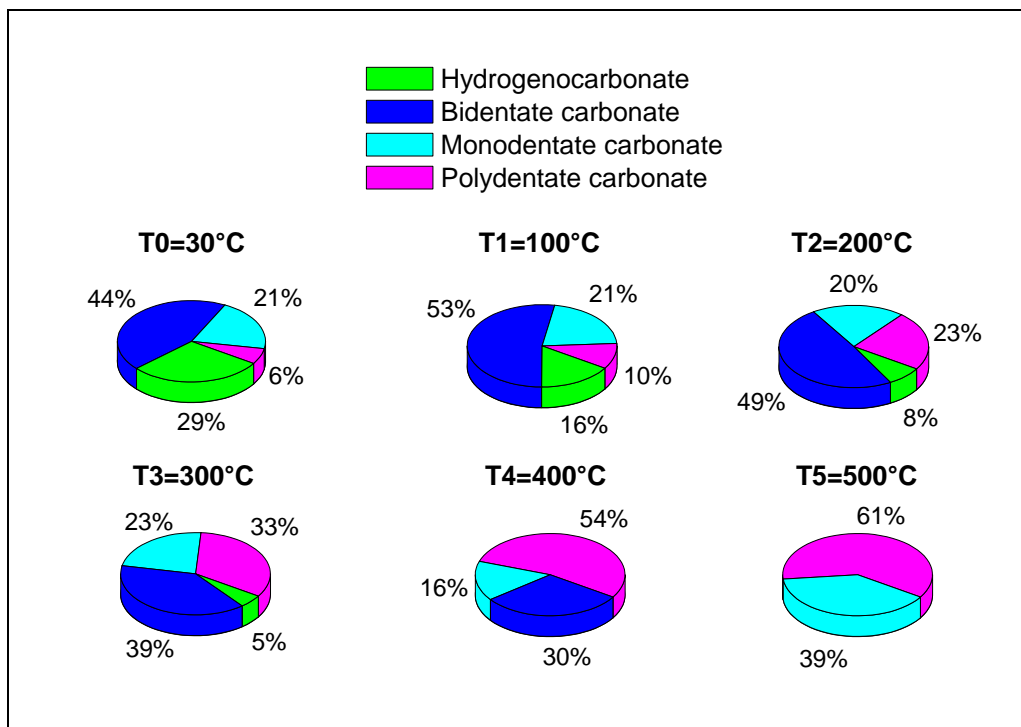


Figure 17: Ratio of remaining species on Ceria149 at different temperatures of desorption.

The kinetic profiles of undoped cerium oxides having different specific surface areas are shown in Figure 18.

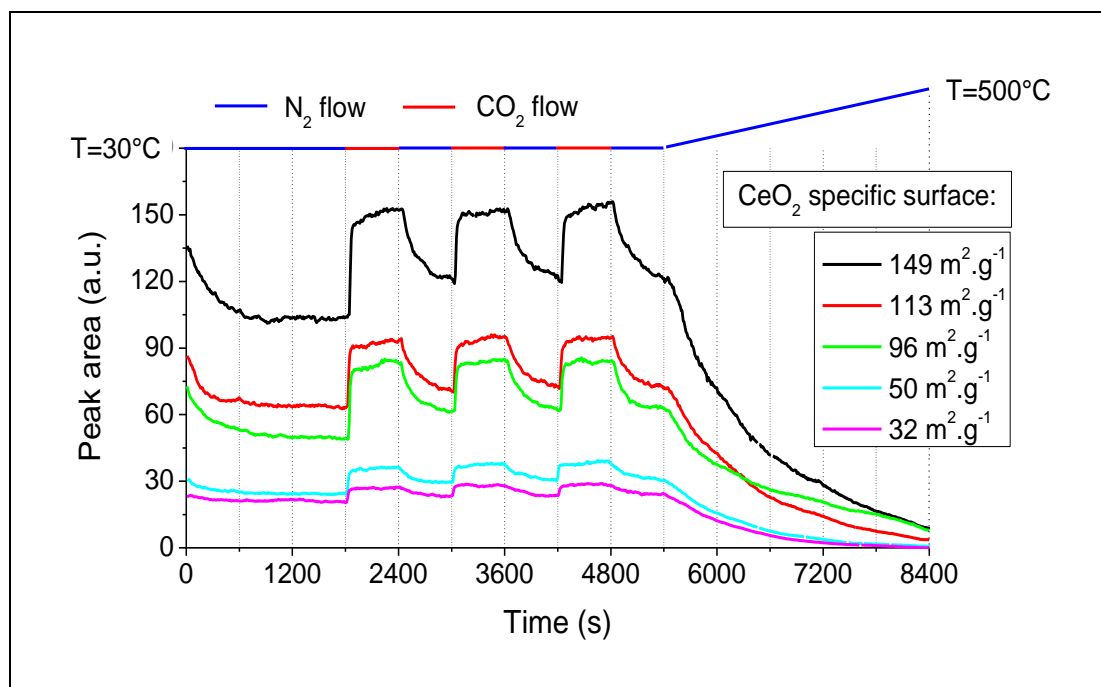


Figure 18: Profiles of cerium oxides having different specific surface areas. The area of peaks, related to adsorbed species, are plotted as a function of experimental protocol.

Overall, the results show that the higher the specific surface area of cerium oxides is, the greater the area of peaks is. Concerning adsorption cycles, we clearly notice the different

adsorption capacities of samples. The variation of the area of bands ( $\Delta a$ ) for each adsorption cycle is shown in Figure 19.

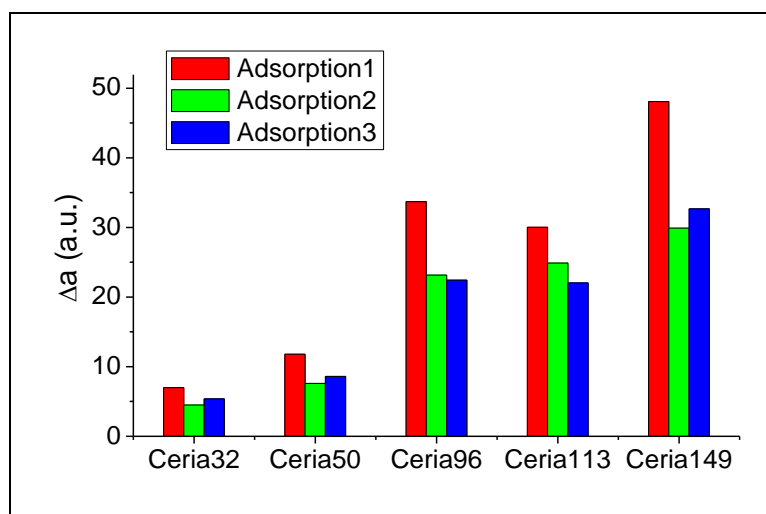


Figure 19: Variation of the area of bands ( $\Delta a$ ) for each adsorption cycle.

The results show the strong influence of specific surface on adsorption capacities. As already reported in primary screening results, once again it was found a linear relationship between specific surface values and adsorption capacities. Figure 20 shows the plot of  $\Delta a$  values as a function of specific surface areas for the first and following adsorption cycles.

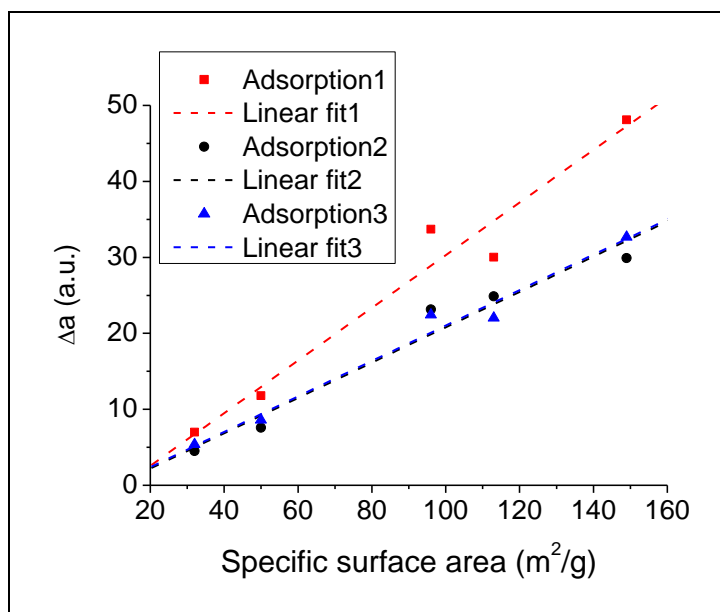


Figure 20: Variation of the area of bands ( $\Delta a$ ) with the specific surface area.

We observe that the linearity of results is more pronounced for the second and the third adsorption process. These results show once again the different strength of  $CO_2$ -adsorbent interactions between the first and following adsorption processes. As the following adsorptions led to weaker interactions, the specific surface area of materials is the mainly influencing parameter of  $CO_2$  capture, explaining therefore the found results. Overall, we have reported similar results for other studied rare earth oxides. The kinetic profiles of some REOs are shown in Figure 21.

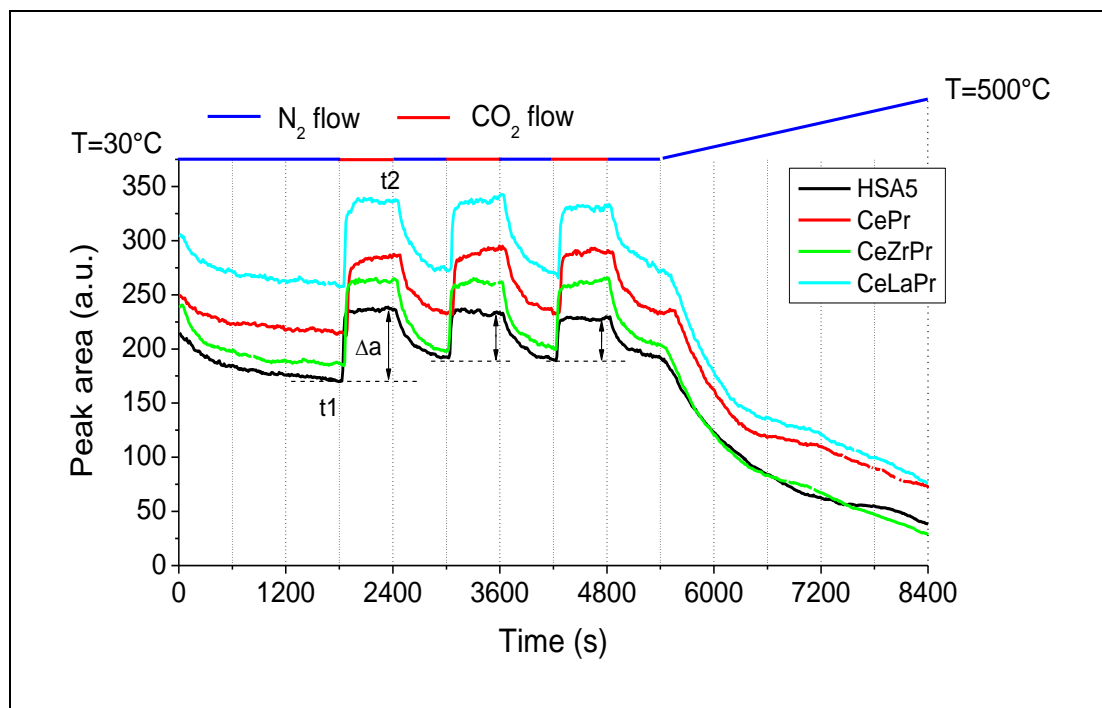


Figure 21: Kinetic profiles of some REOs obtained via DRIFT spectroscopy. The area of peaks, related to adsorbed species, are plotted as a function of experimental protocol.

From these results, we notice that after pretreatment ( $t_1$ ), each sample display different values of area. This indicates different amounts of already existing adsorbed species on adsorbent surfaces before the first adsorption. CeLaPr shows the highest values and undoped ceria HSA5 the lowest ones. These results are related to the basic character of studied samples, doped ceria having the highest basicities.

In the zone of  $\text{CO}_2$  adsorption cycles, the variation of the area of bands ( $\Delta a$ ) has allowed a qualitative analysis of adsorption capacities.  $\Delta a$  values for the adsorption cycles are shown in Figure 22.

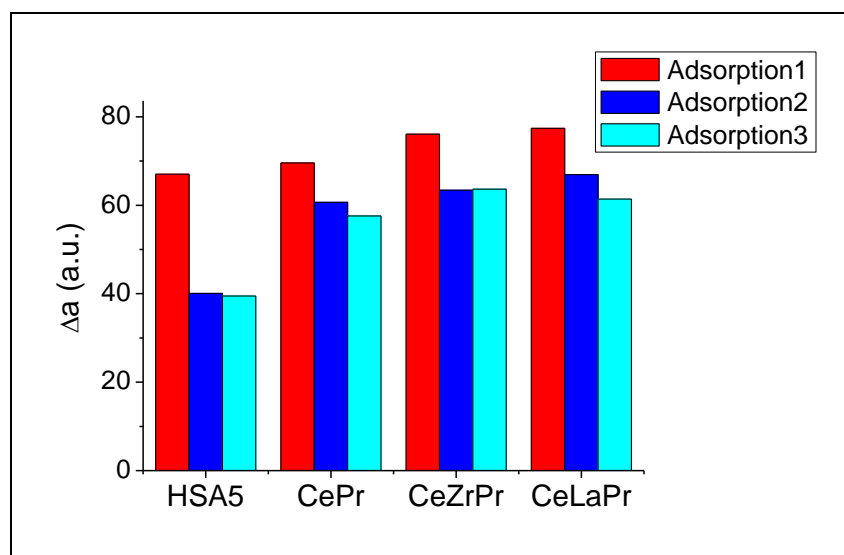


Figure 22: Variation of the area of bands ( $\Delta a$ ) for each adsorption cycle.

In line with results obtained via ATG technique, doped ceria materials (CePr, CeZrPr and CeLaPr) show higher adsorption capacity than undoped ceria. The second and third adsorptions have led to weaker adsorption capacities than the first one. The difference of  $\Delta a$

value between first and following adsorption cycles is more accentuated in the case of HSA5. A priori, these results suggest that doped ceria are not only better for CO<sub>2</sub> capture but also for regeneration step at room temperature.

The DRIFT spectra of some REOs, for the first adsorption process (from t1 to t2), are shown in Figure 23.

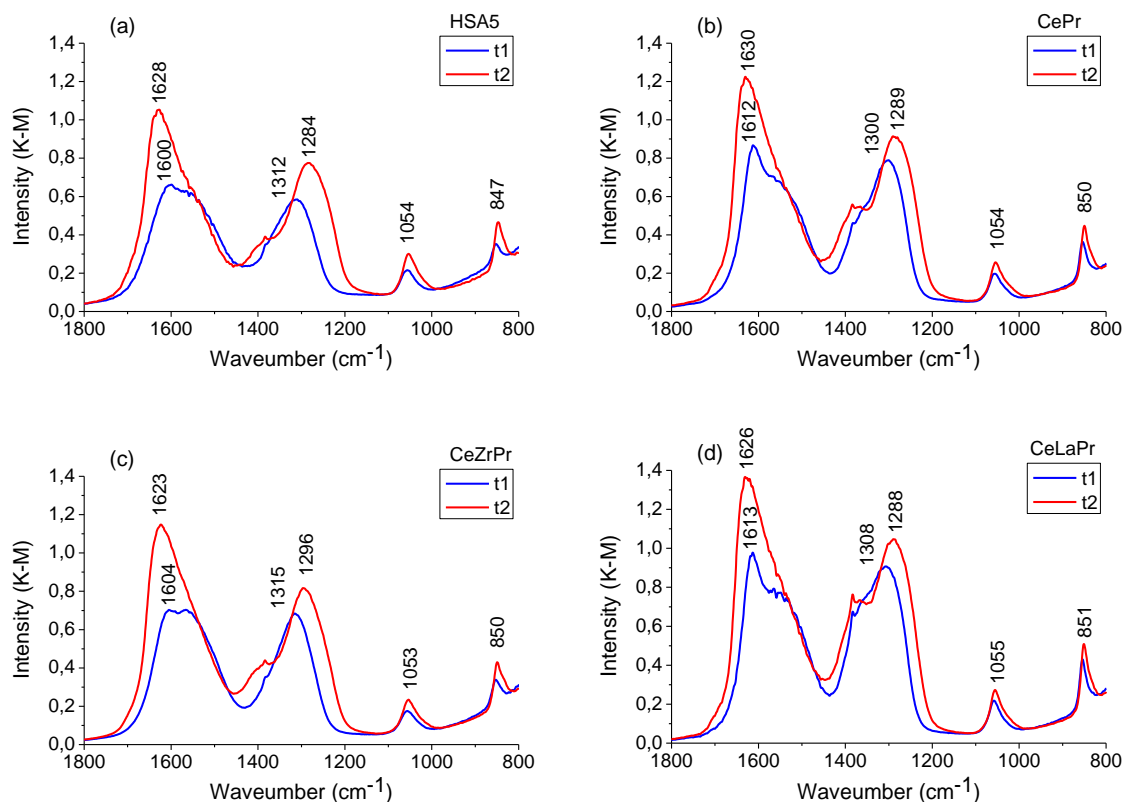


Figure 23: DRIFT spectra of REOs obtained during the first adsorption process. Results for HSA5 (a), CePr (b), CeZrPr (c) and CeLaPr (d).

Overall, as for Ceria149, the evolutions of bands indicate the formation of hydrogencarbonate species. The differences between samples are the relative proportion of already existing adsorbed species on adsorbent surfaces and new formed species. For CePr and CeLaPr, we clearly observe that the amount of already existing species before the first adsorption process (t1 spectra) is higher than for HSA5 and CeZrPr. These results suggest an influence of doped ions on affinity toward CO<sub>2</sub> molecules from atmosphere.

The final step of protocol (temperature swing) enables the overall comparison of desorption rates, and consequently, the thermal stability of species. The percentage of remaining adsorbed species on REOs during temperature swing is shown in Figure 24.

From 30 to 200°C, the small differences between materials and the fast variation of results indicate similar and high desorption rates in this range of temperature for all samples. As observed for Ceria149, the main desorbed species are hydrogencarbonates and bidentate carbonates. These species having the weakest thermal stabilities are easily desorbed from material surface, explaining therefore the observed results. However, for higher temperature swing (up to 500 °C), we observe a distinct desorption rate for each sample. As for higher temperatures we found the most stable species on adsorbent surface, the influence of doped ions are more pronounced. CeLaPr and CePr shows the lowest desorption rates and the highest percentage of remaining species at elevated temperatures. These results can be

explained by the high basic character of these materials. The thermal desorption process is thus more difficult. An interesting result is observed. Even if a higher basic character for CeZrPr is expected in comparison to undoped ceria, CeZrPr shows the highest desorption rates and lowest percentage of remaining species at elevated temperatures. The oxygen mobility can be the reason of this behavior. At elevated temperatures, desorption of species may be facilitated by a partial reduction of material, thereby facilitating the reorganization of sample surface. The doped zirconium cations may reduce the stability between oxygen and cerium ions in the fluorite structure of the adsorbent.

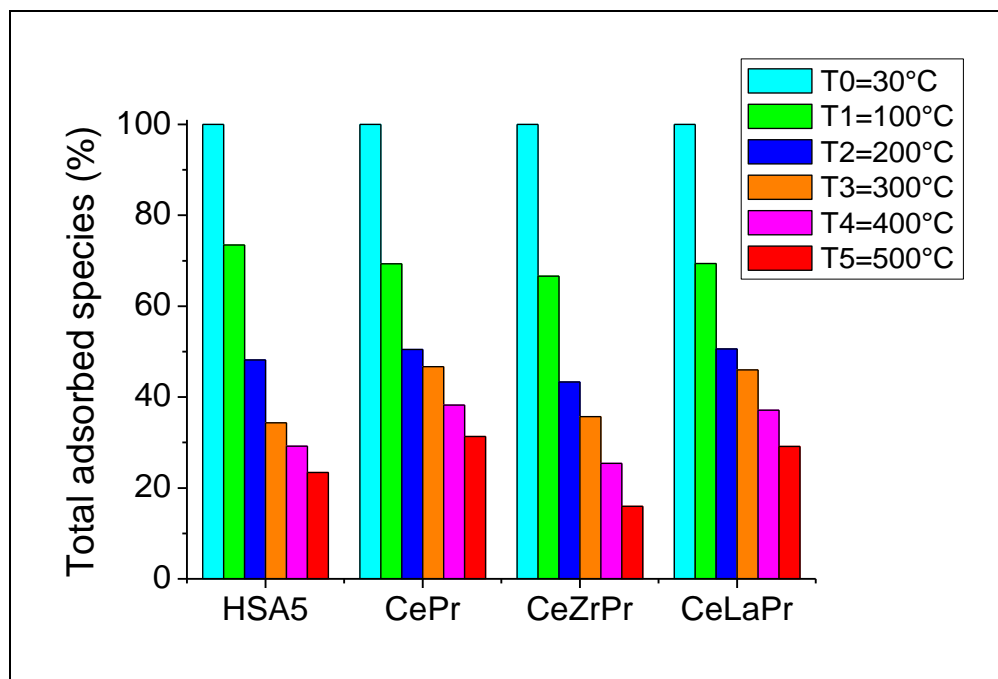


Figure 24: Percentage of remaining adsorbed species on REOs during thermal desorption.

### 3.3 Hybrid materials

Among studied hybrid materials, 33Iminobis/HRS1200 has shown the best performances regarding reversible CO<sub>2</sub> capture at low temperatures. MEA supported silicas have shown good performances only for the first adsorption process. Indeed, screening results indicate the lowest thermal stability of this material among impregnated silicas. In order to perform in-depth investigations, we have selected these two materials for DRIFT study.

#### 3.3.1 33Iminobis impregnated HRS1200

As this adsorbent is composed of amine moiety impregnated over silica support, we have investigated at first, the silica support HRS1200. The spectra of this material under N<sub>2</sub> (a) and CO<sub>2</sub> (b) flow are shown in Figure 25.

HRS1200 is characterized by broad DRIFT bands between 3700 and 3000 cm<sup>-1</sup>, which are assigned to the stretching vibrations of hydrogen-bonded hydroxyl groups and adsorbed water. The presence of adsorbed water is also evidenced by a band at 1630 cm<sup>-1</sup> due to bending vibration mode of H<sub>2</sub>O. We observe as well the band at 3738 cm<sup>-1</sup> due to stretching vibration characteristic of free surface silanol groups, which serve as attachment points for amine moieties. The band at 1098 with broad shoulder at 1200 cm<sup>-1</sup> correspond to (SiO)<sub>n</sub> siloxane stretching vibrations of silica support. The very weak bands at 1984 and 1876 cm<sup>-1</sup> are due to harmonic modes of silica. The bands at 956 and 804 cm<sup>-1</sup> are due to silica support (bending O-Si-O vibrations).

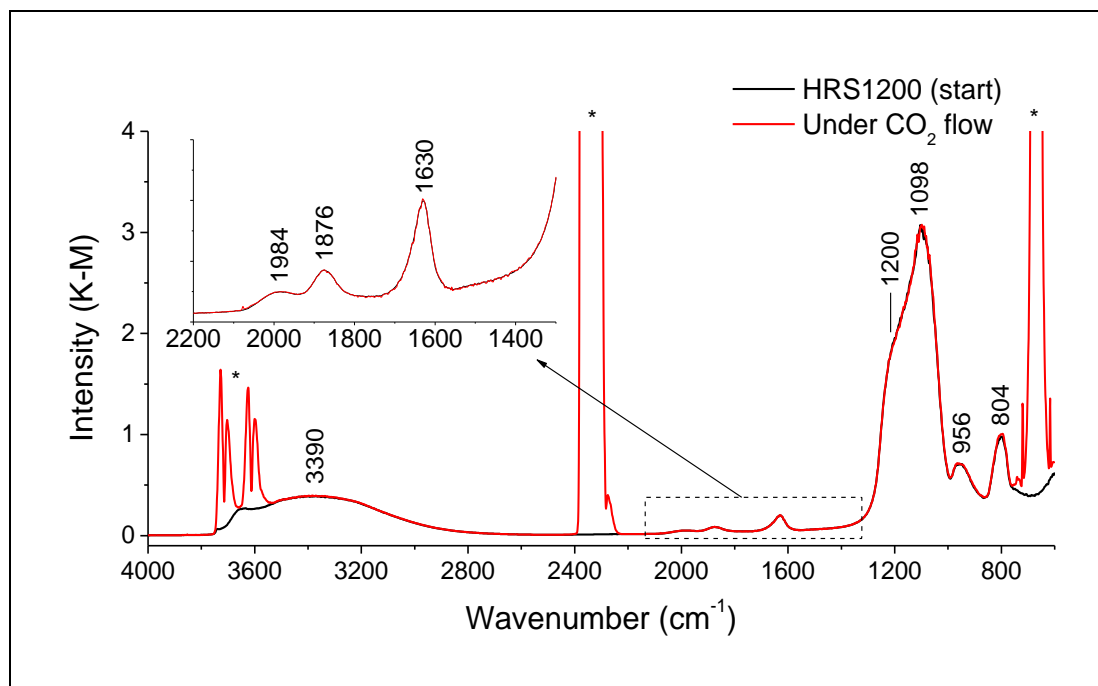


Figure 25: Spectra of HRS1200 under N<sub>2</sub> (a) and CO<sub>2</sub> (b) flow. Inset figure shows the close-up of the spectral range at 2200-1300 cm<sup>-1</sup>. (\*) refers to gas-phase CO<sub>2</sub>.

Our results show that the spectrum of HRS1200 under CO<sub>2</sub> flow is superimposed over the start spectrum of sample (under N<sub>2</sub> flow) and exhibit vibration modes of gas-phase CO<sub>2</sub> ( see bands noted\* in Figure 25). These results confirm that the adsorption of carbon dioxide on HRS1200 leads only to physisorption interactions, and that no bond or carbonate formation with the silica surface takes place. Figure 26 shows the spectra of HRS1200 during temperature swing step.

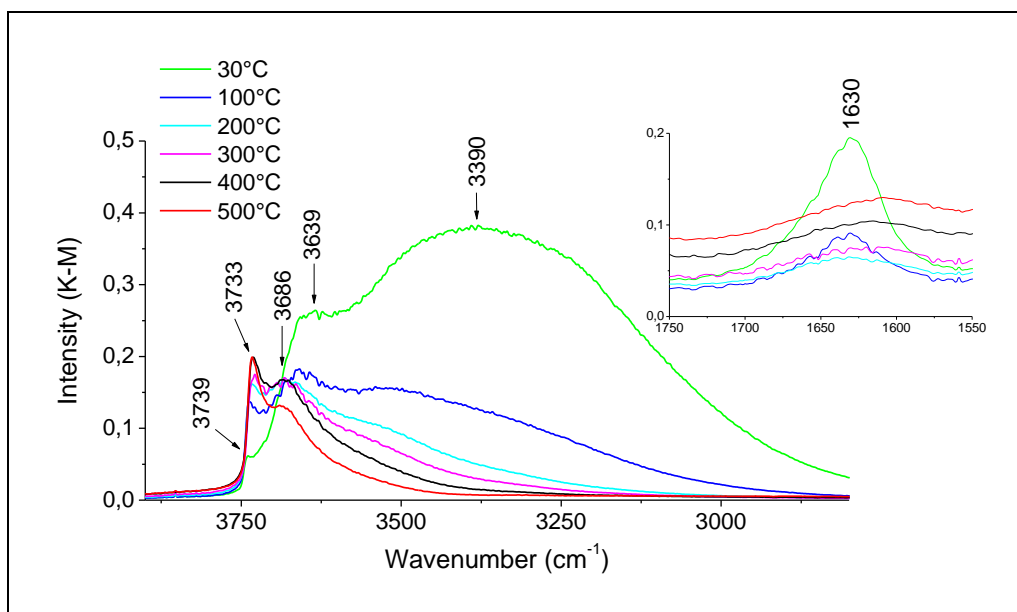


Figure 26: DRIFT spectra of HRS1200 recorded during thermal swing from 30 to 500°C in the spectral range of 3900 to 2800 cm<sup>-1</sup>. Inset figure shows the band evolution at 1630 cm<sup>-1</sup>.

Overall, we have observed a strong decrease of the broad bands centered at 3390 cm<sup>-1</sup> and 1630 cm<sup>-1</sup>, both related to adsorbed water on the support, with increasing temperature. We have also observed the decrease and shift of bands, from 3639 to 3686 cm<sup>-1</sup>, suggesting the

reorganization of hydrogen-bonded OH groups, and the increase and shift of bands, from 3739 to 3733  $\text{cm}^{-1}$ , suggesting the activation of free OH groups during thermal treatment.

In the spectral range of 1750 to 1550  $\text{cm}^{-1}$ , we have stated an offset of the baseline with increasing temperatures. This phenomenon may be due to the influence of emitted thermal radiation with increasing temperatures, which is accentuated by the white color of the sample.

For impregnated HRS1200 with the amine type 33Iminobis, which has two tertiary and one secondary amine group, the spectrum exhibits considerable modifications comparing to that of silica support. Figure 27 shows the DRIFT spectrum of 33Iminobis/HRS1200 just after impregnation process, with comparison to the DRIFT spectrum of HRS1200 and to the ATR (Attenuated Total Reflectance) spectrum of liquid 33Iminobis.

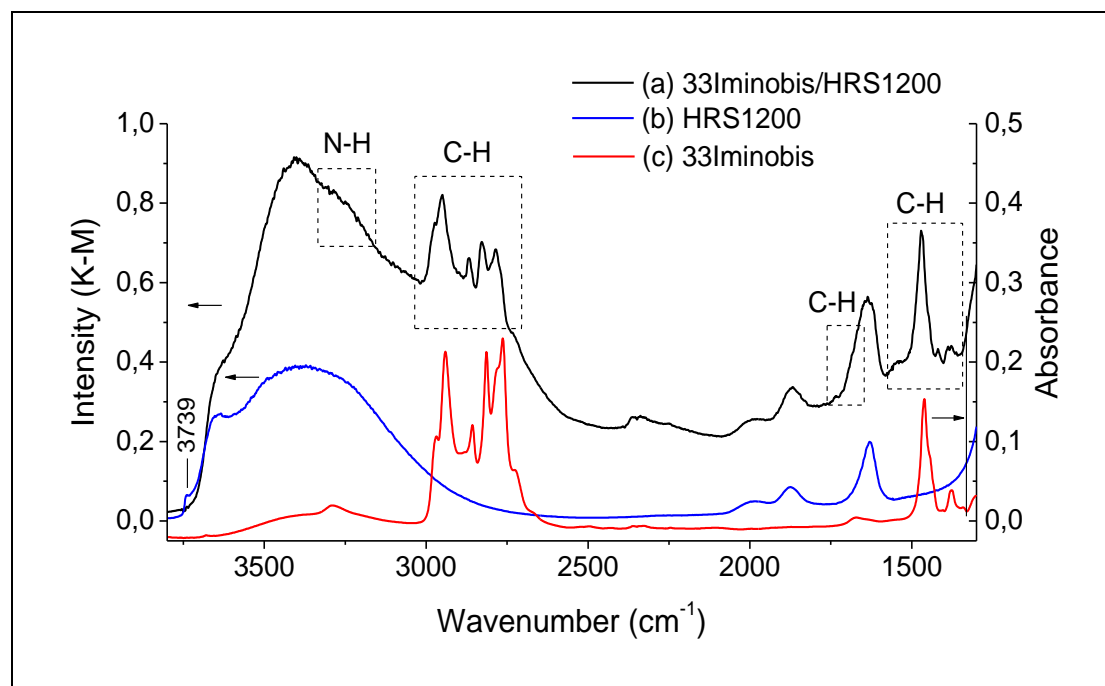


Figure 27: DRIFT spectrum of 33Iminobis/HRS1200 after impregnation process (a), of HRS1200 (b) and ATR spectrum of liquid 33Iminobis (c).

For 33Iminobis/HRS1200, additional bands corresponding to N-H and C-H stretching and bending vibrations are present after impregnation procedure, indicating thus the successful impregnation of 33Iminobis over HRS1200. Moreover, the vanishing of free silanol groups confirms the adsorption of amine moieties on silica support. To assign IR bands, a subtraction spectrum of HRS1200 from 33Iminobis/HRS1200 is shown in Figure 28. The DRIFT spectra were obtained just after pretreatment step ( $\text{N}_2$  flow).

As for the silica support, 33Iminobis/HRS1200 displays a broad OH region (centered at 3390  $\text{cm}^{-1}$ ) which indicates a high affinity toward water molecules. The subtraction spectrum shows a loss band at 3739-3698  $\text{cm}^{-1}$ , which results from the loss of isolated silanols on the surface in comparison with HRS1200 spectrum. The broad medium band at 3280  $\text{cm}^{-1}$  is due to N-H stretching vibrations, associated with the weak N-H bending vibrations at 1660 and 1616  $\text{cm}^{-1}$ . The bands in the spectral range of 3000-2722  $\text{cm}^{-1}$  are due to C-H stretching vibrations of the methyl and propyl moieties of the amine, and the bands at 1469 and 1386  $\text{cm}^{-1}$  are due to the corresponding C-H bending vibrations. The assignment of bands is summarized in Table 4.

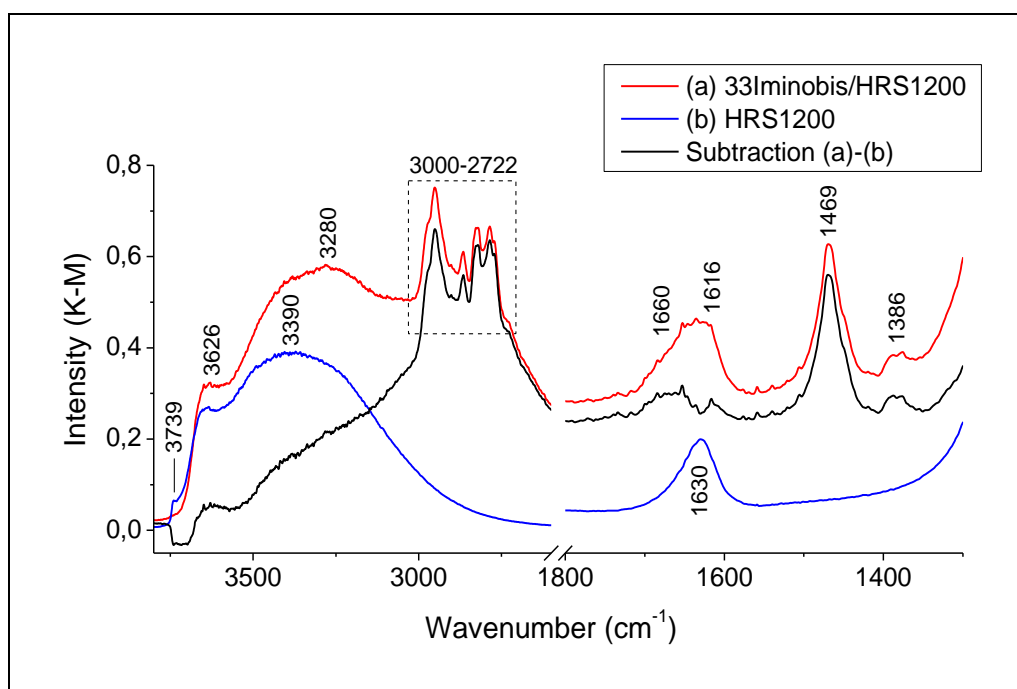


Figure 28: Subtraction spectra (black) of HRS1200 (b) from 33Iminobis/HRS1200 (a).

Table 4: Summary of observed DRIFT bands of 33Iminobis/HRS1200.

wavenumber (cm <sup>-1</sup> )	assignment	correspond to	ref
3739-3698	OH stretching of free surface silanol groups	HRS1200	[51, 142]
3700-3000	OH stretching of hydrogen-bonded OH groups	adsorbed water	[143]
3626	OH stretching of hydrogen-bonded OH groups	HRS1200	[51]
3280	N-H stretching	33Iminobis	[48]
3000-2722	C-H stretching	33Iminobis	[144]
1630	H-O-H bending	adsorbed water	[143]
1660 and 1616	N-H bending	33Iminobis	[145]
1469	C-H bending	33Iminobis	[51]
1386	C-H bending	33Iminobis	[122]
1098 with broad shoulder at 1200	(SiO) <sub>n</sub> siloxane stretching vibrations	HRS1200	[146]

Continuing the investigations, the kinetic profile of 33Iminobis/HRS1200, for pretreatment and adsorption cycle steps, is shown in Figure 29. It has been obtained by integration of the spectral zone (1800-1300 cm<sup>-1</sup>) related to adsorbed species and has been recorded during experimental protocol.

As for REOs, the profile shows a similar behavior compared to mass uptake and thermal profiles. During pretreatment, it has been observed a fast decrease of the area of peaks,

indicating desorption of weakly bound species already existing on sample surface (residual adsorbed species) or indicating partial desorption of amine moieties. At adsorption cycles step, we clearly observe the kinetics of adsorption and desorption at room temperature, which are well correlated to results of adsorption/desorption rates. From the variation of the area of bands ( $\Delta a$ ) we once again state the almost reversibility of CO<sub>2</sub> capture under soft conditions.

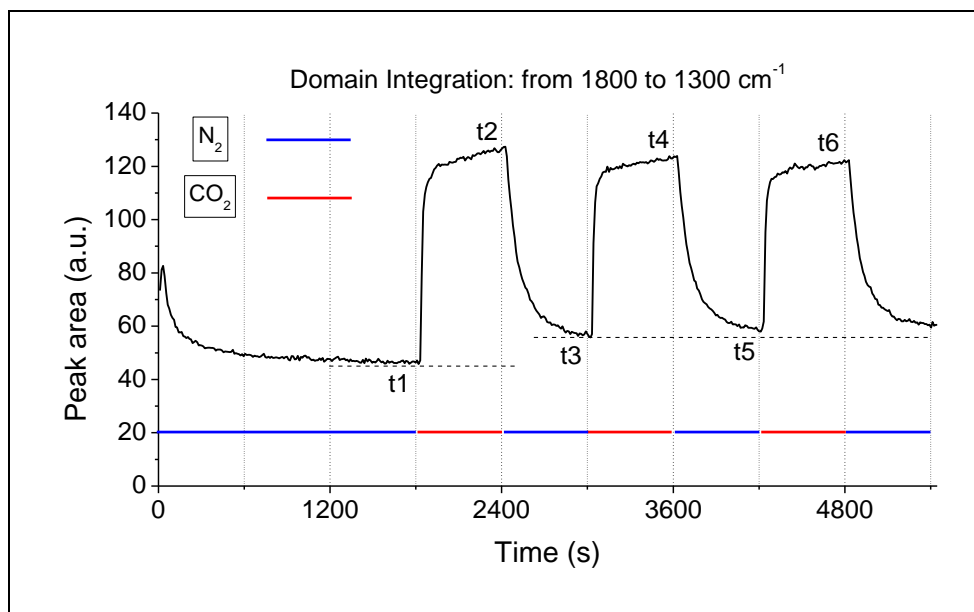


Figure 29: Kinetic profiles of 33Iminobis/HRS1200 recorded during CO<sub>2</sub> adsorption cycles. The area of peaks, related to adsorbed species, has been obtained via DRIFT device.

We now present the analysis of spectra during adsorption cycles, in order to allow the identification of major adsorbed species on 33Iminobis/HRS1200.

Amine chemistry in the liquid phase is well known. The interaction between the basic surface (amine) and acidic CO<sub>2</sub> molecules leads to the formation of ammonium carbamates, ammonium bicarbonate, and carbamic acids (see chapter I: Figure 9 and 10). In aqueous amine, the formation of hydrogencarbonates and carbonates is also possible.

For amine supported silica, CO<sub>2</sub>-adsorbent interactions are still under investigation: the heterogeneous nature of these amine-modified sorbents and their complex FTIR spectra have resulted in conflicting structural assignments by different authors. Latest literature [122, 123, 129] reported the formation of ammonium carbamate ions pairs, carbamic acid and surface bound carbonate. This last one is more strongly bonded and does not desorb under soft conditions (evacuation only).

It is important to emphasize that a comparison with literature is complicated because measurements are performed in different operational conditions. Indeed, it is difficult to assign vibrations to adsorbed species because of the overlapping of bands in the carbon fingerprint region (1800-1100 cm<sup>-1</sup>). Therefore, based on the positions of the bands observed in this study, their behaviors during adsorption/desorption processes and reference to latest literature, we show then the results that allowed us to identify the major adsorbed species on 33Iminobis/HRS1200.

Figure 30 and 31 show the DRIFT spectra of 33Iminobis/HRS1200 before and after CO<sub>2</sub> adsorption for each adsorption cycle, and their respective subtraction spectra.

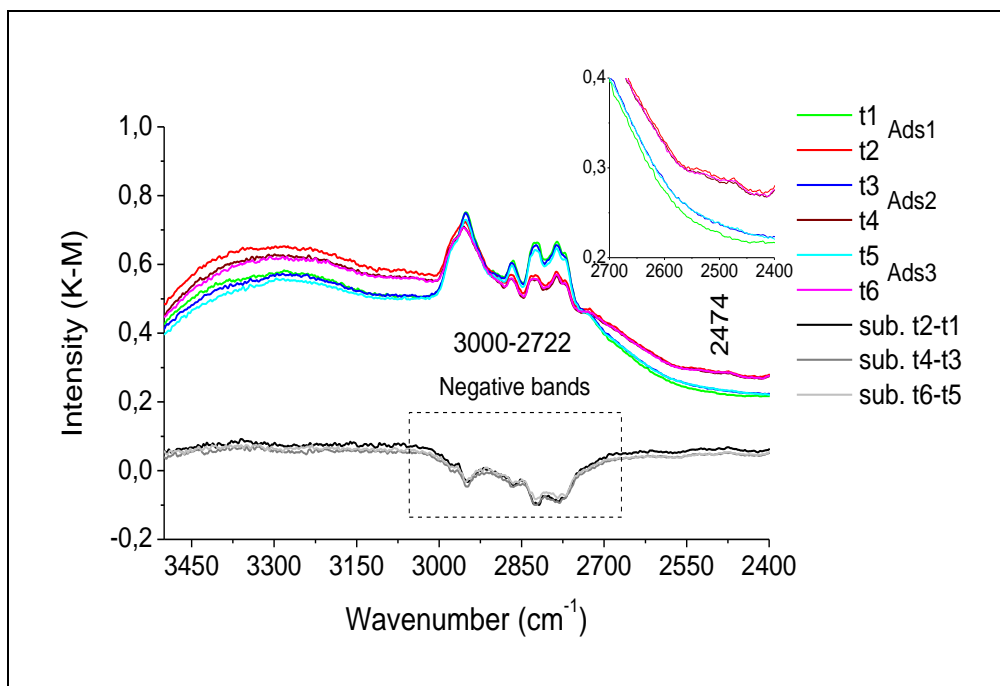


Figure 30: DRIFT spectra of 33Iminobis/HRS1200 recorded during adsorption cycles in the spectral range of 3500-2400 cm<sup>-1</sup>. Inset figure shows the close-up of the band at 2474 cm<sup>-1</sup>.

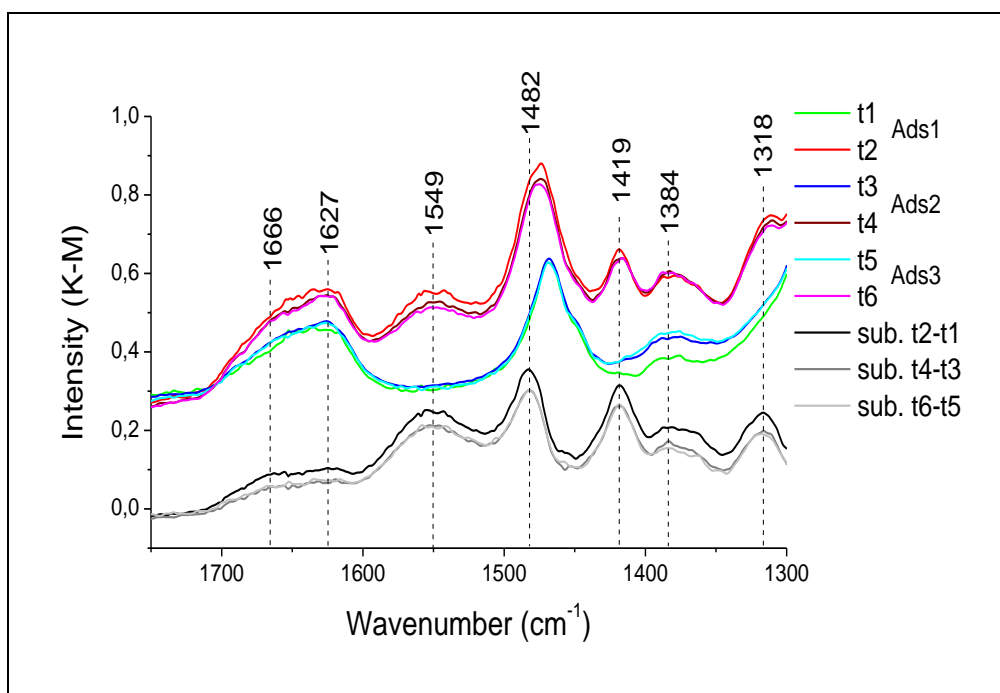


Figure 31: DRIFT spectra of 33Iminobis/HRS1200 recorded during adsorption cycles in the spectral range 1800-1300 cm<sup>-1</sup>.

On Figure 30, the difference spectra for adsorption cycles show negative bands in the region of the C-H stretching (3000-2722 cm<sup>-1</sup>). It means that these bands decrease under CO<sub>2</sub> flow. On the contrary, the corresponding bands due to C-H bending vibrations (1469 and 1386 cm<sup>-1</sup>) increase under CO<sub>2</sub> flow. These results indicate a significant modification of 33Iminobis moieties in the presence of carbon dioxide.

In the spectral range of 1800-1300 cm<sup>-1</sup>, adsorption processes (t1, t3 and t5) lead to intense evolution of bands. On desorption process (t2, t4 and t6), the majority of the amplitude of

these bands disappear and the spectra come back to the start position. Likely screening results, DRIFT results show that evacuation ( $N_2$  flow) at room temperature is sufficient to remove all these species, and indicate that these bands are due to weak bound species. These observations and the results reported by Bacsik *et al.* [123], Danon *et al.* [122] and Knofel *et al.* [129] suggest the formation of a weakly bound alkylammonium carbamate, which is related to a weak broad band centered at  $2474\text{ cm}^{-1}$ , followed by the bands at  $1627$ ,  $1549$ ,  $1482$  and  $1419\text{ cm}^{-1}$ . The band at  $1666\text{ cm}^{-1}$  is assigned to alkylcarbamic acid (carbamic acid) hydrogen bonded to adsorbent surface, according to Bacsik *et al.* and Knofel *et al.*

The cited authors assigned the band at  $1384\text{ cm}^{-1}$  to the symmetric stretch of  $CO_2^-$  (ionic carbamate) and/or to the deformation of O-H (carbamic acid). Regarding the partial irreversibility behavior of this band under soft conditions (only this band does not totally come back to initial position during desorption process, see Figure 31), it appears that this band is due to a more strongly bound species. A band at  $1318\text{ cm}^{-1}$  was observed but not assigned by these authors.

In order to clarify the assignment of bands, Figure 32 shows the kinetic profiles of observed bands for the first adsorption cycle.

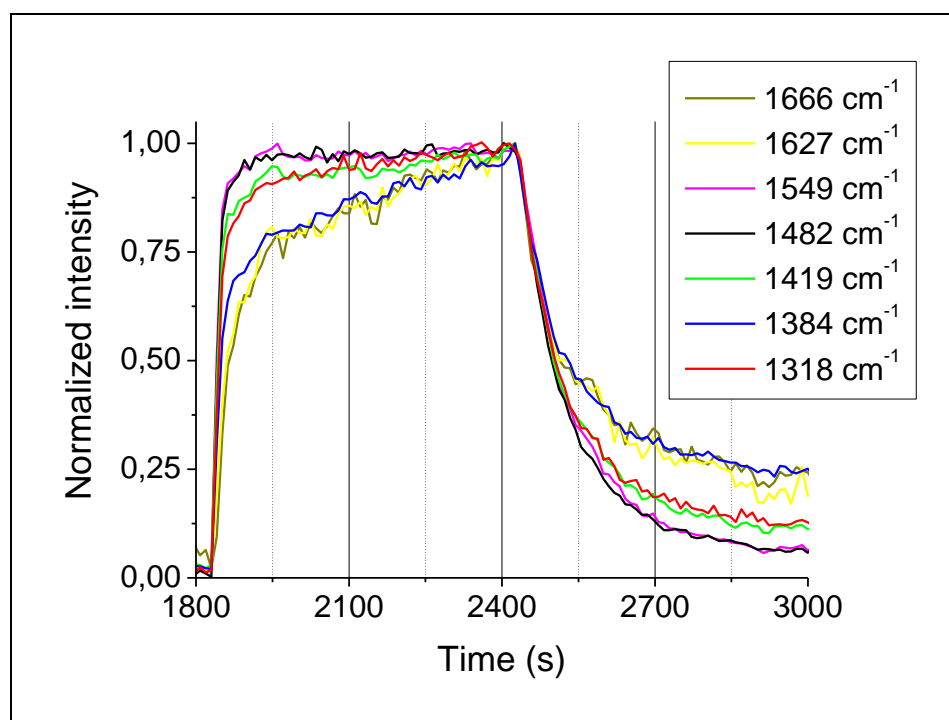


Figure 32: kinetic profiles of 33Iminobis/HRS1200 recorded during the first  $CO_2$  adsorption cycle.

The results show different kinetics of bands during adsorption and desorption process. Overall, we can assemble the bands in two groups: group A, with bands at  $1666$ ,  $1627$  and  $1384\text{ cm}^{-1}$ , which have considerable variation of intensities at long-time period, and group B, with bands at  $1549$ ,  $1482$ ,  $1419$  and  $1318\text{ cm}^{-1}$ , which have rapid variation of intensities at short-time period. Therefore, comparing our results to results reported by previously mentioned authors, we suggest that group A correspond to hydrogen-bonded carbamic acid (excepted for the band at  $1627\text{ cm}^{-1}$ ) and group B to ammonium carbamate ion pairs.

The band at  $1627\text{ cm}^{-1}$  has a different adsorption behavior compared to that of the bands of group B, we assign this band to the ion carbamate  $NH_2^+$ . The distinct kinetic of this band can be explained by the overlapping of the bands at  $1666$  and  $1627\text{ cm}^{-1}$ .

Chang *et al.* [50] and Khatri *et al.* [52] have assigned bands in the spectral range of 1800-1300  $\text{cm}^{-1}$  to hydrogencarbonate and carbonates species, probably because of analogy with  $\text{CO}_2$ -aqueous amine interactions. However, in this work, we have no evidences for the production of such species.

Therefore, we suggest the formation of both ionic carbamate and carbamic acid during  $\text{CO}_2$  adsorption on 33Iminobis/HRS1200. The assignment of bands is summarized in Table 5.

Table 5: Adsorbed species observed over 33Iminobis/HRS1200.

wavenumber ( $\text{cm}^{-1}$ )	assignment	correspond to
2474	sym. $\text{NH}_2^+$ stretch	ionic carbamate
1666	C=O stretch	carbamic acid (hydrogen bonded)
1627	$\text{NH}_2^+$ deformation	ionic carbamate
1549	asym. $\text{CO}_2^-$ stretch	ionic carbamate
1482	sym. $\text{NH}_2^+$ deformation	ionic carbamate
1419	sym. $\text{CO}_2^-$ stretch	ionic carbamate
1384	O-H deformation	carbamic acid (hydrogen bonded)
1318	sym. $\text{CO}_2^-$ stretch	ionic carbamate

We already commented that the main drawback of hybrid materials is their low thermal stability concerning the supported amines groups. In order to study the stability of 33Iminobis over the silica support HRS1200, we have studied the spectra and kinetic evolution of bands during temperature swing step. Figure 33 and 34 shows the spectra evolutions of 33Iminobis/HRS1200 during thermal desorption.

As already reported for silica HRS1200, high temperatures lead to an offset of the spectrum baseline. Indeed, the thermal emission of the sample is more important at high temperatures.

During temperature swing, in the spectral range 3800-2600  $\text{cm}^{-1}$ , we observe the decrease of the bands at (a) 3000-2722  $\text{cm}^{-1}$  related to C-H stretch vibrations. As water is rapidly desorbed from adsorbent surface, we can clearly observe the decrease of the band at 3280  $\text{cm}^{-1}$  due to N-H stretch vibrations. These results indicate desorption of 33Iminobis moieties from silica support. As for results obtained for silica support, we observe the decrease and a blue shift of bands from 3639 to 3682  $\text{cm}^{-1}$ , which indicates the reorganization of OH groups over HRS1200 support. As amine moieties are removed from silica support, we observe the increase of the band at 3734  $\text{cm}^{-1}$ , which indicates the reappearance of free surface silanol groups.

In the spectral range 1800-1300  $\text{cm}^{-1}$ , we observe the decrease of bands at (b) 1739-1555 (overlapping of the bands due to N-H and H-O-H bending vibrations), at (c) 1527-1425 (due to C-H bending vibrations), and at (d) 1422-1348  $\text{cm}^{-1}$  (overlapping of the bands due C-H deformation of the sample and the adsorbed carbamic acid).

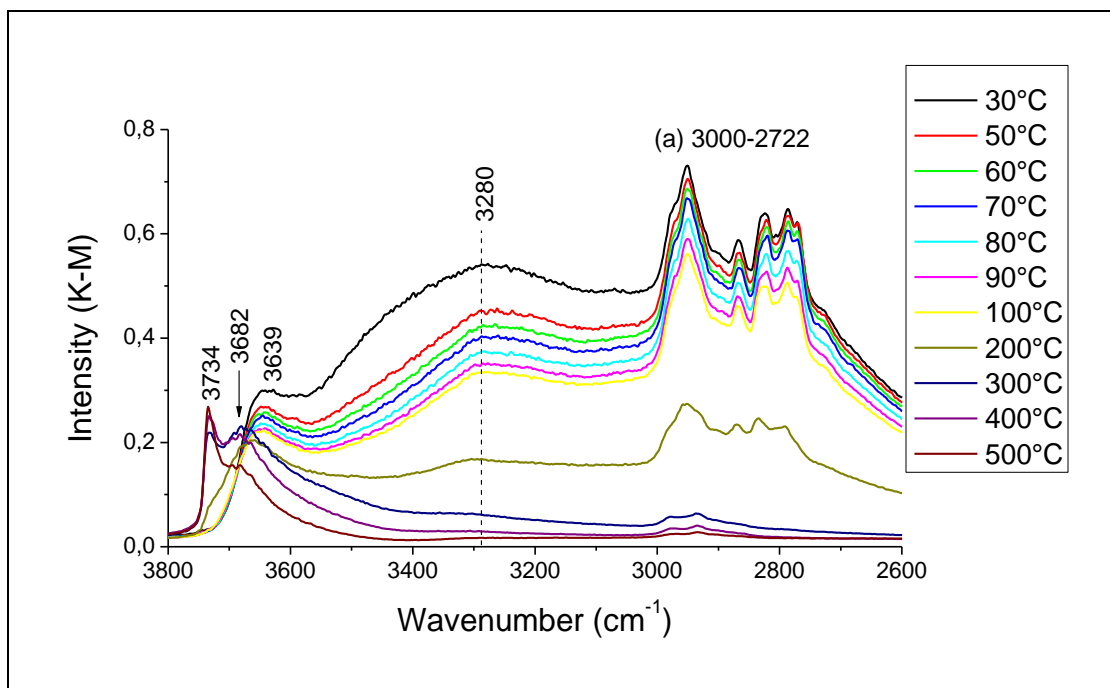


Figure 33: DRIFT spectra of 33Iminobis/HRS1200 during thermal desorption in the spectral range 3800-2600  $\text{cm}^{-1}$ .

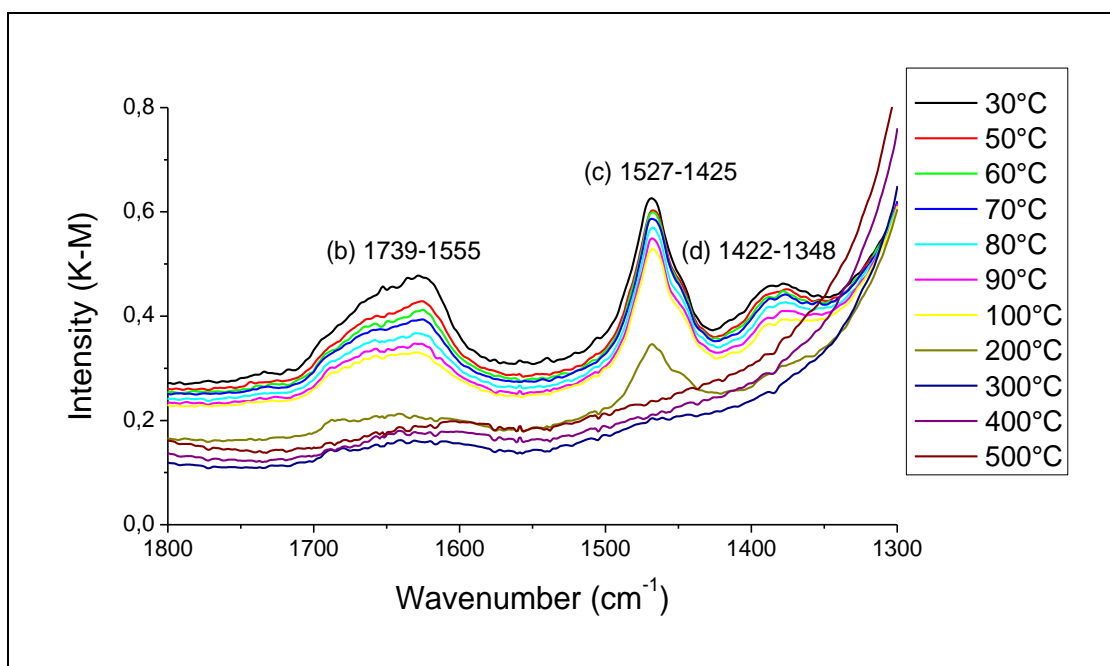


Figure 34: DRIFT spectra of 33Iminobis/HRS1200 during thermal desorption in the spectral range 1800-1300  $\text{cm}^{-1}$ .

By integration of the cited spectral ranges (a), (b), (c) and (d), the kinetic profiles obtained during temperature swing are shown in Figure 35. The evolutions of these bands are the fingerprint of desorption of 33Iminobis from HRS1200.

The results indicate some characteristic temperatures which are related to the removal rates of 33Iminobis moieties from silica support. By analyzing the variations of the peak areas of groups (a) and (c), which represent the impregnated amine moieties, we state that the desorption temperature of 70 °C seems to be the characteristic temperature at which the removal of 33Iminobis from silica support starts. These bands have moderate variations up to

190 °C, and then an intense variation is observed. These results suggest that the temperature of 190 °C is the limit temperature of amine stability over silica support. After this characteristic temperature, the rate of desorption is very intense up to 235 °C, and almost of the amine has been removed from the silica support.

The analysis of band groups (b) and (d) is more difficult because of overlapping of bands related to impregnated amine and adsorbed species. The highest desorption rate is observed for the band group (b) which is mainly related to desorption of water ( $1630\text{ cm}^{-1}$ ). The variation of the band group (d) is quite different from other groups. This behavior can be explained by the simultaneous desorption of hydrogen-bonded acid carbamic and amines moieties from sample surface with a supplementary step around  $115^{\circ}\text{C}$ .

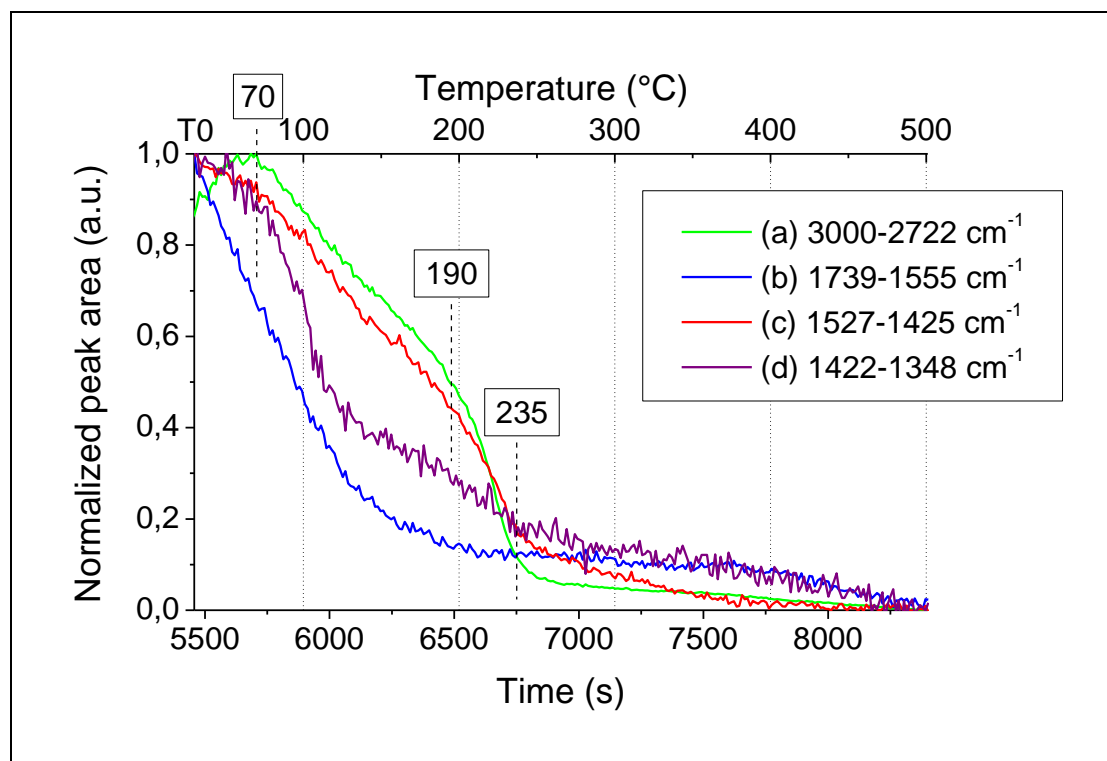


Figure 35: kinetic profiles of 33Iminobis/HRS1200 during thermal desorption. The profiles have been obtained by integration of spectra ranges a, b, c and d.

### 3.3.2 Monoethanolamine impregnated HRS1200

The spectrum of impregnated HRS1200 with the amine type MEA (monoethanolamine) which has a primary amine and a primary alcohol has also been successfully impregnated on the silica support. Figure 36 shows the DRIFT spectrum of MEA/HRS1200 just after impregnation procedure, which is compared to the DRIFT spectrum of HRS1200 and to the ATR spectrum of liquid MEA.

For this hybrid material, we have observed bands due to C-H, N-H and O-H vibrations of MEA moieties impregnated over silica support.

According to studies of vibrational spectrum of MEA by Korolevich *et al.* [147], we have assigned the bands at  $3345\text{ cm}^{-1}$  to the O-H stretch of primary alcohol, the bands at  $3282$  and  $1568\text{ cm}^{-1}$  to  $\text{NH}_2$  stretch and  $\text{NH}_2$  deformation of hydrogen bonded amino group, respectively. The bands at  $2940$  and  $2877\text{ cm}^{-1}$  are due to C-H stretching, the bands at  $1488$  and  $1388\text{ cm}^{-1}$  to C-H deformation modes, finally the band at  $1320\text{ cm}^{-1}$  to O-C-H deformation mode.

Moreover, the MEA impregnation is proved by the loss peak at  $3739\text{ cm}^{-1}$  which indicates the loss of isolated silanol on the surface in comparison with HRS1200.

Because of high the hydrophilic character of the silica support, MEA/HRS1200 displays also a broad band in the OH stretching region ( $3700\text{-}3000\text{ cm}^{-1}$ ).

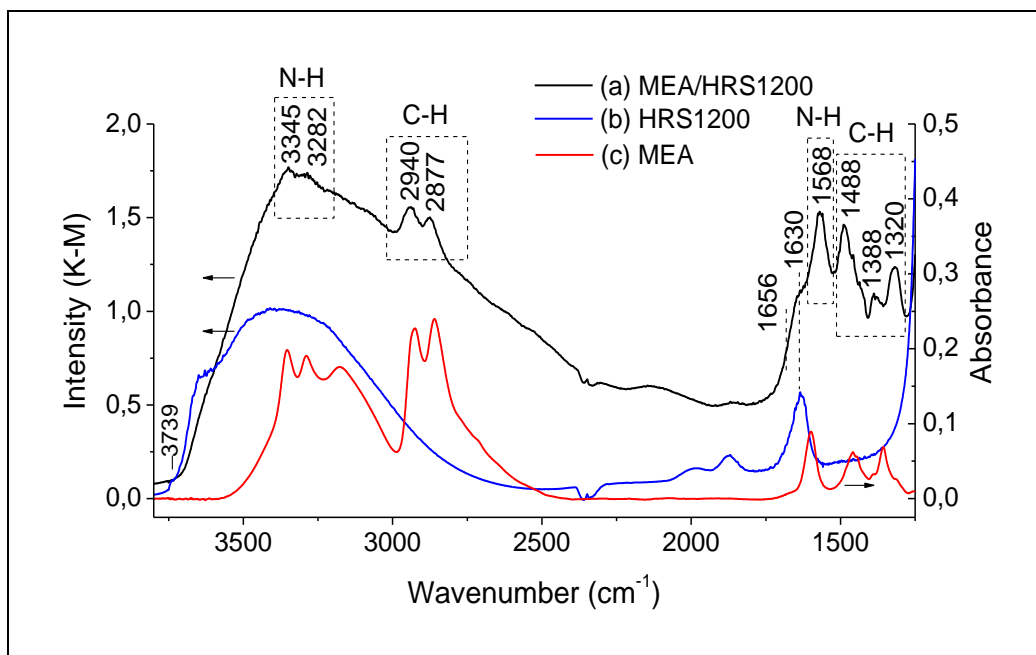


Figure 36: DRIFT spectrum of MEA/HRS1200 after impregnation process (a), of HRS1200 (b) and ATR spectrum of liquid MEA (c).

Even though these results confirm a successful impregnation of MEA over HRS1200, the stability of impregnation (MEA hydrogen-bonded to silica support) was proved to be very weak. Figure 37 shows the DRIFT spectra of MEA/HRS1200 during pretreatment step.

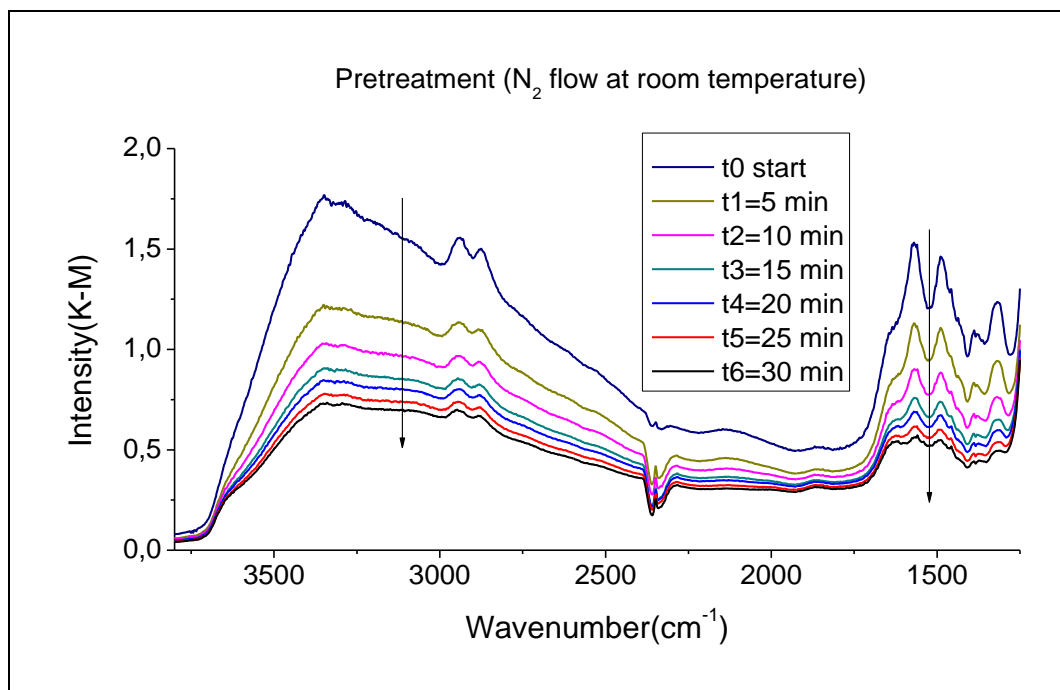


Figure 37: DRIFT spectra of MEA/HRS1200 during pretreatment step.

The results show that IR intensities of the characteristic amine bands start to decrease under N<sub>2</sub> flow only, but the amine group bands do not completely vanish. A small amount of impregnated MEA remains after pretreatment and the sample is then available for the first CO<sub>2</sub> adsorption. The evolution of the DRIFT spectra of MEA/HRS1200 during adsorption cycles and temperature swing step are shown in Figure 38.

In Figure 38 A, the increase of bands during the first CO<sub>2</sub> injection indicates CO<sub>2</sub> adsorption on sample. The subtraction spectra enable to identify the bands related to adsorbed species: 1664, 1626, 1566, 1497, 1381 and 1313 cm<sup>-1</sup>. Compared to results of 33Iminobis/HRS1200, similar bands have been identified during adsorption process (see Table 5). These bands indicate also the formation of ionic carbamate and hydrogen-bonded carbamic acid. The differences in frequencies are due to the different nature of amines in these two hybrid materials.

Figure 38 B and C show the evolution of DRIFT spectra of MEA/HRS1200. The results show that the second and third adsorption process lead to a very weak variation of band intensities, indicating thus a low CO<sub>2</sub> capture capacity after the first adsorption process. This behavior suggests a low amine loading on silica support enable to react with CO<sub>2</sub> molecules.

Figure 38 D shows the spectra evolutions of the sample during thermal desorption. The bands vanish during temperature swing. At 100 °C only, one observes the full vanishing of the characteristic MEA bands. As for screening results, these results confirm the complete desorption of the amine moieties from silica support and indicate the weak thermal stability of this adsorbent.

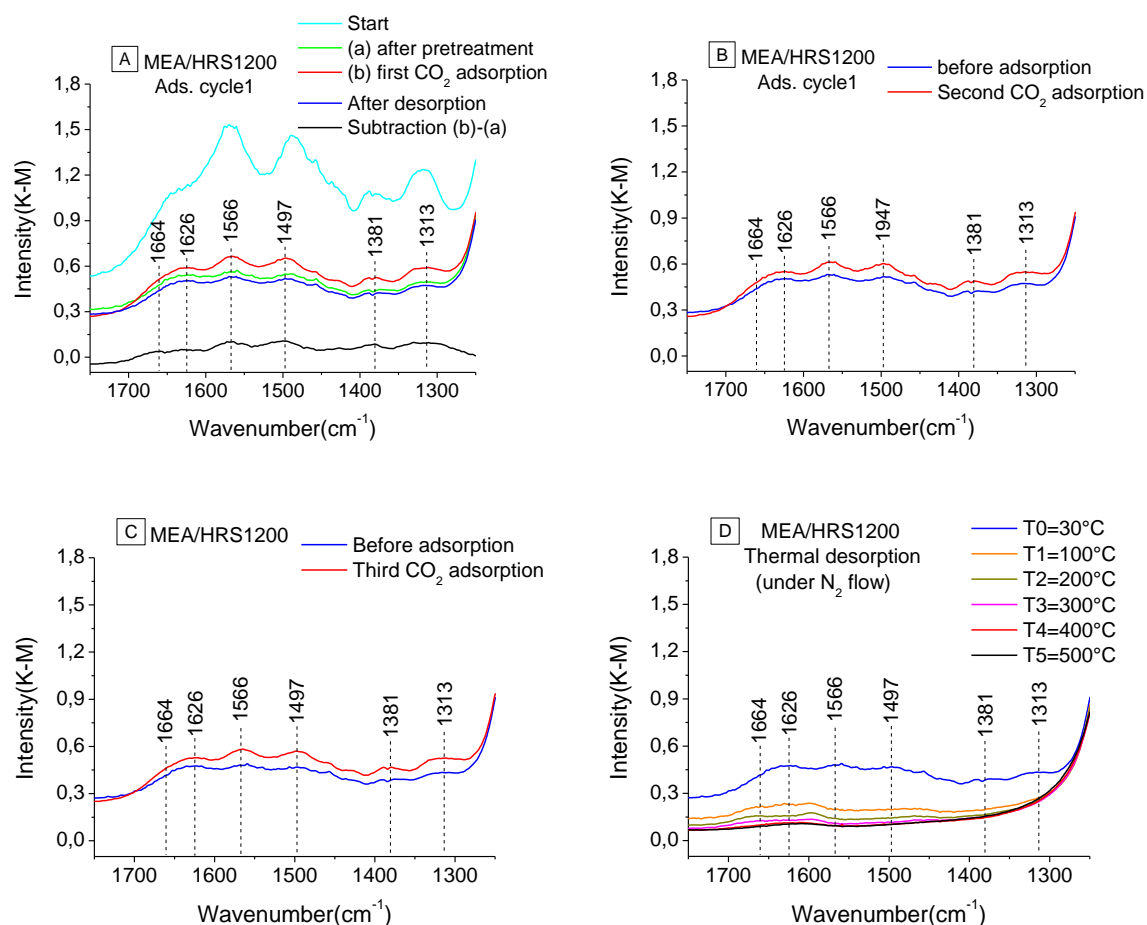


Figure 38: DRIFT spectra of MEA/HRS1200 during CO<sub>2</sub> adsorption cycles and temperature swing.

## 4 Conclusions

In this chapter, we have presented a high-throughput device based on DRIFT spectroscopy to study the chemical interactions between CO<sub>2</sub> and porous materials, and the main results obtained on three types of adsorbents. DRIFT device allows an automatic control of operating conditions and automatic spectra acquisition during a specific designed experimental protocol.

The highlights of our results and discussions are listed below:

### Activated carbon: AC1

1. No spectral changes have been detected after CO<sub>2</sub> adsorptions and desorptions, except for gas-phase CO<sub>2</sub>. We have thus confirmed that CO<sub>2</sub> capture by AC1 is achieved via physisorption process.
2. No bands have been observed in the spectral range related to adsorbed water. This confirms the hydrophobic character of this material.

### Rare Earth Oxides

1. After pretreatment, the broad band around 3445 cm<sup>-1</sup> due to adsorbed water and several bands in the spectral range 1800-800 cm<sup>-1</sup> due to hydrogencarbonate and carbonate species indicate the presence of already existing adsorbed species on the surface of adsorbents. These residual species reduce the amount of sites available for CO<sub>2</sub> capture, consequently, the adsorption capacities of the materials.
2. Under CO<sub>2</sub> flow, increasing bands in the spectral range 1800-800 cm<sup>-1</sup> indicate mainly the formation of hydrogencarbonate species. We have identified two types of these species, hydrogencarbonate of type II being more stable than that of type I.
3. Comparing DRIFT spectra of undoped and doped ceria during CO<sub>2</sub> adsorption cycles, we suggest that the main differences between samples are the relative proportion of already existing adsorbed species on adsorbent surfaces and new formed species.
4. On temperature swing step, the decrease and changes of bands shapes indicate desorption and reorganization of residual species.
5. By means of subtraction spectra and deconvolution technique, we have assigned IR bands to hydrogenocarbonates and to bidentate, monodentate and polydentate carbonates.
6. From the kinetics of desorption, we have established the thermal stability of these species: hydrogencarbonates < bidentate carbonates < monodentate carbonates < polydentate carbonates.
7. The analysis of kinetic profiles suggests that doped ceria are not only better for CO<sub>2</sub> capture but also for regeneration step at room temperature.
8. The analysis of kinetic profiles of doped ceria during temperature swing allowed the analyze of the influence of doped ions on desorption behaviors. The lowest desorption rates and the highest percentage of remaining species at elevated temperatures on CeLaPr and CePr suggest a higher basic character for these oxides. CeZrPr has shown the highest desorption rates and the lowest percentage of remaining species at elevated temperatures, which suggest that the doped zirconium cations may increase the oxygen mobility in the fluorite structure of the adsorbent, thereby facilitating the desorption of species.

9. We have confirmed the linear relationship between specific surface area and adsorption capacities of adsorbents.

Hybrid materials:

a) 33Iminobis impregnated HRS1200

1. No spectral changes after CO<sub>2</sub> adsorptions and desorptions (except for gas-phase CO<sub>2</sub>) on silica support (HRS1200) have been observed. These results confirm that adsorption of carbon dioxide on HRS1200 leads only to weak physisorption interactions.
2. The evolution of IR bands of HRS1200 during temperature swing suggest the reorganization of hydrogen-bonded OH groups of adsorbed water and the activation of free OH groups on the support surface (silanol groups).
3. DRIFT spectrum of 33Iminobis impregnated HRS1200 has shown considerable modifications compared to silica support. Additional bands corresponding to N-H and C-H stretching and bending vibrations of 33Iminobis and the vanishing of free silanol groups confirmed the impregnation of amine moieties on the silica support.
4. By comparing the DRIFT spectra of 33Iminobis/HRS1200 under CO<sub>2</sub> and N<sub>2</sub> flow and by analyzing the kinetic profiles (adsorption cycles), we have identified bands due to ionic carbamate and carbamic acid. Because of the easy desorption of this species under soft conditions (N<sub>2</sub> flow only), we suggest that these species are weakly bound to the silica surface.
5. The analysis of kinetic profiles during temperature swing allowed the identification of characteristic temperatures: 70 °C seems to be the characteristic temperature at which the removal of 33Iminobis from silica support starts and 190 °C is the limit temperature of amine stability over silica support.

b) Monoethanolamine impregnated HRS1200

1. DRIFT bands due to C-H, N-H and O-H vibrations of MEA moieties and the loss of isolated silanol on the material surface confirmed the successful impregnation of MEA over HRS1200.
2. However, the stability of impregnation was proved to be very weak. The characteristic bands of MEA moieties start to decrease under N<sub>2</sub> flow only at room temperature and at 100 °C, one observes the full vanishing of these characteristic bands. These results are in line with screening results.
3. Evolution of bands during the first CO<sub>2</sub> adsorption cycle indicates also the formation of ionic carbamate and carbamic acid.

From this investigation for hybrid materials, we can propose some outlooks:

- New procedures should to be developed in order to increase the thermal stability of the materials. Or the impregnation technique should be improved, or new procedure of synthesis should be employed such as amine covalently tethered to oxide support.
- Even if the analysis of spectra is in line with literature (Bacsik *et al.* [123], Danon *et al.* [122] and Knöfel *et al.*[129]), there is still controversy and further analysis is required before to be able to propose a precise and reliable assignment of spectra. Moreover, a comparison with the reactivity of CO<sub>2</sub> with liquid amines (33Iminobis and MEA) should be performed.

## *CHAPTER V: Investigation Level I*

In the “General Conclusion”, we will gather the information acquired thanks to our four high-throughput steps for an overall comparison of all studied materials.



**CHAPTER VI**  
**Investigation Level II**

-

**Development of a Millifluidic Adsorption Column**



We have seen in the first chapter that CO<sub>2</sub> capture by solid adsorbents is achieved in adsorption columns (adsorbers). The influence of operating conditions (e.g. gas-phase concentration at the inlet of the adsorber and superficial velocities of the gas-phase through the adsorption bed) on breakthrough times and maximum temperature rises must be predicted. When dealing with temperature swing adsorption (TSA), for example, the influence of temperature is critical. Since desorption occurs by increasing temperature, adsorbers are thermally insulated in order to reduce the heat losses with surroundings. This insulation combined with the high heats of adsorption leads to significant temperature rises during the adsorption step. Such warming has a negative impact on the performance of the unit. Dynamic adsorption capacities were shown to be reduced about 10-15% because of excessive bed heating [148]. High temperature rises are also responsible for bed ignition. The control of thermal conditions in the adsorber during the entire operation conditions is a key point. The understanding of CO<sub>2</sub> adsorption behavior, near to realistic configuration, is thus essential.

In order to simulate CO<sub>2</sub> adsorption inside adsorbers, a millifluidics adsorption column has been designed (Figure 1a). This milli-scale device may contribute to high-throughput study of the effects of operating conditions. IR thermography is used as an approach technique to observe the temperature field in the adsorber during CO<sub>2</sub> adsorption (Figure 1b). Consequently, thermal waves may be evaluated and breakthrough times may be estimated.

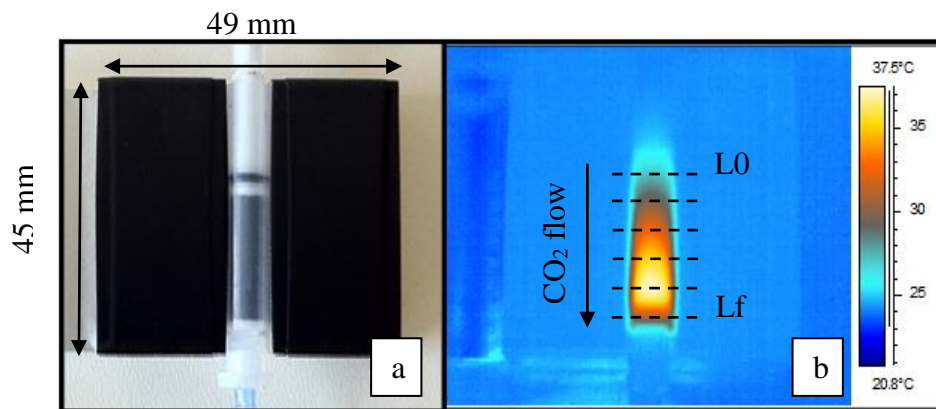


Figure 1: (a) Millifluidic adsorption column. (b) Temperature field during CO<sub>2</sub> adsorption on AC1 (flow rate = 40 ml.min<sup>-1</sup>) at  $t = 60$  s.

The cylindrical adsorber is connected to a gas injection system and placed in an aluminum support. The milli-adsorber has internal diameter  $d_2 = 5$  mm, external diameter  $D_2 = 8$  mm, wall thickness  $e_w = 1.5$  mm and adjustable length  $L$ . It was made of thermoplastic polymer, polypropylene C18 (insulating material,  $\lambda = 0.1 - 0.22$  W.m<sup>-1</sup>.K<sup>-1</sup>), to reduce heat losses with surroundings and thus to maximize the thermal signal received by the IR camera. The aluminum support (high thermal conductivity  $\lambda = 237$  W.m<sup>-1</sup>.K<sup>-1</sup>) was painted in black, to avoid reflections and to homogenize the surface emissivity. CO<sub>2</sub> adsorption occurs thus in isoperibolic conditions, in other words, the temperature around the milli-adsorber is constant and uniform. The heat losses are thus mastered [114].

To illustrate some applications of the device, the activated carbon AC1 has been employed to run an experiment, which consisted in recording the temperature field during CO<sub>2</sub> adsorption for different flow rates (30, 40, 50, 60 and 70 ml.min<sup>-1</sup>) of pure CO<sub>2</sub> injected into the adsorber. The milli-adsorber and its temperature field during CO<sub>2</sub> adsorption (flow rate = 40 ml.min<sup>-1</sup>) at different adsorption times, is shown in Figure 2.

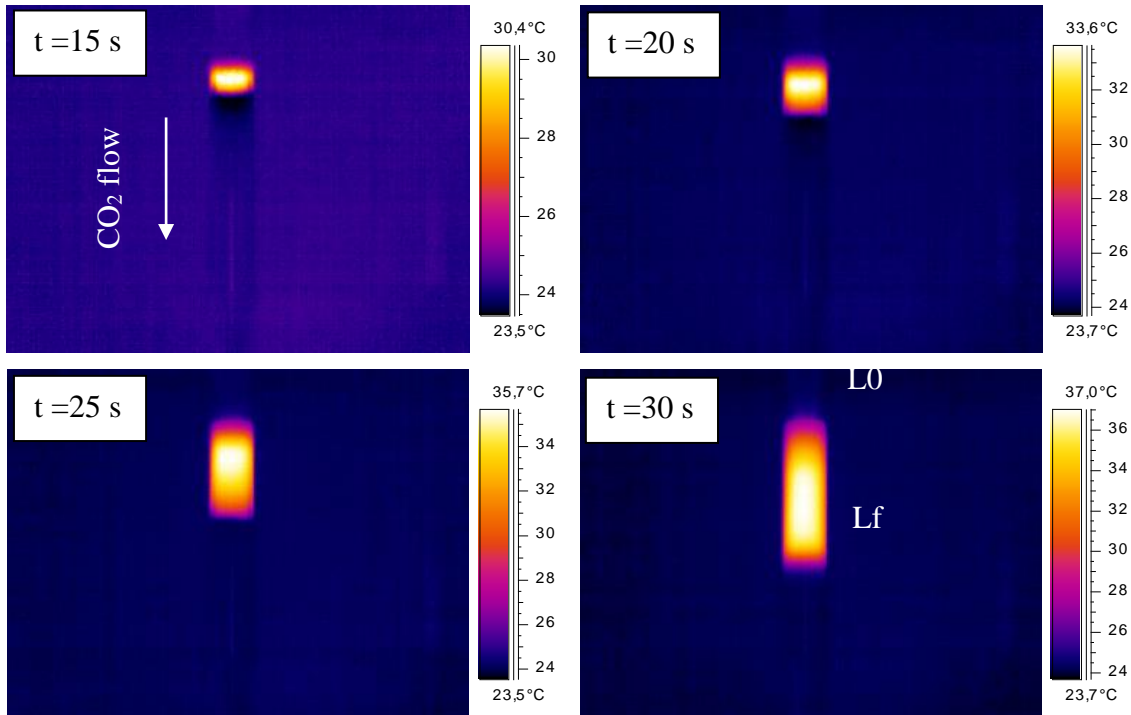


Figure 2: Temperature field during CO<sub>2</sub> adsorption on AC1 at different adsorption times.

The maximum observed temperatures were lower than in the thin-layer approach (Figure 3). This can be explained by two factors: 1) the semi-transparent behavior of the adsorber wall in the infrared region, then the IR signal detected by the IR camera was weaker than in the thin-layer approach. 2) as CO<sub>2</sub> adsorption occurs in isoperibolic conditions, the heat losses are typically greater.

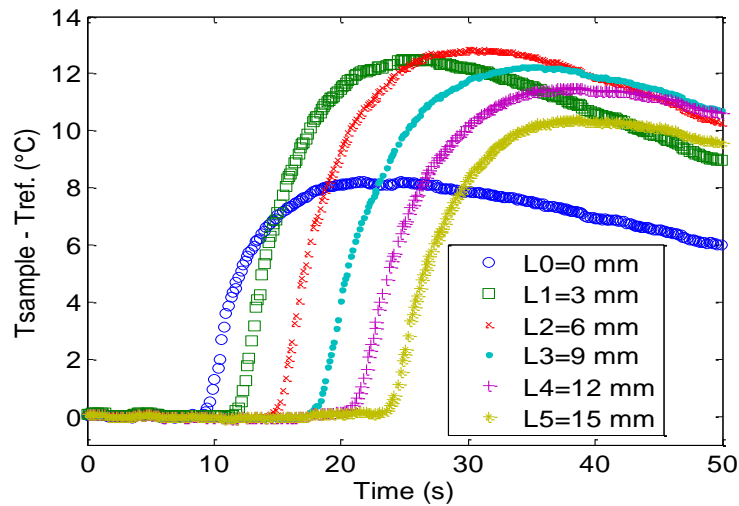


Figure 3: Average temperature in different sections of adsorber, from  $L_0 = 0$  to  $L_f = 15$  mm (see Figure 1b), as a function of adsorption time.

At short-time periods, the thermal behavior in the adsorber is similar to thin-layer configuration. However, in long-time periods, thermal diffusion and dispersion appear to impact the thermal behavior during adsorption process.

A thermal front with constant speed was observed during CO<sub>2</sub> capture. The temperature profile of adsorber during the first seconds of adsorption (Figure 4) shows the propagation of a thermal front along the length of adsorber.

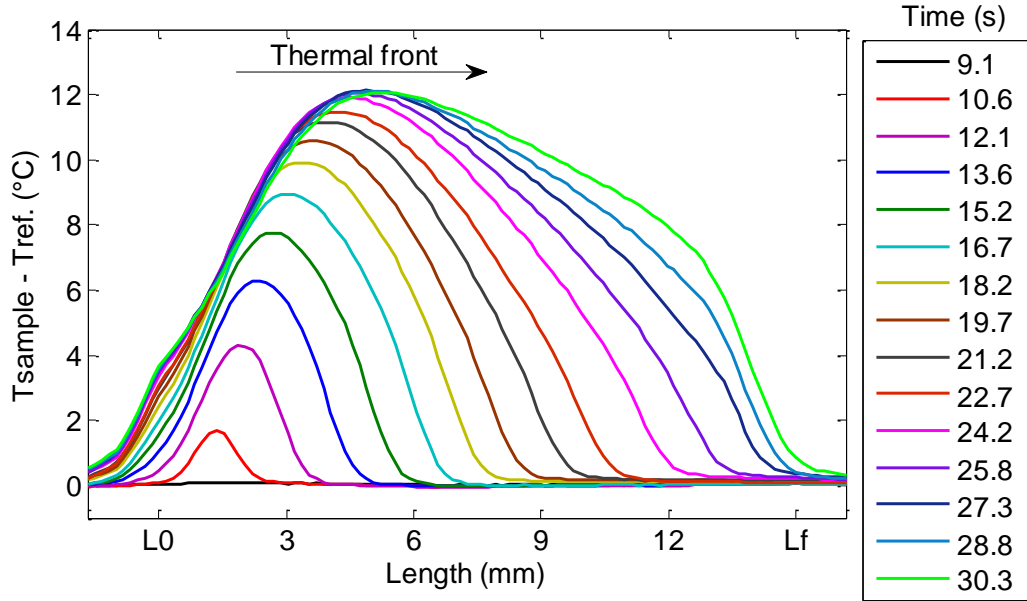


Figure 4: Temperature profile, averaged in the radial direction of adsorber, during the first seconds of CO<sub>2</sub> adsorption process.

The analysis of thermal images and temperature evolutions for each injected flow rate, allowed an estimation of the propagation speed of the thermal front (TFR) in the milli-adsorber. In Figure 5, the temperature field, averaged in the radial direction of the adsorber, is plotted as a function of adsorber length at every image step. Knowing the size of pixel and the sampling frequency, the threshold of the images of Figure 5 allowed the estimation of the slope and confidence interval of the straight lines (dotted lines), which represent the TFR in the adsorber during adsorption process. The estimated values of TFR are shown in Figure 6. The results show the increase of TFR with increasing flow rates.

For a same flow rate traversing an identical volume of both thin-layer and millifluidic bed of adsorbent, a correlation between short-time adsorption (in thin-layer approach) and the thermal front rate (TFR) can be written as:

$$TFR = \frac{e_{fl} \cdot \left( \frac{d_1}{d_2} \right)^2}{\tau_{ST}} \quad (mm / s) \quad (1)$$

where  $e_{fl}$  is the thin-layer thickness (mm),  $\tau_{ST}$  the breakthrough time (s) (temporal window of short-time adsorption, from  $t_i$  to  $t_f$ ) and  $d_1$ ,  $d_2$  the inner diameter of adsorption cup and millifluidic adsorber, respectively.

For example, CO<sub>2</sub> adsorption on the thin-layer of AC1 (CO<sub>2</sub> injection of 40 ml.min<sup>-1</sup> through adsorbent thin-layer with  $e_{fl} = 3$  mm) has led to a breakthrough time of  $\tau_{ST} = 9$  s (Chapter IV, section 4, Figure 8). Applying equation 1 to the found breakthrough time (with  $e_{fl} = 3$  mm,  $d_1 = 8$  mm and  $d_2 = 5$  mm), a thermal front rate of  $TFR = 0.85$  mm.s<sup>-1</sup> was calculated. This result is in good agreement with the estimated TFR in the millifluidic

adsorption column for a same injection flow rate of  $40 \text{ ml}\cdot\text{min}^{-1}$ :  $TFR=0.86 \text{ mm}\cdot\text{s}^{-1}$  (see Figure 6).

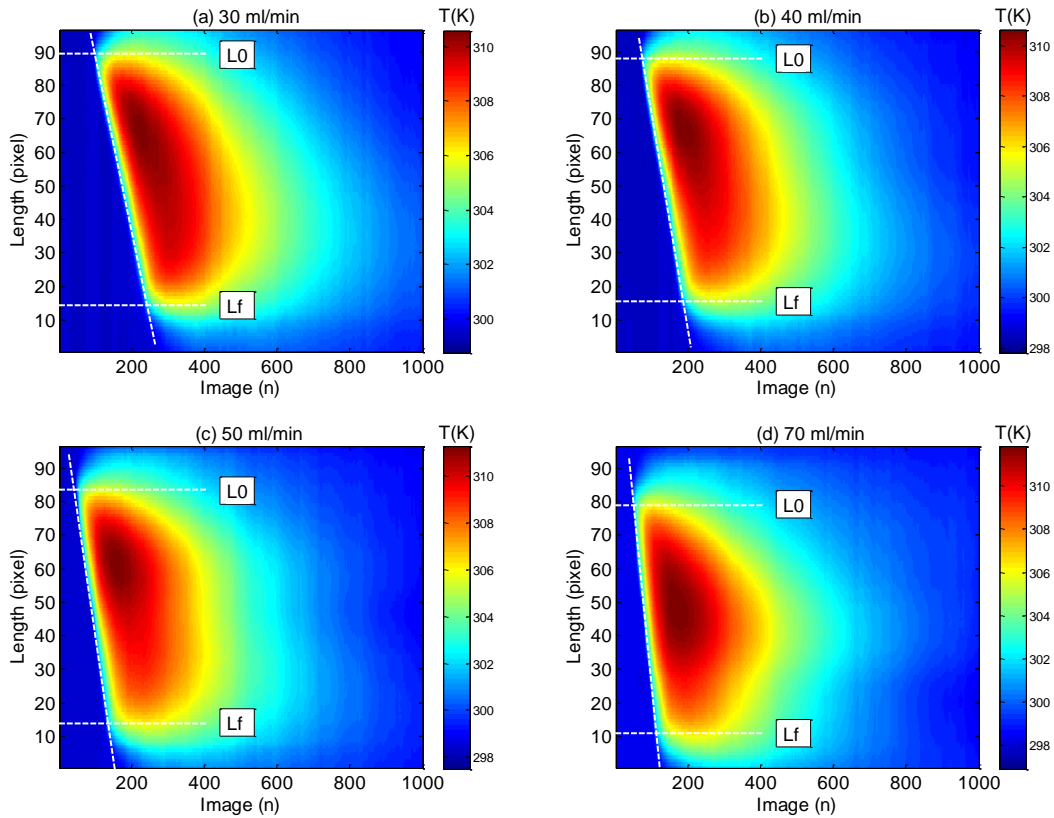


Figure 5: Temperature field, averaged in the radial direction of adsorber, as a function of adsorber length at every image step. Flow rate of 30 (a), 40 (b), 50 (c) and 70 (d)  $\text{ml}\cdot\text{min}^{-1}$ .

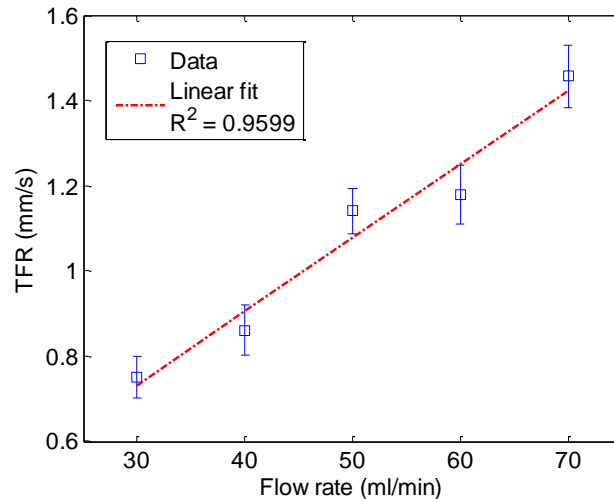


Figure 6: Propagation speed of the thermal front as a function of injected  $\text{CO}_2$  flow rate.

Therefore, thanks to its rapidity, this millifluidic approach is also interesting for preliminary design of processes to be used at industrial scale. For example, the size of the capture system, the time of bed saturation and operational conditions can be evaluated.

It is important to emphasize that we have presented in this chapter the first results obtained. It will be necessary to perform further systematic studies to better understand complex phenomena occurring in the millifluidic column such as heat diffusion and transport.

**GENERAL CONCLUSIONS**  
**and**  
**OUTLOOK**

*GENERAL CONCLUSIONS and OUTLOOK*

# 1 Performance of materials: What is the best material for CO<sub>2</sub> capture?

The answer is: “it depends on the application!” The capture of CO<sub>2</sub> from the postcombustion flue gas at large point source is expected to be one of the largest contributors to the mitigation of green house emissions in the next decades. Nowadays, the majority of investigated capture processes using solid adsorbents operates in cycles, adsorption at low temperature and desorption induced by pressure (PSA) or temperature swing (TSA). Moreover, a profitable capture process imposes other constraints such as rapid adsorption cycles and high energy efficiency. Therefore, a good adsorbent regarding this application must have high adsorption capacity, high selectivity, rapid uptake, easy recycling, and suitable thermal and mechanical properties.

The heat of adsorption for CO<sub>2</sub> should, ideally, have an intermediate value. If it is too high, the sorbent will be difficult to regenerate economically, and, if it is too low, the capacity for adsorbing CO<sub>2</sub> and the selectivity of CO<sub>2</sub> over other gas in the stream will be too small.

However, no ideal adsorbent exist, each adsorbent has strengths and weaknesses that must be considered.

Along our study, we have acquired information about the studied materials that were used: see Table 1 for overall comparison regarding some of these important parameters. In the following sections, a final assessment of CO<sub>2</sub> capture by our solid adsorbents is performed.

Table 1: Overall comparison of studied materials

Material	Nature of sorption	$\Delta H_{ads}$ (kJ/mol)	Adsorption capacity	Thermal stability <sup>(1)</sup>	Adsorption rate	Facility of regeneration <sup>(2)</sup>
REO	chemical	30-40	+	+++	+++	++
Hybrids	chemical	40-60	++++	++	++	++++
Activated carbon	physical	20-30	+++	+++++	+++++	+++++

Note: (1) thermal stability of material (2) full regeneration of material consists in complete removal of adsorbed species.

## 1.1 Rare Earth oxides

CO<sub>2</sub> capture by REO is achieved via chemisorption process with principally the formation of hydrogenocarbonate species over already existing adsorbed species (residual species) on the material surface (monodentate, bidentate and polydentate carbonates). The formation of these weakly bonded species leads to moderate adsorption heats (low chemisorption heats), low adsorption capacities and moderate adsorption rates. The moderate rates of adsorption are controlled by the kinetics of the formation of species on the material surface. Since adsorbent particles are not damaged during temperature swing, REO exhibit high thermal stability.

REO exhibit the lowest adsorption capacities among studied materials. Their adsorption capacities may be improved by thermal desorption of mentioned residual species. However, the costs of a thermal desorption might be large because of the high thermal stability of carbonate species. For a complete removal of such species, a thermal desorption must be achieved by temperature swing up to 500 °C. Moreover, the recycling time may be increased because of this supplementary step.

Doping cations may increase the basicity of surface and the oxygen mobility, as for CeZrPr, which exhibits higher adsorption capacity and easier regeneration than undoped ceria.

Regarding TSA and PSA capture systems, the utilization of REO as adsorbents appears to be unprofitable. However, applications as catalysts for CO<sub>2</sub> valorization appear to be interesting because of the possibility of modulation of the surface properties.

## **1.2 Activated carbons**

CO<sub>2</sub> capture by activated carbons is achieved via physisorption process. CO<sub>2</sub> molecules are attracted by the electrical field of the material surface and no new species are formed. Therefore, the kinetic of adsorption is typically mass transfer limited.

The physisorption of CO<sub>2</sub> over activated carbons leads to low adsorption heats, just above the enthalpy of condensation of CO<sub>2</sub>. Despite these low adsorption heats, a high amount of heat is released during CO<sub>2</sub> capture, which is related to the highest adsorption rates among all studied materials. The high amount of released heat induces an intense increase of the adsorbent temperature. High temperatures reduce the amount of captured CO<sub>2</sub> and impact the overall performance of the adsorbent. Once again because of the interactions of physisorption nature, these materials exhibit a high facility of regeneration under soft conditions (inner flow at room temperature).

Activated carbons (together with hybrid materials) exhibit the highest adsorption capacities, principally because of their high surface areas, and exhibit also a high thermal and mechanical stability.

AC1 (together with 33Iminobis/HRS1200) exhibits the best performances for CO<sub>2</sub> capture among all studied materials.

Therefore, activated carbons have many attractive properties for postcombustion CO<sub>2</sub> capture.

## **1.3 Hybrid materials**

The studied hybrid materials consisted in amine impregnated silica support. The heterogeneous nature of these materials is responsible for large differences in adsorption behaviors. The adsorptive properties depend on the type of impregnated amine moieties and of their solid supports.

CO<sub>2</sub> capture by hybrid materials is achieved via chemisorption process. In the case of 33Iminobis/HRS1200 and MEA/HRS1200, chemisorption process leads to the formation of ionic carbamates and carbamic acid species. These formed species are weakly bonded to the adsorbent surface, resulting in moderate adsorption heats (low chemisorption heats) and therefore, easy material regeneration under soft conditions.

Hybrid materials have high adsorption capacities but low adsorption kinetics. As for REO, their lowest adsorption rates among studied materials are limited by the kinetic of the formation of species on the adsorbent surface.

Because of the high amount of organic content, some hybrid materials have shown weak thermal stability, which is characterized by desorption of amine moieties during the first adsorption cycle. The high amount of heat released during adsorption induces a high temperature variation which causes the removal of amine moieties from silica support. The most remarkable case is CO<sub>2</sub> adsorption on MEA/HRS1200 which shows extreme energetic interactions (the highest adsorption heat among studied materials) for the first CO<sub>2</sub> adsorption only. Following adsorptions lead to weaker adsorbate-adsorbent interactions and, consequently, much weaker adsorption heat. DRIFT investigation revealed that MEA moieties are removed from silicas support under inert flow only.

Among hybrid materials, 33Iminobis/HRS1200 showed the best performances and will be compared to AC1 in the next section.

The use of amine impregnated silica for postcombustion CO<sub>2</sub> capture will principally be limited to low temperature regimes.

### 1.4 AC1 versus 33Iminobis/HRS1200

The amine impregnated silica 33Iminobis/HRS1200 and the activated carbon AC1 have shown the highest adsorption capacities among all studied materials and are regenerable using inert flow at room temperature. Therefore, these materials exhibit the best performances concerning a possible application as adsorbent for postcombustion CO<sub>2</sub> capture at low temperature.

A relative comparison between these materials regarding CO<sub>2</sub> adsorption rate, heat and capacity is shown in Figure 1.

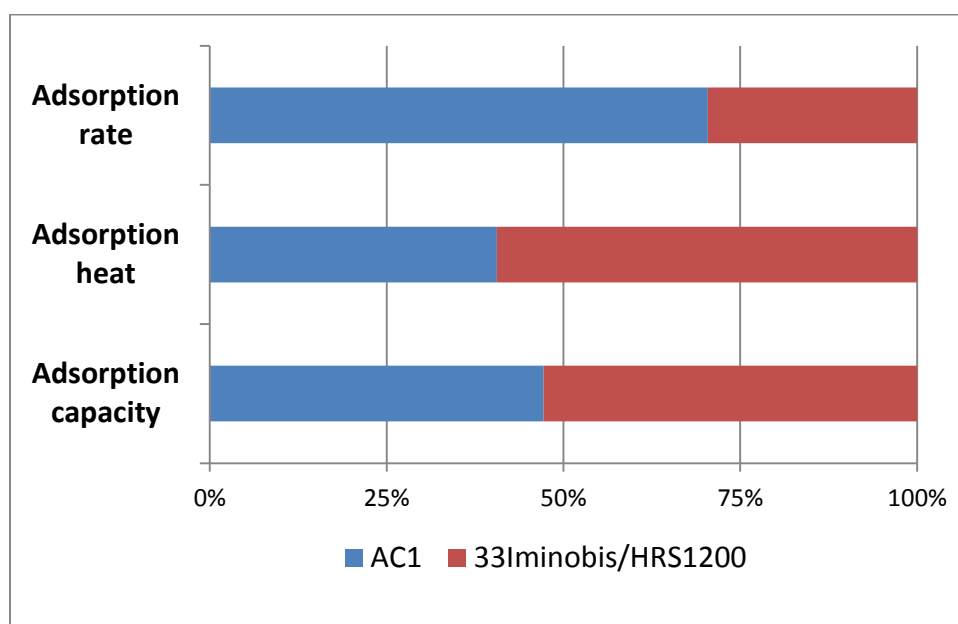


Figure 1: Relative comparison between AC1 and 33Iminobis/HRS1200.

The materials exhibit comparable adsorption capacities. However, because of the different natures of CO<sub>2</sub> adsorption on these materials, AC1 exhibits lower adsorption heat and higher adsorption rate. These features may be decisive in the choice of a profitable CO<sub>2</sub> capture process.

The main difference between these materials is their thermal and mechanical stabilities. AC1 has very good mechanical resistance and thermal stability. 33Iminobis/HRS1200 starts to decompose at 70°C but is relatively stable up to 190°C. Its mechanical resistance is related to

the silica support. Compared to AC1, silica particles are much more fragile. Thermal and mechanical properties of this hybrid material may be a limiting factor regarding multicycle stability.

CO<sub>2</sub> adsorption experiments under humid conditions (not shown here), have proved low influence of water on adsorption capacity of AC1 (hydrophobic character). Otherwise, adsorption capacity of 33Iminobis/HRS1200 is negatively affected by the presence of water possibly because of water's ability to competitively adsorb and/or amine leaching under humid conditions.

Besides the intrinsic performance of adsorbents, the selection of the optimal CO<sub>2</sub> adsorbent will also depend on the adsorbent lifetime, adsorbent costs and specific industrial application.

## **2 Summary and Outlook**

Extensive efforts have been devoted to reduce CO<sub>2</sub> emissions, especially for the development of CO<sub>2</sub> capture technologies. CO<sub>2</sub> capture by solid adsorbents is one of the most promising capture technology due to its high selectivity and low energy penalties.

The study of the physicochemical mechanisms controlling CO<sub>2</sub>-adsorbent interactions is essential when we are looking for efficient CO<sub>2</sub> capture regarding adsorbent performance and the design of capture processes.

In this context, the overall objective of this project was to study CO<sub>2</sub> adsorption interactions from an energetic and chemical point of view, thanks to complementary approaches: Infrared thermography and Infrared spectroscopy.

Moreover, a high-throughput strategy has been followed for tools development as well as for data analysis in order to match the industrial requirements of rapid access to key parameters controlling CO<sub>2</sub> adsorption. This methodology has enabled to investigate the performance of various materials: rare earth oxides (REO), activated carbons and hybrid materials.

The high-throughput strategy consisted in four steps:

1. Primary screening: A high-throughput device based on infrared thermography has been used to investigate the adsorption thermal behavior of thin-layer of adsorbents. This qualitative analysis has enabled, as a first approach, to study the phenomena and to identify material having a good affinity towards CO<sub>2</sub>. Therefore, for the first time, we have evidenced parameters influencing the quantity of heat released, such as CO<sub>2</sub> concentration in the gas-phase, gas flow rate, specific surface area, adsorption and desorption rates and nature of interaction (physisorption/chemisorption). We have also made the first assumptions about adsorption behaviors for each family of materials, for example, CO<sub>2</sub> capture reversibility.
2. Secondary screening: By coupling IR thermography and gravimetric techniques, simultaneous recording of temperature and adsorbed mass evolutions during CO<sub>2</sub> adsorption on adsorbent thin-layer have been achieved. From these data, we have correlated information about thermal and mass transfer phenomena which allowed the partial confirmation of previous assumptions. For example, the capture reversibility and release of heat are strongly influenced by the type of impregnated-amine on silica supports. Moreover, the adsorption capacities of most of materials could be directly estimated from the mass uptake profiles. Overall, hybrid materials and activated carbons have shown the highest adsorption capacities.

## GENERAL CONCLUSIONS and OUTLOOK

A simplified thermal model has been developed to insight into thermal behaviors, which resulted in the estimation of CO<sub>2</sub> adsorption heats ( $\Delta H_{\text{ads}}$ ) and the study of parameters influencing  $\Delta H_{\text{ads}}$  estimations, as heat losses. Therefore, using the experimental data, a pragmatic and high-throughput inverse method of estimation has been implemented. Overall, the highest values of CO<sub>2</sub> adsorption heats ( $\Delta H_{\text{ads}}$ ) have been estimated for hybrid materials, followed by REO and activated carbons. By means of a simplified mass uptake model, other key parameters have been defined to compare the adsorption and desorption rates of studied materials. Activated carbons have shown the highest adsorption and desorption rates, followed by REO and hybrid materials.

Therefore, in these parts of the work we have identified and evaluated key parameters for CO<sub>2</sub> capture by solid adsorbents such as the strength of the interaction ( $\Delta H_{\text{ads}}$ ), adsorption capacities and adsorption kinetics. We could also evidence the thermal stability of materials during cyclic adsorptions at room temperature.

3. Investigation Level I: An experimental setup based on DRIFT spectroscopy has been developed to high-throughput investigations of chemical interactions between CO<sub>2</sub> and materials. So, we have confirmed the nature of interactions and identified the species formed during CO<sub>2</sub> adsorption process for some studied materials. Therefore, CO<sub>2</sub> adsorption on the activated carbon AC1 has been proven to be a pure physisorption process. CO<sub>2</sub> is adsorbed in the form of hydrogenocarbonates and carbonate species on REO, and in the form of ionic carbamates and carbamic acid species on hybrid materials 33Iminobis/HRS1200 and MEA/HRS1200. Furthermore, from the analysis of evolution of adsorbed species during experimental protocol (controlled gas flow and temperature), we have been able to validate previous assessments about adsorption behaviors (kinetics and adsorbed amounts) and to investigate the thermal stability of adsorbents (material degradation) and of adsorbed species. For example, 33Iminobis/HRS1200 is thermally stable up to 190°C.

Finally, the information obtained during screening and DRIFT investigation steps have allowed us to make an overall comparison of materials: Rare Earth oxides are not suitable as adsorbents for postcombustion CO<sub>2</sub> capture principally because of their low adsorption capacities. However, because of the possibility of their surface properties modulation (basicity and oxygen mobility), REO materials are interesting as catalysts for CO<sub>2</sub> valorization (for example for fuel production). Among activated carbon and hybrid materials, two materials aroused interest regarding a reversible CO<sub>2</sub> capture at low temperature: the activated carbon AC1 and the amine impregnated silica 33Iminobis/HRS1200. Both adsorbents have high adsorption capacities and reversible CO<sub>2</sub> capture under soft conditions (without temperature swing). The major differences between materials are their thermal stability and adsorption rates. AC1 owning higher adsorption rate and thermal stability appears to be a more suitable adsorbent.

4. Investigation Level II: We have developed a millifluidic adsorption column in which the temperature field during adsorption process is detected by IR thermography. The millifluidic device has allowed a first high-throughput study of operational conditions influencing temperature evolution and the estimation of the thermal front rate, which is related to bed saturation. Moreover, a multi-scale analysis from thin-layer to adsorbent bed could be achieved. Therefore, we have presented the first results linking the thin-layer data to the propagation speed of the thermal front in the millifluidic adsorption bed. However, it is necessary to perform more experiments in order to

better understand the influence of dispersion and diffusion of heat on thermal behaviors. A thermal modeling should be also suitable to predict adsorber dynamics.

It is important to highlight that this work enabled a rapid access to key parameters governing CO<sub>2</sub>-adsorbent interactions. We have proven the reliability of this methodology by checking the agreements of the information obtained during each high-throughput step. However, to finally certify our results, systematic comparison with classical methods (ATG, DSC) should be performed.

Our experiments have been carried out using a pure CO<sub>2</sub> flow. In order to better approximate the real industrial conditions, CO<sub>2</sub> capture by solid adsorbents should be investigated using CO<sub>2</sub>/N<sub>2</sub> gas mixtures (about 15:85 v/v) which is the standard for the postcombustion stream.

Infrared thermography and Infrared spectroscopy have proven to be a rich combination because of the complementarities of the obtained information: it should be now interesting to couple these two techniques to simultaneously investigate *in-situ* the thermal and chemical phenomena during gas-solid interactions. Moreover, spectral imaging could be obtained, thus allowing direct cartography of adsorption phenomena on solids.

Finally, the developed tools and methodology can be applied for the investigation of any gas-solid interactions, as for heterogeneous catalysis systems.

## **Publications/Conference Papers**

1. J. Mascetti, F. Benevides, I. Moog, L. Rocheron, J.-C. Batsale, J. Jolly, G. Lebourdon, J. Majimel, B. Pavageau, C. Pradere, L. Servant, Caractérisation de l'interaction entre CO<sub>2</sub> et substrat solide : vers une optimisation des procédés industriels de capture?, L'Actualité Chimique, 2013, 371-372.
2. F. Benevides, G. Lebourdon, J. Jolly, C. Pradere, J. Mascetti, B. Pavageau, L. Servant, J.-C. Batsale, Thermal effects of CO<sub>2</sub> capture by solid adsorbents: some approaches by IR image processing, Congrès Français de Mécanique 2013.
3. F. Benevides, G. Lebourdon, J. Jolly, C. Pradere, J. Mascetti, B. Pavageau, L. Servant, J.-C. Batsale, High throughput estimation of heat of adsorptions: thin layer approach based on IR thermography, IPDO-2013.

## REFERENCES

1. IPCC, *Climate Change 2007: Synthesis Report*: [http://www.ipcc.ch/pdf/assessment-report/ar4/syr/ar4\\_syr.pdf](http://www.ipcc.ch/pdf/assessment-report/ar4/syr/ar4_syr.pdf).
2. IEA, *Energy Technology Perspectives 2010*: OECD Publishing.
3. CO2CRC. *CO<sub>2</sub> capture/separation technologies*: [http://www.co2crc.com.au/aboutccs/cap\\_adsorption.html](http://www.co2crc.com.au/aboutccs/cap_adsorption.html)
4. Yang, H., et al., *Progress in carbon dioxide separation and capture: A review*. Journal of Environmental Sciences, 2008. **20**(1): p. 14-27.
5. Plasseraud, L., *Carbon Dioxide as Chemical Feedstock*. Edited by Michele Aresta. ChemSusChem, 2010. **3**(5): p. 631-632.
6. Whipple, D.T. and P.J.A. Kenis, *Prospects of CO<sub>2</sub> Utilization via Direct Heterogeneous Electrochemical Reduction*. The Journal of Physical Chemistry Letters, 2010. **1**(24): p. 3451-3458.
7. Figueroa, J.D., et al., *Advances in CO<sub>2</sub> capture technology—The U.S. Department of Energy's Carbon Sequestration Program*. International Journal of Greenhouse Gas Control, 2008. **2**(1): p. 9-20.
8. Thiruvenkatachari, R., et al., *Post combustion CO<sub>2</sub> capture by carbon fibre monolithic adsorbents*. Progress in Energy and Combustion Science, 2009. **35**(5): p. 438-455.
9. Qi, G., et al., *High efficiency nanocomposite sorbents for CO<sub>2</sub> capture based on amine-functionalized mesoporous capsules*. Energy & Environmental Science, 2011. **4**(2): p. 444-452.
10. Romeo, L.M., et al., *Oxyfuel carbonation/calcination cycle for low cost CO<sub>2</sub> capture in existing power plants*. Energy Conversion and Management, 2008. **49**(10): p. 2809-2814.
11. Li, L., et al., *A review of research progress on CO<sub>2</sub> capture, storage, and utilization in Chinese Academy of Sciences*. Fuel, 2013. **108**(0): p. 112-130.
12. Hoff, K.A., et al., *Modeling and Experimental Study of Carbon Dioxide Absorption in Aqueous Alkanolamine Solutions Using a Membrane Contactor*. Industrial & Engineering Chemistry Research, 2004. **43**(16): p. 4908-4921.
13. Bonenfant, D., M. Mimeault, and R. Hausler, *Determination of the Structural Features of Distinct Amines Important for the Absorption of CO<sub>2</sub> and Regeneration in Aqueous Solution*. Industrial & Engineering Chemistry Research, 2003. **42**(14): p. 3179-3184.
14. Park, S.H., et al., *Correlation and Prediction of the Solubility of Carbon Dioxide in Aqueous Alkanolamine and Mixed Alkanolamine Solutions*. Industrial & Engineering Chemistry Research, 2002. **41**(6): p. 1658-1665.
15. MacDowell, N., et al., *An overview of CO<sub>2</sub> capture technologies*. Energy & Environmental Science, 2010. **3**(11): p. 1645-1669.
16. Liu, Y., et al., *Dynamic performance of CO<sub>2</sub> adsorption with tetraethylenepentamine-loaded KIT-6*. Microporous and Mesoporous Materials, 2010. **134**(1-3): p. 16-21.
17. ADA, *Carbon dioxide capture technology*: <http://www.adaes.com/carbon/co2/>.
18. Choi, S., J.H. Drese, and C.W. Jones, *Adsorbent materials for carbon dioxide capture from large anthropogenic point sources*. ChemSusChem, 2009. **2**(9): p. 796-854.
19. Solvay\_Energy\_Services: [http://www.rhodia.com/en/about\\_us/businesses/energy\\_services/index.tcm](http://www.rhodia.com/en/about_us/businesses/energy_services/index.tcm).
20. Helfferich, F.G., *Principles of adsorption & adsorption processes*, by D. M. Ruthven, John Wiley & Sons, 1984, xxiv + 433 pp. AIChE Journal, 1985. **31**(3): p. 523-524.

21. Francis, M. and S.U.N. Lian-Ming, *Adsorption Aspects théoriques*. Techniques de l'ingénieur Procédés de traitement des eaux potables, industrielles et urbaines, 2003. **base documentaire : TIB318DUO**(ref. article : j2730).
22. Freund, H.J. and M.W. Roberts, *Surface chemistry of carbon dioxide*. Surface Science Reports, 1996. **25**(8): p. 225-273.
23. Burghaus, U., *Surface science perspective of carbon dioxide chemistry—Adsorption kinetics and dynamics of CO<sub>2</sub> on selected model surfaces*. Catalysis Today, 2009. **148**(3–4): p. 212-220.
24. Arenillas, A., et al., *CO<sub>2</sub> capture using some fly ash-derived carbon materials*. Fuel, 2005. **84**(17): p. 2204-2210.
25. Wang, Q., et al., *CO<sub>2</sub> capture by solid adsorbents and their applications: current status and new trends*. Energy & Environmental Science, 2011. **4**(1): p. 42-55.
26. Jacobs, P.A., et al., *Surface probing of synthetic faujasites by adsorption of carbon dioxide. Part 1.-Infra-red study of carbon dioxide adsorbed on Na-Ca-Y and Na-Mg-Y zeolites*. Journal of the Chemical Society, Faraday Transactions 1: Physical Chemistry in Condensed Phases, 1973. **69**(0): p. 1056-1068.
27. Harlick, P.J.E. and F.H. Tezel, *An experimental adsorbent screening study for CO<sub>2</sub> removal from N<sub>2</sub>*. Microporous and Mesoporous Materials, 2004. **76**(1–3): p. 71-79.
28. Sauer, J., et al., *Absolute acidities and site specific properties of zeolite catalysts modelled by advanced computational chemistry technology*. Chemical Physics Letters, 1999. **308**(1–2): p. 147-154.
29. Walton, K.S., M.B. Abney, and M. Douglas LeVan, *CO<sub>2</sub> adsorption in Y and X zeolites modified by alkali metal cation exchange*. Microporous and Mesoporous Materials, 2006. **91**(1–3): p. 78-84.
30. Siriwardane, R.V., et al., *Adsorption of CO<sub>2</sub> on Zeolites at Moderate Temperatures*. Energy & Fuels, 2005. **19**(3): p. 1153-1159.
31. Zhao, Z., et al., *Adsorption of carbon dioxide on alkali-modified zeolite 13X adsorbents*. International Journal of Greenhouse Gas Control, 2007. **1**(3): p. 355-359.
32. Ko, D., R. Siriwardane, and L.T. Biegler, *Optimization of a Pressure-Swing Adsorption Process Using Zeolite 13X for CO<sub>2</sub> Sequestration*. Industrial & Engineering Chemistry Research, 2002. **42**(2): p. 339-348.
33. Matta, G.K.L., et al., *Dynamic isotherms of dye in activated carbon*. Materials Research, 2008. **11**: p. 365-369.
34. Cameron-Carbon-Incorporated, *Activated carbon: manufacture, structure & properties*, 2006: [http://www.cameroncarbon.com/documents/carbon\\_structure.pdf](http://www.cameroncarbon.com/documents/carbon_structure.pdf).
35. Dreisbach, F., R. Staudt, and J.U. Keller, *High Pressure Adsorption Data of Methane, Nitrogen, Carbon Dioxide and their Binary and Ternary Mixtures on Activated Carbon*. Adsorption, 1999. **5**(3): p. 215-227.
36. Bae, Y.-S., et al., *Separation of CO<sub>2</sub> from CH<sub>4</sub> Using Mixed-Ligand Metal–Organic Frameworks*. Langmuir, 2008. **24**(16): p. 8592-8598.
37. Llewellyn, P.L., et al., *High Uptakes of CO<sub>2</sub> and CH<sub>4</sub> in Mesoporous Metal Organic Frameworks MIL-100 and MIL-101*. Langmuir, 2008. **24**(14): p. 7245-7250.
38. Furukawa, H., et al., *Ultrahigh Porosity in Metal-Organic Frameworks*. Science, 2010. **329**(5990): p. 424-428.
39. Demessence, A., et al., *Strong CO<sub>2</sub> Binding in a Water-Stable, Triazolate-Bridged Metal–Organic Framework Functionalized with Ethylenediamine*. Journal of the American Chemical Society, 2009. **131**(25): p. 8784-8786.
40. Britt, D., et al., *Highly efficient separation of carbon dioxide by a metal-organic framework replete with open metal sites*. Proceedings of the National Academy of Sciences of the United States of America, 2009. **106**(49): p. 20637-20640.

41. Dietzel, P.D.C., et al., *Adsorption properties and structure of CO<sub>2</sub> adsorbed on open coordination sites of metal-organic framework Ni<sub>2</sub>(dhtp) from gas adsorption, IR spectroscopy and X-ray diffraction*. Chemical Communications, 2008. **0**(41): p. 5125-5127.
42. Mueller, U., et al., *Metal-organic frameworks-prospective industrial applications*. Journal of Materials Chemistry, 2006. **16**(7): p. 626-636.
43. Gray, M.L., et al., *CO<sub>2</sub> capture by amine-enriched fly ash carbon sorbents*. Separation and Purification Technology, 2004. **35**(1): p. 31-36.
44. Lee, S., et al., *Screening Test of Solid Amine Sorbents for CO<sub>2</sub> Capture*. Industrial & Engineering Chemistry Research, 2008. **47**(19): p. 7419-7423.
45. Vaidya, P.D. and E.Y. Kenig, *CO<sub>2</sub>-Alkanolamine Reaction Kinetics: A Review of Recent Studies*. Chemical Engineering & Technology, 2007. **30**(11): p. 1467-1474.
46. Khatri, R.A., et al., *Carbon Dioxide Capture by Diamine-Grafted SBA-15: A Combined Fourier Transform Infrared and Mass Spectrometry Study*. Industrial & Engineering Chemistry Research, 2005. **44**(10): p. 3702-3708.
47. Yu, J., Y. Le, and B. Cheng, *Fabrication and CO<sub>2</sub> adsorption performance of bimodal porous silica hollow spheres with amine-modified surfaces*. RSC Advances, 2012. **2**(17): p. 6784-6791.
48. Knöfel, C., et al., *Study of Carbon Dioxide Adsorption on Mesoporous Aminopropylsilane-Functionalized Silica and Titania Combining Microcalorimetry and in Situ Infrared Spectroscopy*. The Journal of Physical Chemistry C, 2009. **113**(52): p. 21726-21734.
49. Kuwahara, Y., et al., *Enhanced CO<sub>2</sub> adsorption over polymeric amines supported on heteroatom-incorporated SBA-15 silica: Impact of heteroatom type and loading on sorbent structure and adsorption performance*. Chemistry - A European Journal, 2012. **18**(52): p. 16649-16664.
50. Chang, A.C.C., et al., *In-Situ Infrared Study of CO<sub>2</sub> Adsorption on SBA-15 Grafted with  $\gamma$ -(Aminopropyl)triethoxysilane*. Energy & Fuels, 2003. **17**(2): p. 468-473.
51. Hiyoshi, N., K. Yogo, and T. Yashima, *Adsorption characteristics of carbon dioxide on organically functionalized SBA-15*. Microporous and Mesoporous Materials, 2005. **84**(1-3): p. 357-365.
52. Khatri, R.A., et al., *Thermal and Chemical Stability of Regenerable Solid Amine Sorbent for CO<sub>2</sub> Capture*. Energy & Fuels, 2006. **20**(4): p. 1514-1520.
53. Zhao, Y., Y. Shen, and L. Bai, *Effect of chemical modification on carbon dioxide adsorption property of mesoporous silica*. Journal of Colloid and Interface Science, 2012. **379**(1): p. 94-100.
54. Zelenak, V., et al., *Amine-modified SBA-12 mesoporous silica for carbon dioxide capture: Effect of amine basicity on sorption properties*. Microporous and Mesoporous Materials, 2008. **116**(1-3): p. 358-364.
55. Fisher, J.C., *Thesis: The reduction of CO<sub>2</sub> emissions via CO<sub>2</sub> capture and solid oxide fuel cells*, 2009 The Graduate Faculty of The University of Akron: <http://etd.ohiolink.edu/send-pdf.cgi/Fisher%20James%20C.%20II.pdf?akron1247250147>.
56. Zeleňák, V., et al., *Amine-modified ordered mesoporous silica: Effect of pore size on carbon dioxide capture*. Chemical Engineering Journal, 2008. **144**(2): p. 336-342.
57. Hicks, J.C., et al., *Designing adsorbents for CO<sub>2</sub> capture from flue gas-hyperbranched aminosilicas capable of capturing CO<sub>2</sub> reversibly*. Journal of the American Chemical Society, 2008. **130**(10): p. 2902-2903.

58. Son, W.-J., J.-S. Choi, and W.-S. Ahn, *Adsorptive removal of carbon dioxide using polyethyleneimine-loaded mesoporous silica materials*. *Microporous and Mesoporous Materials*, 2008. **113**(1–3): p. 31-40.
59. Xu, X., et al., *Influence of Moisture on CO<sub>2</sub> Separation from Gas Mixture by a Nanoporous Adsorbent Based on Polyethylenimine-Modified Molecular Sieve MCM-41*. *Industrial & Engineering Chemistry Research*, 2005. **44**(21): p. 8113-8119.
60. Yue, M.B., et al., *Efficient CO<sub>2</sub> Capturer Derived from As-Synthesized MCM-41 Modified with Amine*. *Chemistry – A European Journal*, 2008. **14**(11): p. 3442-3451.
61. Abanades, J.C. and D. Alvarez, *Conversion Limits in the Reaction of CO<sub>2</sub> with Lime*. *Energy & Fuels*, 2003. **17**(2): p. 308-315.
62. Lee, J.B., et al., *Sodium-Based Dry Regenerable Sorbent for Carbon Dioxide Capture from Power Plant Flue Gas*. *Industrial & Engineering Chemistry Research*, 2008. **47**(13): p. 4465-4472.
63. Liang, Y., et al., *Carbon Dioxide Capture Using Dry Sodium-Based Sorbents*. *Energy & Fuels*, 2004. **18**(2): p. 569-575.
64. Zhao, C., X. Chen, and C. Zhao, *Study on CO<sub>2</sub> capture using dry potassium-based sorbents through orthogonal test method*. *International Journal of Greenhouse Gas Control*, 2010. **4**(4): p. 655-658.
65. Maitra, A.M., I. Campbell, and R.J. Tyler, *Influence of basicity on the catalytic activity for oxidative coupling of methane*. *Applied Catalysis A: General*, 1992. **85**(1): p. 27-46.
66. Yingli, B., et al., *Catalytic oxidative coupling of methane over alkali, alkaline earth and rare earth metal oxides*. *Applied Catalysis*, 1988. **39**(0): p. 185-190.
67. Adachi, G., N. Imanaka, and Z.C. Kang, *Binary Rare Earth Oxides*, ISBN 978-1-4020-2569-3, 2005.
68. Mandal, S., et al., *Sm-CeO<sub>2</sub> supported gold nanoparticle catalyst for benzyl alcohol oxidation using molecular O<sub>2</sub>*. *Applied Catalysis A: General*, 2013. **452**: p. 94-104.
69. Gotoh, H., Y. Yamada, and S. Sato, *Dehydration of 1,3-butanediol over rare earth oxides*. *Applied Catalysis A: General*, 2010. **377**(1–2): p. 92-98.
70. Binet, C., M. Daturi, and J.-C. Lavalley, *IR study of polycrystalline ceria properties in oxidised and reduced states*. *Catalysis Today*, 1999. **50**(2): p. 207-225.
71. Vayssilov, G.N., et al., *Reassignment of the Vibrational Spectra of Carbonates, Formates, and Related Surface Species on Ceria: A Combined Density Functional and Infrared Spectroscopy Investigation*. *The Journal of Physical Chemistry C*, 2011. **115**(47): p. 23435-23454.
72. Sato, S., et al., *Basic properties of rare earth oxides*. *Applied Catalysis A: General*, 2009. **356**(1): p. 57-63.
73. Bereketidou, O.A. and M.A. Goula, *Biogas reforming for syngas production over nickel supported on ceria–alumina catalysts*. *Catalysis Today*, 2012. **195**(1): p. 93-100.
74. Jasinski, P., T. Suzuki, and H.U. Anderson, *Nanocrystalline undoped ceria oxygen sensor*. *Sensors and Actuators B: Chemical*, 2003. **95**(1–3): p. 73-77.
75. Maffei, N. and A.K. Kuriakose, *Solid oxide fuel cells of ceria doped with gadolinium and praseodymium*. *Solid State Ionics*, 1998. **107**(1–2): p. 67-71.
76. Jen, H.W., et al., *Characterization of model automotive exhaust catalysts: Pd on ceria and ceria–zirconia supports*. *Catalysis Today*, 1999. **50**(2): p. 309-328.
77. Otsuka-Yao-Matsuo, S., et al., *Oxygen Release Behavior of CeZrO<sub>4</sub> Powders and Appearance of New Compounds and t\**. *Journal of Solid State Chemistry*, 1998. **138**(1): p. 47-54.

78. Abdollahzadeh-Ghom, S., et al., *Improvement of oxygen storage capacity using mesoporous ceria-zirconia solid solutions*. Applied Catalysis B: Environmental, 2011. **108–109**(0): p. 32-38.
79. Slostowski, C., *thesis: Synthèse solvothermale supercritique de nanostructures d'oxyde de cérium* 2012, L'UNIVERSITÉ BORDEAUX 1  
<http://www.theses.fr/2012BOR14661>.
80. Mascetti, J., et al., *Caractérisation de l'interaction entre CO<sub>2</sub> et substrat solide : vers une optimisation des procédés industriels de capture?*, in *L'Actualité Chimique* 2013.
81. Wang, W. and J. Gong, *Methanation of carbon dioxide: An overview*. Frontiers of Chemical Engineering in China, 2011. **5**(1): p. 2-10.
82. Ocampo, F., et al., *CO<sub>2</sub> methanation over Ni-Ceria-Zirconia catalysts: effect of preparation and operating conditions*. IOP Conference Series: Materials Science and Engineering, 2011. **19**(1): p. 012007.
83. Sharma, S., et al., *CO<sub>2</sub> methanation on Ru-doped ceria*. Journal of Catalysis, 2011. **278**(2): p. 297-309.
84. Lavalley, J.C., *Infrared spectrometric studies of the surface basicity of metal oxides and zeolites using adsorbed probe molecules*. Catalysis Today, 1996. **27**(3–4): p. 377-401.
85. Solvay\_Rhodia\_Silica:  
[http://www.rhodia.com/en/about\\_us/businesses/silica/index.tcm](http://www.rhodia.com/en/about_us/businesses/silica/index.tcm)
86. Brunauer, S., et al., *On a Theory of the van der Waals Adsorption of Gases*. Journal of the American Chemical Society, 1940. **62**(7): p. 1723-1732.
87. Siriwardane, R.V., et al., *Adsorption of CO<sub>2</sub> on Molecular Sieves and Activated Carbon*. Energy & Fuels, 2001. **15**(2): p. 279-284.
88. Leal, O., et al., *Reversible adsorption of carbon dioxide on amine surface-bonded silica gel*. Inorganica Chimica Acta, 1995. **240**(1–2): p. 183-189.
89. Knowles, G.P., et al., *Aminopropyl-functionalized mesoporous silicas as CO<sub>2</sub> adsorbents*. Fuel Processing Technology, 2005. **86**(14–15): p. 1435-1448.
90. Serna-Guerrero, R., Y. Belmabkhout, and A. Sayari, *Modeling CO<sub>2</sub> adsorption on amine-functionalized mesoporous silica: 1. A semi-empirical equilibrium model*. Chemical Engineering Journal, 2010. **161**(1–2): p. 173-181.
91. Pré, P., F. Delage, and P. Le Cloirec, *A model to predict the adsorber thermal behavior during treatment of volatile organic compounds onto wet activated carbon*. Environmental Science and Technology, 2002. **36**(21): p. 4681-4688.
92. Delage, F., P. Pre, and P. Le Cloirec, *Mass transfer and warming during adsorption of high concentrations of VOCs on an activated carbon bed: Experimental and theoretical analysis*. Environmental Science and Technology, 2000. **34**(22): p. 4816-4821.
93. SETARAM, *Adsorption and desorption of CO<sub>2</sub> on a catalyst*:  
[http://www.setaram.com/files/application\\_notes/AN611-Adsorption-and-desorption-of-CO2-on-a-catalyst.pdf](http://www.setaram.com/files/application_notes/AN611-Adsorption-and-desorption-of-CO2-on-a-catalyst.pdf).
94. Luo, L. and M. Bailly, *Gestion de la thermique dans les procédés d'adsorption de gaz*. Revue Générale de Thermique, 1996. **35**(418–419): p. 693-697.
95. Yong, L. and K. Sumathy, *Comparison between heat transfer and heat mass transfer models for transportation process in an adsorbent bed*. International Journal of Heat and Mass Transfer, 2004. **47**(8–9): p. 1587-1598.
96. Clause, M., *Thesis: Étude d'un procédé d'adsorption TSA (Temperature Swing Adsorption) à chauffage et refroidissement indirects* 2003.

97. Terzis, A., et al., *Influence of Thermocouple Thermal Inertia in Impingement Heat Transfer Experiments Using Transient Techniques*, in *XXI Biannual Symposium on Measuring Techniques in Turbomachinery 2012*: Valencia, E.
98. Siegel, R. and J.R. Howell, in *THERMAL RADIATION HEAT TRANSFER*, taylor\_&\_francis, Editor 1968.
99. Kreith, F. and M.S. Bohn, *Principios de transferencia de calor*, 2003: p. 481-507.
100. wikipedia, *electromagnetic spectrum*:  
[http://en.wikipedia.org/wiki/Electromagnetic\\_spectrum](http://en.wikipedia.org/wiki/Electromagnetic_spectrum).
101. FLIR, *The ultimate infrared handbook for R&D professionals*.
102. Zholkov, Y.A., *Izmeritel'naya Tekhnika*, 1961: p. 36-37.
103. Younus, A.M.D. and B.-S. Yang, *Intelligent fault diagnosis of rotating machinery using infrared thermal image*. *Expert Systems with Applications*, 2012. **39**(2): p. 2082-2091.
104. Manana, M., et al., *Field winding fault diagnosis in DC motors during manufacturing using thermal monitoring*. *Applied Thermal Engineering*, 2011. **31**(5): p. 978-983.
105. Jadin, M.S. and S. Taib, *Recent progress in diagnosing the reliability of electrical equipment by using infrared thermography*. *Infrared Physics & Technology*, 2012. **55**(4): p. 236-245.
106. Zipser, S., et al., *Combustion Plant Monitoring and Control Using Infrared and Video Cameras*, in *Power Plants and Power Systems Control 2006*, W. Dr. David, Editor 2007, Elsevier Science Ltd: Oxford. p. 249-254.
107. Kaminski, A., et al., *Non-destructive characterisation of defects in devices using infrared thermography*. *Microelectronics Journal*, 1999. **30**(11): p. 1137-1140.
108. Titman, D.J., *Applications of thermography in non-destructive testing of structures*. *NDT & E International*, 2001. **34**(2): p. 149-154.
109. Maillet, D., et al., *Méthodes intégrales et contrôle non destructif par thermographie infrarouge stimulée*. *Revue Générale de Thermique*, 1996. **35**(409): p. 5-13.
110. Guillaumat, L., J.C. Batsale, and D. Mourand, *Real time infra-red image processing for the detection of delamination in composite plates*. *Composites Part A: Applied Science and Manufacturing*, 2004. **35**(7-8): p. 939-944.
111. Bamford, M., et al., *Global and local characterization of the thermal diffusivities of SiCf/SiC composites with infrared thermography and flash method*. *Composites Science and Technology*, 2009. **69**(7-8): p. 1131-1141.
112. Degiovanni, A., J.C. Batsale, and D. Maillet, *Mesure de la diffusivité longitudinale de matériaux anisotropes*. *Revue Générale de Thermique*, 1996. **35**(410): p. 141-147.
113. Bamford, M., J.C. Batsale, and O. Fudym, *Nodal and modal strategies for longitudinal thermal diffusivity profile estimation: Application to the non destructive evaluation of SiC/SiC composites under uniaxial tensile tests*. *Infrared Physics & Technology*, 2009. **52**(1): p. 1-13.
114. Hany, C., et al., *Thermal analysis of chemical reaction with a continuous microfluidic calorimeter*. *Chemical Engineering Journal*, 2010. **160**(3): p. 814-822.
115. Lahiri, B.B., et al., *Medical applications of infrared thermography: A review*. *Infrared Physics & Technology*, 2012. **55**(4): p. 221-235.
116. Colthup, N.B., *Introduction to Infrared and Raman Spectroscopy* 1990: Academic Press.
117. Ryczkowski, J., *IR spectroscopy in catalysis*. *Catalysis Today*, 2001. **68**(4): p. 263-381.
118. Coluccia, S., L. Marchese, and G. Martra, *Characterisation of microporous and mesoporous materials by the adsorption of molecular probes: FTIR and UV-Vis studies*. *Microporous and Mesoporous Materials*, 1999. **30**(1): p. 43-56.

119. Carre, S., et al., *Model reactions as probe of the acid–base properties of aluminas: Nature and strength of active sites. Correlation with physicochemical characterization*. Applied Catalysis A: General, 2010. **372**(1): p. 26-33.
120. Gu, X., et al., *Structural, redox and acid–base properties of V<sub>2</sub>O<sub>5</sub>/CeO<sub>2</sub> catalysts*. Thermochemica Acta, 2006. **451**(1–2): p. 84-93.
121. Hedin, N., et al., *Adsorbents for the post-combustion capture of CO<sub>2</sub> using rapid temperature swing or vacuum swing adsorption*. Applied Energy, 2013. **104**(0): p. 418-433.
122. Danon, A., P.C. Stair, and E. Weitz, *FTIR Study of CO<sub>2</sub> Adsorption on Amine-Grafted SBA-15: Elucidation of Adsorbed Species*. The Journal of Physical Chemistry C, 2011. **115**(23): p. 11540-11549.
123. Bacsik, Z.n., et al., *Temperature-Induced Uptake of CO<sub>2</sub> and Formation of Carbamates in Mesocaged Silica Modified with n-Propylamines*. Langmuir, 2010. **26**(12): p. 10013-10024.
124. Eldridge, G.R., et al., *High-Throughput Method for the Production and Analysis of Large Natural Product Libraries for Drug Discovery*. Analytical Chemistry, 2002. **74**(16): p. 3963-3971.
125. Kawatsura, M. and J.F. Hartwig, *Transition Metal-Catalyzed Addition of Amines to Acrylic Acid Derivatives. A High-Throughput Method for Evaluating Hydroamination of Primary and Secondary Alkylamines*. Organometallics, 2001. **20**(10): p. 1960-1964.
126. Jolly, J., B. Pavageau, and J.-M. Tatibouët, *Time-resolved IR thermographic detection of gaseous molecules adsorption on oxide supports*. Quantitative InfraRed Thermography Journal, 2011. **8**(2): p. 129-137.
127. Ozil, P. and L. Bonnetain, *Theoretical prediction of temperature profiles in an adsorbent fixed-bed*. Chemical Engineering Science, 1978. **33**(9): p. 1233-1237.
128. Rodgers, J. and A. Nicewander, *Thirteen Ways to Look at the Correlation Coefficient*. The American Statistician, 1988. **42**(1): p. 59-66.
129. Knöfel, C., et al., *Study of carbon dioxide adsorption on mesoporous aminopropylsilane- functionalized silica and titania combining microcalorimetry and in situ infrared spectroscopy*. Journal of Physical Chemistry C, 2009. **113**(52): p. 21726-21734.
130. Knöfel, C., et al., *Functionalised micro-/mesoporous silica for the adsorption of carbon dioxide*. Microporous and Mesoporous Materials, 2007. **99**(1–2): p. 79-85.
131. Sircar, S. and J.R. Hufton, *Why Does the Linear Driving Force Model for Adsorption Kinetics Work?* Adsorption, 2000. **6**(2): p. 137-147.
132. Nagelkerke, N.J.D., *A note on a general definition of the coefficient of determination*. Biometrika, 1991. **78**(3): p. 691-692.
133. Ding, L.P., S.K. Bhatia, and F. Liu, *Kinetics of adsorption on activated carbon: application of heterogeneous vacancy solution theory*. Chemical Engineering Science, 2002. **57**(18): p. 3909-3928.
134. Franchi, R.S., P.J.E. Harlick, and A. Sayari, *Applications of Pore-Expanded Mesoporous Silica. 2. Development of a High-Capacity, Water-Tolerant Adsorbent for CO<sub>2</sub>*. Industrial & Engineering Chemistry Research, 2005. **44**(21): p. 8007-8013.
135. Hernández-Huesca, R., L. Díaz, and G. Aguilar-Armenta, *Adsorption equilibria and kinetics of CO<sub>2</sub>, CH<sub>4</sub> and N<sub>2</sub> in natural zeolites*. Separation and Purification Technology, 1999. **15**(2): p. 163-173.
136. Khodakov, A.Y. and L.V.C. Rees, *Effect of propane on the kinetics of carbon dioxide adsorption in NaA zeolites*. Gas Separation & Purification, 1995. **9**(4): p. 253-257.
137. Dormand, J.R. and P.J. Prince, *A family of embedded Runge-Kutta formulae*. Journal of Computational and Applied Mathematics, 1980. **6**(1): p. 19-26.

138. TSYGANENKO, et al. Vol. 59. 1985, Moskva, RUSSIE, FEDERATION DE: Nauka.
139. Hoggan, P.E., et al., *Mechanism of COS Hydrolysis on Alumina*. Journal of Catalysis, 1994. **149**(2): p. 300-306.
140. Daturi, M., et al., *Surface investigation on CeZr<sub>1</sub>-O<sub>2</sub> compounds*. Physical Chemistry Chemical Physics, 1999. **1**(24): p. 5717-5724.
141. Li, C., et al., *Carbon monoxide and carbon dioxide adsorption on cerium oxide studied by Fourier-transform infrared spectroscopy. Part 1.-Formation of carbonate species on dehydroxylated CeO<sub>2</sub>, at room temperature*. Journal of the Chemical Society, Faraday Transactions 1: Physical Chemistry in Condensed Phases, 1989. **85**(4): p. 929-943.
142. Huang, H.Y., et al., *Amine-Grafted MCM-48 and Silica Xerogel as Superior Sorbents for Acidic Gas Removal from Natural Gas*. Industrial & Engineering Chemistry Research, 2002. **42**(12): p. 2427-2433.
143. Tanaka, K. and J.M. White, *Characterization of species adsorbed on oxidized and reduced anatase*. The Journal of Physical Chemistry, 1982. **86**(24): p. 4708-4714.
144. Jiu, J., et al., *Syntheses of highly ordered mesoporous silica by new hybrid template*. Materials Chemistry and Physics, 2004. **86**(2-3): p. 435-439.
145. White, L.D. and C.P. Tripp, *Reaction of (3-Aminopropyl)dimethylethoxysilane with Amine Catalysts on Silica Surfaces*. Journal of Colloid and Interface Science, 2000. **232**(2): p. 400-407.
146. Ojeda, F., et al., *Influence of Hydrogen Incorporation on the Structure and Stoichiometry of Chemically Vapor Deposited Silica Films*. Chemistry of Materials, 2001. **13**(11): p. 3986-3992.
147. Korolevich, M.V., et al., *A study of the vibrational spectrum of monoethanolamine*. Journal of Applied Spectroscopy, 1987. **46**(4): p. 400-403.
148. Delage, F., P. Pré, and P. Le Cloirec, *Mass Transfer and Warming during Adsorption of High Concentrations of VOCs on an Activated Carbon Bed: Experimental and Theoretical Analysis*. Environmental Science & Technology, 2000. **34**(22): p. 4816-4821.

